Czech Technical University in Prague

Faculty of Nuclear Sciences and Physical Engineering

Department of Physics

DOCTORAL THESIS

Study of nuclear effects in hadron-nucleus interactions and in heavy-ion collisions

Prague, 2016

Author: Ing. Michal Křelina

Supervisor: RNDr. Ján Nemčík, CSc.

České vysoké učení technické v Praze

Fakulta jaderná a fyzikálně inženýrská

Katedra fyziky

DISERTAČNÍ PRÁCE

Studium jaderných efektů v hadron-jaderných interakcích a srážkách těžkých iontů

Praha, 2016

Autor: Ing. Michal Křelina

Supervisor: RNDr. Ján Nemčík, CSc.

Bibliografický záznam

Autor:	Ing. Michal Křelina, České vysoké učení technické v Praze, Fakulta jaderná a fyzikálně inženýrská, Katedra fyziky
Název opráce:	Studium jaderných efektů v hadron-jaderných interakcích a srážkách těžkých iontů
Studijní program:	(P3913) Aplikace přírodních věd
Studijní obor:	(3901V016) Jaderné inženýrství
Školitel:	RNDr. Ján Nemčík, CSc. České vysoké učení technické v Praze, Fakulta jaderná a fyzikálně inženýrská, Katedra fyziky & Slovenská akademie věd, Ústav experimentálnej fyziky, Košice
Akademický rok:	2015/2016
Počet stran:	155
Klíčová slova:	Jaderné efekty, QCD, přiblížení barevného dipólu, proton-jaderné a jádro-jaderné srážky, jaderné stínění, Croninův efekt

Bibliographic Entry

Author:	Ing. Michal Krelina, Czech Technical University in Prague, Faculty of Nuclear Sciences and Physical Engineering, Department of physics
Title of Dissertation:	Study of nuclear effects in hadron-nucleus interactions and in heavy-ion collisions
Degree Programme:	Application of natural sciences
Field of Study:	Nuclear engineering
Supervisor:	RNDr. Jan Nemchik, CSc. Czech Technical University in Prague, Faculty of Nuclear Sciences and Physical Engineering, Department of physics & Slovak Academy of Science, Institute of Experimental Physics, Kosice
Academic Year:	2015/2016
Number of Pages:	155
Keywords:	Nuclear effects, QCD, color dipole approach, proton-nucleus and heavy-ion collisions, nuclear shadowing, Cronin effect

Prohlášení

Prohlašuji, že jsem svou dizertační práci vypracoval samostatně a použil jsem pouze podklady (literaturu, projekty, SW atd.) uvedené v přiloženém seznamu.

Nemám závažný důvod proti užití tohoto školního díla ve smyslu § 60 Zákona č.121/2000 Sb., o právu autorském, o právech souvisejících s právem autorským a o změně některých zákonů (autorský zákon).

V Praze dne _______________ ____________________

podpis

Acknowledgement

Foremost I would like to express my gratitude to my supervisor Jan Nemchik for his guidance, expertise, consultations and support throughout my research.

I am also very grateful to Jan Cepila for all the help and advices he has provided during all these years. I want to also thank to Jan Cepila and Miroslav Myska for their feedback on the manuscript.

I would like to thank to all my colleagues from the Department of Physics and study specialization Experimental Nuclear Physics at FNSPE CTU in Prague for stimulating discussions and amazing work environment. Many thanks belong also to my collaborators from Lund University.

Last but not least, I would like to thank my friends and family for their great support.

Title:

Study of nuclear effects in hadron-nucleus interactions and in heavy-ion collisions

Abstract:

We study various nuclear effects occurring in proton-nucleus interactions and heavy-ion collisions. For calculations of the nucleus-to-nucleon ratio, nuclear modification factor (R_{pA}), we employ two different models in order to test theoretical uncertainties. Several different phenomena mainly contribute to a modification of R_{pA} and should be taken into account; the Cronin effect, the effects of quantum coherence (gluon shadowing - GS), and effects based on multiple parton rescatterings during propagation through nuclear medium before a hard collision (initial state interaction - ISI effects). The model based on k_T-factorization was devoted mainly for investigation of modification of R_{pA} in production of hadrons and direct photons. Besides, the color dipole approach was used for study of nuclear effects in production of Drell-Yan (DY) pairs and direct photons since allows to include naturally GS and the Cronin effect. It was found that the Cronin effect leads to a nuclear enhancement at medium values of transverse momenta p_T in the energy range from the FNAL fix-target up to collider LHC experiments. Its magnitude decreases with energy in accordance with data due to a rise of gluon contribution to production cross-section with larger mean transverse momenta. At small Björken x in the target the gluon shadowing leads to a strong nuclear suppression especially in the LHC kinematic region and at forward rapidities. Whereas in the model based on the k_T-factorization the magnitude of GS depends on parameterizations of nuclear parton distribution functions (nuclear PDFs), the color dipole approach allows to independent calculation of this effect. This leads to rather large uncertainties in predictions of nuclear shadowing not only within models under consideration, but also within the same model based on the k_T-factorization using different parameterizations of PDFs. It was investigated that ISI effects lead to a strong suppression at large p_T and forward rapidities. The QCD factorization is broken due to the correlation between projectile and the target. The ISI effects are universal for all known reactions at different energies and, consequently, can be mixed with coherence effects. In order to eliminate the mixing between coherence and ISI effects one should go to small energies corresponding to fix-target experiments, to large p_T-values at RHIC and/or to large invariant masses of DY pairs. For investigation of nuclear effects in dilepton production we used for the first time the Green function formalism, which naturally includes effects of quantum coherence and formation of colorless system in a nuclear

medium. The corresponding predictions for R_{pA} as function of p_T and Björken x can be tested in the future by experiments at RHIC, LHC and planned electron-ion collider or AFTER@LHC.

Název práce:

Studium jaderných efektů v hadron-jaderných interakcích a srážkách těžkých iontů

Abstrakt:

Předmětem této disertační práce je studium jaderných efektů v proton-jaderných a jádro-jaderných srážkách, v níž jsme se zaměřili hlavně na efekty kvantové koherence (jaderné stínění), Croninův efekt a efekt založený na vícenásobných rozptylech partonu při průchodu jaderným médiem před samotnou tvrdou srážkou, tzv. ISI efekt. Tyto efekty jsou studované pomocí jaderného modifikačního faktoru (R_{pA}), který počítáme ve dvou různých modelech. Model založený na QCD k_T-faktorizaci je používán hlavně pro studium produkce hadronů a přímých fotonů. Na druhou stranu, model přiblížení barevného dipólu byl použit pro výpočet Drell-Yanova (DY) procesu a produkci přímých fotonů. Výhodou tohoto modelu je, že efekty jako je Croninův efekt nebo efekty kvantové koherence jsou přirozenou součástí tohoto formalismu. Croninův efekt vede k nadměrné produkci částic v oblasti středních příčných hybností (p_T) pro energie sahající od experimentů ve FNAL po experimenty na urychlovači LHC. Bylo ukázáno, že velikost Croninova efektu klesá s rostoucí energií v souhlasu s experimentálními daty díky rostoucímu příspěvku gluonů ke střední příčné hybnosti partonu. V oblasti malých Björkenovských x dominují efekty kvantové koherence, které vedou k potlačení jaderného modifikačního faktoru zvláště při energiích dosahovaných na LHC nebo při dopředných rapiditách. Velikost jaderného stínění v k_T-faktorizačním modelu závisí na parametrizaci jaderných partonových distribučních funkcí (jaderných PDF), zatímco model přiblížení barevného dipólu umožňuje spočítat efekty stínění nezávisle. To vede k velkým neurčitostem v předpovědích jaderného stínění nejenom mezi oběma modely, ale i v rámci k_T-faktorizačního modelu při použití různých jaderných PDF. Již dříve bylo ukázáno, že ISI efekt vede k silnému potlačení při vysokých p_T a dopředných rapiditách. Tento efekt vede i k narušení QCD faktorizace kvůli korelaci mezi nalétavající a terčovou částicí. Tento efekt je univerzální pro všechny známé reakce při různých energiích a proto může být zaměněn s efekty kvantové koherence. Aby se této záměně předešlo, je potřeba studovat tento efekt při nízkých energiích odpovídajících experimentům s pevným terčíkem, velkých hodnotách p_T nebo velkých invariantních hmotách DY páru. Při studiu jaderných efektů pro Drell-Yanův process byl také po prvé použit formalismus Greenových funkcí, které přirozeně obsahují efekty kvantové koherence a efekty absorpce v jaderném médiu. Publikované předpovědi pro R_{pA} jako funkce p_T nebo Björkenovského x mohou být ověřeny

pomocí experimentů na urychlovačích RHIC a LHC nebo na plánovaném experimentu AFTER@LHC nebo urychlovači EIC.

Contents

List of Figures

Chapter 1

Introduction

During the last 40 years, the various aspects of the strong interaction occurring in processes on nuclear target were studied by physicists. This allowed to obtain supplementary information about nuclear effects which were not observed in hadronic collisions or deep inelastic scattering (DIS). Interactions on nuclear targets at higher energies allow to study gluons that are generally less understood. Especially in small-x region, the non-linear dynamics and saturation phenomena of gluons can be investigated. This can lead to a deeper understanding of strong interactions and its manifestations from the point of view of confinement or hadron masses that are much larger than a sum of their valence quarks. In the case of heavy-ion collisions (HICs), the main attention is dedicated to the discovery and study of phenomena connected with the creation and subsequent evolution of the quark-gluon plasma (QGP) state. The QGP represents a state of matter where it is believed that quarks and gluons exist asymptotically free in the medium.

In order to specify the magnitude of nuclear effects one should provide measurements of nucleus-to-nucleon ratio of production cross-sections, the so-called nuclear modification factor, R_{pA}. The nuclear effects can lead either to a nuclear suppression, $R_{pA} < 1$, or to an enhancement, $R_{pA} > 1$.

Basically, nuclear effects can be divided into initial and final state effects depending on whether they occur before or after the hard scattering. Multiple interactions of projectile partons in a medium can lead to effects of quantum coherence which are controlled by the time scale, called the coherence time (length, l_c). In the case of the Drell-Yan process the coherence length can be approximately expressed as follows,

$$l_c \approx \frac{1}{2m_N x_2}\,, \tag{1.1}$$

where m_N is the nucleon mass and x_2 is the Björken x of the target. The coherence length follows from the quantum mechanical relation of uncertainty and can be interpreted as the lifetime of the coherent state. The effects of quantum coherence are usually related to initial state effects. After the hard scattering as a result of the hadronization process a colorless state is created and propagates then through the medium up to formation of the final hadron. This happens during the time scale, which is called the formation time or length. Interactions of the colorless system during this stage lead to the nuclear absorption, which is treated as the final state effect.

We will analyze the initial state effects in proton-nucleus and nucleus-nucleus collisions taking into account processes where the final state effects are not expected. We will concentrate mainly on theoretical description of such effects as is nuclear shadowing, the Cronin effect and initial state interaction (ISI) effects, since we expect that they give the main contribution to observed nuclear suppression and/or enhancement. The physical interpretation of each effect under consideration is provided within two different models, which are related to different reference frames, infinite momentum frame and target rest frame.

One of the most interesting effect, but suffers from high uncertainties, is the nuclear shadowing. The onset of nuclear shadowing is controlled by the coherence length, and the maximal suppression occurs when $l_c \gg R_A$, where R_A is the nuclear radius. This condition corresponds to rather small Björken $x_2 < 0.01$. Treating the infinite momentum frame, this effect can be seen as a modification of parton distribution functions (nuclear PDFs). Alternatively, the shadowing can be also explained in terms of the color glass condensate (CGC) [1] that is based on the idea of gluon fusion in the Lorentz contracted nucleus. The interpretation of the same phenomenon in the target rest frame corresponds to the shadowing by surface nucleons of the nucleus similar to the Landau-Pomeranchuk-Migdal (LPM) effect [2, 3] in quantum electrodynamics (QED).

The Cronin effect manifests itself at medium large p_T and leads to an enhancement, $R_{pA} > 1$, which is observed in nuclear collisions at various energies form the fix-target FNAL to collider RHIC and LHC experiments. Generally, this effect can be understood as a broadening of the parton mean transverse momentum during its propagation through the medium treating different mechanisms depending on the reference frame.

The next phenomenon studied in this work is connected with the initial state interaction (ISI) effects [4] and can be interpretted as an effective energy loss due to multiple rescatterings of initial-state projectile partons in the medium before a hard collision. This effect aspirates to explain the observed suppressions at high transverse momenta and/or at forward rapidities also in the kinematic regions where another source of suppression -

the coherence effects (shadowing or CGC) are not effective. ISI effects are universal for all known reactions at different energies leading to the breakdown of the QCD factorization [4].

In this work we investigated first all the nuclear effects mentioned above in production of hadrons and direct photons using the model based on the k_T-factorization. Model predictions can be thus compared with experimental data available for a wide range of energies. We found a good agreement with data and analyzed the onset of each effect in different kinematic regions. As the next step we studied for the first time manifestations of the Cronin effect, effects of quantum coherence and ISI effects considering the Drell-Yan process. Although the DY reaction has been already studied in [5,6] including the Cronin effect and shadowing, we present here for the first the comprehensive study including also in addition ISI effects and treating the onset of coherence effects sophistically using the rigorous Green function formalism.

A key feature of the Drell-Yan process is the absence of final state interactions and a corresponding fragmentation, which is associated with an energy loss or absorption phenomena. For this reason the DY process can be considered as a very effective tool for the study of ISI effects [7].

The investigation of ISI effects, especially at LHC, can be very difficult and complicated. For example, the onset of these effects in hadron production at midrapidity requires the measurements of very large transverse momenta of the order of several hundreds of GeV or to go to forward rapidities. However, in this case the ISI effects will be mixed with effects of quantum coherence. For this reason, we present for the first time predictions for nuclear modification factor in the DY process where the contribution of Z^0 boson to the production cross section allows to achieve large invariant mass of dileptons. In comparison with other processes, this is the main advantage of the DY reaction leading to an elimination of coherence effects going to large invariant dilepton masses. In this case one does not need to treat extremely large p_T-values what allows to keep a reasonable high experimental statistics.

At the LHC energies, the long coherence length (LCL) limit, $l_c \gg R_A$, can be safely used. However, at lower energies corresponds to RHIC one should be careful and check the applicability of the LCL limit. Therefore, in this work we treat the rigorous Green function formalism that includes coherence effects naturally. Predictions for nuclear modification factor in the DY process incorporate all effects mentioned above. Moreover, the mastering of the Green function framework also allows to independent and more accurate calculation of not only the gluon shadowing but also final state absorption which is important in other processes during formation of colorless system in a medium created after heavy-ion collisions.

This work is organized as follows. In Chapter 2, the overview of nuclear effects observed in experiments is presented. Moreover, the significance for different final states such as Drell-Yan process, production of direct photons and hadrons is commented and the physical origins of each effect are outlined. Chapter 3 is devoted to the basics of the QCD based k_T-factorization model and to its transition to the nuclear target. Chapter 4 deals with the description of the color dipole framework, especially for proton-nucleus collisions using the Green function technique and its limits. Chapter 5 highlights all individual results in all publications which are part of this work in the Appendix C and summarizes the comparison of both models. Finally, Chapter 6 contains conclusions of this work.

Chapter 2

Nuclear effects

High energy hadronic collisions or deep inelastic scattering are very well understood experimentally as well as theoretically through the quantum chromodynamics (QCD). At the end of seventies, experimental physicists focused on proton-nucleus collisions and later on electron-nucleus (nuclear DIS) interactions. In interactions with so complex and so sophisticated object as is a nucleus, we can expect and study new effects that appear from the number of bounded nucleons that interact strongly with each other. All these effects that arise in proton-nucleus interaction compared to A-times proton-proton collision (corresponding to a nucleus with A non-interacting nucleons) may be called nuclear effects. Note that the term nuclear effects generally represents all effects on nuclear target including effects of hot and dense medium. Nevertheless, within this work under the term nuclear effects only the initial state effects are considered.

Next, nuclear effects can be divided according to their coherent or non-coherent origin. The dynamics of coherence effects is controlled by the coherence length l_c that represents the lifetime of coherence state. The coherence length can be expresses from the quantum mechanical principle of uncertainty approximately as (1.1). The longer the coherence length is the stronger coherence effects are. Coherence effects are strongest for $l_c \gg R_A$, where R_A is the nuclear radius. For more details see Chapter 4.3.1.1. Typical coherence effects are nuclear shadowing or saturation and non-coherent effects are Fermi motion or ISI effects.

One of the most straightforward way how to quantize these effects is the so-called nuclear modification factor defined as nucleus-to-nucleon ratio

$$R_{pA} = \frac{d\sigma^{pA}}{A \cdot d\sigma^{pp}}\,, \tag{2.1}$$

where A is the number of nucleons in nucleus, and σ^{pA} and σ^{pp} are cross-sections on nuclear and proton target. In the case, when measurements on proton target are not available, nuclear effects can be measured e.g. through the forward-backward ratio (ratio of σ^{pA} at forward and backward rapidities)

$$R_{FB} = \frac{d\sigma^{pA}(+|y|)}{d\sigma^{pA}(-|y|)}\,. \tag{2.2}$$

or central-to-peripheral ratio (ratio of σ^{pA} in central collisions and peripheral collisions)

$$R_{CP} = \frac{d\sigma^{pA}|_{central}}{d\sigma^{pA}|_{peripheral}} \tag{2.3}$$

or another variables specific for jets, photons, etc. R_{FB} and R_{CP} measure just relative size of nuclear effects in contrast to nuclear modification factor where the absolute magnitude of nuclear effects is measured.

Based on experimental results, especially on nuclear DIS, there is a general agreement on the main division of nuclear effects as a function of Björken variable, a parton momentum fraction of the nucleus, $x_2(x_{Bj})$. In accordance with [8–12] and references therein four distinct regions can be recognized:

- Suppression from shadowing, saturation and ISI effects, $x_2 < 0.01 \sim 0.1$: a region of possibly strong suppression. It can be understood through the multiple scattering in the nuclear rest frame, or parton fusion in the infinite momentum frame.
- Enhancement, $0.1 < x_2 < 0.3$: a region of the enhancement, sometimes called as Cronin peak or Cronin effect.
- EMC effect, $0.3 < x_2 < 0.8$: a region of the suppression, named after the experiment (European Muon Collaboration) where this suppression was measured for the first time [13]. There is no agreement on the source of this effect. Usually, this suppressions is explained by the nuclear binding effects, pion exchange, etc.
- Fermi motion effect, $x_2 > 0.8$: a region of possible large enhancement. The idea is that for the parton with most of the momentum the quasi-free Fermi motion of the nucleon inside the nucleus becomes important.

All four regions are demonstrated in Fig. 2.1 from [12]. In this work, the EMC effect and Fermi motion are not taken in consideration.

Experiments measuring the deep inelastic scattering on nuclei are the primary source of data for nuclear effects, especially for nuclear PDFs where the kinematics in comparison with proton-nucleus interactions is much more clear. The main variable that is measured is a nuclear ratio of nuclear and proton structure functions F_2 defined as

$$R^{F_2}_{eA}(x_{Bj}, Q^2) = \frac{F_2^A(x_Bj, Q^2)}{AF_2^N(x_Bj, Q^2)}\,, \tag{2.4}$$

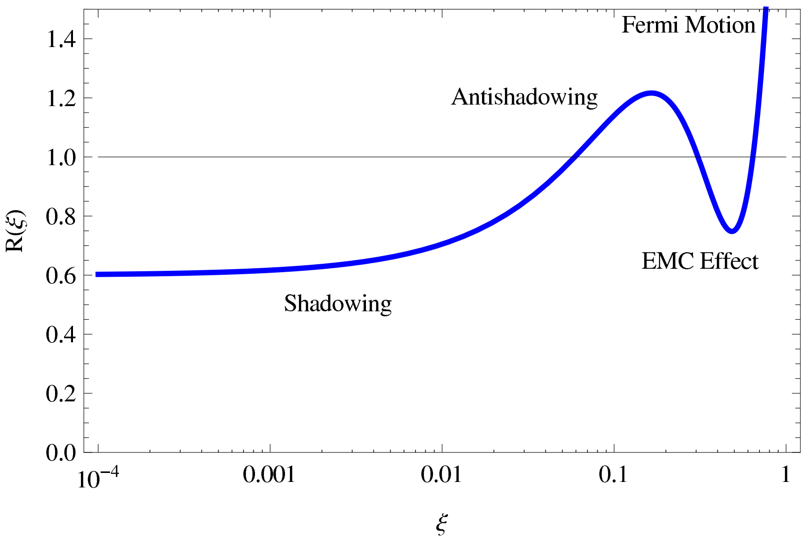

Figure 2.1: An illustration of the expected behavior of the nuclear modification factor where $\xi = x_2$. The figure is taken from [12].

where x_{Bj} and Q^2 are standard variables in DIS. If one considers a DIS process, as is in Fig. 2.2,

$$l(k) + p(P) \to l(k') + X(P'),$$

where k, k', P, P' are four-momentum then

$$q = k - k', \qquad x_{Bj} = \frac{Q^2}{2P \cdot q}, \qquad Q^2 = -q^2 > 0. \tag{2.5}$$

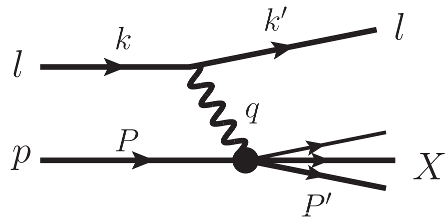

Figure 2.2: An illustration of the deep inelastic scattering.

The main contributions on nuclear DIS are from BCDMS collaboration (experiment NA-4) [14, 15], EMC (experiment NA-28) [13, 16–18] NMC (experiment NA-37) [19–25] or experiment E665 [26, 27]. It does not include potential effects caused by interaction strongly interacting projectile such as initial state interaction effects that will be discussed in more details later. Although, the projects on future nuclear DIS are on the rise especially the electron-ion collider (EIC) [28] that will be located in Thomas Jefferson National Accelerator Facility (JLab) or Brookheaven National Laboratory (BNL), both in the USA. This collider will focus primary on the spin and three-dimensional structure of the nucleon and the physics of high gluon densities (sometimes referred to as small-x physics).

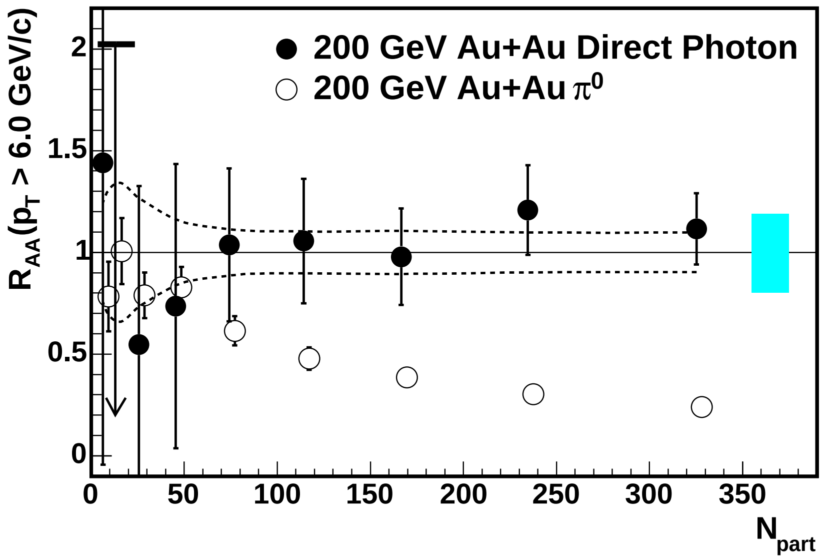

Figure 2.3: Nuclear modification factor at $\sqrt{s}$ = 200 GeV for $Au + Au$ collisions for direct photons and π^0 as function of the number of participants [29].

Next to the nuclear DIS, nuclear effects can be studied through various final states in proton-nucleus and nucleus-nucleus collisions. In this work, we focused on hadrons (charged hadrons, pions, kaons, protons - no vector mesons or heavy baryons), direct photons, Drell-Yan processes and some comments will be related to jets. Hadrons serve as main probes for nuclear effects in $p+A$ and $A+A$ interactions and probes for nuclear effects and hot and dense nuclear matter effects together in heavy-ion collisions. On the other hand, direct photons and Drell-Yan process represent electromagnetic probes for nuclear effects where no fragmentation, no absorption, no energy loss in nucleus-nucleus collisions is expected. Theoretically, both can be an ideal tool to study nuclear effects even in heavy-ion collisions. For example, in the region of medium $p_T \geq 6$ GeV/c where nuclear effects are not expected, all suppression/enhancements are effects of hot and dense nuclear matter as is demonstrated in Fig. 2.3 as a function of centrality in comparison with suppressed neutral pions [29]. Similar situation is presented also in Fig. 2.4 [30] where all mesons are suppressed in $Au + Au$ collisions due to strong interaction in the medium in contrast to electromagnetically interacting direct photons which do not interact with hot and dense nuclear matter. Moreover, the variability of measured mass of DY pair allows to reach various kinematical regions where effects of quantum coherence or ISI effects are dominant only even at small p_T.

Most of effects discussed in this chapter occur in heavy-ion collisions as well as in proton-nucleus interactions or nuclear DIS. However, mainly experimental results and theoretical works for proton-nucleus case are discussed. Moreover, EMC and Fermi motion effects will be omitted due to difficulty to reach kinematical regions at LHC and RHIC where these effects dominate.

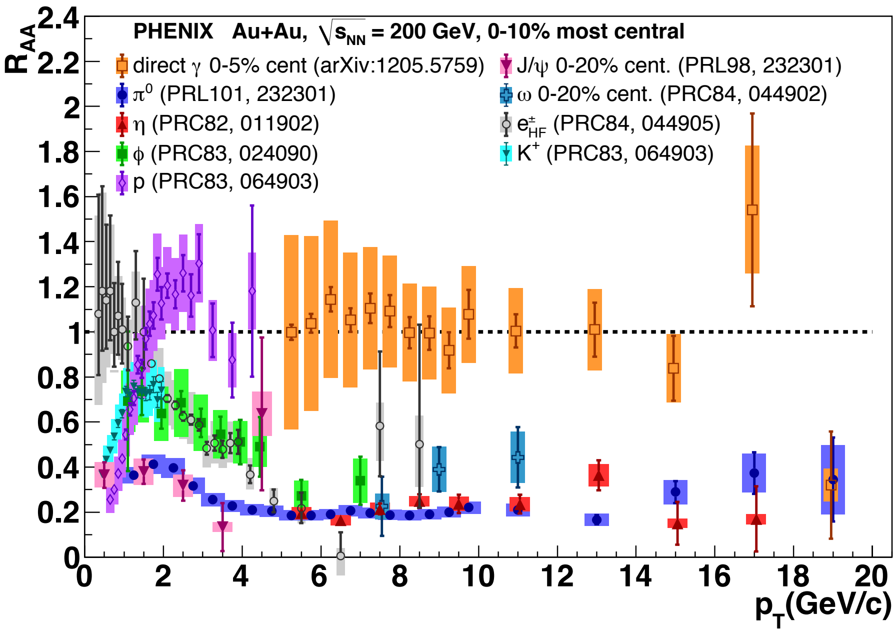

Figure 2.4: Nuclear modification factor at $\sqrt{s} = 200$ GeV for $Au+Au$ collisions as function of p_T for direct photons and various hadrons for central data 0-10% [30].

For more detail on nuclear effects see reviews [10, 11] and references therein.

2.1 Cronin effect

Antishadowing or Cronin effect is one of the first discovered nuclear effects in experimental data in 1974 [31]. Cronin *at al.* in FNAL proton area measured production of hadrons $(\pi^{\pm}, K^{\pm}, p, \bar{p}, d, \bar{d})$ in proton-nucleus (Beryllium, Platinum and Tungsten targets) collisions at incident proton energies of 200, 300, and 400 GeV. It was found that the cross-sections for hadron production scaled with a power of the atomic number A,

$E\frac{d^3\sigma(p_T,A)}{d^3p} = E\frac{d\sigma(p_T,1)}{d^3p}A^{\alpha(p_T)}$, as function of transverse momentum and is larger than one for medium $p_T = 2 \div 6$ GeV/c. This effect is more clear if the nuclear modification factor is introduced, $R_{W/Be}(p_T)$, as in [32]. Then, one can see the absolute magnitude of the Cronin peak that decreases with CMS energy.

Generally, this effect is understood in the framework of higher twist effects or, intuitively, it comes from multiple rescatterings - gluon exchanges of parton before the hard scattering that leads to the nuclear broadening of the p_T-spectra [11]. Namely within the infinite momentum frame based models, the Cronin effects can be interpreted as the modification of parton distribution function in the nucleus, see Chapter 3.4.3, and as soft hadronic rescatterings where each rescattering contribute to the intrinsic momentum broadening [33], see Chapter 3.4.2.

Within the target rest frame, the mechanism leading to the Cronin effect depends on the coherence length. In the region of short coherence length that corresponds to the idea that the fluctuation is created deep inside the nucleus, the incoming projectile parton participates in multiple soft interactions that do not lead to the production of particles, but modify the mean transverse momentum [34]. On the other side, in the regime of long coherence length the fluctuation is created long before the nucleus and interacts with the nucleus coherently and, therefore, cannot interact with each nucleons individually. Nevertheless, the interaction of projectile fluctuation with the nucleus also depends on the size of the fluctuation or intrinsic transverse momentum of the fluctuation, respectively. The harder the fluctuation (the larger the relative intrinsic transverse momentum) between the quark and dilepton is, the stronger is the kick from the target required for the loss of coherence. Large fluctuations have high probability to lose the coherence on the surface of the nucleus which leads to the shadowing at small p_T described below. Small fluctuations, corresponding to high intrinsic transverse momentum, are subject to multiple interactions leading to the larger transverse momentum of the nucleus than a nucleon target, and, hence, is able to disrupt the coherence of the fluctuation. This leads to the enhancement in the cross-section for medium p_T. For high p_T just single high-p_T interaction dominates and eliminates the enhancement by multiple scattering. This phenomena is called the color filtering [5, 35].

Besides FNAL fix-target experiments, the Cronin effect was measured also at high energies at RHIC and LHC colliders. For example, in Fig. 2.5, there is the nuclear modification factor R_{dAu} as function of p_T for different centralities from PHENIX experiment [36]. For pions and kaons one can see the Cronin enhancement with approximate magnitude of 1.2, but for protons an excessive enhancement is observed. This excessive enhancement is referred to as baryon anomaly [37] first observed in $Au + Au$ collisions in PHENIX experiment at RHIC [38, 39].

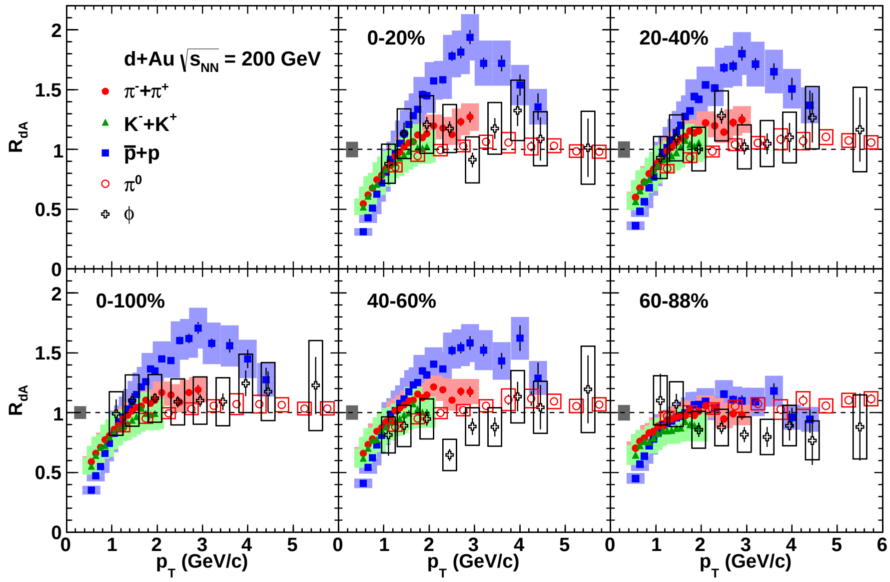

Figure 2.5: Nuclear modification factor R_{dAu} as function of p_T for different centralities from PHENIX experiment [36].

Baryon anomaly poses a challenge for theoretical physicists because nuclear effects (in the sense of initial state effects) are generally considered as final-state-independent effects. Although, there are some papers that try to explain this anomaly as quark recombination [40, 41] or within the hydrodynamics with CGC and jet quenching [42]. All these works explain this anomaly just in heavy-ion context, not for proton-nucleus interactions where the baryon anomaly was also measured later.

At LHC, e.g. in Fig. 2.6 [43], one can see that Cronin peak at LHC can be seen in nuclear modification factor for protons within the baryon anomaly. For light mesons and charged hadrons within the statistic and systematic errors one cannot make conclusion about Cronin peak which can be very small.

Moreover, at LHC kinematics nuclear effects do not apply x_2 distribution as is mentioned above where enhancement is expected for $0.1 < x_2 < 0.3$. For example, at CMS energy $\sqrt{s} = 5020$ GeV the value $x_2 = 0.2$ corresponds to $p_T \sim 500$ GeV/c. If the Cronin effect from different CMS energies is compared, one can conclude that the Cronin peak is still placed between 1 and 6 GeV/c of transverse momentum.

Experimentally, it is very difficult to measure direct photons at low transverse momentum p_T because of many thermal a fragmentation photons which are complicated to

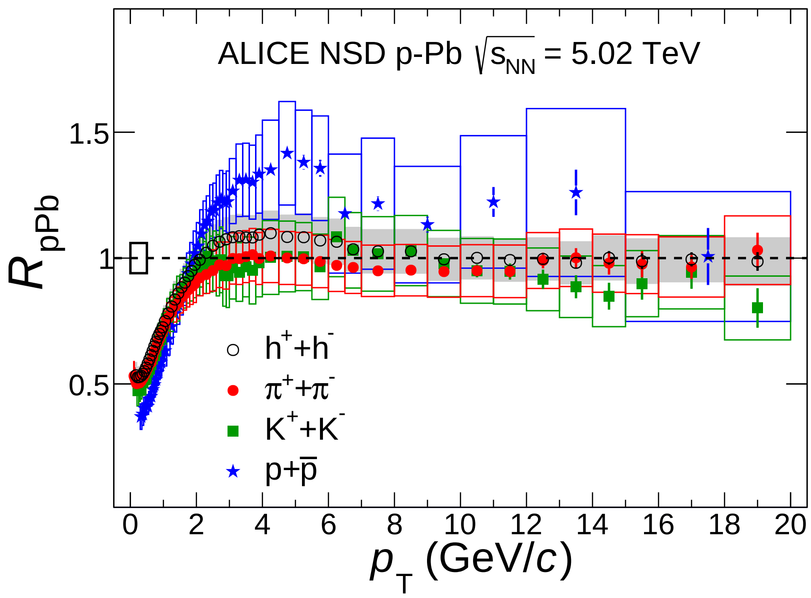

Figure 2.6: Nuclear modification factor R_{pPb} as function of p_T from ALICE experiment [43].

recognize. Therefore, no data exists on nuclear shadowing and Cronin peak for RHIC energies and higher. Typically at RHIC, experimental physicists take direct photons with cut $p_T \geq 6$ GeV/c, shortly behind the expected Cronin peak.

For the Drell-Yan process data exist just for FNAL fix-target experiments on $p + A$ interactions, e.g. [27, 44]. At RHIC the Drell-Yan process is not yet measured. At LHC the measurement of the Drell-Yan process is in progress.

2.2 Nuclear shadowing

Nuclear shadowing represents a suppression emerging in region $x_2 \lesssim 0.1$ where sea quarks and gluons dominate in parton distributions. One can make some conclusions from experimental data for nuclear DIS (experiments NA4, NA28, NA37 and E665 mentioned above):

1. shadowing increases with decreasing x_2 [26],
2. shadowing decreases with increasing Q^2 [24],
3. shadowing increases with the mass number of the nucleus A [23].

Moreover, experimental data from RHIC [36,45–47] and LHC [48] indicate an increase of the shadowing towards most central collisions.

In the infinite momentum frame, nuclear shadowing is interpreted [49] in terms of gluon fusion. Considering moving to very small x_2 and Lorentz contraction in the longitudinal direction in high energy collisions, gluon clouds of surrounding nucleons start to overlap in the transverse plane and the gluon density increases. At certain energy, called saturation scale, the probability of gluon fusion ($qg \to q, gg \to g$) is more probable than the radiation of other gluons and, effectively, the number of gluons decreases and thus the cross-section is suppressed. This principle is described e.g. in the model of the color glass condensate (CGC) [1]. The suppression from the gluon fusion is not taken into the calculation in this work. Nuclear shadowing will be implemented in form of nuclear PDFs, Chapter 3.4.3.

Nuclear shadowing from the perspective of the target rest frame has more intuitive interpretation. In the regime, where the coherence length is greater than nuclear radius, the fluctuation is created long before the nucleus, and the hard interaction with surface nucleons occurs. Then the fluctuation is disrupted and the color field has to be recreated. During the color field recreation, which finishes behind the nucleus, the fluctuation cannot interact with the inner nucleons - inner nucleons are shadowed by the surface nucleons. This phenomenon is the analogy of the Landau-Pomeranchuk-Migdal effect [2, 3] known from the quantum electrodynamics (QED). More details can be found in Chapter 4.3.1.1.

In the case of proton-nucleus collisions, nuclear shadowing is dominantly studied through hadrons. It was measured at RHIC, Fig. 2.5, as well as at LHC, Fig. 2.6. In Fig. 2.5 one can see that the suppression at small p_T increases with centrality.

The same lack of data as for the Cronin effect applies to the direct photons and the Drell-Yan process in the region of nuclear shadowing.

2.3 Suppressions at high p_T and forward rapidities.

One can find signals of other source of suppressions that are observed in experimental data at high p_T and/or at forward rapidities. In the case of the suppression at high p_T observed mainly at RHIC, coherence effects (CGC, nuclear shadowing) are not possible, and therefore another non-coherent source of suppression has to exist. Moreover, similar suppression of non-coherent origin is also observed at forward rapidities in fix-target experiments such as E772 or NA49 where the collision energy is too small for any meaningful coherence effects.

Within this work, an interpretation based on the initial state effects was adopted, for more details see Chapter 3.4.5.

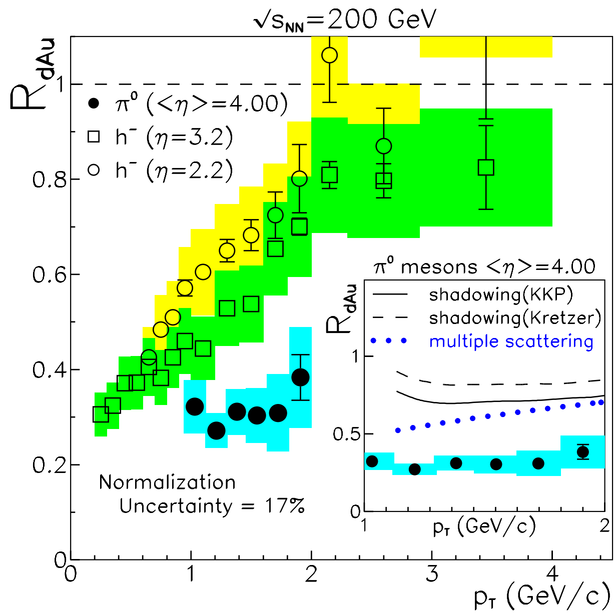

Figure 2.7: Nuclear modification factor R_{dAu} as function of p_T for hadrons at different rapidities [50].

These suppressions can be found at RHIC experiments in π^0 production in $d + Au$ collisions at PHENIX [45] for central collisions. This can imply that this effect can be a function of centrality (impact parameter). Furthermore, there is considerable suppression of π^0 production in forward $d+Au$ collisions [50], see Fig. 2.7. Coherent effects are possible for such forward rapidities at RHIC, but they are not able to reach so high suppression with such great magnitude.

At forward rapidities or, equivalently, at large Feynman x_F, signals can be found in fix-target experiments, e.g. NA49 in hadron production [51], see Fig. 2.8. Coherent effects are not possible in this region due to low collision energy, 158 GeV per nucleon.

Similar suppression as for hadrons at RHIC can be seen also for direct photons for high p_T in central $Au + Au$ collisions [52, 53], see Fig. 2.9. For the Drell-Yan process similar suppression at forward rapidities can be observed at experiment E772 [44].

Moreover, besides suppression of high p_T in hadrons, direct photons and the Drell-Yan process, there is an indication of suppression also for jets at PHENIX [54] and ATLAS [55].

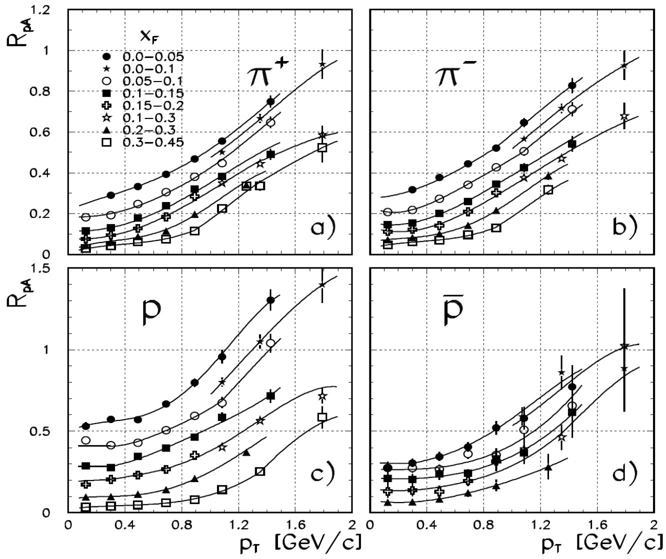

Figure 2.8: Nuclear modification factor R_{pA} as function of p_T for hadrons at different x_F [51].

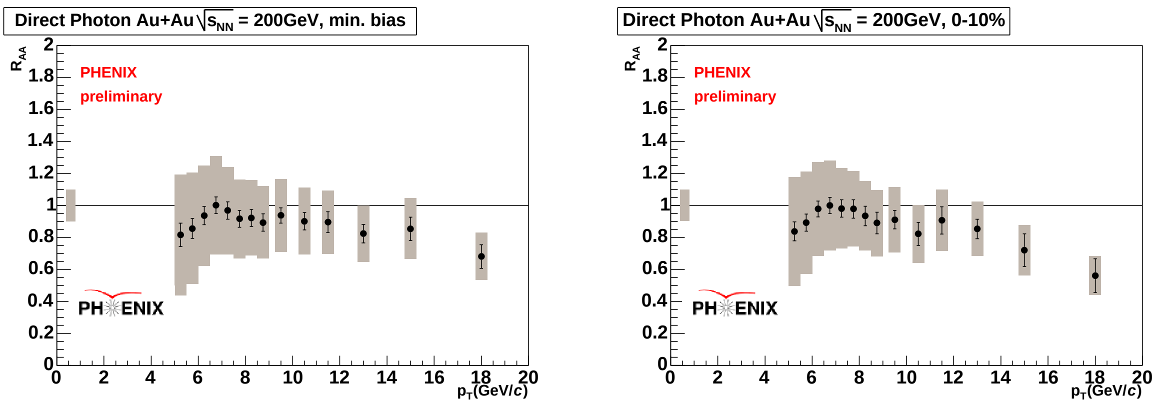

Figure 2.9: Indication of suppression for high-p_T of direct photons in $Au+Au$ collisions at $\sqrt{s} = 200$ GeV for minimum-bias and central collisions [52].

Chapter 3

QCD based k_T-factorization model

3.1 Introduction

During the first part of seventies of the last century, the quantum chromodynamics (QCD) was accepted as the theory of strong interaction [56]. In this theory, the interaction of hadrons is described as an interaction of its constituents - partons - quarks and gluons. The key feature of the QCD is the property of asymptotic freedom [57, 58]. This term describes the weakening of the coupling of partons at short distances or, equivalently, large momentum transfer. Asymptotic freedom allows to use of the well-known perturbative techniques to solve the QCD Lagrangian for the processes where short-distance interactions dominate. This is the reason why the large-momentum-transfer processes play a key role in particle physics.

The size of asymptotic freedom necessary for the perturbative techniques can be expressed by the QCD scale Λ_{QCD} for momentum-transfer dependence of strong running coupling constant α_s. Because this scale is of the order of several hundred MeV, there are kinematical regions, where the α_S is sufficiently small, and the perturbative theory can be used.

Then, the whole picture of hadron hard scattering processes within the QCD based factorization, sometimes called QCD improved parton model, can be seen as follows, see Fig. 3.1. The large-momentum-transfer process can be factorized into two parts by utilizing the impulse representation. The probability of finding parton a in a hadron A with a momentum fraction x_a is denoted by the parton distribution function $f_{a/A}(x_a)$. The probability of obtaining a hadron C with a momentum fraction z_c from a parton c is denoted by the fragmentation function $D_{C/c}(z_c)$. These functions represent a non-perturbative part of QCD and have to be determined experimentally. The interaction between partons can be calculated by the perturbative QCD. The hadronic cross-section for the process is then summed over all possible constituent scatterings, each of which is weighted by the appropriate parton distribution and fragmentation functions. For some

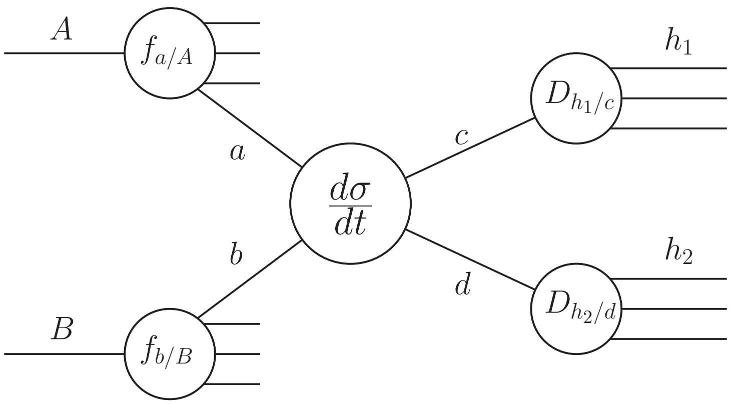

Figure 3.1: Schematic view of the hard scattering process factorized into parton distribution functions (f), parton fragmentation function (D), and the partonic cross-section $d\sigma/d\hat{t}$.

general overview the following references [59–61] can be studied.

The QCD based factorization model as well as the naive parton model [62, 63] are formulated in the infinite momentum frame where it is assumed that transverse momentum of parton inside hadron is small and therefore negligible. This assumption allowed the formulation of parton distribution functions, integrated over the transverse distribution. However these models work well for a lot of processes, as will be described in Chapter 3.3.3, they fail for some processes such as Drell-Yan dilepton production or correlation of heavy quarks.

The idea of the QCD based k_T-factorization model coming from the second half of the seventies of the last century, see [61, 64] or for review [32, 65]. In this approach, next to the PDFs that describe longitudinal momentum distribution the intrinsic transverse momentum is taken into account. This extension is called transverse momentum dependent (TMD) parton distribution functions and corresponds to the unintegrated quarks and gluon distribution functions where, in this work, a naive model based on the Gaussian distribution of the transverse momentum was adopted.

3.2 Kinematics and notation

Note, that for binary processes $A + B \to C + X$, A and B denote incoming or initial-state hadrons and C denotes outgoing or observed final-state hadron. Upper-case letters $(A, B, C, ...)$ describe initial-state and final state hadrons. Their four-momenta p are labeled with corresponding upper-case subscript $(p_A, p_B, p_C, ...)$. Lower-case letters $(a, b, c, ...)$ denote partons and their four-momenta are labeled accordingly $(p_a, p_b, p_c, ...)$.

The invariant inclusive cross-section for the reaction $A+B \to h+X$ for producing a hadron h at high p_T in the CMS of A and B is given by

$$\begin{aligned} E\frac{d^3\sigma^{(AB\to h\,X)}}{d^3p} &= K\sum_{abcd}\int dx_a\,dx_b\,dz_c\,f_{a/A}(x_a,Q^2)\,f_{b/B}(x_b,Q^2)\,D_{h/c}(z_c,\mu_F^2) \\ &\quad\times\frac{\hat{s}}{\pi z_c^2}\,\frac{d\sigma^{(ab\to cd)}}{d\hat{t}}\,\delta(\hat{s}+\hat{t}+\hat{u}), \end{aligned} \tag{3.1}$$

where the sum is over all possible hard subprocesses, K is the normalization factor, Q^2 is a square of momentum transfer, μ_F is a fragmentation scale, $d\sigma/d\hat{t}$ is a partonic cross-section, and the δ function is necessary for the momentum conservation. E, resp. p is energy, resp. momentum of a parton c, $\hat{s}, \hat{t}, \hat{u}$ are parton Mandelstam variables and x_a, x_b, z_c are fractions of momentum of parton inside the hadron.

Longitudinal fractions of hadron momenta carried by parton are defined as

$$x_a = \frac{p_a}{p_A}, \quad x_b = \frac{p_b}{p_B}, \quad z_c = \frac{p_C}{p_c}. \tag{3.2}$$

For large transverse momentum processes it is useful to define x-variables

$$x_T = \frac{2p_T}{\sqrt{s}} \quad \text{and} \quad x_F = \frac{2p_l}{\sqrt{s}}, \tag{3.3}$$

where p_T is the transverse and p_l is the longitudinal component of momentum with respect to the beam direction. Neglecting the mass of hadrons implies the allowed ranges of x_T and x_F to be $(0, 1)$ and $(-1, 1)$ respectively. Next useful variable is the rapidity y which is defined as

$$y = \frac{1}{2}\ln\frac{E+p_l}{E-p_l}. \tag{3.4}$$

For massless particles (mass is negligible for high energy processes), pseudorapidity η is equivalent to the rapidity. Pseudorapidity is defined as $\eta = \ln\cot\theta/2$, where θ is the laboratory system scattering angle.

It is beneficial to use the Mandelstam variables for hadrons

$$s = (p_A + p_B)^2, \quad t = (p_A - p_C)^2 \quad \text{and} \quad u = (p_B - p_C)^2$$

and for partons

$$\hat{s} = (p_a + p_b)^2, \quad \hat{t} = (p_a - p_c)^2 \quad \text{and} \quad \hat{u} = (p_b - p_c)^2. \tag{3.5}$$

Mandelstam variables satisfy $\hat{s} + \hat{t} + \hat{u} = 0$ for massless partons.

The momentum four-vector of initial-state hadrons is chosen in the simplest form

$$p = (E, \vec{p}) = (E, 0, 0, p_l),$$

where E is the energy of a hadron and p_l is the magnitude of the momentum in the direction of the beam. In the CMS it holds $E_A = E_B$ and $p_{l_A} = -p_{l_B}$ for two identical colliding hadrons.

Energy of a colliding hadron can be calculated from the Mandelstam variable

$$s = (p_A + p_B)^2 = 4E^2 \quad \Rightarrow \quad E = \frac{\sqrt{s}}{2},$$

and since for massless particles $E = |\vec{p}|$ holds, so $E = p_l$ and the final form of four-momenta is

$$p_A = \frac{1}{2}\sqrt{s}\,(1, 0, 0, 1) \quad \text{and} \quad p_B = \frac{1}{2}\sqrt{s}\,(1, 0, 0, -1). \tag{3.6}$$

The momentum $\vec{p}_C$ can be separated to the longitudinal and the transverse part $\vec{p}_C = \vec{p}_T + \vec{p}_l$ and so

$$p_C = (E, p_T, 0, p_l) = p_T \left(\frac{E}{p_T}, 1, 0, \frac{p_l}{p_T} \right).$$

The four-momentum can be written as

$$p_C = p_T \left(\frac{E}{\sqrt{E^2 - p_l^2}}, 1, 0, \frac{p_l}{\sqrt{E^2 - p_l^2}} \right) = p_T(\cosh y, 1, 0, \sinh y). \tag{3.7}$$

The proof of last step:

$$\cosh y = \cosh \ln \sqrt{\frac{E + p_l}{E - p_l}} = \frac{1}{2} \left(\sqrt{\frac{E + p_l}{E - p_l}} + \sqrt{\frac{E - p_l}{E + p_l}} \right) = \frac{E}{\sqrt{E^2 - p_l^2}}$$

and

$$\sinh y = \sinh \ln \sqrt{\frac{E + p_l}{E - p_l}} = \frac{1}{2} \left(\sqrt{\frac{E + p_l}{E - p_l}} - \sqrt{\frac{E - p_l}{E + p_l}} \right) = \frac{p_l}{\sqrt{E^2 - p_l^2}}.$$

Next, the application of Eq. (3.2) to the Eq. (3.6) and (3.7) yields to

$$p_a = \frac{1}{2} x_a \sqrt{s}(1, 0, 0, 1) \quad p_b = \frac{1}{2} x_a \sqrt{s}(1, 0, 0, -1) \quad \text{and} \quad p_c = \frac{p_T}{z_c}(\cosh y, 1, 0, \sinh y). \tag{3.8}$$

Now, it is appropriate to express the parton Mandelstam variables as

$$\begin{aligned}\hat{s} &= (p_a + p_b)^2 \\ &= \left(\frac{\sqrt{s}}{2}\,(x_a + x_b, 0, 0, x_a - x_b)\right)^2 \\ &= \frac{s}{4}\,\left[(x_a + x_b)^2 - (x_a - x_b)^2\right] \\ &= x_a x_b s,\end{aligned}$$

$$\begin{aligned}\hat{t} &= (p_a - p_c)^2 \\ &= \left(\frac{x_a\sqrt{s}}{2} - \frac{p_T}{z_c}\cosh y, -\frac{p_T}{z_c}, 0, \frac{x_a\sqrt{s}}{2} - \frac{p_T}{z_c}\sinh y\right)^2 \\ &= \frac{p_T^2}{z_c^2}\,\left(\cosh^2 y - \sinh^2 y - 1\right) + \frac{x_a\sqrt{s}}{z_c}\,p_T(\sinh y - \cosh y) \\ &= -\frac{x_a}{z_c}\,\sqrt{s}p_T e^{-y}\end{aligned}$$

and evaluation of the $\hat{u}$ is very similar to the $\hat{t}$. Finally, the summary of all Mandelstam variables on the parton level is presented

$$\hat{s} = x_a x_b s, \quad \hat{t} = -\frac{x_a}{z_c}\,p_T\sqrt{s}\,e^{-y} \quad \text{and} \quad \hat{u} = -\frac{x_b}{z_c}\,p_T\sqrt{s}\,e^{y}. \tag{3.9}$$

Next, Eq. (3.9) can be used to evaluate the δ function in the Eq. (3.1)

$$\begin{aligned}\delta(\hat{s} + \hat{t} + \hat{u}) &= \delta\left(\hat{s} - \frac{x_a}{z_c}\,\sqrt{s}p_T e^{-y} - \frac{x_b}{z_c}\,\sqrt{s}p_T e^{y}\right) \\ &= \delta\left[\frac{1}{z_c}\,\left(z_c\hat{s} - x_a\sqrt{s}p_T e^{-y} - x_b\sqrt{s}p_T e^{y}\right)\right] \\ &= z_c\delta\left[\hat{s}\left(z_c - \frac{p_T}{\sqrt{s}x_b}\,e^{-y} - \frac{p_T}{\sqrt{s}x_a}\,e^{y}\right)\right] \\ &= \frac{z_c}{\hat{s}}\,\delta\left(z_c - \frac{x_T}{2x_b}\,e^{-y} - \frac{x_T}{2x_a}\,e^{y}\right)\end{aligned}$$

and to integrate Eq. (3.1) over z_c leading to

$$z_c = \frac{x_T}{2x_b}\,e^{-y} + \frac{x_T}{2x_a}\,e^{y}. \tag{3.10}$$

Then, by applying the upper boundary condition $z_c \leq 1$ to (3.10) the minimal value of x_b is obtained

$$x_{b_{min}} = \frac{x_a x_T e^{-y}}{2x_a - x_T e^{y}} \tag{3.11}$$

and similarly by applying of the upper boundary condition $x_b \leq 1$ the minimum of x_a is obtained

$$x_{a_{min}} = \frac{x_T e^y}{2 - x_T e^{-y}} \,. \tag{3.12}$$

If the last condition $x_a \leq 1$ is applied, the general kinematic restriction is obtained

$$\cosh y \leq \frac{\sqrt{s}}{2 p_T} \,. \tag{3.13}$$

Finally, by evaluating the δ function in (3.1), integrating over z_c (3.10) and by application of the minimal value of x_a (3.12) and x_b (3.11) the following final expression can be obtained

$$\begin{aligned} E\frac{d^3\sigma^{(AB\to h\;X)}}{d^3p} &= K \sum_{abcd} \int_{x_{a_{min}}}^{1} dx_a \int_{x_{b_{min}}}^{1} dx_b\, f_{a/A}(x_a, Q^2)\, f_{b/B}(x_b, Q^2) \\ &\quad \times D_{h/c}(z_c, \mu_F^2) \frac{1}{\pi z_c} \frac{d\sigma^{(ab\to cd)}}{d\hat{t}} \,, \end{aligned} \tag{3.14}$$

where

$$z_c = \frac{x_T}{2x_b}\, e^{-y} + \frac{x_T}{2x_a}\, e^{y}, \quad x_{b_{min}} = \frac{x_a\, x_T\, e^{-y}}{2x_a - x_T\, e^{y}} \quad \text{and} \quad x_{a_{min}} = \frac{x_T\, e^{y}}{2 - x_T\, e^{-y}} \,. \tag{3.15}$$

3.3 Proton target

In this section, basics of proton-proton cross-section including perturbative QCD and non-perturbative effects are described.

3.3.1 Perturbative QCD

The theory of strong interaction is described by the quantum chromodynamics a non-abelian gauge theory based on the $SU(3)$ symmetry group. The Lagrangian density has the form [66]

$$\mathcal{L}_{QCD} = \bar{\psi}_i (i\gamma^\mu \partial_\mu - m)\psi_j - g G^a_\mu \bar{\psi}_i \gamma^\mu T^a_{ij} \psi_j - \frac{1}{4}\, G^a_{\mu\nu} G^{\mu\nu}_a \,, \tag{3.16}$$

where ψ is Dirac (quark) field, indexes i, j represent the $SU(3)$ gauge group elements, g is a coupling constant, γ^μ are Dirac matrices, T^a_{ij} are generators of the $SU(3)$ gauge group,

$G^a_{\mu\nu} = \partial_\mu G^a_\nu + \partial_\nu G^a_\mu - g f^{abc} G^b_\mu G^c_\nu$ represents the gluonic field strength tensor where f^{abc} are the structure constants of $SU(3)$ and m is the mass of a quark.

For processes with sufficiently large transverse momentum, the perturbative techniques can be applied on QCD Lagrangian. The leading-order (LO) calculation of perturbative QCD will be considered. For this leading-logarithm approximation, the running strong coupling constant has the form [66]

$$\alpha_S(Q^2) = \frac{12\pi}{(33 - 2n_f)\ln{(Q^2/\Lambda^2_{QCD})}}\,, \tag{3.17}$$

where n_f denotes for the number of flavors, Q^2 is the transferred momentum and Λ_{QCD} is the fundamental QCD scale constant.

In the leading-logarithm approximation the case of hadron or jet production includes all relevant subprocesses containing quark-quark, quark-gluon and gluon-gluon scattering. All two-body scattering differential cross-sections for jet/hadron production are in Table 3.1 and corresponding Feynman diagrams are shown in Fig. 3.2.

Subprocess	Cross-section
$qq' \to qq'$	$\frac{4}{9}\,\frac{s^2+u^2}{t^2}$
$qq \to qq$	$\left[\frac{4}{9}\left(\frac{s^2+u^2}{t^2} + \frac{s^2+t^2}{u^2}\right) - \frac{8}{27}\,\frac{s^2}{tu}\right]$
$q\bar{q} \to q'\bar{q}'$	$\frac{4}{9}\,\frac{s^2+u^2}{t^2}$
$qq \to qq$	$\left[\frac{4}{9}\left(\frac{s^2+u^2}{t^2} + \frac{u^2+t^2}{s^2}\right) - \frac{8}{27}\,\frac{u^2}{st}\right]$
$gq \to gq$	$\left[-\frac{4}{9}\left(\frac{s}{u} + us\right) + \frac{s^2+u^2}{t^2}\right]$
$q\bar{q} \to gg$	$\left[\frac{32}{27}\left(\frac{t}{u} + ut\right) - \frac{8}{3}\,\frac{t^2+u^2}{s^2}\right]$
$gg \to q\bar{q}$	$\left[\frac{1}{6}\left(\frac{t}{u} + ut\right) - \frac{8}{3}\,\frac{t^2+u^2}{s^2}\right]$
$gg \to gg$	$\frac{9}{2}\left[3 - \frac{tu}{s^2} - \frac{su}{t^2} - \frac{st}{u^2}\right]$

Table 3.1: Table of parton scatterings cross-sections for hadron production at LO with a factor $\pi\alpha_S^2/\hat{s}$ factored out.

In case of direct photons production, quark-quark and quark-gluon subprocesses involving photon has to be considered. Differential cross-sections for direct photons production are in Table 3.2 and corresponding Feynman diagrams are shown at Fig. 3.3.

Because experimental data correspond to the sum of all orders of perturbation series and include all non-perturbative effects, at least a compensation of LO and higher order contributions is necessary. One way is to calculate processes within the next-to-leading order (NLO) or next-to-next-to-leading order (NNLO) including loops and multiparticle

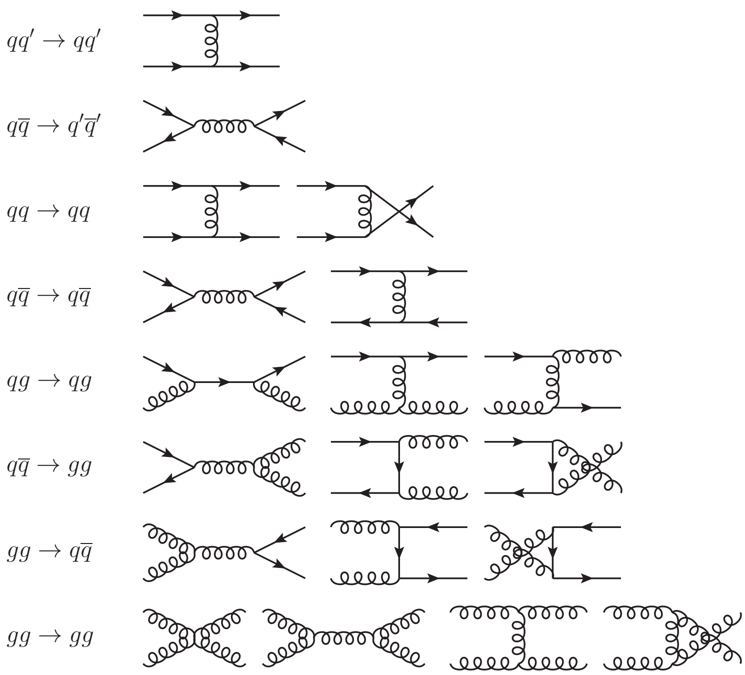

Figure 3.2: The Feynman diagrams for tree-level partonic subprocesses for jet/hadron production.

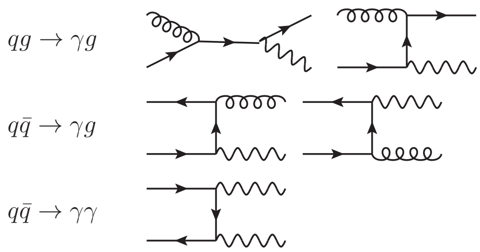

Figure 3.3: The Feynman diagrams for tree-level partonic subprocesses for direct photons production.

Subprocess	Cross-section
$gq \to \gamma q$	$-\frac{1}{3}\, e_q^2 \left(\frac{u}{s} + \frac{s}{u}\right)$
$q\bar{q} \to \gamma g$	$\frac{8}{9}\, e_q^2 \left(\frac{u}{t} + \frac{t}{u}\right)$
$q\bar{q} \to \gamma\gamma$	$\frac{2}{3}\, e_q^4 \left(\frac{t}{u} + \frac{u}{t}\right)$

Table 3.2: Table of parton scatterings cross-sections for hadron production at LO with factors $\pi\alpha_{EM}\alpha_S/\hat{s}$ and $\pi\alpha_{EM}^2/\hat{s}$ factored out of the single and double photon subprocesses, respectively.

production ($2 \to 3$, $2 \to 4$). Diagrams containing loops lead to infrared and ultraviolet singularities that are necessary to eliminate. That can be done by using regularization and some renormalization scheme leading to complex calculations of higher-order terms.

Another way is using the so-called K-factor. It can be defined in perturbative series for some processes at parton level as

$$\sigma_0 + \alpha_S \sigma_1 + ... = K\sigma_0, \tag{3.18}$$

where σ_i are contributions of i-th order, or it can be defined as

$$K = \frac{\sigma^{exp}}{\sigma^{th}}, \tag{3.19}$$

where σ^{exp} is the measured cross-section and σ^{th} is the calculated cross-section at LO. There are several approaches to choose the K-factor. For example, K-factor as an effective function of $\approx \exp(\alpha_s)$ is used in [67]. In [68] the K-factor is extracted from jets as a function of $\sqrt{s}$ and $p_{T,jet}$ but in most papers, e.g. [32] or [69], it is taken ad-hoc as a fixed number.

Obviously, the K-factor depends on the CMS energy and on a process in consideration. It varies for pure QCD processes, Drell-Yan process and for electroweak sector production.

3.3.2 Parton distribution functions, fragmentation functions

Parton distribution functions are usually interpreted as the probability densities to find a parton within a hadron with its momentum fraction between x and $x + dx$ at scale Q^2. Similarly, fragmentation functions represent the probability of obtaining a hadron h with a momentum fraction between z and $z + dz$ at scale μ_f.

The factorization theorem implies the independence of parton fragmentation and distribution functions on the hard scale Q^2. This allows to obtain both functions by fitting experimental data from the deep-inelastic scattering or e^-e^+ annihilation. These fits were obtained at relevant factorization scales Q_0^2 for parton distribution functions, resp. fragmentation scale μ_{F_0} for fragmentation functions and they can be evaluated on scales Q^2, resp. μ_F by a set of integro-differential evolution equations - DGLAP (Dokshitzer-Gribov-Lipatov-Altarelli-Parisi) evolution equations [70–72]

$$\frac{df_{q_i/A}(x, Q^2)}{dt} = \frac{\alpha_s(Q^2)}{2\pi} \int_x^1 \frac{dy}{y} \left[P_{qq}(x/y) f_{q_i/A}(y, Q^2) + P_{qg}(x/y) f_{q_i/A}(y, Q^2)\right] \tag{3.20}$$

and

$$\frac{df_{g/A}(x,Q^2)}{dt} = \frac{\alpha_s(Q^2)}{2\pi}\int_x^1 \frac{dy}{y}\left[\sum_q P_{gq}(x/y)f_{q_i/A}(y,Q^2) + P_{gg}(x/y)f_{g/A}(y,Q^2)\right], \tag{3.21}$$

where $f(x,Q^2)$ is the distribution function of a quark or a gluon, t is defined as $\ln(Q^2/\Lambda^2_{QCD})$, and the subscript q denotes quark flavors.

The kernels P_{ij} have the physics interpretation as the probability densities that a parton of type i radiates a quark or gluon and becomes a parton of type j carrying fraction x/y of the momentum of parent's parton.

The general procedure for obtaining the distribution function is as follows.

1. Make a choice on experimental data
2. Select the factorization scheme, e.g. $\overline{\text{MS}}$ (a renormalization scheme describing how the divergent parts are absorbed)
3. Choose the parametric form for the input parton distributions at Q_0^2
4. Evolution to any value of Q^2
5. Calculate χ^2 between evolved distribution and data
6. By adjusting the parameterizations of the input distributions minimize the χ^2

The input parton distributions are usually of form

$$xf_i = a_i\, x^{b_i}(1-x)^{c_i}, \tag{3.22}$$

where a_i, b_i and c_i are free parameters. More details can be found e.g. in [73].

Author uses PDFs CTEQ6 [74], MSTW2008 [75], CT10 [76], HERAPDF1.5 [77] and NNPDF2.1 [78] parametrizations.

Note that for calculation of proton anti-proton collisions the distribution function for u and d quarks have to be exchanged with their antiparticles $\bar{u}$ and $\bar{d}$.

The fragmentation of partons into hadrons can be explained only by using models. The most used model is the independent fragmentation model (IFM) [79]. For the full description of the final state the event generators based on string or cluster models are needed. Data for fragmentation functions were obtained primarily from e^-e^+ collisions at e.g. KEK, DESY, SLAC or CERN.

The following fragmentation functions were used: KKP [80] (Kniehl-Kramer-Pötter, 2000), DDS [81] (de Florian-Daniel-Sassot, 2007) and Kretzer [82] (2000).

3.3.3 Intrinsic transverse momentum

The QCD based factorization model, sometimes referred to QCD collinear parton model, was successful in describing high-p_T particle production in high energy $p+p$ collisions, $\sqrt{s} > 50$ GeV, [83]. On the other hand, this model fails to account for data for angular correlation of produced heavy quarks, and the total transverse momentum distribution of the heavy quark pairs [84, 85], or the Drell-Yan lepton pairs [86, 87]. Due to the uncertainty principle, one can expect that an average intrinsic transverse momentum has at least a few hundred MeV, reflecting the hadron size. Besides, next source of initial k_T are higher order perturbative QCD processes, e.g. $2 \to 3$, with additional radiated gluons. In fact, it is difficult to recognize true intrinsic and pQCD generated transverse momentum.

One of the most direct measurement of the k_T-smearing provides the Drell-Yan process, $q\bar{q} \to l^+l^-$, where the mean transverse momentum $\langle p_T^2 \rangle$ corresponds directly to the mena intrinsic transverse momentum $\langle k_T^2 \rangle$. It was shown that corresponding intrinsic $\langle k_T^2 \rangle = 0.95$ GeV^2 [87] and $\langle k_T^2 \rangle = 0.6$ GeV^2 after accounting for NLO subprocesses, respectively. [88].

One can imagine that this effect is analogous to the Fermi motion of nucleons in a nucleus and can lead to a smearing of the p_T spectra. The k_T-smearing distribution function is a phenomenological parametrization and can be extracted from measurements of dimuon, diphoton and dijet pairs. This effect was investigated e.g. in [32,61,65,89–93].

In this work, a more phenomenological approach is adopted where the intrinsic transverse momentum distribution is described by the Gaussian distribution

$$g_N(k_T, Q^2) = \frac{1}{\pi \langle k_T^2 \rangle_N} \, e^{-k_T^2/\langle k_T^2 \rangle_N}, \tag{3.23}$$

which introduces a new non-perturbative parameter, the mean intrinsic transverse momentum $\langle k_T^2 \rangle$. In the first approximation, $\langle k_T^2 \rangle$ is a constant different for each CMS energy but it can differ a little as function of p_T [94]. Next, one can consider that $\langle k_T^2 \rangle$ depends on the momentum scale Q^2 of the hard process [32, 61]

$$\langle k_T^2 \rangle_N(Q^2) = \langle k_T^2 \rangle_0 + 0.2\, \alpha_S(Q^2) Q^2, \tag{3.24}$$

where $\langle k_T^2 \rangle_0$ differs also for each CMS energy of the collisions.

In this work a CMS-energy-independent approach were developed [95, 96] based on Eq. 3.24 with the consideration that the mean intrinsic transverse momentum changes with CMS energy due to different ratio of quarks and gluons involved in the collision.

Here, $\langle k_T^2 \rangle_0$ was determined with values 0.2 GeV^2 for quarks and 0.8 GeV^2 for gluons. Therefore, the mean intrinsic transverse momentum increases with CMS energy due to increasing gluon contribution.

3.3.4 Proton-proton cross-section

The overall expression for the inclusive differential cross-section for hadron production then reads

$$\begin{aligned} E\frac{d^3\sigma^{(pp\to h\ X)}}{d^3p} &= K\sum_{abcd}\int dx_a dx_b dz_c d^2k_{Ta} d^2k_{Tb} g_p(k_{Ta},Q^2) g_p(k_{Tb},Q^2) f_{a/A}(x_a,Q^2) \\ &\times f_{b/B}(x_b,Q^2) D_{h/c}(z_c,\mu_F^2)\frac{\hat{s}}{\pi z_c^2}\frac{d\sigma^{(ab\to cd)}}{d\hat{t}}\delta(\hat{s}+\hat{t}+\hat{u}), \end{aligned} \tag{3.25}$$

where one integral can be carried out as is described in Appendix A.1 and remaining integrals have to be computed numerically.

The inclusive differential cross-section for direct photon production has a form

$$\begin{aligned} E\frac{d^3\sigma^{(pp\to \gamma\ X)}}{d^3p} &= K\sum_{abcd}\int dx_a dx_b d^2k_{Ta} d^2k_{Tb} g_p(k_{Ta},Q^2) g_p(k_{Tb},Q^2) f_{a/A}(x_a,Q^2) \\ &\times f_{b/B}(x_b,Q^2)\frac{\hat{s}}{\pi}\frac{d\sigma^{(ab\to cd)}}{d\hat{t}}\delta(\hat{s}+\hat{t}+\hat{u}) \end{aligned} \tag{3.26}$$

where, similarly as for hadron production, one integral can be carried out as is described in section A.1 and remaining integrals have to be computed numerically.

3.4 Nuclear target

This section describes basic formula for proton-nucleus and nucleus-nucleus cross-section and all nuclear effects used in this this model.

3.4.1 Proton-nucleus and nucleus-nucleus cross-section

The formula for the inclusive differential cross-section for proton-nucleus interaction is based on $p+p$ cross-section (3.25) where an integral over an impact parameter and a function describing the distribution of nucleons in the nucleus have to be added. Then one can add a nuclear modification e.g. nuclear PDF, nuclear broadening etc.

The formula for inclusive differential cross-section for hadron production reads

$$\begin{aligned} E\frac{d^3\sigma^{(p\,A\to h\;X)}}{d^3p} &= K\sum_{abcd}\int d^2b\,T_A(b)\int dx_a\,dx_b\,dz_c\,d^2k_{Ta}\,d^2k_{Tb}\,g_A(k_{Ta},Q^2,b) \\ &\quad \times g_p(k_{Tb},Q^2)\,f_{a/p}(x_a,Q^2)\,f_{b/A}(b,x_b,Q^2) \\ &\quad \times D_{h/c}(z_c,\mu_F^2)\frac{1}{\pi z_c}\,\frac{d\sigma^{(ab\to cd)}}{d\hat{t}} \end{aligned} \tag{3.27}$$

and for direct photons production

$$\begin{aligned} E\frac{d^3\sigma^{(p\,A\to\gamma\;X)}}{d^3p} &= K\sum_{abcd}\int d^2b\,T_A(b)\int dx_a\,dx_b\,d^2k_{Ta}\,d^2k_{Tb}\,g_A(k_{Ta},Q^2,b) \\ &\quad \times g_p(k_{Tb},Q^2)\,f_{a/p}(x_a,Q^2)\,f_{b/A}(b,x_b,Q^2) \\ &\quad \times\frac{1}{\pi}\,\frac{d\sigma^{(ab\to cd)}}{d\hat{t}}\,. \end{aligned} \tag{3.28}$$

The nuclear thickness function or nuclear profile function $T_A(b)$ gives the number of nucleons in the nucleus A per unit area along a direction z separated from the center of the nucleus by an impact parameter b

$$T_A(b) = \int dz\,\rho(b,z), \tag{3.29}$$

where $\rho(b,z)$ is a parametrization of the distribution normalized to the number of nucleons A

$$\int d^2b\,T_A(b) = A. \tag{3.30}$$

In this work, the two-parameter Fermi model (2pF) (also known as Wood-Saxon distribution) for heavy ions was chosen as the parametrization of ρ in the form

$$\rho(r) = \frac{\rho_0}{1+e^{\frac{r-c}{z}}} \tag{3.31}$$

where $r = \sqrt{b^2+z^2}$, ρ_0 is determined by the normalization in (3.30) and c and z are model parameters.

Values of parameters for two-parameter Fermi model from [97] were used.

Due to the fact that this work is focused on initial state effects, in case of heavy-ion collisions only a direct photon production is studied. The inclusive differential cross-section for direct photon production in $A+B$ collisions reads

$$
\begin{aligned}
E\frac{d^3\sigma^{(A\,B\to\gamma\;X)}}{d^3p} \quad &= \quad K\sum_{abcd}\int d^2s\,d^2b\,T_A(s)T_B(|\vec{b}-\vec{s}|)\int dx_a\,dx_b\,d^2k_{Ta}\,d^2k_{Tb} \\
&\times g_A(k_{Tb},Q^2,s)\,g_B(k_{Ta},Q^2,|\vec{b}-\vec{s}|)\,f_{a/A}(x_a,Q^2,s) \\
&\times f_{b/B}(x_b,Q^2,|\vec{b}-\vec{s}|)\,\frac{1}{\pi}\,\frac{d\sigma^{(ab\to cd)}}{d\hat{t}}\,,
\end{aligned}
\tag{3.32}
$$

where partons from both nuclei are affected by the nuclear PDFs of own mother nucleus and both propagate through the other nucleus.

In the following subsections all nuclear effects that were used in this work are described.

3.4.2 Nuclear broadening

Nuclear broadening or k_T-broadening is an extension of the intrinsic transverse momentum, described in chapter 3.3.3, to the nucleus where the initial transverse momentum k_T of the beam partons is broadened. The k_T-broadening stands for high-energy parton propagating through a nuclear medium that experiences multiple soft scatterings and so increases its transverse momentum. It can be imagined as parton multiple gluonic exchanges with nucleons. Assuming that each scattering provides a k_T kick that can be described also by the Gaussian distribution, one can just change the width of the initial k_T distribution

$$
\langle k_T^2\rangle_A(Q^2,b) = \langle k_T^2\rangle_N(Q^2) + \Delta k_T^2(b), \tag{3.33}
$$

where $\langle k_T^2\rangle_N(Q^2)$ describe distribution of initial transverse momentum within the nucleon and the nuclear broadening term $\Delta k_T^2(b)$ describes multiple scattering in nucleus with b-dependent k_T distribution

$$
g_A(k_T,Q^2,b) = \frac{1}{\pi\langle k_T^2\rangle_A}\,e^{-k_T^2/\langle k_T^2\rangle_A}. \tag{3.34}
$$

In this work, the nuclear broadening $\Delta k_T^2(b)$ is expressed within the color dipole formalism as

$$
\Delta k_T^2(b) = 2\,C\,T_A(b), \tag{3.35}
$$

where the factor C is calculated as

$$
C = \left.\frac{d\sigma_{q\bar{q}}^N}{dr^2}\right|_{r=0}, \tag{3.36}
$$

from the dipole cross-section $\sigma_{q\bar{q}}^N$ at $r = 0$.

Majority of authors, e.g. [32, 94], take the broadening term expressed as

$$\Delta k_T^2(b) = C h_{pA}(b), \tag{3.37}$$

where the term $h_{pA}(b)$ is the effective number of collisions at impact parameter b. The constant C is the average transverse momentum squared that can be extracted from data [94] or can be scale-dependent $C(Q^2)$ [32]. The effective number of collisions usually has a form $h_{pA}(b) = \nu_A(b) - 1$, where $\nu_A(b) = \sigma_{NN} T_A(b)$ that corresponds to all possible collisions except the hard interaction producing a particle. In [94] the prescription of $\nu_A(b)$ is investigated in more detail.

3.4.3 Nuclear PDF

One of the most straightforward way how to include nuclear effects is using nuclear modification of parton distribution functions - nuclear PDFs. Basically, all nuclear PDF parameterizations are based on fitting of accessible data, mainly from nuclear DIS and nuclear Drell-Yan process, within the QCD collinear factorization theorem at LO or NLO order. Last decade the data from RHIC and LHC on hadrons, direct photons, di-jet or $W^\pm$ and Z^0 boson production are also used for the global fit.

Currently, several nuclear PDF sets are available: EKS98 [98], EPS09 [99], HKN07 [100], nDS [81], nCTEQ15 [101], DSZS [102].

Most of these parameterizations consider only the spatial averaged nuclear PDFs, probed in minimum-bias nuclear collisions as functions of momentum fraction x and scale Q^2 and flavour. Illustrative comparison of some nuclear PDF sets is in Fig. 3.4. For EKS98 and EPS09 an update on impact parameter dependent nPDF [103] based on RHIC data for different centrality exists. More recent parameterizations provide also uncertainties and error sets.

Nuclear PDF is then implemented for each flavor i as

$$f_{i/A}(x_b, Q^2, b) = R_i^A(x_b, Q, b)\, f_{i/p}(x, Q^2), \tag{3.38}$$

where $f_{i/A}$ is the nuclear parton distribution function and $f_{i/p}$ is standard parton distribution function and R_f^A is nuclear modification factor normalized to one nucleon.

One should be also careful about the double counting of the Cronin enhancement from nuclear PDF and nuclear broadening together.

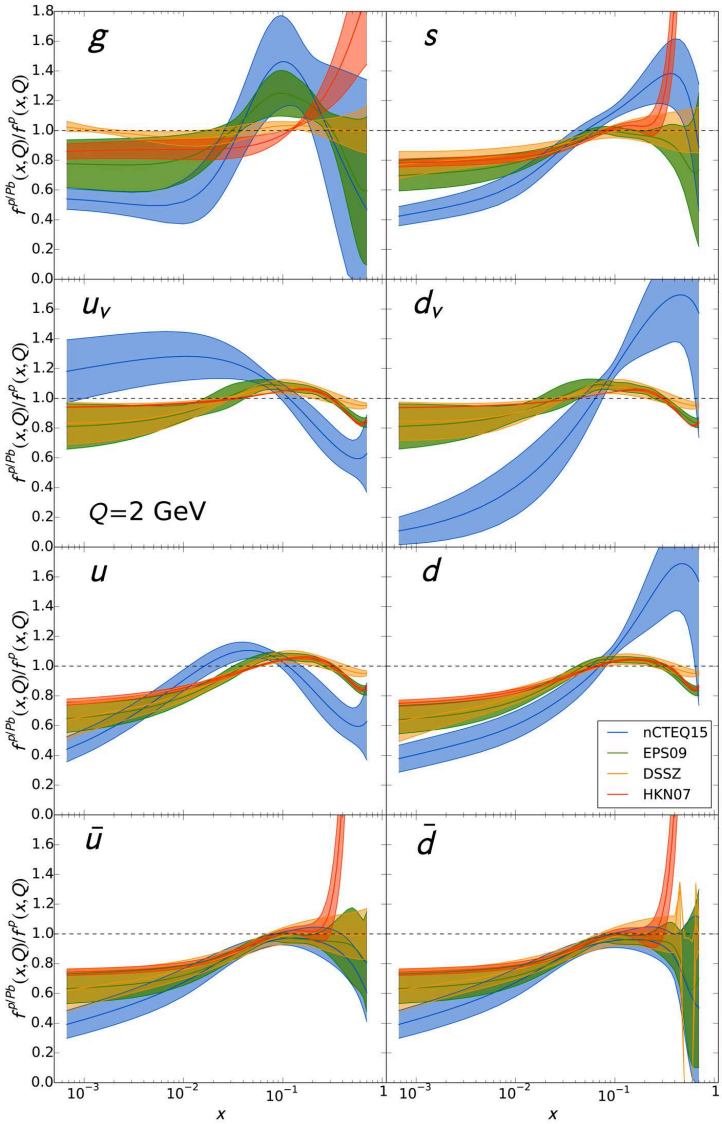

Figure 3.4: Comparison of nCTEQ15 [101], EPS09 [99], DSZS [102] and HKN07 [100] for lead at scale $Q = 2$ GeV [101].

3.4.4 Isospin effect

Isospin effect comes from the difference between the proton-nucleus and neutron-nucleus collisions due to the different distribution of valence quarks. Therefore, this effect is important mainly for nucleus-nucleus collisions and in the large-x region where the valence quarks dominate.

This effect can be included by an appropriate modification of the structure of PDFs

$$f_{i/N}(x,Q^2) = \frac{Z}{A} f_{i/p}(x,Q^2) + \left(1 - \frac{Z}{A}\right) f_{i/n}(x,Q^2)\,, \tag{3.39}$$

where $f_{i/N}(x,Q^2)$ represents parton distribution function of nucleon, and Z is the proton number of the target.

For example, in the case of deuteron, the isospin effect leads to the suppression $R_{dAu} \sim 0.83$, or $R_{AuAu} \sim 0.80$ for the heavy-ion collisions.

3.4.5 Initial State Interaction

One of the mechanisms, which has an ambitions to explain the suppression at high-p_T and forward rapidities described in Chapter 2.3, is an initial state interaction (ISI) effects [4] where the participation of the projectile hadron in the multiple interactions during the propagation through the nucleus leads to the dissipation of energy. This dissipation of the energy is proportional to the energy of the projectile hadron and, therefore, is present at all energies.

This effect can be interpreted in the Fock states representation. The projectile hadron can be in each time decomposed over different states. Then the interaction of Fock states with the target leads to the modification of weight of these Fock states depending on the type of interaction.

In each Fock state, the projectile momentum fraction is distributed among all constituents depending on the multiplicity. For the kinematics, where the leading parton carries most of the momentum, $x \to 1$, less momentum fraction is left for the rest constituents. Such configuration have the lower probability is the higher constituent multiplicity.

Moreover, in the case of the nuclear target, where the initial state multiple interactions enhance the weight factor of higher Fock states, it can be viewed as an effective energy loss. It is because higher Fock states with higher multiplicity have less probability for having the projectile parton $x \to 1$. A detailed description and interpretation of the corresponding additional suppression was presented also in [104–106].

The initial state energy loss (ISI effect) is an effect that dominates at forward rapidities, $x_L = 2p_L/\sqrt{s}$ and/or high p_T, $x_T = 2p_T/\sqrt{s}$. Correspondingly, the proper variable which controls this effect is $\xi = \sqrt{x_L^2 + x_T^2}$. This effect was derived and evaluated in [4, 107] within the Glauber approximation where each interaction in the nucleus lead to a suppression $S(\xi) \approx 1-\xi$. Summing up over the multiple initial state interactions at impact parameter b, one arrives at a nuclear ISI-modified PDF

$$f_{a/A}(x, Q^2) \Rightarrow f^A_{a/A}(x, Q^2, b) = C_v f_{a/A}(x, Q^2) \frac{e^{-\xi\sigma_{eff}T_A(b)} - e^{-\sigma_{eff}T_A(b)}}{(1-\xi)(1-e^{-\sigma_{eff}T_A(b)})}, \tag{3.40}$$

where $\sigma_{eff} = 20$ mb [4] is the hadronic cross-section which effectively determines the rate of multiple interactions, and normalization factor C_v is fixed by the Gottfried sum rule.

This effect aspirates to describe the suppressions mentioned in Chapter 2.3. Further, ISI effect predicts a substantial suppressions at high p_T at RHIC energy and lower, and at forward rapidities at all energies that can be verified by the future measurement at RHIC and LHC. Moreover, the correlation between nuclear target and the projectile, where the ISI effects, implemented as the modification of PDF of the projectile, is function of target momentum fraction x_2, leads to a breakdown of the QCD factorization theorem [4] that supposes the independency of projectile and target.

Chapter 4

Color Dipole Approach

4.1 Introduction

Models based on QCD (Chapter 3) work well for proton-proton collisions, but its use for nuclear collisions is much more complicated because of non-intuitive transition to nuclear collisions and its specifics properties, e.g. non-perturbative effects such as color confinement or effects of quantum coherence.

An alternative model to QCD based models, much more suitable especially for nuclear collisions, is the so-called color dipole model originally proposed in [108] for hadronic interactions, and, consequently, it was applied to DIS [109] and to the Drell-Yan process [110] that was basically studied also in [6,111,112]. In contrast to QCD based models, the color dipole approach is formulated in the target rest frame and, therefore, the interpretation of processes is different because the space-time interpretation is not Lorentz invariant.

This difference can be described e.g. in the Drell-Yan production in Fig. 4.1. In the QCD based models, defined in the infinite momentum frame, the Drell-Yan process looks like an annihilation of quark and anti-quark from each proton at leading order level, see Fig. 4.1 a). In the color dipole approach its looks like a bremsstrahlung from an incoming quark. There are two possibilities of bremsstrahlung, experimentally indistinguishable, before and after the interaction with the target, Fig. 4.1 b).

One of the key features used in the color dipole model is an expansion of the projectile, e.g. quark, into the Fock states [110]

$$|q\rangle = |q\rangle + |q\gamma^*\rangle + |q\gamma^* G\rangle + ..., \tag{4.1}$$

where first two states are most probable, and each higher Fock state is heavier and has shorter lifetime and, therefore, can be neglected for the proton-proton and low energy

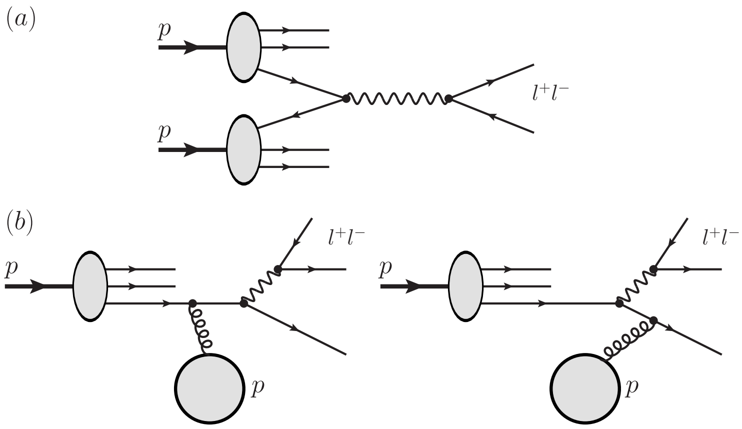

Figure 4.1: Sketch of the Drell-Yan process in a) QCD based model in the infinite momentum frame and b) color dipole approach in the target rest frame.

nuclear collisions. For high energy proton-nucleus or nucleus-nucleus collisions the importance of higher Fock states, e.g. $|q\gamma^* G\rangle$, grows, and lead to effects such as gluon shadowing that will be described later in this chapter.

Overall inclusive cross-section is then calculated as a convolution of parton distribution function (PDF), $|q\gamma^*\rangle$ Fock state wave function and a dipole cross-section representing an interaction of the target with the dipole.

Only the Drell-Yan process and direct photon production are considered within the color dipole approach in this work.

4.2 Proton target

In this section, basics of proton-proton cross-section within the color dipole framework are described.

4.2.1 Quark-nucleon cross-section

In the lowest approximation, including only $|q\gamma^*\rangle$ Fock state, the interaction of the projectile quark with the nucleon in the case of proton-proton collision can be seen as a gamma bremsstrahlung from an incoming quark as in Fig. 4.2.

Differential quark-nucleon cross-section can be expressed by factorization in the light-

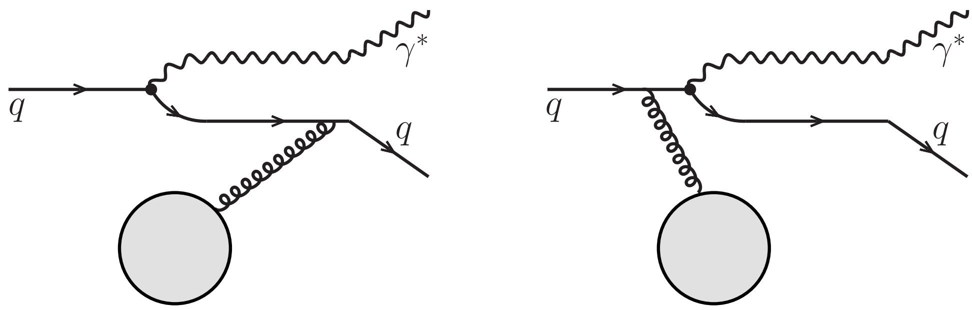

Figure 4.2: Bremsstrahlung of $\gamma^* q$ fluctuation in the interaction with the target nucleon.

cone (LC) form [6, 111, 112]

$$\frac{d^3\sigma^{(qN\to\gamma X)}}{d(\ln\alpha)d^2p_T} = \frac{1}{(2\pi)^2}\int d^2\rho_1\, d^2\rho_2\, e^{i\vec{p}_T(\vec{\rho}_1-\vec{\rho}_2)}\Psi^*_{\gamma^* q}(\alpha,\vec{\rho}_2)\Psi_{\gamma^* q}(\alpha,\vec{\rho}_1)\sigma_\gamma(\vec{\rho}_1,\vec{\rho}_2,\alpha), \quad (4.2)$$

where

$$\sigma_\gamma(\vec{\rho}_1,\vec{\rho}_2,\alpha) = \frac{1}{2}\left\{\sigma^N_{q\bar{q}}(\alpha\rho_1) + \sigma^N_{q\bar{q}}(\alpha\rho_2) - \sigma^N_{q\bar{q}}(\alpha|\vec{\rho}_1-\vec{\rho}_2|)\right\}, \quad (4.3)$$

where $\Psi_{\gamma^* q}(\alpha,\vec{\rho})$ is the wave function of $|q\gamma^*\rangle$ state, $\sigma^N_{q\bar{q}}(\rho)$ denotes the dipole cross-section of the interaction of the dipole with the target nucleon, α is the momentum fraction of incoming quark which is carried by the photon, and $\vec{\rho}_1$ and $\vec{\rho}_2$ are the transversal sizes of $|\gamma^* q\rangle$ state.

The wave function of $|\gamma^* q\rangle$ state ($q \to q + \gamma^*$) has different form for transversal and longitudinal polarised photon [112]

$$\Psi^{T,L}_{\gamma^* q}(\vec{\rho},\alpha) = \frac{Z_f\sqrt{\alpha_{EM}}}{2\pi}\,\chi^\dagger_f \hat{\mathcal{O}}^{T,L}\chi_i \mathrm{K}_0(\eta\rho) \quad (4.4)$$

where Z_f denotes the fraction of quark charge, α_{EM} is the electromagnetic coupling constant, $\chi_{f,i}$ are spinors of incoming and outgoing quarks, $\mathrm{K}_0(x)$ is the modified Bessel function of second kind, sometimes called as the MacDonald's function, and

$$\eta^2 = \alpha^2 m_q^2 + (1-\alpha)M^2, \quad (4.5)$$

where M is an invariant mass of the virtual photon γ^* (corresponding to the dilepton mass), m_q refers to the effective quark mass. The whole situation is sketched in Fig. 4.3. In this figure, $\vec{\rho}$ is the transverse momentum between a quark and a photon, then their distance from the center of gravity is $(1-\alpha)\vec{\rho}$ and $\alpha\vec{\rho}$, respectively.

Operators $\hat{\mathcal{O}}^{T,L}$ have following form [112]

$$\hat{\mathcal{O}}^T = i m_q \alpha^2 \vec{e}^{\,*}\cdot(\vec{n}\times\vec{\sigma}) + \alpha\,\vec{e}^{\,*}\cdot(\vec{\sigma}\times\vec{\nabla}) - i(2-\alpha)\vec{e}^{\,*}\cdot\vec{\nabla}, \quad (4.6)$$

$$\hat{\mathcal{O}}^L = 2M(1-\alpha), \tag{4.7}$$

where $\vec{e}^*$ is an unit vector of the photon polarization (perpendicular to $\vec{n}$), $\vec{n}$ is an unit vector in the direction of the incoming quark that is the same as axis z, $\vec{n} = \vec{e}_z$, $\vec{\sigma}$ is the vector of the Pauli matrices, and $\vec{\nabla}$ is a two dimensional gradient acting on the transverse coordinate $\vec{\rho}$.

For direct photon production one can take $M = 0$.

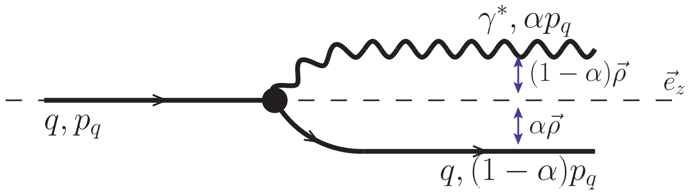

Figure 4.3: Feynman diagram representation of the $\gamma^* q$ fluctuation.

Wave functions in (4.2) can be modified by (4.6) and (4.7) to

$$\begin{aligned}\sum_{i,f} \Psi^{T*}_{\gamma^* q}(\vec{\rho}_2, \alpha)\Psi^{T}_{\gamma^* q}(\vec{\rho}_1, \alpha) = Z_f^2 \frac{\alpha_{EM}}{2\pi^2} \, &\left[m_f^2 \alpha^4 \mathrm{K}_0(\eta\rho_1)\mathrm{K}_0(\eta\rho_2) \right. \\ &\left. + (1+(1-\alpha)^2)\eta^2 \frac{\vec{\rho}_1 \cdot \vec{\rho}_2}{\rho_1\rho_2} \, \mathrm{K}_1(\eta\rho_1)\mathrm{K}_1(\eta\rho_2)\right],\end{aligned} \tag{4.8}$$

$$\sum_{i,f} \Psi^{L*}_{\gamma^* q}(\vec{\rho}_2, \alpha)\Psi^{L}_{\gamma^* q}(\vec{\rho}_1, \alpha) = Z_f^2 \frac{\alpha_{EM}}{\pi^2} \, M^2(1-\alpha)^2 \mathrm{K}_0(\eta\rho_1)\mathrm{K}_0(\eta\rho_2), \tag{4.9}$$

that is averaging over the polarization of the incoming quark and summed over polarizations of the outgoing quark and photon.

Integrals in (4.2) can be partly integrated analytically up to one remaining integral. After some algebra the qN cross-section reads

$$\begin{aligned}\frac{d^3\sigma^{(qN\to\gamma X)}}{d(\ln\alpha)d^2p_T} &= \frac{\alpha_{EM}}{2\pi^2}\left[(m_q^2\alpha^4 + 2M^2(1-\alpha)^2)\left(\frac{1}{p_T^2+\eta^2}\,\mathcal{I}_1 - \frac{1}{4\eta}\,\mathcal{I}_2\right)\right. \\ &+ \left.(1+(1-\alpha)^2)\left(\frac{\eta p_T}{p_T^2+\eta^2}\,\mathcal{I}_3 - \frac{1}{2}\,\mathcal{I}_1 + \frac{\eta}{2}\,\mathcal{I}_2\right)\right],\end{aligned} \tag{4.10}$$

where

$$\mathcal{I}_1 = \int_0^\infty d^2\rho\,\rho\,\mathrm{J}_0(p_T\rho)\mathrm{K}_0(\eta\rho)\sigma^N_{q\bar{q}}(\alpha\rho), \tag{4.11}$$

$$\mathcal{I}_2 = \int_0^\infty d^2\rho\,\rho^2\mathrm{J}_0(p_T\rho)\mathrm{K}_1(\eta\rho)\sigma^N_{q\bar{q}}(\alpha\rho), \tag{4.12}$$

$$\mathcal{I}_3 = \int_0^\infty d^2\rho\,\rho\,\mathrm{J}_1(p_T\rho)\mathrm{K}_1(\eta\rho)\sigma^N_{q\bar{q}}(\alpha\rho). \tag{4.13}$$

The derivation of (4.10) can be found in [113] or [114].

For some particular cases, the qN cross-section (4.2) can be also integrated analytically over p_T with result

$$\frac{d\sigma^{(qN\to\gamma X)}}{d(\ln\alpha)} = \int d^2\rho\,|\Psi_{\gamma^* q}(\alpha,\vec{\rho})|^2\sigma_{q\bar{q}}^N(\alpha\rho), \tag{4.14}$$

and

$$\begin{aligned}\frac{d\sigma^{(qN\to\gamma X)}}{d(\ln\alpha)} &= \frac{\alpha_{EM}}{\pi}\int d\rho\,\rho[(m_q^2\alpha^4 + 2M^2(1-\alpha)^2)\mathrm{K}_0^2(\eta\rho)\\ &+ (1+(1-\alpha)^2)\eta^2\mathrm{K}_1^2(\eta\rho)]\sigma_{q\bar{q}}^N(\alpha\rho),\end{aligned} \tag{4.15}$$

respectively.

The only free parameter in the color dipole approach is the effective quark mass m_q. The value of the quark mass m_q should correspond to one used in the particular dipole cross-section. Larger discussion about the effect of the effective quark mass can be found in [6, 114].

Note that the contribution of the Z^0 boson to the cross-section should be included for investigating of the Drell-Yan process with higher mass. The including of the Z^0 boson into the color dipole framework is described in Appendix A.2.

4.2.2 Dipole cross-section

Dipole cross-section is an universal quantity in high energy physics that can be used for description of various processes, e.g. DIS, Drell-Yan process or pion-proton scattering. The idea of the dipole cross-section comes from the eighties [108] with application on deep inelastic scattering where $|q\bar{q}\rangle$ Fock state is considered, and, basically, represents two gluon exchange (in the Regge phenomenology this corresponds to the exchange of one pomeron) between $q\bar{q}$ dipole and proton target. Hence, this formalism can be used only for high energy processes, $x_2 \lesssim 0.01$. In the Born approximation the dipole cross-section is energy-independent and depends on transverse separation and x_2. The energy dependence is generated by the radiation of soft gluons that can be resumed in the leading log approximation [115]

$$\sigma_{q\bar{q}}^N(x_2,\rho) = \frac{4\pi}{3}\rho^2\alpha_S\int\frac{d^2k_T}{k_T^2}\frac{[1-\exp(i\vec{k}_T\cdot\vec{\rho})]}{k_T^2\rho^2}\frac{\partial(x_2 G(x_2,k_T^2))}{\partial\log(k_T^2)}, \tag{4.16}$$

where $\vec{k}_T$ is the transverse momentum of the dipole exchanged with target, α_S is the strong running coupling constant at the relevant scale, and $G(x_2,k_T^2)$ is the unintegrated gluon density.

Factor $[1 - \exp(i\vec{k}_T \cdot \vec{\rho})]$ represents the so-called screening factor that leads to the vanishing of the dipole cross-section for $\rho \to 0$. This factor is a key feature of color transparency phenomenon [35, 108, 116]. It was proved that for small dipole separations the quadratic approximation of the dipole cross-section can be used

$$\sigma_{q\bar{q}}^N(\rho) = C\rho^2. \tag{4.17}$$

There are more ways how to get the factor C. Two approaches are mainly mentioned in the literature. The factor C can correspond to the first term in the Taylor expansion of the dipole cross-section parametrization at $\rho = 0$

$$C = \left.\frac{d\sigma_{q\bar{q}}^N(\rho)}{d\rho^2}\right|_{\rho=0}, \tag{4.18}$$

or can be estimated from the limit condition on long coherence length (LCL) limit (will be described later) [117]

$$\begin{aligned} &\frac{\int d^2b \int d^2\rho \left|\Psi_{\gamma^* q}^{T,L}(\vec{\rho}, \alpha, Q^2)\right|^2 \left\{1 - \exp\left[-\frac{1}{2}C(s)\alpha^2\rho^2 T_A(b)\right]\right\}}{\int d^2\rho \left|\Psi_{\gamma^* q}^{T,L}(\vec{\rho}, \alpha, Q^2)\right|^2 C(s)\alpha^2\rho^2} \\ = &\frac{\int d^2b \int d^2\rho \left|\Psi_{\gamma^* q}^{T,L}(\vec{\rho}, \alpha, Q^2)\right|^2 \left\{1 - \exp\left[-\frac{1}{2}\sigma_{q\bar{q}}^N(\alpha\rho, s) T_A(b)\right]\right\}}{\int d^2\rho \left|\Psi_{\gamma^* q}^{T,L}(\vec{\rho}, \alpha, Q^2)\right|^2 \sigma_{q\bar{q}}^N(\alpha\rho, s)}. \end{aligned} \tag{4.19}$$

On the other hand, at large dipole separations it is assumed to be saturated. Because of a lot of uncertainties in the theoretical description of the dipole cross-section, e.g. unknown unintegrated gluon distribution, behavior at large separations and other, phenomenological parametrizations based on fitted experimental data are used.

GBW

One of the oldest and best known parametrization was provided by Golec-Biernat and Wusthoff (GBW) [118]. This simple parametrization do not take into account any QCD evolution and originally is based on the old HERA data from 1997, update of fitting parameters on newer HERA data were published by Kowalsky, Motyka and Watt [119]. This parametrization has a form

$$\sigma_{q\bar{q}}^N(\rho, x) = \sigma_0 \left(1 - \exp\left[-\frac{\rho^2 Q_0^2}{4\left(\frac{x}{x_0}\right)^2}\right]\right), \tag{4.20}$$

where $Q_0^2 = 1\,\mathrm{GeV}^2$ and fitting parameters are showed in Tab. 4.1. This model includes one pomeron exchange only.

n_{fl}	m_{uds}[GeV]	m_c[GeV]	x-range	Q^2 [GeV^2]	σ_0 [mb]	x_0	λ	ref.
3	0.14	-	< 0.01	-	29.12	0.41×10^{-4}	0.227	[118]
4	0.14	1.5	< 0.01	-	23.03	3.04×10^{-4}	0.288	[118]
3	0.14	-	< 0.01	0.25-45	20.1	5.16×10^{-4}	0.289	[119]
4	0.14	1.4	< 0.01	0.25-45	23.9	1.11×10^{-4}	0.287	[119]
4	0.14	1.4	< 0.01	0.75-650	22.5	1.69×10^{-4}	0.317	[119]

Table 4.1: Parameters for the GBW model.

KST

KST model of the dipole cross-section was published by Kopeliovich, Schaefer, Tarasov [120]. This model works well for $Q^2 \sim 20\,\mathrm{GeV}^2$ and lower and is based on H1 (1995) and ZEUS (1992) data. This model has a form

$$\sigma_{q\bar{q}}^N(\rho, s_q) = \sigma_0(s_q)\left(1 - \exp\left[-\frac{\rho^2}{r_0^2(s_q)}\right]\right), \tag{4.21}$$

where s_q is energy of the incoming quark, next

$$\sigma_0(s_q) = \sigma_{tot}^{\pi p}(s_q)\left(1 + \frac{3r_0^2(s_q)}{8\langle r_{ch}^2(s_q)\rangle}\right), \tag{4.22}$$

$$r_0^2(s_q) = 0.88\left(\frac{s_q}{s_0}\right)^{-0.14} \mathrm{fm}, \tag{4.23}$$

$$s_0 = 1000\ \mathrm{GeV}^2, \qquad \langle r_{ch}^2(s_q)\rangle = 0.44\,\mathrm{fm}^2. \tag{4.24}$$

Parametrization from [121] with data from [122] was used for pion-proton cross-section $\sigma_{tot}^{\pi p}(s_q)$

$$\sigma_{tot}^{\pi p}(s_q) = 23.6\left(\frac{s_q}{s_0}\right)^{0.08} + 1.432\left(\frac{s_q}{s_0}\right)^{-0.45} \mathrm{mb}, \tag{4.25}$$

where the first term corresponds to the pomeron exchange and the second to the reggeon exchange.

BGBK

This parametrization by Bartels, Golec-Biernat and Kowalski [123] was created by including of the DGLAP evolution into the GBW model

$$\sigma_{q\bar{q}}^N(\rho, x) = \sigma_0\left(1 - \exp\left[-\frac{\pi^2\rho^2\alpha_s(\mu^2)xg(x,\mu^2)}{3\sigma_3}\right]\right), \tag{4.26}$$

with the scale

$$\mu^2 = \frac{C}{\rho^2} + \mu_0^2. \tag{4.27}$$

There, $g(x,\mu^2)$ contains LO DGLAP evolution of gluons only (quarks are neglected due to small fractions x_2) [70–72]

$$\frac{\partial xg(x,\mu^2)}{\partial \ln \mu^2} = \frac{\alpha_S(\mu^2)}{2\pi} \int_x^1 dz\, P_{gg}(z) \frac{x}{z}\, g\left(\frac{x}{z}, \mu^2\right) \tag{4.28}$$

where the gluon density at initial scale $Q_0^2 = 1$ GeV^2 is parameterized as

$$xg(x, Q_0^2) = A_g x^{-\lambda_g}(1-x)^{5.6}, \tag{4.29}$$

where C, μ_0^2, A_g and λ_g are parameters fitted from the DIS data.

IP-Sat

IP-Sat model is generalization of BGBK model accounting the impact parameter dependence of the dipole cross-section by Rezaeian, Siddikov, de Klundert and Venogopalan [124]

$$\sigma_{q\bar{q}}^N(\rho, x) = 2 \int d^2 b \left(1 - \exp\left[-\frac{\pi^2\rho^2}{2N_c}\, \alpha_S(\mu^2) xg(x,\mu^2) T_G(b)\right]\right) \tag{4.30}$$

with the Gaussian impact parameter dependence

$$T_G(b) = \frac{1}{2\pi B_G}\, \mathrm{e}^{-\frac{b^2}{2B_G}}, \tag{4.31}$$

where $B_G = 4$ GeV^2 is a free parameter extracted from the t-dependence of the exclusive $e+p$ data. Fitted parameters are in Tab. 4.2.

n_{fl}	m_{uds}[GeV]	m_c[GeV]	x-range	Q^2 [GeV^2]	μ_0^2 [GeV^2]	A_g	λ_g	ref.
4	0.0	1.27	< 0.01	0.75-650	1.51	2.308	0.058	[124]
4	0.0	1.4	< 0.01	0.75-650	1.428	2.373	0.052	[124]

Table 4.2: Parameters for the IP-Sat model.

One can encounter also other parameterizations with next parameterizations, e.g. model by Iancu, Itakura and Munier (IIM, sometimes denoted as CGC) [119, 125]; Albacete, Armesto, Milhano and Salgado (rcBK) [126]; Albacete, Armesto, Milhano, Quiroga Arias and Salgado (AAMQS) [127], both including Balitsky-Kovchegov evolution; Forshaw and Shaw [128] including reggeon exchange only.

4.2.3 Proton-proton cross-section

Overall inclusive differential cross-section for the Drell-Yan production in proton-proton collisions consists of the convolution of PDFs, qN cross-section and some appropriate kinematics [110]

$$\frac{d^4\sigma^{(pp\to l^-l^+X)}}{dM^2dx_Fd^2p_T} = \frac{d\sigma^{(\gamma^*\to l^+l^-)}}{dM^2}\frac{x_1}{x_1+x_2}\int_{x_1}^{1}\frac{d\alpha}{\alpha^2}\Sigma_q\left(f_q\left(\frac{x_1}{\alpha}\right)+f_{\bar{q}}\left(\frac{x_1}{\alpha}\right)\right)\frac{d^3\sigma^{(qN\to\gamma^*X)}}{d(\ln\alpha)d^2p_T}\,, \tag{4.32}$$

where the cross-section for dilepton production reads

$$\frac{d\sigma^{(\gamma^*\to l^+l^-)}}{dM^2} = \frac{\alpha_{EM}}{3\pi M^2}\,. \tag{4.33}$$

Momentum fractions of quarks x_1 and x_2 can be expressed using Feynman x_F or equivalently using rapidity y

$$\begin{aligned} x_1 &= \frac{1}{2}\left(\sqrt{x_F^2+4\tau}+x_F\right) = \sqrt{\tau}\exp(y), \\ x_2 &= \frac{1}{2}\left(\sqrt{x_F^2+4\tau}-x_F\right) = \sqrt{\tau}\exp(-y), \end{aligned} \tag{4.34}$$

where

$$\tau = \frac{M^2+p_T^2}{s} = x_1x_2, \tag{4.35}$$

$$x_F = x_1 - x_2. \tag{4.36}$$

It can be proven, that the upper limit of the integral over α is smaller than one [114]

$$\alpha \leq 1 - \frac{p_T^2}{x_1s - M^2}\,. \tag{4.37}$$

The scale in quark PDFs is taken in the form [129]

$$Q^2 = p_T^2 + (1-x_1)M^2. \tag{4.38}$$

For the case of p_T-integrated qN cross-section which can be used for rapidity distribution or dilepton mass distribution (if experimental data use enough small p_T cut otherwise (4.32) have to be integrated from particular $p_{T,min}$ to $p_{T,max}$), inclusive differential cross-section reads

$$\frac{d^2\sigma^{(pp\to l^-l^+X)}}{dM^2dx_F} = \frac{d\sigma^{(\gamma^*\to l^+l^-)}}{dM^2}\frac{x_1}{x_1+x_2}\int_{x_1}^{1}\frac{d\alpha}{\alpha^2}\Sigma_q\left(f_q\left(\frac{x_1}{\alpha}\right)+f_{\bar{q}}\left(\frac{x_1}{\alpha}\right)\right)\frac{d\sigma^{(qN\to\gamma^*X)}}{d(\ln\alpha)}\,, \tag{4.39}$$

where momentum fractions x_1 and x_2 are same as in (4.34) but

$$\tau = \frac{M^2}{s} = x_1 x_2. \tag{4.40}$$

And the scale is taken in the form

$$Q^2 = M^2. \tag{4.41}$$

For the direct photons the Eq. (4.32) is used with $M = 0$ and $\frac{d\sigma(\gamma^* \to l^+ l^-)}{dM^2} = 1$.

Next useful relations for cross-section are presented in Appendix A.4.

4.3 Nuclear target

This section describes basic formula for proton-nucleus cross-section and all formulas for quark-nucleus cross-sections.

4.3.1 Quark-nucleus cross-section

The calculation of proton-nucleus and nucleus-nucleus collisions is the main asset of the color dipole approach that naturally incorporates some nuclear effects such as nuclear shadowing or Cronin enhancement.

The dynamics and the magnitude of these effects are controlled by the coherence length l_c. In the term of coherence length, the theory can be simplified for limits, short coherence length or long coherence length limits otherwise one should use the Green function formalism or phenomenological formfactor. All these aspects will be described in the following chapters.

Note that all these methods are applied for the lowest Fock state $|q\gamma^*\rangle$ only. So, they include just quark effects such as quark shadowing or quark broadening. However, the nuclear target is also sensitive to higher Fock states e.g. $|q\gamma^* G\rangle, |q\gamma^* 2G\rangle, ...$ that lead to the next effects such as gluon shadowing. The influence of higher Fock states will be commented in the section about the gluon shadowing.

All these methods have a property that is common to all and is typical for the color dipole approach. This feature is called the color transparency and is connected to the transverse separation of the fluctuation. If the dipole cross-section $\sigma_{q\bar{q}}^N$ is small and goes to zero then the quark-nucleus cross-section is equal to the A-times quark-nucleon cross-section and the nucleus seems to be transparent for the projectile. On the other hand, if the dipole cross-section $\sigma_{q\bar{q}}^N$ is large then the probability of the interaction with the surface nucleons is the highest. These surface nucleons shadow the inner nucleons where the color field regenerate and is ready to the next interaction again far behind the nucleus.

4.3.1.1 Coherence length

For the nuclear target in the color dipole picture, the time that the projectile is creating e.g. $|q\gamma^*\rangle$ Fock state has to be studied. This time, when the projectile is frozen in $|q\gamma^*\rangle$ fluctuation, is called coherence time t_c controlled by the uncertainty relation, and can be interpreted as the lifetime of the corresponding Fock state. Assuming that projectile moves at the speed of light the coherence length can be defined as $l_c = t_c c$.

Coherence time or length controls the number of scatterings of the projectile with the nuclear target and, therefore, the magnitude of various nuclear effects. These nuclear effects has an origin in the coherent interaction of the nucleons [130, 131]. It is useful to distinguish two limiting cases in which the theory simplifies:

Short coherence length (SCL). In the SCL limit, the coherence length l_c becomes smaller than inter-particle spacing in the nucleus $l_c < 1 \div 2$ fm, where, consequently, the fluctuation has a time to interact only with one nucleon. Thus, all nucleons contribute equally to the cross-section. This is the so-called Bethe-Heitler regime [132].

Long coherence length (LCL). The LCL limit corresponds to the case when the coherence length is greater than nuclear radius, $l_c > R_A$. In this case, the projectile interacts with the whole nucleus at the surface. This region corresponds to the Landau-Pomeranchuk-Migdal effect [2, 3]. The shadowing and antishadowing are maximal.

Regions between the SCL and LCL are generally more difficult to express. The most strict approach is the Green function method [133, 134] that will be described in this chapter. Another, more simple approach, is based on a simple interpolation between the SCL and LCL limits using the longitudinal formfactor $F_A(q_c, b)$ where $q_c = 1/l_c$ corresponds to the longitudinal momentum transferred in the reaction [114, 130, 135].

The coherence length in the case of the Drell-Yan process for the $|q\gamma^*\rangle$ fluctuation is given by the uncertainty relation

$$l_c = \frac{2E_q}{M_{q\gamma}^2}\,, \tag{4.42}$$

where E_q and m_q refer to the energy and mass of the projectile quark, and $M_{q\gamma}$ is the effective mass of the $|q\gamma^*\rangle$ fluctuation

$$M_{q\gamma}^2 = \frac{M^2}{1-\alpha} + \frac{m_q^2}{\alpha} + \frac{p_T^2}{\alpha(1-\alpha)}\,, \tag{4.43}$$

where M is a virtual photon mass (corresponds to the dilepton pair mass), p_T is the transverse momentum of the photon, and α is the light-cone momentum fraction of the projectile quark carried by the photon. After some algebra assuming $E_q = \frac{x_1}{\alpha} E_p$ where x_1 is a light-cone momenta of the projectile proton taken by the photon, E_p is the energy of incoming proton related to the CMS invariant energy $s = 2m_N^2 + 2E_p m_N \sim 2E_p m_N$, and by using of the relation $x_1 x_2 = \frac{M^2+p_T^2}{s}$ the final formula for the coherence length can be obtained

$$l_c = \frac{1}{2m_N x_2} \frac{(M^2+p_T^2)(1-\alpha)}{(1-\alpha)M^2 + \alpha^2 m_q^2 + p_T^2} \,. \tag{4.44}$$

It can be shown [130] that the mean coherence length has a form

$$\langle l_c \rangle = \frac{1}{2m_N x_2} \tag{4.45}$$

leading to the scaling of coherence effects with x_2 used in the QCD based factorization models.

In contrast, in the target rest frame this scaling is more complicated. Assuming limit case $x_1 \to 1$, where $\alpha > x_1$, leads to $l_c \to 0$ as follow from (4.44) where the dominator suppress the mean coherence length, and means that nuclear effects vanish.

4.3.1.2 Long coherence length

The long coherence length limit, as was mentioned above, corresponds to the case when the coherence length is greater than nuclear radius, $l_c > R_A$. This allows to projectile in the coherent state to experience multiple rescatterings inside the nucleus without producing any on-shell particles.

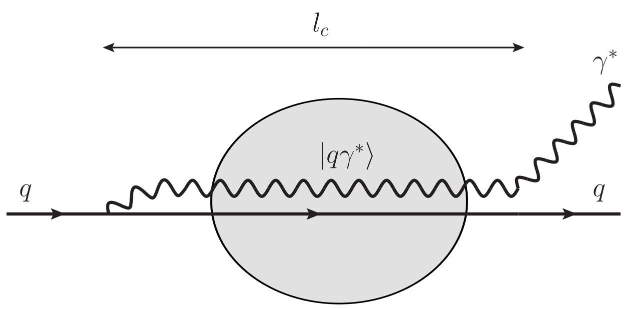

Figure 4.4: The sketch of long coherence length limit.

The LCL limit corresponds to the situation when the fluctuation arises long before the projectile quark enters the nuclear target, and the decoherence occurs far behind the nucleus. All nucleons in the nucleus having the same impact parameter participate coherently in the interaction with the projectile, as shown in Fig. 4.4. In terms of Fock components it can be assumed that the transverse separation ρ of the fluctuation is fixed, and does not vary during the propagation through the nucleus in the LCL limit corresponding to high energy interaction.

It was proven in [108] that if the fluctuation with constant transverse separation in the impact parameter space is an eigenstate of the interaction, the cross-section can be calculated by replacing the dipole cross-section on nucleon $\sigma^N_{q\bar{q}}$ with the dipole cross-section on the nucleus $\sigma^A_{q\bar{q}}$. The $\sigma^A_{q\bar{q}}$ can be calculated using the Glauber eikonalization [5, 112]

$$\sigma^N_{q\bar{q}}(\alpha\rho, x_2) \Rightarrow \sigma^A_{q\bar{q}}(\alpha\rho, x_2) = 2\int d^2b\left(1-\left(1-\frac{1}{2A}\,\sigma^N_{q\bar{q}}(\alpha\rho, x_2)T_A(b)\right)^A\right), \tag{4.46}$$

where $T_A(b)$ is the nuclear thickness function.

4.3.1.3 Short coherence length

The short coherence length limit can be used for the cases where the coherence length is shorter than the inter-nucleon separation, $l_c < 1 \div 2$ fm. The lifetime of the fluctuation is short, and is able to interact with one nucleon inside the nucleus only, so, nucleons cannot act coherently on it. In comparison with the LCL limit, the transverse separation is not fixed, but it varies with every new creation of the fluctuation. Therefore, the Glauber eikonalization that require fixed transverse separation cannot be used. The result is that there is no shadowing in this limit.

More details of this theory can be found in [34, 131] or you can see [114] for the review. Shortly, the final formula for the SCL limit reads

$$\sigma^{qA}(\alpha, \vec{p}_T) = \frac{1}{(2\pi)^2}\int d^2k_T\, d^2r_T\, e^{-\frac{1}{4}b_0^2r_T^2}e^{-\frac{1}{4}\sigma^N_{q\bar{q}}(r_T,x_q)\langle T_A\rangle}\sigma^{qN}(\alpha, |\vec{p}_T-\alpha\vec{k}_T|), \tag{4.47}$$

where σ^{qA} and σ^{qN} denote for quark-nucleus and quark-nucleon cross-section, respectively. $b_0^2 = \frac{2}{3\pi\langle r^2_{ch}\rangle}$ stands for the mean value of the primordial transverse momentum squared of the quark, $\langle r^2_{ch}\rangle = 0.79 \pm 0.03$ fm represents the mean square charge radius of a proton, x_q is a fraction of the proton momenta carried by the quark and $\langle T_A\rangle$ is the average thickness function defined as

$$\langle T_A\rangle = \frac{1}{A}\int d^2b\, T_A^2(b). \tag{4.48}$$

4.3.1.4 Green function technique

The Green function technique [112] represents an universal method how to describe interactions with the nuclear target for whole kinematical region in terms of the coherence length. As can be seen in Figs. 4.5 and 4.6, this method should be primary applied mainly for lower energies at RHIC, for forward rapidities at FNAL fix-target experiments or for planned experiment e.g. AFTER@LHC [136] which would use the proton and nuclear beam from LHC for various nuclear fix targets. Otherwise, limiting cases of the LCL and SCL limits that have simpler form can be used in the case of Drell-Yan process or production of direct photons. The Green function formalism is also important for the calculation of the gluon shadowing (see Chapter 4.3.1.5) where dominant scales are small and, hence, the coherence length has to be treated exactly.

Besides treating the coherence length exactly, the Green function framework has next advantages and benefits. As will be described later, the Green function contains a potential that describes the absorption in the medium. The absorption is less important in the case of the Drell-Yan process and direct photons, but it has a much greater importance for the production of hadrons e.g. vector mesons [137]. Further, the Green function formalism is used in DIS where the lowest Fock state contains a pair $q\bar{q}$ and, therefore, the interaction between them is introduced [113, 133, 134, 138].

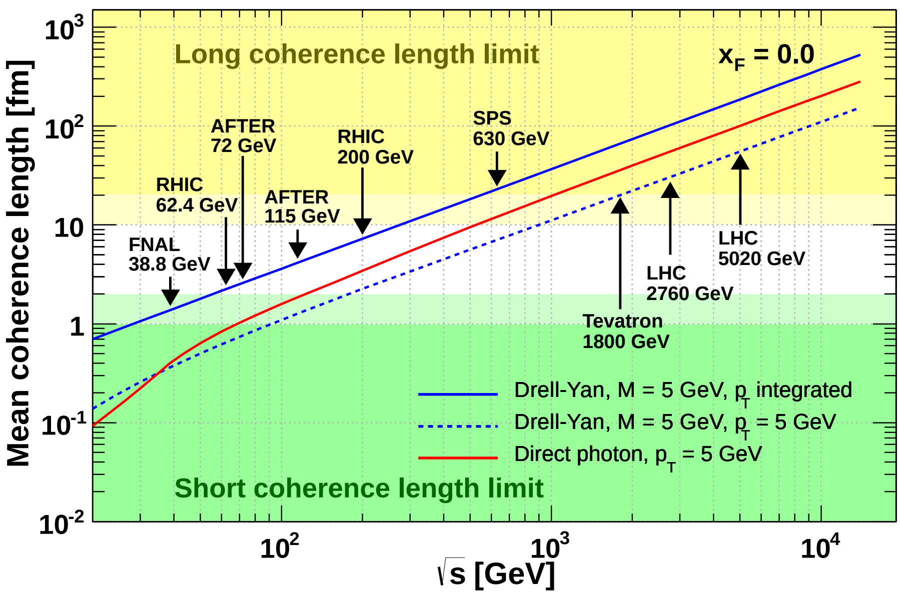

Figure 4.5: The mean coherence length for Drell-Yan and direct photon production at $x_F = 0.0$.

The quark-nucleus cross-section using the Green function technique consists of two

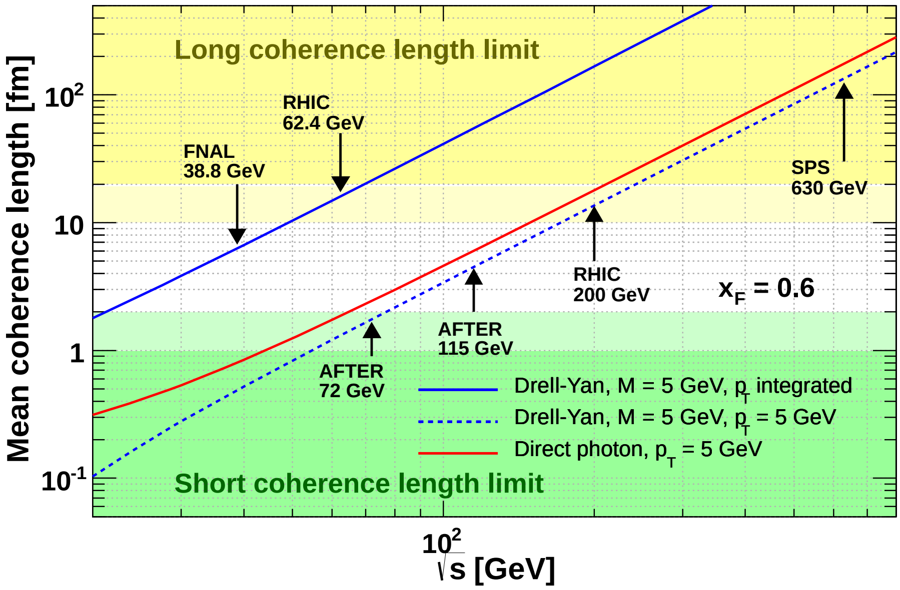

Figure 4.6: The mean coherence length for Drell-Yan and direct photon production at $x_F = 0.6$.

parts

$$
\begin{aligned}
\frac{d\sigma^{(qA\to\gamma X)}}{d(\ln\alpha)} &= A\frac{d\sigma^{(qp\to\gamma X)}}{d(\ln\alpha)} - \frac{d\Delta\sigma^{(qA\to\gamma X)}}{d(\ln\alpha)} \\
&= A\frac{d\sigma^{(qp\to\gamma X)}}{d(\ln\alpha)} - \frac{1}{2}\,\mathrm{Re}\int d^2b\int_{-\infty}^{\infty}dz_1\int_{z_1}^{\infty}dz_2\int d^2\rho_1\,d^2\rho_2 \\
&\times\ \Psi^*_{\gamma^* q}(\alpha,\vec{\rho}_2)\rho_A(b,z_2)\sigma^N_{q\bar{q}}(\alpha\rho_2)G(\vec{\rho}_2,z_2|\vec{\rho}_1,z_1) \\
&\times\ \rho_A(b,z_1)\sigma^N_{q\bar{q}}(\alpha\rho_1)\Psi_{\gamma^* q}(\alpha,\vec{\rho}_1),
\end{aligned}
\tag{4.49}
$$

where the Green function $G(\vec{\rho}_2, z_2|\vec{\rho}_1, z_1)$ fulfills the two dimensional Schrödinger equation

$$
\left[i\frac{\partial}{\partial z_2} + \frac{\Delta(\vec{\rho}_2)-\eta^2}{2E_q\alpha(1-\alpha)} + V(b,\vec{\rho}_2,z_2)\right]G(\vec{\rho}_2,z_2|\vec{\rho}_1,z_1) = i\delta(z_2-z_1)\delta^2(\vec{\rho}_2-\vec{\rho}_1). \tag{4.50}
$$

Second term on l.h.s. is analogous to the kinetic term in the Schrödinger equation and cares about the phase shift for the propagating $q\gamma^*$ fluctuation. The two dimensional Laplacian acts on the transverse coordinate, the kinetic term $(\Delta(\vec{\rho}_2)-\eta^2)/2E_q\alpha(1-\alpha)$ takes care of the varying effective mass of the $q\gamma^*$ pair, and imaginary potential $V(b,\vec{\rho}_2,z_2)$ reads

$$
V(b,\vec{\rho},z) = -\frac{i}{2}\,\rho_A(b,z)\sigma^N_{q\bar{q}}(\alpha\rho). \tag{4.51}
$$

This imaginary potential, similarly to the Glauber theory, accounts for all higher order scattering terms. One can see a similarity with the optical theorem where the absorption in the medium is also described by the imaginary potential.

For convenience, the factor $\exp(-iq_L^{min}(z_2-z_1))$ that describes the longitudinal motion is included into the Green function $G(\vec{\rho}_2, z_2|\vec{\rho}_1, z_1)$ [113].

The second term in (4.49) can be interpreted as follow, see Fig. 4.7. At the point z_1 the projectile quark creates a $|q\gamma^*\rangle$ state with an initial separation $\vec{\rho}_1$. Then the $|q\gamma^*\rangle$ fluctuation propagates through the nucleus along arbitrary curved trajectories which are summed over, and arrives at the point z_2 with a transverse separation $\vec{\rho}_2$. The initial and the final separations are controlled by the light-cone wave functions of the $|q\gamma^*\rangle$ Fock state of the projectile $\Psi_{q\gamma^*}(\alpha\vec{\rho})$. During the propagation through the nucleus the $|q\gamma^*\rangle$ Fock state interacts with bound nucleons via the dipole cross-section $\sigma^N_{q\bar{q}}(\alpha\vec{\rho})$ which depends on the local transverse separation $\vec{\rho}$.

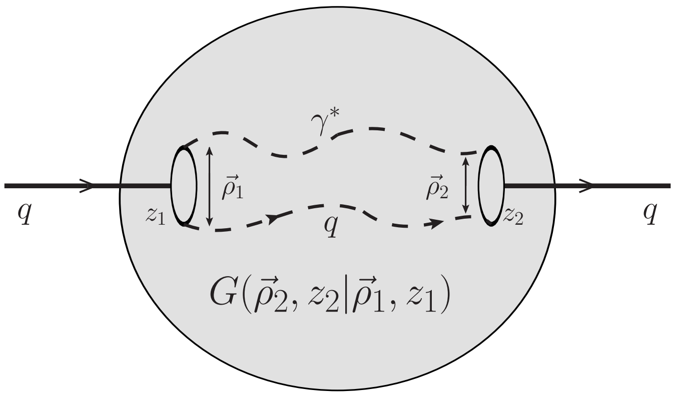

Figure 4.7: Propagation of the $\gamma^* q$ fluctuation through the nucleus for the finite coherence length that is described by the Green function $G(\vec{\rho}_2, z_2|\vec{\rho}_1, z_1)$

If the high energy limit $E_q \to \infty$ is considered, the kinetic term in (4.50) can be neglected resulting in

$$G(\vec{\rho}_2, z_2|\vec{\rho}_1, z_1)|_{E_q\to\infty} = \delta^2(\vec{\rho}_1 - \vec{\rho}_2) \exp\left[i\int_{z_1}^{z_2} dz\, V(b, \vec{\rho}_2, z)\right], \qquad (4.52)$$

where it follows that the transverse separation is fixed. Putting the (4.52) into (4.49) the case of LCL limit can be obtained [112].

The Schrödinger equation (4.50) with the potential (4.51) can be solved numerically or analytically for small-ρ approximation.

The quark-nucleus cross-section with the p_T dependence is much more complex [112]

$$\begin{aligned}
\frac{d^3\sigma^{(qA\to\gamma^* X)}}{d(\ln\alpha)\,d^2p_T} &= \frac{\alpha_{EM}}{(2\pi)^4 4E_q^2(1-\alpha)^2}\,2\mathrm{Re}\int_{-\infty}^{\infty}dz_1\int_{z_1}^{\infty}dz_2\int d^2b\,d^2k_T\,d^2\rho_1\,d^2\rho_2\\
&\times\ \exp\left[i\alpha\vec{p}_2\cdot\vec{\rho}_2-i\alpha\vec{p}_1\cdot\vec{\rho}_1-i\int_{z_2}^{\infty}dz\,V(b,\vec{\rho}_2,z)-i\int_{-\infty}^{z_1}dz\,V(b,\vec{\rho}_1,z)\right]\\
&\times\ \hat{\Gamma}^*(\vec{\rho}_2)\hat{\Gamma}(\vec{\rho}_1)G(\vec{\rho}_2,z_2|\vec{\rho}_1,z_1), \qquad (4.53)
\end{aligned}$$

respectivelly

$$\begin{aligned}
\frac{d^3\sigma^{(qA\to\gamma^* X)}}{d(\ln\alpha)\,d^2p_T} &= \frac{\alpha^2}{(2\pi)^4}\left\{\mathrm{Re}\int_{-\infty}^{\infty}dz\int d^2b\,d^2k_T\,d^2\rho_1\,d^2\rho_2\,d^2\rho\right.\\
&\times\ \exp\left[i\alpha\vec{p}_2\cdot\vec{\rho}_2-i\alpha\vec{p}_1\cdot\vec{\rho}_1-i\int_{z}^{\infty}dz'\,V(b,\vec{\rho}_2,z')-i\int_{-\infty}^{z}dz'\,V(b,\vec{\rho}_1,z')\right]\\
&\times\ \Psi^{T,L^*}_{\gamma^*q}(\vec{\rho}_2-\vec{\rho},\alpha)i\left[2V(b,\vec{\rho},z)-V(b,\vec{\rho}_1,z)-V(b,\vec{\rho}_2,z)\right]\Psi^{T,L}_{\gamma^*q}(\vec{\rho}_1-\vec{\rho},\alpha)\\
&+\ 2\mathrm{Re}\int_{-\infty}^{\infty}dz_1\int_{z_1}^{\infty}dz_2\int d^2b\,d^2k_T\,d^2\rho_1\,d^2\rho_2\,d^2\rho_1'\,d^2\rho_2'\\
&\times\ \exp\left[i\alpha\vec{p}_2\cdot\vec{\rho}_2-i\alpha\vec{p}_1\cdot\vec{\rho}_1-i\int_{z_2}^{\infty}dz\,V(b,\vec{\rho}_2,z)-i\int_{-\infty}^{z_1}dz\,V(b,\vec{\rho}_1,z)\right]\\
&\times\ \Psi^{T,L^*}_{\gamma^*q}(\vec{\rho}_2-\vec{\rho}_2',\alpha)\left[V(b,\vec{\rho}_2,z_2)-V(b,\vec{\rho}_2',z_2)\right]G(\vec{\rho}_2',z_2|\vec{\rho}_1',z_1)\\
&\times\ \left.\left[V(b,\vec{\rho}_1,z_1)-V(b,\vec{\rho}_1',z_1)\right]\Psi^{T,L}_{\gamma^*q}(\vec{\rho}_1-\vec{\rho}_1',\alpha)\right\}, \qquad (4.54)
\end{aligned}$$

where

$$\begin{aligned}
\vec{p}_1 &= -\frac{\vec{p}_T}{\alpha}\ ,\\
\vec{p}_2 &= \vec{k}_T-\frac{1-\alpha}{\alpha}\,\vec{p}_T\ , \qquad (4.55)
\end{aligned}$$

and $\vec{k}_T$ is the transverse momentum of the quark.

In (4.53) operators $\widehat{\Gamma}$ read

$$\widehat{\Gamma}(\vec{\rho})=\chi_f^\dagger\left[2M(1-\alpha)+i\,m_f\,\alpha^2\,(\vec{n}\times\vec{\sigma})\cdot\vec{e^*}+\alpha\,(\vec{\sigma}\times\vec{\nabla}_\rho)\cdot\vec{e^*}-i\,(2-\alpha)\,\vec{\nabla}_\rho\cdot\vec{e^*}\right]\chi_i. \qquad (4.56)$$

Solution for small-ρ approximation

As was mentioned in Section 4.2.2, if the mean transverse separation is small, the dipole cross-section can be approximated in squared form $\sigma^N_{q\bar{q}}(\alpha\rho)=C\alpha^2\rho^2$. Moreover, expressions for qN or qA can be considerable simplified if the nuclear density function is approximated by the step function

$$\rho_A(b,z)=\rho_0\theta(R_A^2-b^2-z^2), \qquad (4.57)$$

where the constant density $\rho_0 = 0.16\,\mathrm{fm}^{-3}$ is used. This approximation works remarkable well, especially for heavy nuclei [139].

Then, the potential in (4.51) has a form

$$V(b,\vec{\rho},z) \approx -\frac{i}{2}\,C\alpha^2\rho^2\rho_A\theta(R_A^2 - b^2 - z^2). \tag{4.58}$$

and the Schrödinger equation (4.50) can be solved analytically as two-dimensional harmonic oscillator (2DHO) [140]

$$G(\vec{\rho}_2,z_2|\vec{\rho}_1,z_1) = \frac{a\,\mathrm{e}^{-iq_L^{min}\Delta z}}{2\pi\sinh\left(\omega\Delta z\right)}\;\exp\left\{-\frac{a}{2}\left[(\rho_1^2+\rho_2^2)\coth(\omega\Delta z) - \frac{2\vec{\rho}_1\cdot\vec{\rho}_2}{\sinh(\omega\Delta z)}\right]\right\}, \tag{4.59}$$

where $\Delta z = z_2 - z_1$ and 2DHO variables read

$$a = (-1+\mathrm{i})\sqrt{\rho_A E_q\alpha^3(1-\alpha)C/2}, \tag{4.60}$$

$$\omega = -(1+\mathrm{i})\sqrt{\rho_A C\alpha/(2E_q(1-\alpha))}. \tag{4.61}$$

Longitudinal momentum q_L^{min} has form

$$q_L^{min} = \frac{\eta^2}{2E_q\alpha(1-\alpha)}\,. \tag{4.62}$$

where E_q labels for the energy of the incoming quark

$$E_q = \frac{x_1}{\alpha}\,\frac{s-2M_N^2}{2M_N}\,. \tag{4.63}$$

With this analytical solution of the Green function the quark-nucleus cross-section (4.54) can be simplified. One solution was presented by Raufeisen [113] where the final solution is divided into six integrals. In Appendix A.3 we present own solution consists of two, more complex, terms.

Exact numerical solution

The solution for the arbitrary dipole cross-section parametrization and real nuclear density cannot be obtain by any nice analytical form for the Green function, but the numerical solution of the two-dimensional differential Schrödinger equation (4.50) have to be applied. This solution was published for first time in [49] for the DIS. We extended this solution for the Drell-Yan process and direct photon production.

First, the procedure of the numerical solution will be shown for the p_T-integrated qA cross-section (4.49) and analytical procedure can be applied for the p_T-dependent qA cross-section (4.54) with more complicated boundary conditions.

For the process of numerical solution it is desirable to rewrite (4.49) in order to get rid of delta functions in (4.50) that are inconvenient for the numerical solution

$$g_1(\vec{\rho}_2, z_2|z_1) = \int d^2\rho_1\, \mathrm{K}_0(\eta\rho_1)\sigma^N_{q\bar{q}}(\alpha\rho_1) G(\vec{\rho}_2, z_2|\vec{\rho}_1, z_1), \tag{4.64}$$

$$\frac{\vec{\rho}_2}{\rho_2}\cdot \vec{g}_2(\vec{\rho}_2, z_2|z_1) = \int d^2\rho_1\, \mathrm{K}_1(\eta\rho_1)\sigma^N_{q\bar{q}}(\alpha\rho_1)\frac{\vec{\rho}_1}{\rho_1} G(\vec{\rho}_2, z_2|\vec{\rho}_1, z_1). \tag{4.65}$$

These reformulated Green functions fulfil following evolution equations

$$i\frac{\partial}{\partial z_2}\, g_1(\vec{\rho}_2, z_2|z_1) = \left[\frac{1}{2\mu_{q\bar{q}}}\left(\eta^2 - \frac{\partial^2}{\partial^2\rho_2} - \frac{1}{\rho_2}\frac{\partial}{\partial\rho_2}\right) + V(z_2, \vec{\rho}_2, \alpha)\right] g_1(\vec{\rho}_2, z_2|z_1), \tag{4.66}$$

$$i\frac{\partial}{\partial z_2}\, g_2(\vec{\rho}_2, z_2|z_1) = \left[\frac{1}{2\mu_{q\bar{q}}}\left(\eta^2 - \frac{\partial^2}{\partial^2\rho_2} - \frac{1}{\rho_2}\frac{\partial}{\partial\rho_2} + \frac{1}{\rho_2^2}\right) + V(z_2, \vec{\rho}_2, \alpha)\right] g_2(\vec{\rho}_2, z_2|z_1) \tag{4.67}$$

with boundary conditions

$$g_1(\vec{\rho}_2, z_2|z_1)|_{z_1=z_2} = \mathrm{K}_0(\eta\rho_2)\sigma^N_{q\bar{q}}(\alpha\rho_2), \tag{4.68}$$

$$g_2(\vec{\rho}_2, z_2|z_1)|_{z_1=z_2} = \mathrm{K}_1(\eta\rho_2)\sigma^N_{q\bar{q}}(\alpha\rho_2). \tag{4.69}$$

The second term in (4.49) has a form

$$\begin{aligned}\frac{d\Delta\sigma^{(qA\to\gamma X)}}{d(\ln\alpha)} &= \alpha_{EM}\mathrm{Re}\int db\, b\int_{-\infty}^{\infty} dz_1 \int_{z_1}^{\infty} dz_2 \int d\rho_2\, \rho_2 \rho_A(b, z_1)\rho_A(b, z_2)\sigma^N_{q\bar{q}}(\alpha\rho_2)\\ &\times \left[(1+(1-\alpha)^2)\eta^2 \mathrm{K}_1(\eta\rho_2) g_2(\vec{\rho}_2, z_2|z_1)\right.\\ &+ \left.(m_f^2\alpha^4 + 2M^2(1-\alpha)^2)\mathrm{K}_0(\eta\rho_2) g_1(\vec{\rho}_2, z_2|z_1)\right].\end{aligned} \tag{4.70}$$

The time-dependent two-dimensional Schrödinger equations (4.66) and (4.67) by a modification of the method based on the Crank-Nicholson algorithm [141–143]. Details of this method for numerical solution are presented in Appendix A in [49].

4.3.1.5 Gluon shadowing

So far, all calculations within the color dipole approach contained the lowest Fock state $|q\gamma^*\rangle$ including a quark only. By introducing of higher Fock states containing gluons, $|q\gamma^* G\rangle, |q\gamma^* 2G\rangle, \ldots$, new effects in connection with gluons can be included.

The correction on the gluon shadowing within the color dipole approach was calculated in [5] or see [114] for detailed review. The main idea and the most important parts of the gluon shadowing calculation will be summarized. First, it is assumed that the gluon shadowing should be universal, because this shadowing corresponds to the gluon part of the particular Fock state, and can be calculated i.e. from DIS where this calculation can be made easily. Second, the factor $R_G(x, Q^2)$ is calculated in the light-cone Green function technique [120], described in chapter 4.3.1.4 where the $|q\bar{q}G\rangle$ Fock state of a longitudinally polarized photons is considered. This can be understood in the following way, the light-cone wave function for the transition $\gamma_L^* \to q\bar{q}$ does not allow for large, aligned jet configurations. Then, all $q\bar{q}$ dipoles from longitudinal photons have size $\sim 1/Q^2$ and the gluon can propagate relatively far from the $q\bar{q}$-pair, therefore this configuration can be approximated by the $|GG\rangle$ Fock state. Consequently, the distance of the gluon from the $q\bar{q}$ dipole in the impact parameter space determines the magnitude of the gluon shadowing. From the experimental data the mean separation size was set to $\rho_0 = 0.3$ fm [5] which is also the limit where this approximation is valid. Finally, it has to be assumed that $Q^2 \gg 1/\rho_0^2$, otherwise the $q\bar{q}$ dipole is not point-like in comparison to the size of $|q\bar{q}G\rangle$ Fock state.

Next, it is assumed that the gluon shadowing is implemented as the modification of the dipole cross-section

$$\sigma_{q\bar{q}}^N(\alpha\rho, x) \Rightarrow \sigma_{q\bar{q}}^N(\alpha\rho, x) R_G(x, Q^2), \tag{4.71}$$

where $R_G(x, Q^2)$ stands for gluon shadowing factor

$$R_G(x, Q^2) = \frac{G_A(x, Q^2)}{A G_N(x, Q^2)} \sim 1 - \frac{\Delta\sigma_L^{\gamma A}(x, Q^2)}{A\sigma_L^{\gamma p}(x, Q^2)}, \tag{4.72}$$

where $\sigma_L^{\gamma p}$ is the DIS cross-section where the longitudinal polarization is considered because of large Q^2 where the longitudinal polarization dominates.

The total photoabsorption cross-section $\Delta\sigma^{\gamma A} = \sigma_{tot}^{\gamma A} - A\sigma^{\gamma p}$ can be calculated from the diffractive dissociation cross-section $\gamma N \to XN$ [144–146] where at the lowest order the cross-section reads

$$\begin{aligned} \Delta\sigma^{\gamma A} &= 8\pi \mathrm{Re} \int d^2 \int_{-\infty}^{\infty} dz_1 \int_{-\infty}^{\infty} dz_2 \Theta(z_2 - z_1) \rho_A(b, z_1) \rho_A(b, z_2) \\ &\times \int dM_X^2 e^{-iq_l(z_2 - z_1)} \left. \frac{d^2\sigma(\gamma N \to X\,N)}{dM_X^2 dq_T^2} \right|_{q_T=0}, \end{aligned} \tag{4.73}$$

where $q_L = (Q^2 + M_X^2)/2E_\gamma$ is the longitudinal and q_T is the transversal momentum transfer, E_γ is the photon energy in the target rest frame, M_X is an invariant mass of the particular excited state, $\rho_A(b, z)$ is the nuclear density and z_1, z_2 are longitudinal coordinates. And the diffractive cross-section after the evaluation reads

$$
\begin{aligned}
& 8\pi\,\mathrm{Re}\int dM_X^2\, e^{-iq_L z}\left.\frac{d^2\sigma(\gamma N\to XN)}{dM_X^2 dq_T^2}\right|_{q_T=0} \\
= & \;\mathrm{Re}\int_0^1 d\alpha_q\int_x^{0.1} d\ln\alpha_G \frac{16\alpha_{EM}C_{GG}^2\alpha_S(Q^2)}{3\pi^2Q^2\tilde{b}^2}\sum_q Z_q^2 \\
\times & \;((1-2\xi-\xi^2)e^{-\xi}+\xi^2(3+\xi)E_1(\xi) \\
\times & \left(\frac{t}{w}+\frac{\sinh(\Omega\Delta z)}{t}\ln\left(1-\frac{t^2}{u^2}\right)+\frac{2t^3}{uw^2}+\frac{t\sinh(\Omega\Delta z)}{w^2}+\frac{4t^3}{w^3}\right), \qquad (4.74)
\end{aligned}
$$

where

$$\Delta z = z_2 - z_1, \qquad (4.75)$$

$$\Omega = \frac{iB}{\alpha_G(1-\alpha_G)\nu}, \qquad (4.76)$$

$$B^2 = \tilde{b}^4 - i\alpha_G(1-\alpha_G)\nu C_{eff}\rho_A, \qquad (4.77)$$

$$\nu = \frac{Q^2}{2m_N x}, \qquad (4.78)$$

$$\xi = ixm_N\Delta z, \qquad (4.79)$$

$$t = \frac{B}{\tilde{b}^2}, \qquad (4.80)$$

$$u = t\cosh(\Omega\Delta z)+\sinh(\Omega\Delta z), \qquad (4.81)$$

$$w = (1+t^2)\sinh(\Omega\Delta z)+2t\cosh(\Omega\Delta z), \qquad (4.82)$$

$$\tilde{b} = (0.65\mathrm{GeV})^2+\alpha_G Q^2. \qquad (4.83)$$

The gluon-gluon-nucleon cross-section is parameterized in the form

$$\sigma_{GG}^N(\rho,\tilde{x}) = C_{eff}(\tilde{x})\rho^2, \qquad (4.84)$$

where $\tilde{x} = x/\alpha_G$. To prevent a situation $\tilde{x} > 0.1$ for $\alpha \to x$, where the dipole formulation is no longer valid, the following prescription is employed

$$\tilde{x} = \min(x/\alpha, 0.1). \qquad (4.85)$$

The parameter C_{eff} is then determined from the asymptotic condition

$$\frac{\int d^2b\, d^2\rho|\Psi_{qG}(\rho)|^2(1-\exp(-\frac{1}{2}C_{eff}(\tilde{x})\rho^2T_A(b)))}{\int d^2\rho|\Psi_{qG}(\rho)|^2C_{eff}(\tilde{x})\rho^2} \qquad (4.86)$$

$$= \frac{\int d^2b\, d^2\rho|\Psi_{qG}(\rho)|^2(1-\exp(-\frac{9}{8}\sigma_{q\bar{q}}^N(\rho,\tilde{x})T_A(b)))}{\int d^2\rho|\Psi_{qG}(\rho)|^2\frac{9}{4}\sigma_{q\bar{q}}^N(\rho,\tilde{x})}, \qquad (4.87)$$

where the light-cone wave function for radiation of a quark from a gluon reads [120]

$$|\Psi_{qG}(\rho)|^2 = \frac{4\alpha_S(Q^2)}{3\pi^2}\frac{\exp\left(-\tilde{b}^2\rho^2\right)}{\rho^2}. \qquad (4.88)$$

Finally, the scale was set to

$$Q^2 = \frac{1}{\rho^2} + 4\ \mathrm{GeV}^2. \tag{4.89}$$

An example of the gluon shadowing on lead as function of momentum fraction x integrated over impact parameter b is in Fig. 4.8 for different scales and in Fig. 4.9 for different centralities.

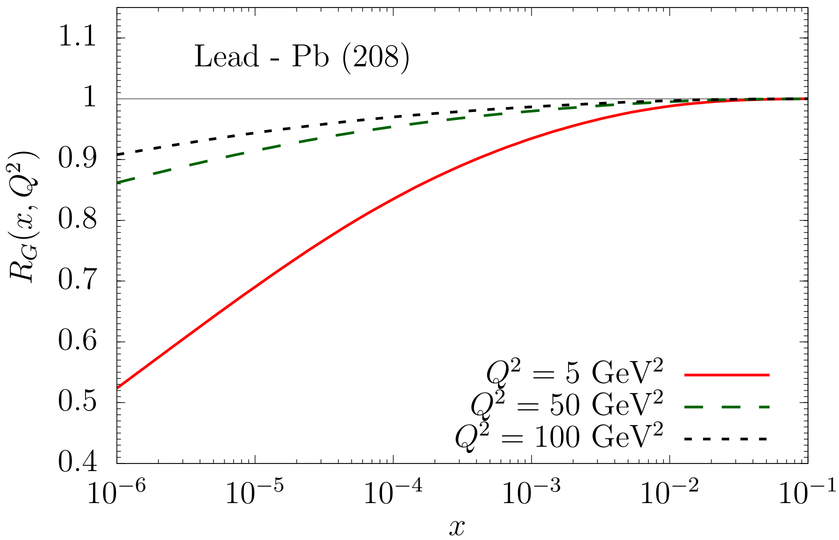

Figure 4.8: Gluon shadowing factor integrated over b for different scales Q^2.

4.3.2 Proton-nucleus cross-section

The overall proton-nucleus cross-section for Drell-Yan production is similar to proton-proton cross-section 4.2.3

$$\frac{d^4\sigma^{(pA\to l^- l^+ X)}}{dM^2 dx_F d^2 p_T} = \frac{d\sigma^{(\gamma^*\to l^+ l^-)}}{dM^2} \frac{x_1}{x_1 + x_2} \int_{x_1}^{1} \frac{d\alpha}{\alpha^2} \Sigma_q \left(f_q \left(\frac{x_1}{\alpha} \right) + f_{\bar{q}} \left(\frac{x_1}{\alpha} \right) \right) \frac{d^3\sigma^{(qA\to\gamma^* X)}}{d(\ln\alpha) d^2 p_T}, \tag{4.90}$$

and similarly p_T-integrated proton-nucleus cross-section

$$\frac{d^2\sigma^{(pA\to l^- l^+ X)}}{dM^2 dx_F} = \frac{d\sigma^{(\gamma^*\to l^+ l^-)}}{dM^2} \frac{x_1}{x_1 + x_2} \int_{x_1}^{1} \frac{d\alpha}{\alpha^2} \Sigma_q \left(f_q \left(\frac{x_1}{\alpha} \right) + f_{\bar{q}} \left(\frac{x_1}{\alpha} \right) \right) \frac{d\sigma^{(qA\to\gamma^* X)}}{d(\ln\alpha)}, \tag{4.91}$$

where variables x_1, x_2, Q^2 and others kinematical variables have same form as in Chapter 4.2.3.

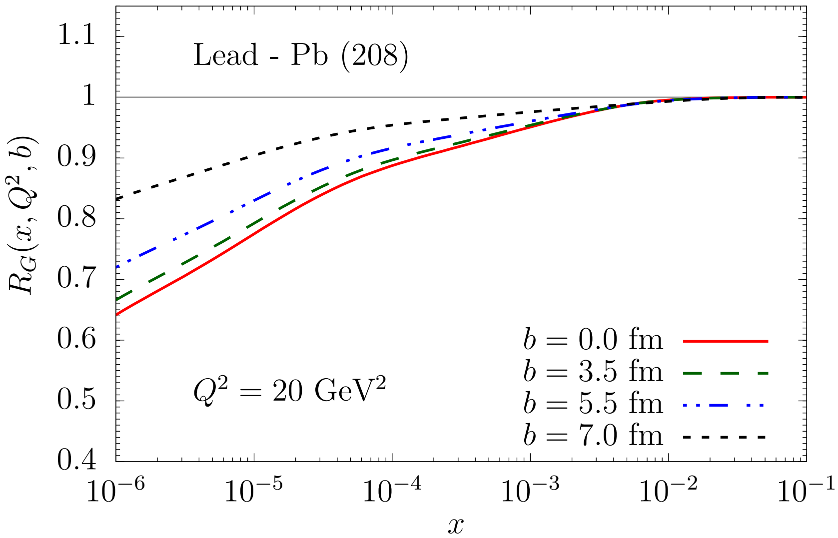

Figure 4.9: Gluon shadowing factor as function of the impact parameter b for different centrality and fixed scale.

At the level of proton-nucleus cross-section one can include other effects such as the isospin effect, Chapter 3.4.4, or the ISI effects, Chapter 3.4.5, or isospin effect, Chapter 3.4.4, in the same way as in QCD based models in the form of the modification of parton distribution functions.

Chapter 5

Results

This chapter provides highlights of results published in papers and proceedings where all achieved results are commented in detail. All publication are also part on this work in Appendix C. In the second part, basic facts and comments on comparison of both models used in this work are written.

5.1 QCD based k_T-factorization model

First two papers [96], [147] focus on hadron production at RHIC and LHC energies. In both, the nuclear shadowing, Cronin effect and ISI effects are studied where in second paper two different dipole cross-sections (GBW and IP-Sat) were used, and the impact on the shape and size of the Cronin effects was compared. Both give predictions for hadron production at forward rapidities where significant suppression due to ISI effects is expected. Third paper [95], apart from first two papers, investigates also lower energies corresponding to fix-target experiments in FNAL.

Next paper [148] also includes direct photons. Direct photons are compared with data from RHIC and LHC, and heavy-ion collisions $Pb + Pb$ and $Au + Au$ were studied where the impact of ISI effects is much greater than in proton-nucleus collisions.

In paper [149] comparison of direct photons production within the QCD based k_T-factorization model and the color dipole approach (provided by J. Cepila) have been done. Both models describe reasonable well data for direct photon production in $p + p$ collisions. The QCD based k_T-factorization model shows better agreement with data in the low-p_T region. This fact is a consequence of an absence of the more precise determination of the dipole cross section in this kinematic region. A significant difference between predictions of the shape and magnitude of the Cronin enhancement from both models was found. It is expected better agreement between both models using more precise recent parameterizations of the dipole cross-section. In the large-p_T region a good agreement of both models was found. Finally, the ISI effects give same results for both models as is expected.

5.2 Color dipole model

The paper [150] that emerged from [151] deals with the Drell-Yan production within the color dipole approach at high energies where the LCL limit can be safely used. The Drell-Yan process next to the virtual photon includes also production of Drell-Yan via the Z^0 boson that gives significant contribution at high dilepton masses, mainly at LHC. In this paper, nuclear effects are studied in p_T, rapidity η and dilepton mass distributions that allow to study kinematical regions where different nuclear effects are dominant. The effects of quark and gluon shadowing, Cronin peak and ISI effects are discussed. Next, the impact of four different dipole cross-sections was investigated. Finally, predictions for Drell-Yan process at RHIC and at forward rapidities at LHC and for dilepton-hadron correlations (provided by V. Goncalves) are provided.

Last proceedings [152], according to which the next paper is in preparation, involves the study of color dipole model using the Green function technique at low energies, below the RHIC. Results for dilepton mass distribution using exact numerical solution and for p_T distribution for solution for squared dipole cross-section and uniform nuclear density are presented. For the first time, prediction for the experiment AFTER@LHC is provided. Also, prediction for the Drell-Yan production at RHIC is also provided where the Green function technique predicts larger Cronin peak than LCL limit.

5.3 Comparison of both models

The goal of this section is to summarize the main advantages and disadvantages for both models. Some comparisons for both models were provided e.g. in [153]. First, advantages(+) and disadvantages(−) are summarized.

QCD based k_T-factorization model:

+ Works well for proton-proton collisions.
+ Based on the first principle, from QCD Lagrangian.
+ Easier calculation of different final states (hadrons, direct photons, jets, ...).
+ Studied for longer time, i.e. a lot of higher order calculations and more Monte Carlo generators.

− For LO the K-factor has to be used as naive compensation of NLO and higher orders.
− Transverse momentum distribution is added phenomenologically.
− Divergence for $p_T \to 0$, out of perturbative region.
− Free choice of factorization and renormalization scales.
− Non-intuitive transition to nuclear target.

Color dipole approach:

+ Works also in non-perturbative regions.
+ Intuitive transition to nuclear target.
+ Naturally includes some nuclear effects.
+ No need of K-factor.

− Strong dependency on dipole cross-section.
− Limitation of dipole cross-section for $x_2 \leq 0.01$.
− More difficult to calculate higher Fock states.

Parameterizations of dipole cross-sections can be improved by the measurement of the unintegrated gluon distribution function. This can be measured e.g. in the ultra-peripheral collisions but much more data are needed. Better prospects for the unintegrated gluon distribution functions are coming from the upcoming electron-ion collider (EIC) program in USA.

Both models interpret nuclear shadowing and Cronin effects within their reference frame. Both models predict Cronin effect at same position in relation to transverse momentum, but they vary in the shape and magnitude in according to dipole cross-section used in case of color dipole approach, or parameters of nuclear broadening, or using of Cronin effects from nuclear PDFs in the case of QCD based models. Usually, predictions of Cronin effect from both models are in agreement with experimental data within their statistical and systematical errors.

More complicated situation arises for nuclear shadowing where one can distinguish even shadowing from quarks and gluons. There can be found greater differences in the determining of the magnitude of shadowing but more data for smaller x_2 are missing.

Finally, mechanism of ISI effects gives same results for both models and can be verified by the future measurements at RHIC, LHC or AFTER@LHC where large forward rapidities will be measured.

Chapter 6

Summary and conclusions

In this work the nuclear effects in proton-nucleus and nucleus-nucleus collisions were studied using both the QCD based k_T-factorization model and the color dipole approach. We analyzed the onset of nuclear shadowing, enhancement (the Cronin effect) and the effective energy loss caused by multiple rescatterings of a parton during its propagation through a medium in production of hadrons, direct photons and Drell-Yan pairs.

The main results, which have been achieved and published, are the following:

- The effects of quantum coherence, the nuclear enhancement and ISI effects were studied in production of hadrons and direct photons within the model based on k_T-factorization and we found a good agreement of our predictions for the nuclear attenuation factor with available experimental data. Due to a nuclear broadening described in terms of the dipole cross-section a parameter-free model was developed that is universal for all energies of collisions where pQCD can be applied.
- In particular, it was demonstrated that the shape of the Cronin effect depends on the parametrization of the dipole cross-section used in calculations and the magnitude of the Cronin peak decreases with the collision energy due a rise of gluon contribution to production cross-section with larger mean transverse momenta.
- We showed that the effective energy loss due to ISI effects are able to describe a strong suppression at large p_T indicated by experimental data. We demonstrated that the Drell-Yan process can be treated as a very effective tool for investigations of net ISI effects at large values of dilepton invariant masses, M, including for the first time the contribution of Z^0 boson to DY cross-section. We performed for the first time corresponding predictions for the nuclear modification factor at large M in various kinematical regions where the coherence effects are not expected and

found a significant suppression that can be tested in the future by experiments at the LHC.

- In order to test theoretical uncertainties the magnitude of nuclear shadowing was compared using two different models where we found large variations in predictions due to different sources (nuclear PDFs vs. independent calculation of GS) of this effect entering in both models. The large uncertainties in predictions of the onset of shadowing was found also within the same model based on the QCD factorization using different parameterizations of nuclear PDFs.
- We investigated for the first time the nuclear effects in the Drell-Yan process using rigorous the Green function formalism which allows to treat an arbitrary magnitude of the coherence length and is effective also in kinematic regions where LCL limit cannot be used safely. The mastering of the Green function technique represents a powerful tool that can be used also for more precise calculation of gluon shadowing or absorption that is important for formation of colorless system in heavy-ion collisions.

Bibliography

[1] E. Iancu, A. Leonidov, and L. D. McLerran, Phys. Lett. **B510**, 133 (2001), arXiv:hep-ph/0102009.

[2] L. Landau and I. Pomeranchuk, Dokl.Akad.Nauk Ser.Fiz. **92**, 535 (1953).

[3] A. B. Migdal, Phys.Rev. **103**, 1811 (1956).

[4] B. Z. Kopeliovich, J. Nemchik, I. K. Potashnikova, M. B. Johnson, and I. Schmidt, Phys. Rev. **C72**, 054606 (2005), arXiv:hep-ph/0501260.

[5] B. Kopeliovich, J. Raufeisen, A. Tarasov, and M. Johnson, Phys.Rev. **C67**, 014903 (2003), arXiv:hep-ph/0110221.

[6] B. Z. Kopeliovich, J. Raufeisen, and A. V. Tarasov, Phys. Lett. **B503**, 91 (2001), arXiv:hep-ph/0012035.

[7] J.-C. Peng and J.-W. Qiu, Prog. Part. Nucl. Phys. **76**, 43 (2014), arXiv:1401.0934.

[8] S. V. Akulinichev, S. Shlomo, S. A. Kulagin, and G. M. Vagradov, Phys. Rev. Lett. **55**, 2239 (1985).

[9] L. L. Frankfurt and M. I. Strikman, Phys. Rept. **160**, 235 (1988).

[10] M. Arneodo, Phys. Rept. **240**, 301 (1994).

[11] N. Armesto, J. Phys. **G32**, R367 (2006), arXiv:hep-ph/0604108.

[12] R. J. Fries and C. Nonaka, Prog. Part. Nucl. Phys. **66**, 607 (2011), arXiv:1012.1881.

[13] European Muon, J. Ashman *et al.*, Phys. Lett. **B202**, 603 (1988).

[14] BCDMS, G. Bari *et al.*, Phys. Lett. **B163**, 282 (1985).

[15] BCDMS, A. C. Benvenuti *et al.*, Phys. Lett. **B189**, 483 (1987).

[16] European Muon, M. Arneodo *et al.*, Phys. Lett. **B211**, 493 (1988).

[17] European Muon, M. Arneodo *et al.*, Nucl. Phys. **B333**, 1 (1990).

[18] European Muon, J. Ashman *et al.*, Z. Phys. **C57**, 211 (1993).

[19] New Muon, P. Amaudruz *et al.*, Z. Phys. **C51**, 387 (1991).

[20] New Muon, P. Amaudruz *et al.*, Z. Phys. **C53**, 73 (1992).

[21] New Muon, P. Amaudruz *et al.*, Nucl. Phys. **B441**, 3 (1995), arXiv:hep-ph/9503291.

[22] New Muon, M. Arneodo *et al.*, Nucl. Phys. **B441**, 12 (1995), arXiv:hep-ex/9504002.

[23] New Muon, M. Arneodo *et al.*, Nucl. Phys. **B481**, 3 (1996).

[24] New Muon, M. Arneodo *et al.*, Nucl. Phys. **B481**, 23 (1996).

[25] New Muon, M. Arneodo *et al.*, Nucl. Phys. **B487**, 3 (1997), arXiv:hep-ex/9611022.

[26] E665, M. R. Adams *et al.*, Phys. Rev. Lett. **68**, 3266 (1992).

[27] E665, M. R. Adams *et al.*, Z. Phys. **C67**, 403 (1995), arXiv:hep-ex/9505006.

[28] A. Accardi *et al.*, (2012), arXiv:1212.1701.

[29] PHENIX, S. S. Adler *et al.*, Phys. Rev. Lett. **94**, 232301 (2005), arXiv:nucl-ex/0503003.

[30] M. J. Tannenbaum, J. Phys. Conf. Ser. **589**, 012019 (2015), arXiv:1404.6232.

[31] J. W. Cronin *et al.*, Phys. Rev. **D11**, 3105 (1975).

[32] X.-N. Wang, Phys. Rev. **C61**, 064910 (2000), arXiv:nucl-th/9812021.

[33] A. Accardi, (2002), arXiv:hep-ph/0212148.

[34] M. Johnson, B. Kopeliovich, and A. Tarasov, Phys. Rev. C **63**, 035203 (2001), arXiv:hep-ph/0006326.

[35] G. Bertsch, S. J. Brodsky, A. Goldhaber, and J. Gunion, Phys.Rev.Lett. **47**, 297 (1981).

[36] PHENIX, A. Adare *et al.*, Phys. Rev. **C88**, 024906 (2013), arXiv:1304.3410.

[37] PHENIX, T. Chujo, Eur. Phys. J. **C49**, 23 (2007), arXiv:nucl-ex/0608020.

[38] PHENIX, K. Adcox *et al.*, Phys. Rev. Lett. **88**, 242301 (2002), arXiv:nucl-ex/0112006.

[39] PHENIX, S. S. Adler *et al.*, Phys. Rev. Lett. **91**, 172301 (2003), arXiv:nucl-ex/0305036.

[40] R. J. Fries, B. Muller, C. Nonaka, and S. A. Bass, Phys. Rev. Lett. **90**, 202303 (2003), arXiv:nucl-th/0301087.

[41] V. Greco, C. M. Ko, and P. Levai, Phys. Rev. Lett. **90**, 202302 (2003), arXiv:nucl-th/0301093.

[42] T. Hirano and Y. Nara, Phys. Rev. **C69**, 034908 (2004), arXiv:nucl-th/0307015.

[43] ALICE, J. Adam *et al.*, (2016), arXiv:1601.03658.

[44] D. M. Alde *et al.*, Phys. Rev. Lett. **64**, 2479 (1990).

[45] PHENIX, S. S. Adler *et al.*, Phys. Rev. Lett. **98**, 172302 (2007), arXiv:nucl-ex/0610036.

[46] PHENIX, S. S. Adler *et al.*, Phys. Rev. **C77**, 014905 (2008), arXiv:0708.2416.

[47] BRAHMS, I. Arsene *et al.*, Phys. Rev. Lett. **93**, 242303 (2004), arXiv:nucl-ex/0403005.

[48] ALICE, J. Adam *et al.*, Phys. Rev. **C91**, 064905 (2015), arXiv:1412.6828.

[49] J. Nemchik, Phys.Rev. **C68**, 035206 (2003), arXiv:hep-ph/0301043.

[50] STAR, J. Adams *et al.*, Phys. Rev. Lett. **97**, 152302 (2006), arXiv:nucl-ex/0602011.

[51] B. Boimska, *Transverse characteristics of hadron production in elementary and nuclear collisions at the CERN SPS energies*, PhD thesis, Warsaw, Inst. Nucl. Studies, 2004.

[52] PHENIX, T. Sakaguchi, Nucl. Phys. **A805**, 355 (2008), arXiv:0708.4265.

[53] PHENIX, S. Afanasiev *et al.*, Phys. Rev. Lett. **109**, 152302 (2012), arXiv:1205.5759.

[54] PHENIX, D. V. Perepelitsa, Nucl. Phys. **A904-905**, 1003c (2013).

[55] ATLAS, G. Aad *et al.*, Phys. Lett. **B748**, 392 (2015), arXiv:1412.4092.

[56] H. Fritzsch, M. Gell-Mann, and H. Leutwyler, Phys. Lett. **B47**, 365 (1973).

[57] D. J. Gross and F. Wilczek, Phys. Rev. Lett. **30**, 1343 (1973).

[58] H. D. Politzer, Phys. Rev. Lett. **30**, 1346 (1973).

[59] E. Reya, Phys. Rept. **69**, 195 (1981).

[60] J. F. Owens, Surveys High Energ. Phys. **3**, 65 (1982).

[61] J. F. Owens and J. D. Kimel, Phys. Rev. **D18**, 3313 (1978).

[62] R. P. Feynman, Conf. Proc. **C690905**, 237 (1969).

[63] J. D. Bjorken and E. A. Paschos, Phys. Rev. **185**, 1975 (1969).

[64] R. P. Feynman, R. D. Field, and G. C. Fox, Phys. Rev. **D18**, 3320 (1978).

[65] J. F. Owens, Rev. Mod. Phys. **59**, 465 (1987).

[66] R. K. Ellis, W. J. Stirling, and B. R. Webber, Camb. Monogr. Part. Phys. Nucl. Phys. Cosmol. **8**, 1 (1996).

[67] A. Lipatov, M. Malyshev, and N. Zotov, JHEP **1112**, 117 (2011), arXiv:1110.6582.

[68] G. Barnafoldi, P. Levai, G. Papp, G. I. Fai, and Y. Zhang, Heavy Ion Phys. **18**, 79 (2003), arXiv:nucl-th/0206006.

[69] J. F. Owens, E. Reya, and M. Gluck, Phys. Rev. **D18**, 1501 (1978).

[70] V. N. Gribov and L. N. Lipatov, Sov. J. Nucl. Phys. **15**, 438 (1972).

[71] G. Altarelli and G. Parisi, Nucl. Phys. B **126**, 298 (1977).

[72] Y. L. Dokshitzer, Sov. Phys. JETP **46**, 641 (1977).

[73] CTEQ, R. Brock *et al.*, Rev. Mod. Phys. **67**, 157 (1995).

[74] J. Pumplin *et al.*, JHEP **07**, 012 (2002), arXiv:hep-ph/0201195.

[75] A. Martin, W. Stirling, R. Thorne, and G. Watt, Eur. Phys. J. C **63**, 189 (2009), arXiv:0901.0002.

[76] H.-L. Lai *et al.*, Phys. Rev. **D82**, 074024 (2010), arXiv:1007.2241.

[77] ZEUS, H1, V. Radescu, Combination and QCD Analysis of the HERA Inclusive Cross Sections, in *Proceedings, 35th International Conference on High energy physics (ICHEP 2010)*, 2013, arXiv:1308.0374.

[78] The NNPDF Collaboration, R. D. Ball *et al.*, Nucl. Phys. B **855**, 153 (2012), arXiv:1107.2652.

[79] R. D. Field and R. P. Feynman, Nucl. Phys. **B136**, 1 (1978).

[80] B. A. Kniehl, G. Kramer, and B. Potter, Nucl. Phys. B **582**, 514 (2000), arXiv:hep-ph/0010289.

[81] D. de Florian, R. Sassot, and M. Stratmann, Phys. Rev. D **75**, 114010 (2007), arXiv:hep-ph/0703242.

[82] S. Kretzer, Phys. Rev. **D62**, 054001 (2000), arXiv:hep-ph/0003177.

[83] F. Borzumati and G. Kramer, Z. Phys. **C67**, 137 (1995), arXiv:hep-ph/9502280.

[84] BEATRICE, M. Adamovich *et al.*, Phys. Lett. **B348**, 256 (1995).

[85] BEATRICE, Yu. Aleksandrov *et al.*, Phys. Lett. **B433**, 217 (1998).

[86] D. C. Hom *et al.*, Phys. Rev. Lett. **37**, 1374 (1976).

[87] D. M. Kaplan *et al.*, Phys. Rev. Lett. **40**, 435 (1978).

[88] R. D. Field, AIP Conf. Proc. **55**, 97 (1979).

[89] X.-N. Wang, Phys. Rept. **280**, 287 (1997), arXiv:hep-ph/9605214.

[90] X.-N. Wang, Phys. Rev. Lett. **81**, 2655 (1998), arXiv:hep-ph/9804384.

[91] A. P. Contogouris, R. Gaskell, and S. Papadopoulos, Phys. Rev. **D17**, 2314 (1978).

[92] D. W. Sivers, S. J. Brodsky, and R. Blankenbecler, Phys. Rept. **23**, 1 (1976).

[93] L. Apanasevich *et al.*, Phys. Rev. **D59**, 074007 (1999), arXiv:hep-ph/9808467.

[94] Y. Zhang, G. I. Fai, G. Papp, G. G. Barnafoldi, and P. Levai, Phys. Rev. **C65**, 034903 (2002), arXiv:hep-ph/0109233.

[95] M. Krelina and J. Nemchik, Nucl. Phys. Proc. Suppl. **245**, 239 (2013).

[96] M. Krelina and J. Nemchik, EPJ Web Conf. **60**, 20023 (2013).

[97] H. D. Vries, C. D. Jager, and C. D. Vries, Atomic Data and Nuclear Data Tables **36**, 495 (1987).

[98] K. Eskola, V. Kolhinen, and C. Salgado, Eur. Phys. J. C **9**, 61 (1999), arXiv:hep-ph/9807297.

[99] K. J. Eskola, H. Paukkunen, and C. A. Salgado, JHEP **04**, 065 (2009), arXiv:0902.4154.

[100] M. Hirai, S. Kumano, and T.-H. Nagai, Phys. Rev. C **76**, 065207 (2007), arXiv:0709.3038.

[101] K. Kovarik *et al.*, (2015), arXiv:1509.00792.

[102] D. de Florian, R. Sassot, P. Zurita, and M. Stratmann, Phys. Rev. **D85**, 074028 (2012), arXiv:1112.6324.

[103] I. Helenius, K. J. Eskola, H. Honkanen, and C. A. Salgado, JHEP **07**, 073 (2012), arXiv:1205.5359.

[104] B. Z. Kopeliovich, J. Nemchik, I. K. Potashnikova, and I. Schmidt, Phys. Rev. **C86**, 054904 (2012), arXiv:1208.4951.

[105] J. Nemchik, V. Petracek, I. K. Potashnikova, and M. Sumbera, Phys. Rev. **C78**, 025213 (2008), arXiv:0805.4267.

[106] B. Z. Kopeliovich, J. Nemchik, I. K. Potashnikova, and I. Schmidt, Int. J. Mod. Phys. **E23**, 1430006 (2014).

[107] B. Z. Kopeliovich and J. Nemchik, J. Phys. **G38**, 043101 (2011).

[108] B. Z. Kopeliovich, L. I. Lapidus, and A. B. Zamolodchikov, JETP Lett. **33**, 595 (1981), [Pisma Zh. Eksp. Teor. Fiz.33,612(1981)].

[109] N. N. Nikolaev and B. Zakharov, Z.Phys. **C49**, 607 (1991).

[110] B. Kopeliovich, In *Hirschegg 1995, Proceedings, Dynamical properties of hadrons in nuclear matter* 102-112 (1995), arXiv:hep-ph/9609385.

[111] S. J. Brodsky, A. Hebecker, and E. Quack, Phys. Rev. **D55**, 2584 (1997), arXiv:hep-ph/9609384.

[112] B. Z. Kopeliovich, A. V. Tarasov, and A. Schafer, Phys. Rev. **C59**, 1609 (1999), arXiv:hep-ph/9808378.

[113] J. Raufeisen, *QCD coherence effects in high-energy reactions with nuclei*, PhD thesis, CFNSM, Rupertus Carola University of Heidelberg, 2000, arXiv:hep-ph/0009358.

[114] J. Cepila, *Coherence effects in hadron-nucleus and heavy ion collisions at high energies*, PhD thesis, FNSPE, Czech Technical University in Prague, 2013.

[115] N. N. Nikolaev and B. Zakharov, Phys.Lett. **B332**, 184 (1994), arXiv:hep-ph/9403243.

[116] S. J. Brodsky and A. H. Mueller, Phys.Lett. **B206**, 685 (1988).

[117] B. Z. Kopeliovich, J. Raufeisen, and A. V. Tarasov, Phys.Rev. **C62**, 035204 (2000), arXiv:hep-ph/0003136.

[118] K. J. Golec-Biernat and M. Wusthoff, Phys.Rev. **D59**, 014017 (1998), arXiv:hep-ph/9807513.

[119] H. Kowalski, L. Motyka, and G. Watt, Phys.Rev. **D74**, 074016 (2006), arXiv:hep-ph/0606272.

[120] B. Z. Kopeliovich, A. Schafer, and A. V. Tarasov, Phys.Rev. **D62**, 054022 (2000), arXiv:hep-ph/9908245.

[121] A. Donnachie and P. Landshoff, Phys.Lett. **B296**, 227 (1992), arXiv:hep-ph/9209205.

[122] Particle Data Group, R. M. Barnett *et al.*, Phys.Rev. **D54**, 1 (1996).

[123] J. Bartels, K. J. Golec-Biernat, and H. Kowalski, Phys. Rev. **D66**, 014001 (2002), arXiv:hep-ph/0203258.

[124] A. H. Rezaeian, M. Siddikov, M. Van de Klundert, and R. Venugopalan, Phys.Rev. **D87**, 034002 (2013), arXiv:1212.2974.

[125] E. Iancu, K. Itakura, and S. Munier, Phys.Lett. **B590**, 199 (2004), arXiv:hep-ph/0310338.

[126] J. L. Albacete, N. Armesto, J. G. Milhano, and C. A. Salgado, Phys. Rev. **D80**, 034031 (2009), arXiv:0902.1112.

[127] J. L. Albacete, N. Armesto, J. G. Milhano, P. Quiroga-Arias, and C. A. Salgado, Eur. Phys. J. **C71**, 1705 (2011), arXiv:1012.4408.

[128] J. R. Forshaw and G. Shaw, JHEP **0412**, 052 (2004), arXiv:hep-ph/0411337.

[129] B. Kopeliovich and A. Rezaeian, Int.J.Mod.Phys. **E18**, 1629 (2009), arXiv:0811.2024.

[130] M. Johnson *et al.*, Phys.Rev. **C65**, 025203 (2002), arXiv:hep-ph/0105195.

[131] M. Johnson, B. Kopeliovich, and I. Schmidt, Phys.Rev. **C75**, 064905 (2007), arXiv:hep-ph/0701015.

[132] H. Bethe and W. Heitler, Proc.Roy.Soc.Lond. **A146**, 83 (1934).

[133] B. Kopeliovich, J. Raufeisen, and A. Tarasov, Phys.Lett. **B440**, 151 (1998), arXiv:hep-ph/9807211.

[134] J. Raufeisen, A. V. Tarasov, and O. O. Voskresenskaya, Eur. Phys. J. **A5**, 173 (1999), arXiv:hep-ph/9812398.

[135] B. Z. Kopeliovich, J. Nemchik, A. Schafer, and A. V. Tarasov, Phys. Rev. Lett. **88**, 232303 (2002), arXiv:hep-ph/0201010.

[136] S. J. Brodsky, F. Fleuret, C. Hadjidakis, and J. P. Lansberg, Phys. Rept. **522**, 239 (2013), arXiv:1202.6585.

[137] B. Z. Kopeliovich, J. Nemchik, and I. Schmidt, Phys. Rev. **C76**, 025210 (2007), arXiv:hep-ph/0703118.

[138] B. Zakharov, Phys.Atom.Nucl. **61**, 838 (1998), arXiv:hep-ph/9807540.

[139] B. Kopeliovich and B. Povh, Phys. Lett. **B367**, 329 (1996), arXiv:hep-ph/9509362.

[140] R. Feynman and A. Hibbs, *Quantum mechanics and path integrals,*International series in pure and applied physics (McGraw-Hill, 1965).

[141] N. Giordano, *Computational physics* (Prentice Hall, 1997).

[142] A. Goldberg, H. M. Schey, and J. L. Schwartz, Am.J.Phys. **35** (1967).

[143] J. Crank and P. Nicolson, Math.Proc.Camb.Phil.Soc. **43**, 50 (1947).

[144] V. Gribov, Sov.Phys.JETP **29**, 483 (1969).

[145] V. Gribov, Sov.Phys.JETP **30**, 709 (1970).

[146] V. Karmanov and L. Kondratyuk, Sov.Phys.JETP Lett. **18**, 266 (1973).

[147] M. Krelina and J. Nemchik, EPJ Web Conf. **66**, 04016 (2014).

[148] M. Krelina and J. Nemchik, Production of photons and hadrons on nuclear targets, in *Proceedings, 18th Conference of Czech and Slovak Physicists, with participation of Hungarian and Polish Physical Societies*, pp. 53–54, 2015.

[149] M. Krelina, J. Ceppila, and J. Nemchik, Challenges of direct photon production at forward rapidities and large pT, 2015, will be published in Journal of Physics Conference Series.

[150] E. Basso, V. P. Goncalves, M. Krelina, J. Nemchik, and R. Pasechnik, (2016), arXiv:1603.01893.

[151] M. Krelina, E. Basso, V. P. Goncalves, J. Nemchik, and R. Pasechnik, Nuclear effects in Drell-Yan production at the LHC, 2015, will be published in EPJ Web of Conf.

[152] M. Krelina, E. Basso, V. P. Goncalves, J. Nemchik, and R. Pasechnik, Systematic study of real photon and Drell-Yan pair production in p+A (d+A) interactions, 2015, will be published in EPJ Web of Conf.

[153] J. Raufeisen, J.-C. Peng, and G. C. Nayak, Phys. Rev. **D66**, 034024 (2002), arXiv:hep-ph/0204095.

[154] R. P. Feynman, R. D. Field, and G. C. Fox, Nucl. Phys. **B128**, 1 (1977).

[155] R. Pasechnik, B. Kopeliovich, and I. Potashnikova, Phys. Rev. **D86**, 114039 (2012), arXiv:1204.6477.

Appendix A

A.1 Intrinsic transverse momentum kinematics

In this Appendix, the basic kinematics for the k_T-smearing is provided.

Generally, the k_T-smearing can be added into the calculation by a reformulation of the parton distribution functions as

$$dx_a\, f_{a/A}(x_a, Q) \to dx_a\, d^2k_{aT}\, g_N(k_{Ta}, Q^2)\, f_{a/N}(x_a, Q^2), \tag{A.1}$$

where momentum fractions can be redefined as

$$x_a = \frac{E_a + p_{La}}{\sqrt{s}}, \quad x_b = \frac{E_b - p_{Lb}}{\sqrt{s}}, \tag{A.2}$$

where p_L is a longitudinal momentum in the beam direction. Then, from the four-momentum vectors $p_a = (E_a, \vec{k}_{Ta}, p_{\shortparallel a})$ and $p_b = (E_b, \vec{k}_{Tb}, p_{\shortparallel b})$ with

$$E_a = \frac{k_{Ta}^2}{2\sqrt{s}x_a} + \frac{x_a\sqrt{s}}{2}, \quad p_{\shortparallel a} = \frac{x_a\sqrt{s}}{2} - \frac{k_{Ta}^2}{2\sqrt{s}x_a} \tag{A.3}$$

and

$$E_b = \frac{k_{Tb}^2}{2\sqrt{s}x_b} + \frac{x_b\sqrt{s}}{2}, \quad p_{\shortparallel b} = \frac{k_{Tb}^2}{2\sqrt{s}x_b} - \frac{x_b\sqrt{s}}{2} \tag{A.4}$$

the Mandelstam variables can be expressed. By the same definition as in (3.5) the Mandelstam variable $\hat{s}$ takes the form

$$\hat{s} = x_a x_b s + \frac{k_{Ta}^2 k_{Tb}^2}{x_a x_b s} - 2\vec{k}_{Ta} \cdot \vec{k}_{Tb}. \tag{A.5}$$

It is very useful to use polar coordinates

$$d^2k_T \to dk_T\, d\phi\, J(k_T, \phi), \tag{A.6}$$

where $J(k_T, \cos\phi)$ is a Jacobian in the form

$$J(k_T, \phi) = k_T. \tag{A.7}$$

After that, the $\hat{s}$ variable takes the final form

$$\hat{s} = x_a x_b s + \frac{k_{Ta}^2 k_{Tb}^2}{x_a x_b s} - 2k_{Ta}k_{Tb}\left(\cos\phi_a \cos\phi_b + \sin\phi_a \sin\phi_b\right). \tag{A.8}$$

Similarly, $\hat{t}$ and $\hat{u}$ Mandelstam variables can be expressed as

$$\hat{t} = -\frac{p_T}{z_c}\left(x_a\sqrt{s}e^{-y} + \frac{k_{Ta}^2}{\sqrt{s}\,x_a}\,e^{y} - 2k_{Ta}\cos\phi_a\right) \tag{A.9}$$

and

$$\hat{u} = -\frac{p_T}{z_c}\left(x_b\sqrt{s}e^{y} + \frac{k_{Tb}^2}{\sqrt{s}\,x_b}\,e^{-y} - 2k_{Tb}\cos\phi_b\right). \tag{A.10}$$

Moreover, similarly as in (3.9) to (3.12), the integration over z_c can be performed using a delta function with result

$$z_c = \frac{p_T}{\hat{s}}\left[\sqrt{s}\left(x_a e^{-y} + x_b e^{y}\right) + \frac{1}{\sqrt{s}}\left(\frac{k_{Ta}^2}{x_a}\,e^{y} + \frac{k_{Tb}^2}{x_b}\,e^{-y}\right) - 2\left(k_{Ta}\cos\phi_a + k_{Tb}\cos\phi_b\right)\right] \tag{A.11}$$

and applying boundary conditions $z_c \leq 1$ on (A.11) leads to the quadratic equation for $x_{b\,min}$. The results for $x_{b\,min}$ is

$$\begin{aligned} x_{b\,min} = {} & e^{-y}(-e^{2y}\,k_{Ta}^2\,p_T\,\sqrt{s} - p_T\,s^{3/2}\,x_a^2 - 2e^{y}\,s\,x_a(v - p_T\,w) \\ & \pm\sqrt{u})\,/\,(2\,s^{3/2}\,x_a\,(e^{y}\,p_T - \sqrt{s}\,x_a)), \end{aligned} \tag{A.12}$$

where

$$\begin{aligned} u &= 4\,e^{y}\,k_{Tb}^2\,s^{3/2}\,x_a(e^{y}\,p_T - \sqrt{s}\,x_a)(e^{y}\,k_{Ta}^2 - p_T\,\sqrt{s}\,x_a) \\ &+ (e^{2y}\,k_{Ta}^2\,p_T\,\sqrt{s} + 2\,e^{y}\,v - p_T\,s\,x_a\,w + p_T\,s^{3/2}\,x_a^2)^2, && \text{(A.13)} \\ v &= k_{Ta}\,k_{Tb}(\cos\phi_a\cos\phi_b + \sin\phi_a\sin\phi_b), && \text{(A.14)} \\ w &= k_{Ta}\,\cos\phi_a + k_{Tb}\,\cos\phi_b, && \text{(A.15)} \end{aligned}$$

and by applying the other condition $x_{b\,min} \leq 1$ same roots of quadratic equations are obtained for both roots of $x_{a\,min}$

$$\begin{aligned} x_{a\,min} = {} & (k_{Tb}^2\,p_T\,\sqrt{s} + e^{2y}\,p_T\,s^{3/2} + 2\,e^{y}\,s(v - p_T\,w) \\ & \pm\sqrt{u})\,/\,(2\,e^{y}\,s^2 - 2\,p_T\,s^{3/2}), \end{aligned} \tag{A.16}$$

where

$$\begin{aligned} u &= 4\,e^{y}\,k_{Ta}\,k_{Tb}\,s^{3/2}(e^{y}\sqrt{s} - p_T)(e^{y}\,p_T\,\sqrt{s} - k_{Ta}k_{Tb}) \\ &+ s\,(k_{Ta}\,k_{Tb}\,p_T + 2e^{y}\,\sqrt{s}(v - p_T\,w) + e^{2y}\,p_T\,s)^2, && \text{(A.17)} \\ v &= k_{Ta}\,k_{Tb}(\cos\phi_a\cos\phi_b + \sin\phi_a\sin\phi_b), && \text{(A.18)} \\ w &= k_{Ta}\,\cos\phi_a + k_{Tb}\,\cos\phi_b. && \text{(A.19)} \end{aligned}$$

Next, restrictions on the initial transverse momentum $k_{Ta} < x_a \sqrt{s}$ and $k_{Tb} < x_b \sqrt{s}$ can be obtained. In some cases, some of Mandelstam variables can approach zero, if the initial k_T is too large. That is a problem for the partonic cross-section which could then diverge. This problem is solved by adding a regularization mass μ^2 to denominators of the partonic cross-sections with the value $\mu = 0.2\,\mathrm{GeV}$ for quarks and $\mu = 0.8\,\mathrm{GeV}$ for gluons as in [32].

Finally, one should add a radial variable x_R [154] in (A.1)

$$dx_i \Rightarrow \frac{dx_i}{x_{Ri}}\,, \tag{A.20}$$

which represents a energy fraction carried by the quarks

$$x_{Ri}^2 = x_i^2 + 4k_{Ti}^2/s, \tag{A.21}$$

where x_i is a longitudinal momentum fraction, k_{Ti} is a transverse momentum and s is the square of CMS energy.

It is expected that the k_T-smearing leads to an increase of the cross-section as discussed in [65].

Similar derivation of k_T-kinematics for hadrons can be made also for direct photons (case for $z_c = 1$) with following results: momentum fraction x_b can be expressed as

$$\begin{aligned} x_b = {} & (2\,e^y\,s\,v\,x_a - e^{2y} k_{Ta}^2\,p_T\,\sqrt{s} - p_T\,s^{3/2} x_a^2 \\ & \pm \sqrt{u})\,/\,(2\,e^y\,s^{3/2}\,x_a(e^y\,p_T - \sqrt{s}\,x_a)), \end{aligned} \tag{A.22}$$

where

$$\begin{aligned} u &= s(4\,e^y\,k_{Tb}^2\,\sqrt{s}\,x_a(e^y\,p_T - \sqrt{s}\,x_a)(e^y\,k_{Ta}^2 - p_T\,\sqrt{s}\,x_a) \\ &+ (e^{2y}\,k_{Ta}^2\,p_T + p_T\,s\,x_a^2 - 2\,e^y\,\sqrt{s}\,x_a\,v)^2), \end{aligned} \tag{A.23}$$

$$v = k_{Ta}\,p_T\,\cos\phi_a + k_{Tb}\,p_T\,\cos\phi_b - k_{Ta}\,k_{Tb}\,\cos(\phi_a - \phi_b), \tag{A.24}$$

and then minimal value of the integral variable x_a as

$$\begin{aligned} x_{a\,min} = {} & (k_{Tb}^2\,p_T\,\sqrt{s} + e^{2y}\,p_T\,s^{3/2} - 2\,e^y\,s\,v \\ & \pm \sqrt{u})\,/\,(2\,s^{3/2}(e^y\,\sqrt{s} - p_T)), \end{aligned} \tag{A.25}$$

where

$$\begin{aligned} u &= s(4\,e^y\,k_{Ta}^2\,\sqrt{s}(e^y\,\sqrt{s} - p_T)(e^y\,p_T\,\sqrt{s} - k_{Tb}^2) \\ &+ (k_{Tb}^2\,p_T + e^{2y}\,p_T\,s - 2\,e^y\,v)^2), \end{aligned} \tag{A.26}$$

$$v = k_{Ta}\,p_T\,\cos\phi_a + k_{Tb}\,p_T\,\cos\phi_b - k_{Ta}\,k_{Tb}\,\cos(\phi_a - \phi_b). \tag{A.27}$$

A.2 Wave function with gauge bosons

The goal of this Appendix is to extent the $q\gamma^*$ wave function to general qG^* wave function where G^* stands for gauge bosons $G^* = \gamma^*, Z^0, W^\pm$ [155].

The proton-proton cross-section for gauge boson production can be expressed as

$$\frac{d^4\sigma^{(pp\to G^*X)}}{dx_F d^2p_T} = \frac{x_1}{x_1+x_2}\int_{x_1}^1 \frac{d\alpha}{\alpha^2}\Sigma_f\left(f_f\left(\frac{x_1}{\alpha}\right)+f_{\bar f}\left(\frac{x_1}{\alpha}\right)\right)\frac{d^3\sigma^{(qp\to qG^*X)}}{d(\ln\alpha)d^2p_T}, \tag{A.28}$$

where functions f_f denote PDFs. The factorization scale for PDFs has a form $\mu^2 = p_T^2 + (1-x_1)M^2$. The Drell-Yan process cross-section studied within this work focuses on the inclusive $G = \gamma^*, Z^0$ production cross-section as follows

$$\frac{d^4\sigma^{(pp\to l^-l^+X)}}{d^2p_T dM^2 d\eta} = \mathcal{F}_G(M)\frac{d^4\sigma^{(pp\to G^*X)}}{d^2p_T d\eta}, \tag{A.29}$$

where

$$\mathcal{F}_\gamma(M) = \frac{\alpha_{EM}}{3\pi M^2}, \qquad \mathcal{F}_Z(M) = \mathrm{Br}(Z^0\to l^-l^+)\rho_Z(M), \tag{A.30}$$

where the branching ratio $\mathrm{Br}(Z^0\to l^-l^+)\cong 0.101$, and the invariant mass distribution of the Z^0 boson in the narrow approximation is

$$\rho_Z(M) = \frac{1}{\pi}\frac{M\Gamma_Z(M)}{(M^2-m_Z^2)^2+M^2\Gamma_Z^2(M)}. \tag{A.31}$$

The generalized total decay width reads

$$\Gamma_Z(M) = \frac{\alpha_{EM}M}{6\sin^2 2\theta_W}\left(\frac{160}{3}\sin^4\theta_W - 40\sin^2\theta_W + 21\right) \tag{A.32}$$

with the Weinberg mixing angle θ_W, $\sin^2\theta_W \cong 0.23$.

The quark-nucleon cross-section has same form as in (4.2)

$$\begin{aligned}\frac{d^3\sigma^{(qN\to GX)}}{d(\ln\alpha)d^2p_T} &= \frac{1}{(2\pi)^2}\int d^2\rho_1\, d^2\rho_2\, e^{i\vec p_T(\vec\rho_1-\vec\rho_2)}\Psi_{T,L}^{V-A,*}(\alpha,\vec\rho_2,m_f)\Psi_{T,L}^{V-A}(\alpha,\vec\rho_1,m_f)\\ &\times \frac{1}{2}\left\{\sigma_{q\bar q}^N(\alpha\rho_1)+\sigma_{q\bar q}^N(\alpha\rho_2)-\sigma_{q\bar q}^N(\alpha|\vec\rho_1-\vec\rho_2|)\right\}\end{aligned} \tag{A.33}$$

except for the sum over quark polarizations and vector and axial-vector wave functions

$$\begin{aligned}&\sum_{quark pol.}\Psi_{T,L}^{V-A,*}(\alpha,\vec\rho_2,m_f)\Psi_{T,L}^{V-A}(\alpha,\vec\rho_1,m_f)\\ &= \Psi_{T,L}^{V,*}(\alpha,\vec\rho_2,m_f)\Psi_{T,L}^{V}(\alpha,\vec\rho_1,m_f)+\Psi_{T,L}^{A,*}(\alpha,\vec\rho_2,m_f)\Psi_{T,L}^{A}(\alpha,\vec\rho_1,m_f).\end{aligned} \tag{A.34}$$

Each component reads [155]

$$\begin{aligned}\Psi_V^T\Psi_V^{T*} &= \frac{(\mathcal{C}_f^G)^2(g_{v,f}^G)^2}{2\pi^2}\Big[m_f^2\alpha^4\mathrm{K}_0(\eta\rho_1)\mathrm{K}_0(\eta\rho_2) \\ &+ (1+(1-\alpha)^2)\eta^2\frac{\vec{\rho}_1\cdot\vec{\rho}_2}{\rho_1\rho_2}\mathrm{K}_1(\eta\rho_1)\mathrm{K}_1(\eta\rho_2)\Big] \qquad (A.35)\\ \Psi_V^L\Psi_V^{L*} &= \frac{(\mathcal{C}_f^G)^2(g_{v,f}^G)^2}{\pi^2}M^2(1-\alpha)^2\mathrm{K}_0(\eta\rho_1)\mathrm{K}_0(\eta\rho_2) \qquad (A.36)\\ \Psi_A^T\Psi_A^{T*} &= \frac{(\mathcal{C}_f^G)^2(g_{a,f}^G)^2}{2\pi^2}\Big[m_f^2\alpha^2(1-\alpha)^2\mathrm{K}_0(\eta\rho_1)\mathrm{K}_0(\eta\rho_2) \\ &+ (1+(1-\alpha)^2)\eta^2\frac{\vec{\rho}_1\cdot\vec{\rho}_2}{\rho_1\rho_2}\mathrm{K}_1(\eta\rho_1)\mathrm{K}_1(\eta\rho_2)\Big] \qquad (A.37)\\ \Psi_A^T\Psi_A^{T*} &= \frac{(\mathcal{C}_f^G)^2(g_{a,f}^G)^2}{\pi^2}\frac{\eta^2}{M^2}\Big[\eta^2\mathrm{K}_0(\eta\rho_1)\mathrm{K}_0(\eta\rho_2) \\ &+ \alpha^2m_f^2\frac{\vec{\rho}_1\cdot\vec{\rho}_2}{\rho_1\rho_2}\mathrm{K}_1(\eta\rho_1)\mathrm{K}_1(\eta\rho_2)\Big] \qquad (A.38)\end{aligned}$$

where $\mu^2 = \alpha^2m_f^2 + (1-\alpha)M^2$, $\mathrm{K}_0(x)$ is modified Bessel function of the second kind, and the coupling factors $\mathcal{C}_f^G$ are defined as

$$\mathcal{C}_f^\gamma = \sqrt{\alpha_{EM}}Z_f,\ \ \mathcal{C}_f^Z = \frac{\sqrt{\alpha_{EM}}}{\sin 2\theta_W},\ \ \mathcal{C}_f^{W^+} = \frac{\sqrt{\alpha_{EM}}}{2\sqrt{2}\sin\theta_W}V_{f_uf_d},\ \ \mathcal{C}_f^{W^-} = \frac{\sqrt{\alpha_{EM}}}{2\sqrt{2}\sin\theta_W}V_{f_df_u}, \qquad (A.39)$$

with the vectorial coupling at the leading order for vector case

$$g_{v,f}^\gamma = 1,\quad g_{v,f_u}^Z = \frac{1}{2}-\frac{4}{3}\sin^2\theta_W,\quad g_{v,f_d}^Z = -\frac{1}{2}-\frac{2}{3}\sin^2\theta_W,\quad g_{v,f}^W = 1, \qquad (A.40)$$

and for the axial-vector case

$$g_{a,f}^\gamma = 0,\qquad g_{a,f_u}^Z = \frac{1}{2},\qquad g_{a,f_d}^Z = -\frac{1}{2},\qquad g_{a,f}^W = 1, \qquad (A.41)$$

Here, $f_u = u, c, t$ and $f_d = d, s, b$ are flavors, $V_{f_uf_d}$ refer to the CKM matrix elements.

For quark masses the following masses are used $m_{uds} = 0.14, m_c = 1.4, m_b = 4.5$ and $m_t = 172$ GeV.

A.3 Solution of the Green function in the form of the HO

In this appendix, the solution of (4.54) for small-ρ approximation, $\sigma_{q\bar{q}}^N = C\rho^2$, and for uniform nuclear density approximation, $\rho_A(b,z) = \rho_0\theta(R_A^2 - b^2 - z^2)$ will be presented.

These approximations allow to solve 2D Schrödinger equation (4.50) analytically with result in form (4.59) with (4.60) and (4.61).

Basic idea of this solution is to substitute for Bessel functions K_0 and K_1 in wave functions by their integral representation

$$\mathrm{K}_0(\eta\rho) = \frac{1}{2}\int_0^\infty \frac{dt}{t}\exp\left(-t-\frac{\eta^2\rho^2}{4t}\right), \tag{A.42}$$

$$\frac{1}{\eta\rho}\mathrm{K}_1(\eta\rho) = \frac{1}{4}\int_0^\infty \frac{dt}{t^2}\exp\left(-t-\frac{\eta^2\rho^2}{4t}\right), \tag{A.43}$$

$$\tag{A.44}$$

and solve it as multiple Gaussian integrals leading to the analytical solution for integrals over transverse coordinates.

Then, the result can be expressed as the sum of two terms

$$\frac{d^3\sigma^{(qA\to\gamma^* X)}}{d(\ln\alpha)\,d^2p_T} = \mathcal{I}_A + \mathcal{I}_B, \tag{A.45}$$

where the first term, $\mathcal{I}_A$, gives dominant contribution similar to LCL limit

$$\begin{aligned}\mathcal{I}_A &= Z_f^2\frac{\alpha_{EM}}{(2\pi)^3}\,\mathrm{Re}\int_0^{R_A} dL\,L\int_0^{2L} dz\int_0^\infty dt\,du\,C\alpha^2\rho_0\exp[-u-t]\\ &\times \left[(m_f^2\alpha^4+2M^2(1-\alpha)^2)\frac{1}{2u}\frac{1}{2t}\mathcal{I}_{A,0}-(1+(1-\alpha)^2)\eta^4\frac{1}{4u^2}\frac{1}{4t^2}\mathcal{I}_{A,1}\right]\end{aligned} \tag{A.46}$$

where subintegrals have forms

$$\begin{aligned}\mathcal{I}_{A,0} &= \frac{\pi^2}{16A^3D^3}\exp\left[-\frac{D+AE^2}{4AD}p_T^2\right]\\ &\times \left(-4B^2D+(BE-2D)^2p_T^2+4A(4D-E^2p_T^2)+4A(4(B-D)D+E(2D-BE)p_T^2)\right)\end{aligned} \tag{A.47}$$

$$\begin{aligned}\mathcal{I}_{A,1} &= \frac{\pi^2}{128A^4D^5}\exp\left[-\frac{D+AE^2}{4AD}p_T^2\right]\\ &\times \left(-32D^2(-B^3+4AB(B-D)+4A^2(B+D))+16D(-BB(BE-2D)(BE-D)\right.\\ &+ 2A^2E(D(E-2)+2BE)+2A(2B^2E^2-BDE(4+E)+D^2(1+2E)))p_T^2\\ &+ \left.E(BE-2D)(4D^2+(B^2-4AB-4A^2)E^2+D(8AE-4BE))p_T^2\right)\end{aligned} \tag{A.48}$$

where

$$
\begin{aligned}
A &= \frac{\eta^2}{4u} + \tfrac{1}{2} C\alpha^2\rho_0 z, && \text{(A.49)}\\
B &= C\alpha^2\rho_0 z, && \text{(A.50)}\\
C &= \frac{\eta^2}{4t} + \tfrac{1}{2} C\alpha^2\rho_0 z, && \text{(A.51)}\\
D &= \frac{4AC - B^2}{4A}, && \text{(A.52)}\\
E &= \frac{2(2A - B)}{4A}. && \text{(A.53)}
\end{aligned}
$$

The second term $\mathcal{I}_B$ gives corrections to the first term for small p_T. For high p_T this term can be neglected. This term has a form

$$
\begin{aligned}
\mathcal{I}_B &= Z_f^2 \frac{\alpha_{EM}}{(2\pi)^4} \,\mathrm{Re} \int_0^{R_A} dL\, L \int_0^{2L} dz \int_0^{2L-z} d\Delta z \int_0^{\infty} dt\, du\, C^2 \alpha^4 \rho_0^2 \frac{a\, \mathrm{e}^{-iq_L^{min}\Delta z}}{\sinh(\omega \Delta z)} \\
&\times \left[(m_f^2 \alpha^4 + 2M^2(1-\alpha)^2) \frac{1}{2u} \frac{1}{2t} \mathcal{I}_{B,0} - (1 + (1-\alpha)^2) \eta^4 \frac{1}{4u^2} \frac{1}{4t^2} \mathcal{I}_{B,1} \right], \quad \text{(A.54)}
\end{aligned}
$$

where subintegrals have form

$$
\begin{aligned}
\mathcal{I}_{B,0} &= \frac{\pi^3}{256 G^3 H^3 J^5} \exp\left[-\frac{J + GK^2}{4GJ} p_T^2 \right] \\
&\times \big(32J^2 \left(B(B-4G)I^2 + 2(HB(B-4G) + GI^2)J + 8GHJ^2 \right) - 16J(HJ(2J - BK) \\
&\times (2J + 4GK - BK) + I^2(J^2 + B(B-4G)K^2 + JK(G(4+K) - 2B))) p_T^2 \\
&+ I^2K^2(BK - 2J)((B-4G)K - 2J)\, p_T^4 \big), \quad \text{(A.55)}\\
\mathcal{I}_{B,1} &= \frac{\pi^3 I}{4096 G^4 H^4 J^7} \exp\left[-\frac{J + GK^2}{4GJ} p_T^2 \right] \\
&\times \big(128J^3 \left(3(4G - B)B^2I^2 + 8(H(4G-B)B^2 + G(G-B)I^2)J + 32GH(G-B)J^2 \right) \\
&- 32J^2(8(G-B)J^2(I^2 + 4HJ) + 2J(3B(3B - 8G)I^2 + 8(HB(3B - 8G) + GI^2)J \\
&+ 32GHJ^2)K + (9(4G - B)B^2I^2 + 16(H(4G-B)B^2 + G(G-B)I^2)J \\
&+ 32GH(G-B)J^2)K^2) p_T^2 + 4JK(8HJ(2J + 4GK - BK)(BK - 2J)^2 \\
&+ I^2(16J^3 + 9(4G - B)B^2K^3 + 4JK^2(9B^2 + 2G^2K - 2GB(12 + K)) \\
&+ 4J^2K(2G(7 + 2K) - 11B))) p_T^4 + I^2K^3(BK - 2J)^2((B - 4G)K - 2J)\, p_T^6 \big), \quad \text{(A.56)}
\end{aligned}
$$

where

$$B = H\alpha^2\rho_0 z, \tag{A.57}$$
$$F = \frac{a}{2}\coth(\omega\Delta z) + \tfrac{1}{2}H\alpha^2\rho_0 z, \tag{A.58}$$
$$G = \tfrac{1}{2}H\alpha^2\rho_0 z + \frac{\eta^2}{4u}, \tag{A.59}$$
$$H = \frac{a}{2}\coth(\omega\Delta z) + \frac{\eta^2}{4t}, \tag{A.60}$$
$$I = \frac{a}{\sinh(\omega\Delta z)}, \tag{A.61}$$
$$J = \frac{4FGH - HB^2 - GI^2}{4GH}, \tag{A.62}$$
$$K = \frac{4GH - 2HB}{4GH}. \tag{A.63}$$

A.4 Cross-section kinematics

Here, some useful relations for cross-section transformations will be presented.

Some Drell-Yan data are presented for several bins in invariant mass together with the mean value $\langle M\rangle$ for each bin. It is useful, according to the mean value theorem, to integrate the cross-section of gamma decay to dilepton

$$\sigma^{(\gamma^*\to l^+l^-)} = \int_{M^2_{min}}^{M^2_{max}} dM^2 \frac{d\sigma^{(\gamma^*\to l^+l^-)}}{dM^2} = \frac{\alpha_{EM}}{3\pi}\ln\frac{M^2_{max}}{M^2_{min}} \tag{A.64}$$

and the rest of $p+p$ cross-section is calculated as

$$\frac{d^3\sigma^{(pp\to l^-l^+X)}}{dx_F d^2p_T} = \sigma^{(\gamma^*\to l^+l^-)} \frac{x_1}{x_1+x_2}\int_{x_1}^{1}\frac{d\alpha}{\alpha^2}\Sigma_q\left(f_q\left(\frac{x_1}{\alpha}\right)+f_{\bar q}\left(\frac{x_1}{\alpha}\right)\right)\left.\frac{d^3\sigma^{(qp\to\gamma^*X)}}{d(\ln\alpha)d^2p_T}\right|_{M^2=\langle M\rangle^2}. \tag{A.65}$$

Next, for direct photon production it is convenient to use the form same as for hadrons

$$E\frac{d^3\sigma^{(pp\to\gamma X)}}{d^3p} = \sqrt{M^2+p_T^2+\frac{s}{4}x_F^2}\,\frac{2}{\sqrt{s}}\,\frac{d^3\sigma^{(pp\to\gamma X)}}{dx_F d^2p_T}. \tag{A.66}$$

For comparison with Drell-Yan data from LHC experiments it is useful to express the cross-section in term of pseudorapidity instead of Feynman x_F

$$\frac{d^3\sigma^{(pp\to l^-l^+X)}}{d\eta d^2p_T} = \left(\frac{2}{\sqrt{s}}\sqrt{M^2+p_T^2}\cosh\eta\right)\frac{d^3\sigma^{(pp\to l^-l^+X)}}{dx_F d^2p_T}, \tag{A.67}$$

where $x_{1,2} = \frac{1}{2}\sqrt{x_F^2 + 4\tau} \pm x_F$ transform to $x_{1,2} = \sqrt{\tau}e^{\pm\eta}$, where $\tau = \frac{M^2+p_T^2}{s}$. Other forms of provided data at LHC are dilepton cross-section as function of dilepton mass $\frac{d\sigma^{(pp\to l^- l^+ X)}}{dM}$, transverse momentum $\frac{d\sigma^{(pp\to l^- l^+ X)}}{dp_T}$, rapidity $\frac{d\sigma^{(pp\to l^- l^+ X)}}{d\eta}$ and total cross-section, usually used for Z^0 boson production, $\sigma_{tot}^{(pp\to l^- l^+ X)}$, where typical limits for the integration over dilepton mass are $M_{min} = 60$ GeV and $M_{max} = 120$ GeV, can be obtained by integration of (4.32) over the rest differential variables.

Appendix B

List of publications

Papers & proceedings

- E. Basso, V. P. Goncalves, M. Krelina, J. Nemchik, and R. Pasechnik; *Nuclear effects in Drell-Yan pair production in high-energy pA collisions*; (2016), arXiv:1603.01893
- M. Krelina, E. Basso, V. Goncalves, J. Nemchik and R. Pasechnik; *Systematic study of real photon and Drell-Yan pair production in p+A (d+A) interactions*; will be published in EPJ Web of Conf.
- M. Krelina, E. Basso, V. Goncalves, J. Nemchik and R. Pasechnik; *Nuclear effects in Drell-Yan production at the LHC*; will be published in EPJ Web of Conf.
- M. Krelina, J. Cepila, J. Nemchik; *Challenges of direct photon production at forward rapidities and large* p_T; will be published in Journal of Physics Conference Series
- M. Krelina, J. Nemchik; *Production of photons and hadrons on nuclear targets*; ISBN 978-80-244-4726-1, 2015
- M. Krelina, J. Nemchik; *Cronin effect at different energies: from RHIC to LHC*; EPJ Web of Conf. 66, 04016 (2014)
- M. Krelina, J. Nemchik; *Nuclear effects in hadron production in nucleon-nucleus collisions*; Nuclear Physics B (Proc. Suppl.) 245 (2013) 239-242
- M. Krelina, J. Nemchik; *Production of hadrons in proton-nucleus collisions: from RHIC to LHC*; EPJ Web of Conf. 60 (2013) 20023

Oral presentations

- Science coffee seminar - "*Nuclear effects within the color dipole approach*", Lund University, Faculty of Science, Theoretical High Energy Physics, 20.8.2015 (invited talk)
- 18th Conference of Czech and Slovak Physicists, "*Nuclear effects in nucleon-nucleus collisions and nucleus-nucleus collisions*", Olomouc, Czech Republic, 16.-19.9.2014
- 10th International Workshop on High-pT Physics in the RHIC/LHC era, "*Challenges of direct photon production at forward rapidities and large p_T*", SUBATECH Nantes, France, 9.-12.9.2014
- High Energy Physics in the LHC Era - 5th International Workshop, "Nuclear effects of high-pT hadrons in pA interactions",, Valparaiso, Chile, 16.-20.12.2013
- 25th Indian-Summer School - Understanding Hot & Dense QCD Matter, Prague, Czech Republic, 2.-6.9.2013
- Hadron Structure 2013, "*Nuclear effects in hadron production in nucleon-nucleus collisions*", Tatranske Matliare, Slovakia, 30.6. - 4.7.2013

Poster presentations

- ISMD 2015 (XLV International Symposium on Multiparticle Dynamics), Wildbad Kreuth, Germany, 27.9-3.10.2015, 2 posters; Franco Rimondi Association award for the best theoretical poster
- Quark Matter 2015, Kobe, Japan, 27.9-3.10.2015, 2 posters
- INPC 2013 (Internationa Nuclear Physics Conference 2013), Firenze, Italy, 2.-7.6.2013
- LHCP 2013 (LHC Physics Conference 2013), Barcelona, Spain, 13.-18.5.2013
- Schladming Winter School 2013 - Extreme QCD in and out of Equilibrium, Schladming, Austria, 23. February - 2.3.2013
- Ecole Joliot-Curie 2012 - Nuclei through the looking glass, Frejus, France, 30.9.-5.10.2012

Appendix C

Published results

EPJ Web of Conferences 66, 04016 (2014)
DOI: 10.1051/epjconf/20146604016

Cronin effect at different energies: from RHIC to LHC

Michal Krelina[1,a] and Jan Nemchik[1,2,b]

[1] *Czech Technical University in Prague, FNSPE, Brehova 7, 11519 Prague, Czech Republic*
[2] *Institute of Experimental Physics SAS, Watsonova 47, 04001 Kosice, Slovakia*

Abstract. Using the QCD improved parton model we study production of hadrons with large transverse momenta p_T in proton-proton and proton-nucleus collisions at different energies corresponding to experiments at RHIC and LHC. For investigation of large-p_T hadrons produced on nuclear targets we include additionally the nuclear modification of parton distribution functions and the nuclear broadening calculated within the color dipole formalism. We demonstrate that complementary effect of initial state interactions causes a significant suppression at large p_T and at forward rapidities. We provide a good description of the Cronin effect at medium-high p_T and the nuclear suppression at large p_T in agreement with available data from experiments at RHIC and LHC. In the LHC energy range this large-p_T suppression expected at forward rapidities can be verified by the future measurements.

1 Introduction

Experimental and theoretical investigation of inclusive hadron (h) production at different transverse momenta p_T in proton-nucleus ($p + A$) with respect to proton-proton ($p + p$) collisions allows to study various nuclear phenomena through the nucleus-to-proton ratio, the so called nuclear modification factor, $R_A(p_T) = \sigma_{p+A\to h+X}(p_T)/A\,\sigma_{p+p\to h+X}(p_T)$, where A is the mass number.

The Cronin effect, observed already in 1975 [1] as the ratio $R_A(p_T) > 1$ at medium-high p_T, was studied in [2] within the color dipole formalism. Predicted magnitude and the shape of this effect was verified later by the PHENIX data [3] at RHIC and recently by the ALICE experiment [4] at LHC. However, other models presented in [5] do not provide a good description of the last ALICE data [4].

Besides Cronin enhancement of particle production at medium-high p_T the PHENIX data [3] on π^0 production in $d + Au$ collisions at mid rapidity ($y = 0$) indicate a suppression at large p_T, $R_A(p_T) < 1$. Moreover, the BRAHMS and STAR data [6] at forward rapidities demonstrate even much stronger suppression. This forward region is expected to be studied also at LHC since the target Bjorken x is e^y times smaller than at $y = 0$. This allows to investigate a stronger onset of coherent phenomena (shadowing, Color Glass Condensate (CGC)), which are expected to suppress particle yields.

Interpretations of large-y suppression at RHIC and LHC via CGC should be done with a great care since the assumption that CGC is the dominant source of suppression leads to severe problems with understanding of a wider samples of data at smaller energies (see examples in [7]) where no coherence effects are possible. This supports a manifestation of another mechanism proposed in [7] and applied for description of various processes in $p(d) + A$ interactions [8] and in heavy ion collisions [9]. Such a

[a] e-mail: michal.krelina@fjfi.cvut.cz
[b] e-mail: nemcik@saske.sk

mechanism is valid at any energy and is responsible for a significant suppression of particle production at $\xi \to 1$, where $\xi = \sqrt{x_F^2 + x_T^2}$ with Feynman x_F and variable $x_T = 2p_T/\sqrt{s}$ defined at given c.m. energy $\sqrt{s}$. Dissipation of energy due to initial state interactions (ISI) [7] leads to breakdown of the QCD factorization at large ξ and we rely on the factorization formula, Eq. (4), where we replace the proton parton distribution function (PDF) by the nuclear modified one, $f_{a/p}(x, Q^2) \Rightarrow f_{a/p}^{(A)}(x, Q^2, b)$, where

$$f_{a/p}^{(A)}(x, Q^2, b) = C_v f_{a/p}(x, Q^2) \frac{e^{-\xi\sigma_{eff} T_A(b)} - e^{-\sigma_{eff} T_A(b)}}{(1-\xi)\left(1 - e^{-\sigma_{eff} T_A(b)}\right)} \tag{1}$$

with $\sigma_{eff} = 20\,\text{mb}$ and with the normalization factor C_v fixed by the Gottfried sum rule.

2 Cross section calculations

For calculations of the inclusive hadron production in $p + p$ and $p(d) + A$ interactions we adopt the QCD improved parton model. The corresponding invariant inclusive cross section of the process $p + p \to h + X$ is then given by the standard convolution expression based on QCD factorization [10],

$$E\frac{d^3\sigma^{pp\to hX}}{d^3p} = K\sum_{abcd}\int d^2k_{Ta} d^2k_{Tb} \frac{dx_a}{x_{Ra}} \frac{dx_b}{x_{Rb}} F_p^a(x_a, k_{Ta}^2, Q^2) F_p^b(x_b, k_{Tb}^2, Q^2) D_{h/c}(z_c, \mu_F^2) \frac{1}{\pi z_c} \frac{d\hat{\sigma}^{ab\to cd}}{d\hat{t}}, \tag{2}$$

where functions $F_p^i(x_i, k_{Ti}^2, Q^2) = x_i f_{i/p}(x_i, Q^2) g_p(k_{Ti}^2, Q^2)$, K is the normalization factor, $K \approx 1.0-1.5$ depending on the energy, x_a, x_b are fractions of longitudinal momentum of colliding partons, z_c is a fraction of the parton momentum carried by a produced hadron, $d\hat{\sigma}/d\hat{t}$ is the hard parton scattering cross section and radial variable is defined as $x_{Ri}^2 = x_i^2 + 4k_{Ti}^2/s$.

The distribution of the initial parton transverse momentum is described by the Gaussian form [11]

$$g_p(k_T, Q^2) = \frac{1}{\pi\langle k_T^2\rangle_N(Q^2)} e^{-k_T^2/\langle k_T^2\rangle_N(Q^2)} \quad \text{with} \quad \langle k_T^2\rangle_N(Q^2) = \langle k_T^2\rangle_0 + 0.2\,\alpha_S(Q^2) Q^2, \tag{3}$$

where $\langle k_T^2\rangle_0 = 1.5\ \text{GeV}^2$ for RHIC and $\langle k_T^2\rangle_0 = 0.5\ \text{GeV}^2$ for LHC energy in order to obtain the best description of hadron spectra in $p + p$ collisions as is depicted in Fig.1. For the hard parton scattering cross section we use regularization masses $\mu_q = 0.2\,\text{GeV}$ and $\mu_G = 0.8\,\text{GeV}$ for quark and gluon propagators, respectively [2].

For the process $p + A \to h + X$ the corresponding invariant differential cross section reads,

$$\begin{aligned} E\frac{d^3\sigma^{pA\to hX}}{d^3p} = K\sum_{abcd}\int d^2b T_A(b) \int d^2k_{Ta} d^2k_{Tb} \frac{dx_a}{x_{Ra}} \frac{dx_b}{x_{Rb}} g_A(x_a, k_{Ta}, Q^2, b)\, g_p(k_{Tb}, Q^2) \\ \times x_a f_{a/p}(x_a, Q^2) x_b f_{b/A}(b, x_b, Q^2) D_{h/c}(z_c, \mu_F^2) \frac{1}{\pi z_c} \frac{d\hat{\sigma}^{ab\to cd}}{d\hat{t}}, \end{aligned} \tag{4}$$

where $T_A(b)$ is the nuclear thickness function. The nuclear parton distribution functions (NPDFs) $f_{b/A}(x_b, Q^2) = R_f^A(x_b, Q^2)\left[\frac{Z}{A} f_{b/p}(x_b, Q^2) + \left(1 - \frac{Z}{A}\right) f_{b/n}(x_b, Q^2)\right]$ were obtained using the nuclear modification factor $R_f^A(x_b, Q^2)$ with EPS09 [12] and nDS [13] parametrizations. The nuclear modified distribution of the initial parton transverse momentum has the form

$$g_A(x, k_T, Q^2, b) = \frac{1}{\pi\langle k_T^2\rangle_A(x, Q^2, b)} e^{-k_T^2/\langle k_T^2\rangle_A(x, Q^2, b)}, \quad \text{where} \quad \langle k_T^2\rangle_A(Q^2, b) = \langle k_T^2\rangle_N(Q^2) + \Delta k_T^2(x, b). \tag{5}$$

Here $\Delta k_T^2(x, b) = 2\,C(x)\,T_A(b)$ [14] represents nuclear broadening (NB) evaluated within the color dipole formalism. The factor $C(x)$ is related to the dipole cross section $\sigma_{\bar{q}q}$ as $C(x) =$

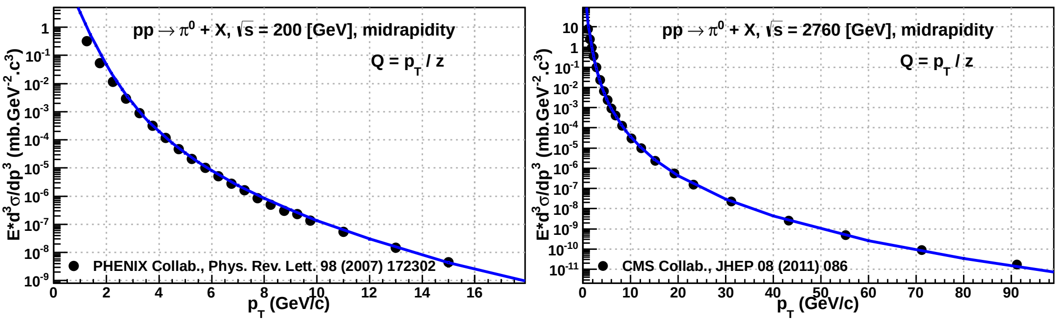

Figure 1. Single inclusive hadron spectra in $p + p$ collisions vs. data at $\sqrt{s} = 200$ and 2760 GeV.

$d\sigma_{\bar{q}q}(x,r)/dr^2|_{r=0}$. NB for gluons is larger due to the Casimir factor 9/4. In all calculations we take the scale $Q^2 = \mu_F^2 = p_T^2/z_c^2$. For PDFs and fragmentation functions we use MSTW2008 [15] and DSS [16] parametrization, respectively. For the dipole cross section we adopt the GBW parametrization from [17] and Impact-Parameter dependent Saturation Model (IP-Sat) from [18].

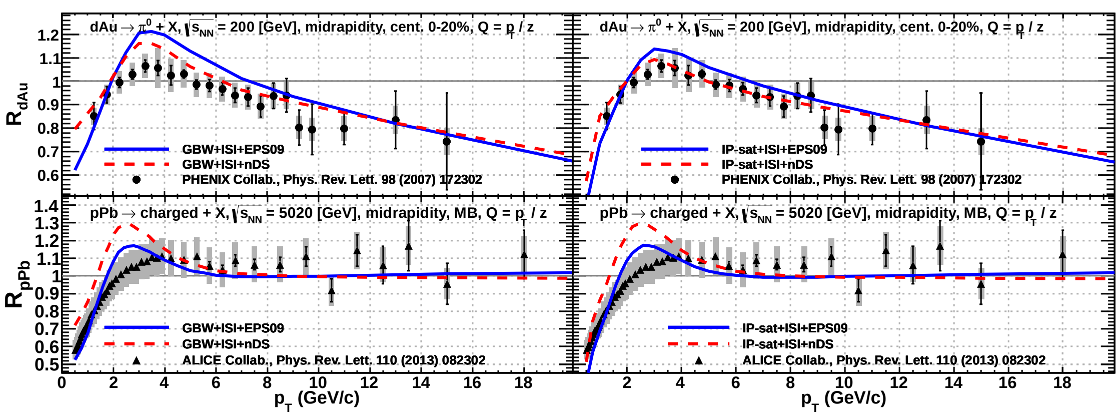

Figure 2. Prediction for the Cronin effect vs. PHENIX [3] and ALICE [4] data.

In Fig. 2 we present predictions for the Cronin effect at mid rapidity in inclusive hadron production at RHIC and LHC in a good agreement with PHENIX data [3] for central (0-20%) d+Au collisions and with data from the ALICE [4] experiment. In all calculations we include ISI effects given by Eq. (1). NPDFs with EPS09 [12] and nDS [13] parametrization are depicted by the solid and dashed lines, respectively. Nuclear broadening is calculated using GBW [17] (left boxes) and IP-Sat [18] (right boxes) parametrization of the dipole cross section, respectively. Note that ISI effects are irrelevant at LHC but cause a significant large-p_T suppression at RHIC.

While we predict in the LHC energy range a weak onset of ISI effects at $y = 0$ resulting in $R_{p+Pb}(p_T) \to 1$ (see Fig. 2), at forward rapidities we expect a significant nuclear large-p_T suppression as is shown in Fig. 3 for several $y = 2$, 3 and 4. The dotted lines represent calculations without ISI effects and NPDFs. The dashed lines include additionally ISI effects given by Eq. (1) and solid lines represent the full calculation including both ISI effects and NPDFs with EPS09 parametrization [12]. Here in all calculations we use IP-Sat parametrization [18] of the dipole cross section.

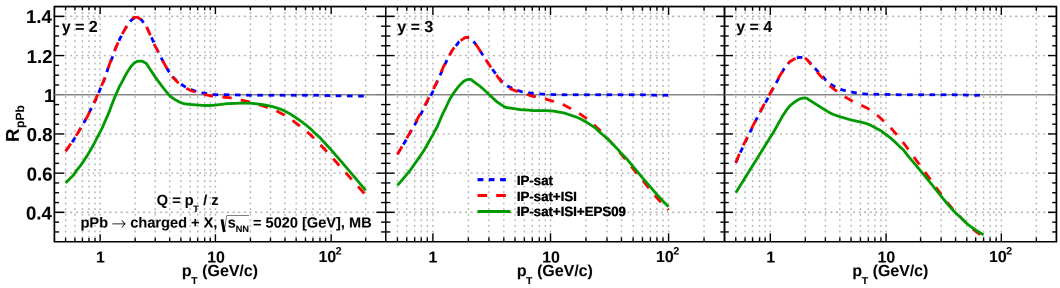

Figure 3. Nuclear modification factor $R_{p+Pb}(p_T)$ for hadron production at $\sqrt{s} = 5.02$ TeV and at $y = 2, 3$ and 4.

3 Conclusions

We provide a good description of data on the Cronin effect at medium-high p_T at RHIC and LHC energies adopting the QCD improved parton model. Nuclear broadening is calculated within the color dipole formalism using two different parametrizations of the dipole cross section. At large p_T we demonstrate a strong onset of ISI effects at RHIC even at mid rapidity causing a significant suppression. In the LHC kinematic region ISI effects are irrelevant at $y = 0$ but we predict a strong large-p_T suppression at forward rapidities that can be verified by the future measurements.

Acknowledgements

This work has been supported by the grant 13-02841S of the Czech Science Foundation (GAČR), by the Grant VZ MŠMT 6840770039, by the Slovak Research and Development Agency APVV-0050-11 and by the Slovak Funding Agency 2/0092/10.

References

[1] J.W. Cronin, et al., Phys. Rev. D. **11**, 3105 (1975).
[2] B.Z. Kopeliovich, et al., Phys. Rev. Lett. **88**, 232303 (2002).
[3] S.S. Adler, et al. (PHENIX Collaboration), Phys. Rev. Lett. **98**, 172302 (2007).
[4] B. Abelev, et al. (ALICE Collaboration), Phys. Rev. Lett. **110**, 082302 (2013).
[5] J. Albacete, N. Armesto, et al., Int. J. Mod. Phys. E**22**, 1330007 (2013)
[6] I. Arsene, et al. (BRAHMS Collaboration), Phys. Rev. Lett. **93**, 242303 (2004); J. Adams, et al. (STAR Collaboration), Phys. Rev. Lett. **97**, 152302 (2006).
[7] B. Z. Kopeliovich et al., Phys. Rev. C**72**, 054606 (2005); B. Z. Kopeliovich and J. Nemchik, J. Phys. G**38**, 043101 (2011).
[8] J. Nemchik, et al., Phys. Rev. C**78**, 025213 (2008); Nucl. Phys. A**830**, 611c (2009).
[9] B.Z. Kopeliovich and J. Nemchik, Phys. Rev. C**86**, 054904 (2012).
[10] R. P. Feynman, R. D. Field and G. C. Fox, Phys. Rev. D**18**, 3320 (1978).
[11] X. N. Wang, Phys. Rev. C**61**, 064910 (2000).
[12] K. J. Eskola, H. Paukkunen and C. .A. Salgado, JHEP **0904**, 065 (2009).
[13] D. de Florian and R. Sassot, Phys. Rev. D**69**, 074028 (2004).
[14] M. B. Johnson, B. Z. Kopeliovich and A. V. Tarasov, Phys. Rev. C**63**, 035203 (2001).
[15] A. D. Martin, W. J. Stirling, R. S. Thorne and G. Watt, Eur. Phys. J. C**63**, 189-285 (2009).
[16] D. de Florian, R. Sassot and M. Stratmann, Phys. Rev. D**75**, 114010 (2007).
[17] K. Golec-Biernat and M. Wüsthoff, Phys. Rev. D**59**, 014017 (1998).
[18] A. H. Rezaeian, at al., Phys. Rev. D**87**, 034002 (2013).

EPJ Web of Conferences **60**, 20023 (2013)
DOI: 10.1051/epjconf/20136020023

Production of hadrons in proton-nucleus collisions: from RHIC to LHC

Michal Krelina[1,a] and Jan Nemchik[1,2,b]

[1] *Czech Technical University in Prague, FNSPE, Brehova 7, 11519 Prague, Czech Republic*
[2] *Institute of Experimental Physics SAS, Watsonova 47, 04001 Kosice, Slovakia*

Abstract. We study nuclear effects in production of large$-p_T$ hadrons on nuclear targets at different energies corresponding to RHIC and LHC experiments. For calculations we employ the QCD improved parton model including the intrinsic parton transverse momenta and the nuclear broadening. Besides nuclear modification of parton distribution functions we include also the complementary effect of initial state interactions causing a significant nuclear suppression at large$-p_T$ and at forward rapidities violating so the QCD factorization. Numerical results for nucleus-to-nucleon ratios are compared with available data from experiments at RHIC and LHC. We perform also predictions for nuclear effects at LHC expected at forward rapidities.

1 Introduction

Recent experimental measurements of particle production at different transverse momenta p_T in proton-nucleus ($p + A$) collisions at RHIC and LHC allows to study various nuclear phenomena. This gives a good baseline for interpretation of the recent heavy-ion results.

Nuclear effects in inclusive hadron (h) production are usually studied through the nucleus-to-nucleon ratio, the so called nuclear modification factor, $R_A(p_T) = \sigma_{p+A\to h+X}(p_T)/A\,\sigma_{p+p\to h+X}(p_T)$.

The Cronin effect, resulting in $R_A(p_T) > 1$ at medium-high p_T, was studied in [1] within the color dipole formalism. Corresponding predictions were confirmed later by data from the PHENIX Collaboration [2] at RHIC and recently by the ALICE experiment [3] at LHC. However, none from other models presented in a review [4] was able to describe successfully the last ALICE data [3].

Another interesting manifestation of nuclear effects leads to nuclear suppression at large p_T, $R_A(p_T) < 1$. Such a suppression is indicated by the PHENIX data [2] on π^0 production in d+Au collisions at mid rapidity, $y = 0$. However, much stronger suppression has been investigated at forward rapidities by the BRAHMS ($y = 1, 2$ and 3.2) and STAR ($y = 4$) Collaborations [5]. This forward region is expected to be studied also at LHC since the target Bjorken x is $\exp(y)$ times smaller than at $y = 0$. This allows to investigate already in the RHIC kinematic region the coherent phenomena (shadowing, Color Glass Condensate (CGC)), which are expected to suppress particle yields.

The interpretation of large-y suppression at RHIC via CGC [6] should be done with a great care since the assumption that CGC is the dominant source of suppression leads to severe problems with understanding of a wider samples of data at smaller energies (see examples in [7]) where no coherence effects are possible. These data demonstrate the same pattern of nuclear suppression increasing with Feynman x_F and/or with $x_T = 2p_T/\sqrt{s}$, where $\sqrt{s}$ is c. m. energy. Threfore it is natural to expect that the mechanisms, which cause the nuclear suppression at lower energies, should be also important and cannot be ignored at the energy of RHIC and LHC. Such a mechanism related to initial state interactions (ISI), which is not related to coherence and is valid at any energy, was proposed in [7] and applied for description of various processes in $p(d) + A$ interactions [8] and in heavy ion collisions [9].

In this paper we perform predictions for $R_A(p_T)$ in hadron production in $p(d) + A$ interactions at RHIC and LHC within the QCD improved parton model. First we verify a successful description of particle spectra in $p + p$ collisions. For evaluation of the Cronin effect we include nuclear breoadening calculated within the color dipole formalism [10]. We demonstrate that nuclear modification of the parton distribution functions leads to a modification of $R_A(p_T)$ especially at small and medium p_T. Effects of ISI cause a strong nuclear suppression at large p_T and/or at forward rapidities. Model calculations of $R_A(p_T)$ are in a good agreement with PHENIX and STAR data at RHIC and with the first data from the ALICE experiment at LHC. We preform also calculations for $R_A(p_T)$ at forward rapidities in the LHC kinematic region. Predicted strong nuclear suppression can be verified in the future by the CMS and ALICE experiments.

2 $p + p$ collisions

Within the QCD improved parton model for the invariant inclusive cross section of the process $p+p \to h+X$ we use the standard convolution expression based on QCD factor-

[a] e-mail: michal.krelina@fjfi.cvut.cz
[b] e-mail: nemcik@saske.sk

Article available at http://www.epj-conferences.org or http://dx.doi.org/10.1051/epjconf/20136020023

ization [11]

$$E\frac{d^3\sigma^{pp\to hX}}{dp^3} = K\sum_{abcd}\int d^2k_{Ta}d^2k_{Tb}\frac{dx_a}{x_{Ra}}\frac{dx_b}{x_{Rb}}$$
$$\times g_p(k_{Ta},Q^2)\,g_p(k_{Tb},Q^2)\,f_{a/p}(x_a,Q^2)\,f_{b/p}(x_b,Q^2)$$
$$\times D_{h/c}(z_c,\mu_F^2)\,\frac{1}{\pi z_c}\,\frac{d\hat{\sigma}^{ab\to cd}}{d\hat{t}} \qquad (1)$$

where K is the normalization factor, $K \approx 1.0 - 1.5$ depending on the energy, $d\hat{\sigma}/d\hat{t}$ is the hard parton scattering cross section, x_a, x_b are fractions of longitudinal momenta of colliding partons and z_c is a fraction of the parton momentum carried by a produced hadron. The radial variable is defined as $x_{Ri}^2 = x_i^2 + 4k_{Ti}^2/s$.

The intrinsic parton transverse momentum distribution g_N is described by the Gaussian distribution

$$g_N(k_T,Q^2) = \frac{1}{\pi\langle k_T^2\rangle_N(Q^2)}e^{-k_T^2/\langle k_T^2\rangle_N(Q^2)}\,, \qquad (2)$$

with a non-perturbative parameter $\langle k_T^2\rangle_N(Q^2)$ representing the mean intrinsic transverse momentum with the scale dependent parametrization taken from [12]

$$\langle k_T^2\rangle_N(Q^2) = 2.0(\mathrm{GeV}^2) + 0.2\,\alpha_S(Q^2)Q^2\,. \qquad (3)$$

For the hard parton scattering cross section we use regularization masses $\mu_q = 0.2\,\mathrm{GeV}$ and $\mu_G = 0.8\,\mathrm{GeV}$ for quark and gluon propagators, respectively [1].

In all calculations we took the scale $Q^2 = \mu_F^2 = p_T^2/z_c^2$. The parton distribution and fragmentation functions were taken with NNPDF2.1 paramatrization [13] and with DSS parametrization [14], respectively.

3 $p + A$ collisions

The invariant differential cross section for inclusive high-p_T hadron production in $p + A$ collisions reads

$$E\frac{d^3\sigma^{pA\to hX}}{dp^3} = K\sum_{abcd}\int d^2bT_A(b)\int d^2k_{Ta}d^2k_{Tb}\frac{dx_a}{x_{Ra}}\frac{dx_b}{x_{Rb}}$$
$$\times g_A(b,k_{Ta},Q^2)\,g_p(k_{Tb},Q^2)\,f_{a/p}(x_a,Q^2)\,f_{b/A}(b,x_b,Q^2)$$
$$\times D_{h/c}(z_c,\mu_F^2)\frac{1}{\pi z_c}\frac{d\hat{\sigma}^{ab\to cd}}{d\hat{t}}\,, \qquad (4)$$

where $T_A(b)$ is the nuclear thickness function normalized to the mass number A. The nuclear parton distribution functions (NPDF) $f_{b/A}(b, x_b, Q^2)$ were obtained using the nuclear modification factor $R_f^A(x_b, Q)$ from EPS09 [15] or nDS [16] for each flavour,

$$f_{b/A}(x_b,Q^2) = R_f^A(x_b,Q^2)\Big[\tfrac{Z}{A}f_{b/p}(x_b,Q^2)$$
$$+\left(1-\tfrac{Z}{A}\right)f_{b/n}(x_b,Q^2)\Big]. \qquad (5)$$

The k_T-broadening Δk_T^2 represents a propagation of the high-energy parton through a nuclear medium that experiences multiple soft rescatterings. It can be imagined as parton multiple gluonic exchanges with nucleons. The initial parton transverse momentum distribution $g_A(k_T, Q^2, b)$ of a projectile nucleon going through the target nucleon at impact parameter b has the same Gaussian form as in $p+p$ collisions,

$$g_A(k_T,Q^2,b) = \frac{1}{\pi\langle k_T^2\rangle_A}(Q^2,b)e^{-k_T^2/\langle k_T^2\rangle_A(Q^2,b)}\,, \qquad (6)$$

but with impact parameter dependent variance

$$\langle k_T^2\rangle_A(Q^2,b) = \langle k_T^2\rangle_N(Q^2) + \Delta k_T^2(b), \qquad (7)$$

where we take k_T-broadening $\Delta k_T^2(b) = 2\,C\,T_A(b)$ evaluated within the color dipole formalism [10]. The variable C is related to the dipole cross section $\sigma_{\bar{q}q}$ describing the interaction of the $\bar{q}q$ pair with a nucleon as

$$C = \left.\frac{d\sigma_{\bar{q}q}^N(r)}{dr^2}\right|_{r=0}\,. \qquad (8)$$

Note that for gluons the nuclear broadening is larger due to the Casimir factor 9/4. For the dipole cross section we adopt the GBW parametrization [17].

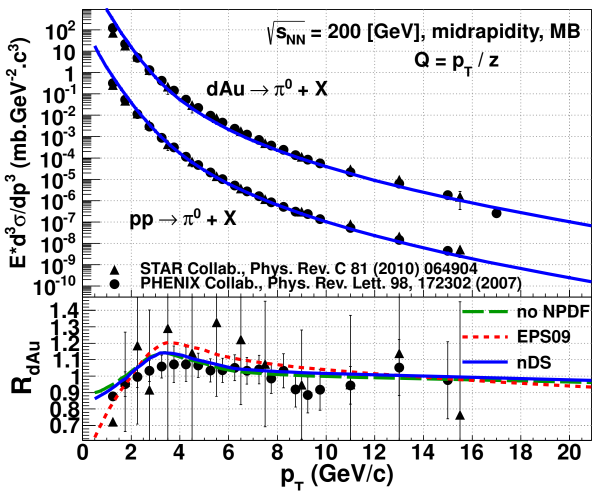

Figure 1. Single inclusive pion spectra in $p + p$ and $d + Au$ collisons and $R_{dAu}(p_T)$ vs. PHENIX [2] and STAR [18] data.

In Fig. 1 we present inclusive π^0-spectra and R_{dAu} at RHIC c.m. energy 200 GeV in a good agreement with data from the PHENIX [2] and STAR [18] experiments. While the dashed line in calculations of $R_{dAu}(p_T)$ corresponds to the pure effect of nuclear broadening the dotted and solid line additionaly include NPDF with parametrization EPS09 and nDS, respectively.

The recent data on hadron production in $p + Pb$ collisions from the ALICE experiment [3] at LHC allow to test our model predictions. The corresponding comparison is presented in Fig. 2 demonstrating a reasonable agreement. While the dashed line represents predictions without NPDFs, the dashed and solid lines including different parametrizations of NPDFs bring our calculations to a better agreement with data at small and medium-high p_T.

4 Initial State Interactions

It was presented in [7–9] that there is a significant suppression of hadron production at $\xi \to 1$, where $\xi = \sqrt{x_F^2 + x_T^2}$.

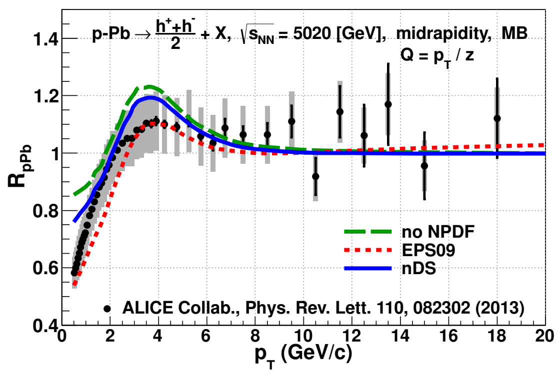

Figure 2. Predictions for the Cronin effect vs. ALICE data [3].

Such a suppression is observed experimentally at large x_F for variety of reactions at small energies (see examples in [7]) and is indicated also in $d + Au$ collisions at RHIC [2]. The interpretation of this effect is based on dissipation of energy due to initial state interactions. As a result the QCD factorization is expected to be broken at large ξ and we rely on the factorization formula, Eq. (4), where we replace the proton PDF by the nuclear modified one, $f_{a/p}(x, Q^2) \Rightarrow f_{a/p}^{(A)}(x, Q^2, b)$, where

$$f_{a/p}^{(A)}(x, Q^2, b) = C_v f_{a/p}(x, Q^2) \frac{e^{-\xi \sigma_{eff} T_A(b)} - e^{-\sigma_{eff} T_A(b)}}{(1-\xi)\,(1 - e^{-\sigma_{eff} T_A(b)})} \quad (9)$$

with $\sigma_{eff} = 20$ mb and the normalization factor C_v is fixed by the Gottfried sum rule.

Besides predictions at $y = 0$ in Fig. 2 where ISI effects are irrelevant we present also calculations for $R_{p+Pb}(p_T)$ at forward rapidities, where we expect a significant nuclear suppression at large p_T due to ISI effects. The results are shown in Fig. 3 for rapidities $y = 0$, 2 and 4. The dotted lines represent calculations without ISI effects and NPDFs. The dashed lines include additionally ISI effects and solid lines represent the full calculation including both ISI effects and NPDFs.

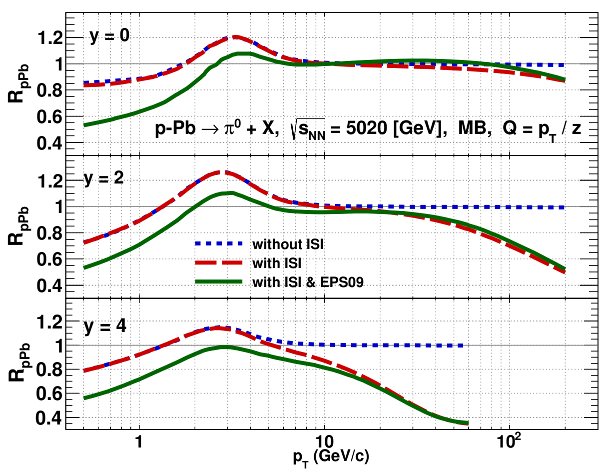

Figure 3. Nuclear modification factor $R_{p+Pb}(p_T)$ for hadron production at c.m. energy 5.02 TeV and at several rapidities.

5 Conclusions

Using the QCD improved parton model we predict the correct magnitude and the shape of the Cronin effect in accordance with data from experiments at RHIC and LHC. Initial state energy loss is expected to suppress significantly inclusive hadron production at large p_T and/or at forward rapidities. Effects of ISI at LHC are irrelevant at $y = 0$ but we predict a strong suppression at forward rapidities that can be verified by the future measurements.

Acknowledgements

This work has been supported by the grant 13-02841S of the Czech Science Foundation (GAČR), by the Grant VZ MŠMT 6840770039, by the Slovak Research and Development Agency APVV-0050-11 and by the Slovak Funding Agency 2/0092/10.

References

[1] B.Z. Kopeliovich, et al., Phys. Rev. Lett. **88**, 232303 (2002).

[2] S.S. Adler, et al. (PHENIX Collaboration), Phys. Rev. Lett. **98**, 172302 (2007).

[3] B. Abelev, et al. (ALICE Collaboration), Phys. Rev. Lett. **110**, 082302 (2013).

[4] J. Albacete, N. Armesto, et al., Int. J. Mod. Phys. E**22**, 1330007 (2013)

[5] I. Arsene, et al. (BRAHMS Collaboration), Phys. Rev. Lett. **93**, 242303 (2004); J. Adams, et al. (STAR Collaboration), Phys. Rev. Lett. **97**, 152302 (2006).

[6] D. Kharzeev, Y. V. Kovchegov and K. Tuchin, Phys. Lett. B**99**, 23 (2004).

[7] B Z. Kopeliovich et al., Phys. Rev. C**72**, 054606 (2005); B.Z. Kopeliovich and J. Nemchik, J. Phys. G**38**, 043101 (2011).

[8] J. Nemchik, et al., Phys. Rev. C**78**, 025213 (2008); Nucl. Phys. A**830**, 611c (2009).

[9] B.Z. Kopeliovich and J. Nemchik, Phys. Rev. C**86**, 054904 (2012).

[10] M. B. Johnson, B. Z. Kopeliovich and A. V. Tarasov, Phys. Rev. C**63**, 035203 (2001).

[11] R. P. Feynman, R. D. Field and G. C. Fox, Phys. Rev. D**18**, 3320 (1978).

[12] X. N. Wang, Phys. Rev. C**61**, 064910 (2000).

[13] R. D. Ball, et al. (NNPDF Collaboration), Nucl. Phys. B**855**, 153 (2012).

[14] D. de Florian, R. Sassot and M. Stratmann, Phys. Rev. D**75**, 114010 (2007).

[15] K. J. Eskola, H. Paukkunen and C. .A. Salgado, JHEP **0908**, 065 (2009).

[16] D. de Florian and R. Sassot, Phys. Rev. D**69**, 074028 (2004).

[17] K. Golec-Biernat and M. Wüsthoff, Phys. Rev. D**59**, 014017 (1998).

[18] B. Abelev, et al. (STAR Collaboration), Phys. Rev. C**81**, 064904 (2010).

Available online at www.sciencedirect.com

ScienceDirect

Nuclear Physics B (Proc. Suppl.) 245 (2013) 239–242

NUCLEAR PHYSICS B PROCEEDINGS SUPPLEMENTS

www.elsevier.com/locate/npbps

Nuclear effects in hadron production in nucleon-nucleus collisions

Michal Krelina[a], Jan Nemchik[a,b]

[a]Czech Technical University in Prague, FNSPE, Brehova 7, 11519 Prague, Czech Republic
[b]Institute of Experimental Physics SAS, Watsonova 47, 04001 Kosice, Slovakia

Abstract

We investigate nuclear effects in production of large-p_T hadrons in nucleon-nucleus collisions corresponding to a broad energy range from the fix-target up to RHIC and LHC experiments. For this purpose we use the QCD improved parton model including the intrinsic parton transverse momenta. This model is firstly tested reproducing well the data on p_T spectra of hadrons produced in proton-proton collisions at different energies. For investigation of large-p_T hadrons produced on nuclear targets we include additionally the nuclear broadening and the nuclear modification of parton distribution functions. We also demonstrate that at large-p_T and at forward rapidities the complementary effect of initial state interactions (ISI) causes a significant nuclear suppression. Numerical results for nucleus-to-nucleon ratios are compared with available data from the fix-target and collider experiments. We perform also predictions at forward rapidities which are expected to be measured in the future at LHC.

Keywords: proton-nucleus collisions, nuclear modification factor, Cronin effect, effect of initial state interactions

1. Introduction

Existing experimental measurements of particle production at different transverse momenta p_T in proton-nucleus ($p + A$) collisions and at different energies clearly demonstrate a manifestation of various nuclear effects, which are usually studied through the nucleus-to-nucleon ratio, the so called nuclear modification factor, defined for inclusive hadron (h) production as $R_A(p_T) = \sigma_{p+A\to h+X}(p_T)/A\,\sigma_{p+p\to h+X}(p_T)$, where A is the mass number. This gives a good baseline for interpretation of the recent heavy-ion results.

The enhancement of hadron production in $p + A$ with respect to $p + p$ collisions, $R_A(p_T) > 1$, at medium-high p_T is known as the Cronin effect [1] and was studied in [2] within the color dipole formalism. Corresponding predictions were confirmed later by data from the PHENIX Collaboration [3] at RHIC and recently by the ALICE experiment [4] at LHC. However, none from other models presented in a review [5] was able to describe successfully the last ALICE data [4].

On the other hand, the PHENIX data [3] on π^0 production in central d+Au collisions at mid rapidity, $y = 0$, indicate a suppression at large p_T, $R_A(p_T) < 1$. However, as is demonstrated by the BRAHMS and STAR data [6], the forward rapidity region is even much more suitable for investigation of large-p_T suppression since the target Bjorken x is exp(y)-times smaller than at $y = 0$. This allows to investigate already in the RHIC kinematic region the coherent phenomena (shadowing, Color Glass Condensate), which are expected to suppress particle yields.

The interpretation of large-y suppression at RHIC via only coherent phenomena leads to severe problems with understanding of a wider samples of data at smaller energies (see examples in [7]) where no coherence effects are possible. These data demonstrate the same pattern of nuclear suppression increasing with Feynman x_F and/or with $x_T = 2p_T/\sqrt{s}$, where $\sqrt{s}$ is c. m. energy. This leads to an expectation that the mechanism, which causes the nuclear suppression at low energies, should

Email addresses: michal.krelina@fjfi.cvut.cz (Michal Krelina), nemcik@saske.sk (Jan Nemchik)

http://dx.doi.org/10.1016/j.nuclphysbps.2013.10.045

be also important and cannot be ignored at the energy of RHIC and LHC. Such a mechanism related to initial state interactions (ISI), which is not related to coherence and is valid at any energy, was proposed in [7] and applied for description of various processes in $p(d) + A$ interactions [8] and in heavy ion collisions [9].

In the present paper we will study a manifestation of nuclear effects included in our predictions for nuclear modification factor like isospin corrections, nuclear modification of parton distribution functions (shadowing), nuclear broadening (Cronin effect) and ISI effects.

2. $p + p$ collisions

For evaluation of the invariant cross section of the process $p + p \to h + X$ we use the standard convolution expression based on QCD factorization [10]

$$E\frac{d^3\sigma^{pp\to hX}}{dp^3} = K\sum_{abcd}\int d^2k_{Ta}d^2k_{Tb}\frac{dx_a}{x_{Ra}}\frac{dx_b}{x_{Rb}} \times g_p(k_{Ta},Q^2)\,g_p(k_{Tb},Q^2)\,F_{a/p}(x_a,Q^2)\,F_{b/p}(x_b,Q^2) \times D_{h/c}(z_c,\mu_F^2)\,\frac{1}{\pi z_c}\,\frac{d\hat{\sigma}^{ab\to cd}}{d\hat{t}}\,, \quad (1)$$

where $F_{i/p}(x_i, Q^2) = x_i\, f_{i/p}(x_i, Q^2)$ with parton distribution functions (PDF) $f_{i/p}(x_i, Q^2)$, K is the normalization factor (not important for us), $K \approx 1.0 - 1.5$ depending on the energy, $d\hat{\sigma}/d\hat{t}$ is the hard parton scattering cross section, x_a, x_b are fractions of longitudinal momenta of colliding partons and z_c is a fraction of the parton momentum carried by a produced hadron. The radial variable is defined as $x_{Ri}^2 = x_i^2 + 4k_{Ti}^2/s$.

The distribution of the initial parton transverse momentum is described by the Gaussian form [11],

$$g_p(k_T, Q^2) = \frac{1}{\pi\langle k_T^2\rangle_N(Q^2)}e^{-k_T^2/\langle k_T^2\rangle_N(Q^2)} \quad (2)$$

with the scale dependent parametrization of the mean intrinsic transverse momentum from [11],

$$\langle k_T^2\rangle_N(Q^2) = \langle k_T^2\rangle_0 + 0.2\,\alpha_S(Q^2)\,Q^2\,, \quad (3)$$

where $\langle k_T^2\rangle_0 = 0.2$ GeV^2 and 2.0 GeV^2 for quarks and gluons, respectively. Such a large value of $\langle k_T^2\rangle_0$ for gluons results from a small gluon propagation radius [12]. We verified that the invariant cross section (1) with parametrization (2) provides a good description of hadron spectra at different energies.

For the hard parton scattering cross section we use regularization masses $\mu_q = 0.2$ GeV and $\mu_G = 0.8$ GeV [2] for quark and gluon propagators, respectively. In all calculations we take the scale $Q^2 = \mu_F^2 = p_T^2/z_c^2$. For PDFs and fragmentation functions we use MSTW2008 [13] and DSS [14] parametrization, respectively.

3. $p + A$ collisions. Nuclear effects

The invariant differential cross section for inclusive high-p_T hadron production in $p + A$ collisions reads

$$E\frac{d^3\sigma^{pA\to hX}}{dp^3} = K\sum_{abcd}\int d^2bT_A(b)\int d^2k_{Ta}d^2k_{Tb}\frac{dx_a}{x_{Ra}}\frac{dx_b}{x_{Rb}} \times g_A(b,k_{Ta},Q^2)\,g_p(k_{Tb},Q^2)\,F_{a/p}(x_a,Q^2)\,F_{b/A}(b,x_b,Q^2) \times D_{h/c}(z_c,\mu_F^2)\frac{1}{\pi z_c}\frac{d\hat{\sigma}^{ab\to cd}}{d\hat{t}}\,, \quad (4)$$

where $T_A(b)$ is the nuclear thickness function at given impact parameter b normalized to the mass number A and $F_{i/A}(b, x_i, Q^2) = x_i\, f_{i/A}(b, x_i, Q^2)$.
Eq. (4) includes the following nuclear effects:

Isospin effect. This effect is important in the large-x region where the valence quarks dominate. It is incorporated in Eq. (4) as the following modification of PDFs,

$$f_{i/N}(x, Q^2) = \tfrac{Z}{A} f_{i/p}(x, Q^2) + \left(1 - \tfrac{Z}{A}\right) f_{i/n}(x, Q^2)\,, \quad (5)$$

where Z is the proton number of the target.

Nuclear modification of PDFs. The nuclear parton distribution functions (NPDFs) are associated with nuclear shadowing at sufficiently small x and are obtained using the nuclear modification factor $R_i^A(x, Q^2)$ with EPS09 [15] or nDS [16] parametrization,

$$f_{i/A}(x, Q^2) = R_i^A(x, Q^2) f_{i/N}(x, Q^2). \quad (6)$$

Nuclear broadening. In Eq. (4) the nuclear intrinsic parton transverse momentum distribution $g_A(k_T, Q^2, b)$ of a projectile nucleon going through the target nucleon at impact parameter b has the same Gaussian form as in $p + p$ collisions,

$$g_A(k_T, Q^2, b) = \frac{1}{\pi\langle k_T^2\rangle_A(Q^2, b)}e^{-k_T^2/\langle k_T^2\rangle_A(Q^2,b)}\,, \quad (7)$$

but with impact parameter dependent variance

$$\langle k_T^2\rangle_A(Q^2, b) = \langle k_T^2\rangle_N(Q^2) + \Delta k_T^2(b)\,, \quad (8)$$

where we take the nuclear k_T-broadening $\Delta k_T^2(x, b) = 2\,C(x)\,T_A(b)$ evaluated within the color dipole formalism [17]. The factor $C(x)$ is related to the dipole cross section $\sigma_{\bar{q}q}$, which describes the interaction of the $\bar{q}q$ pair with a nucleon, as $C(x) = \left.\frac{d\sigma^N_{\bar{q}q}(x,r)}{dr^2}\right|_{r=0}$. Note that for gluons the nuclear broadening is larger due to the Casimir factor 9/4. For the dipole cross section we adopt the GBW parametrization from [18] and Impact-Parameter dependent Saturation Model (IP-Sat) from [19].

Initial state interactions. It was demonstrated in [7, 8, 9] that a significant suppression of hadron production arises at $\xi \to 1$, where $\xi = \sqrt{x_F^2 + x_T^2}$. Observed suppression at RHIC at forward rapidities (large

x_F) [6] is usually interpreted by the onset of coherence effects. However, a similar large-x_F suppression is observed also for variety of reactions at small energies (see examples in [7]) where no effects of coherence are possible. Even indicated large-p_T suppression in central $d + Au$ collisions by the PHENIX data [3] cannot be explained by the onset of coherence effects. This supports an existence of a complementary mechanism based on a dissipation of energy due to ISIs leading to breakdown of the QCD factorization at large ξ [7]. Here we rely on the factorization formula, Eq. (4), where we replace the proton PDF by the nuclear modified one, $f_{a/p}(x, Q^2) \Rightarrow f_{a/p}^{(A)}(x, Q^2, b)$, where

$$f_{a/p}^{(A)}(x, Q^2, b) = N f_{a/p}(x, Q^2) \frac{e^{-\xi\sigma_{eff}T_A(b)} - e^{-\sigma_{eff}T_A(b)}}{(1-\xi)\left(1 - e^{-\sigma_{eff}T_A(b)}\right)} \quad (9)$$

with $\sigma_{eff} = 20\,\mathrm{mb}$ and the normalization factor N is fixed by the Gottfried sum rule. Note that corrections, Eq. (9), correspond to sufficiently long coherence length, $l_c = \sqrt{s}/m_N k_T \gtrsim R_A$, where R_A is the nuclear radius. In the opposite case, when $l_c \lesssim 1 \div 2$ fm, corrections for ISI effects are weaker due to substitution $T_A(b) \Rightarrow T_A(b)/2$.

4. Comparison with data

As far as we have a good description of the data for proton target, we have no further adjustable parameters and can predict nuclear effects. At a small energy corresponding to FNAL fixed target experiments [20] besides Cronin enhancement at medium-high p_T and nuclear modification of PDFs one should not expect any nuclear effects. However, we predict a significant onset of ISI effects causing a supplementary suppression rising with p_T. Such a situation is depicted as a difference between the solid and dotted lines in Fig. 1 where the results of parameter-free calculations for the production of charged pions are compared with fixed target data on the ratio of the tungsten and beryllium cross sections, $R_{W/Be}(p_T)$, at $\sqrt{s} = 27.4$ GeV [20] as function of p_T. While the dotted line includes besides NPDFs also nuclear broadening calculated with KST dipole cross section [12], the solid line includes additionally ISI effects, Eq. (9).

In the RHIC energy range at $y = 0$ besides Cronin enhancement at medium-high p_T and small isotopic corrections at large p_T one should not expect any nuclear effects since no coherence effects are possible. However, the PHENIX data [3] indicate large-p_T suppression, which is more evident for central $d + Au$ collisions, as is demonstrated in Fig. 2 (lower box). Such a suppression is caused by ISI effects, Eq. (9), and is

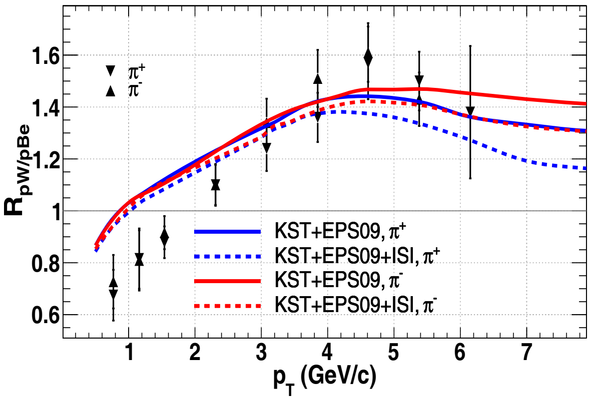

Figure 1: Ratio of the charged pion production cross sections for tungsten and beryllium as a function of the transverse momentum of the produced pions. The dotted lines include only nuclear broadening and NPDFs, while the solid ones include additionally ISI effects, Eq. (9) with a modification for short l_c. The data are taken from the fixed target experiments [20].

depicted by the solid lines, while the dotted lines, representing calculations without ISI effects, overestimate the PHENIX data at large p_T. In Fig. 2 the red and blue lines correspond to nuclear broadening calculated with IP-Sat [19] and GBW [18] parametrizations, respectively.

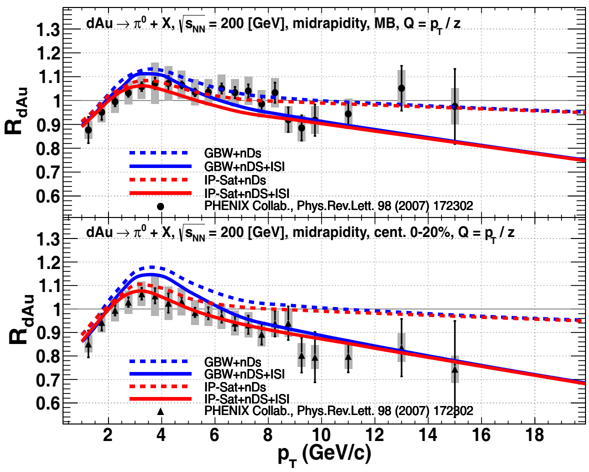

Figure 2: Nuclear modification factor $R_{d+Au}(p_T)$ for π^0 production in $d + Au$ collisions at $\sqrt{s} = 200$ GeV vs. PHENIX data [3], minimum bias (MB) - upper box and centrality $0 - 20\,\%$ - lower box. Nuclear broadening is calculated for two different parametrizations of the color dipole cross sections, GBW [18] and IP-Sat [19]

While we predict at $y = 0$ a significant onset of ISI effects at RHIC energies and at energies corresponding to fixed target FNAL experiments, one should not expect such effects at LHC since the corresponding Bjorken x

is very small. The recent data on charge hadron production in $p+Pb$ collisions from the ALICE experiment [4] confirm such an expectation as is demonstrated in Fig. 3, where $R_{p+Pb}(p_T) \approx 1$ at large p_T. The ALICE data [4] presented in Fig. 3 allow so to test only our model predictions for the Cronin enhancement at medium-high p_T and the corresponding comparison demonstrates a good agreement. The solid and dotted lines represent calculations at $y = 0$ using NPDFs with the EPS09 and nDS parametrization, respectively. However, ISI effects causing a significant large-p_T suppression can be arisen at forward rapidities as is depicted in Fig. 3 by the dashed and dot-dashed lines calculated at $y = 2$ and $y = 4$, respectively, using the nDS parametrization of NPDFs. The upper and lower panel corresponds to calculations of nuclear broadening using GBW [18] and IP-Sat [19] parametrization of the dipole cross section, respectively.

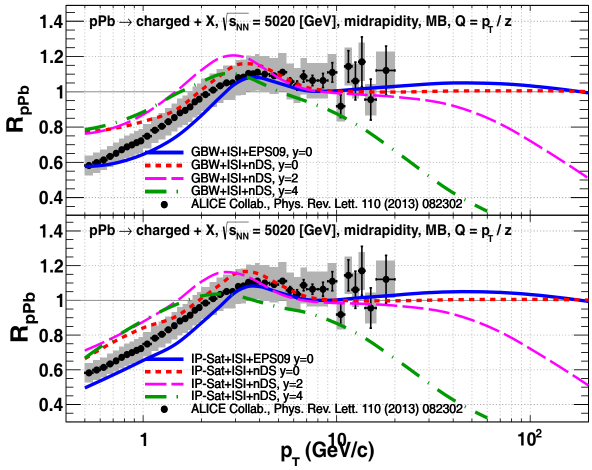

Figure 3: Nuclear modification factor $R_{p+Pb}(p_T)$ for charge hadron production at several rapidities, $y = 0, 2$ and 4. The data at mid rapidity are taken from [4].

5. Conclusions

Using the QCD improved parton model we present a good description of data on the nuclear modification factor as function of p_T covering a broad energy interval starting from the fix-target experiments at FNAL through the experiments at RHIC and finishing at the recent experiments at LHC. In predictions we include various nuclear effects like the Cronin enhancement of particle production, isotopic corrections, coherent effects (shadowing) at small Bjorken x and ISI effects, Eq. (9). The nuclear broadening is calculated within the color dipole formalism using different parametrizations of the dipole cross section. In the all energy interval we predict the correct magnitude and the shape of the Cronin effect in accordance with available data from the fixed-target FNAL experiments and collider experiments at RHIC and LHC. We demonstrate a manifestation of ISI effects at FNAL energy $\sqrt{s} = 27.4$ GeV causing an additional suppression in a reasonable agreement with corresponding data. In the RHIC energy range ISI effects cause a significant large-p_T suppression at $y = 0$ in accordance with RHIC data on pion production in central $d + Au$ collisions. Such a large-p_T suppression corresponds to breakdown of the QCD factorization. In the LHC kinematic region ISI effects are irrelevant at $y = 0$, but we predict a strong suppression at forward rapidities that can be verified by the future measurements.

Acknowledgments

This work has been supported in part by the grant 13-02841S of the Czech Science Foundation (GAČR), by the Grant VZ MŠMT 6840770039, by the Slovak Research and Development Agency APVV-0050-11 and by the Slovak Funding Agency, Grant 2/0092/10.

References

[1] J.W. Cronin, et al., Phys. Rev. D. **11**, 3105 (1975).
[2] B.Z. Kopeliovich, et al., Phys. Rev. Lett. **88**, 232303 (2002).
[3] S.S. Adler, et al. (PHENIX Collaboration), Phys. Rev. Lett. **98**, 172302 (2007).
[4] B. Abelev, et al. (ALICE Collaboration), Phys. Rev. Lett. **110**, 082302 (2013).
[5] J. Albacete, N. Armesto, et al., Int. J. Mod. Phys. E**22**, 1330007 (2013)
[6] I. Arsene, et al. (BRAHMS Collaboration), Phys. Rev. Lett. **93**, 242303 (2004); J. Adams, et al. (STAR Collaboration), Phys. Rev. Lett. **97**, 152302 (2006).
[7] B Z. Kopeliovich et al., Phys. Rev. C**72**, 054606 (2005); B.Z. Kopeliovich and J. Nemchik, J. Phys. G**38**, 043101 (2011).
[8] J. Nemchik, et al., Phys. Rev. C**78**, 025213 (2008); Nucl. Phys. A**830**, 611c (2009).
[9] B.Z. Kopeliovich and J. Nemchik, Phys. Rev. C**86**, 054904 (2012).
[10] R. P. Feynman, R. D. Field and G. C. Fox, Phys. Rev. D**18**, 3320 (1978).
[11] X. N. Wang, Phys. Rev. C**61**, 064910 (2000).
[12] B. Z. Kopeliovich, A. Schfer and A. V. Tarasov,, Phys. Rev. D**62** (2000) 054022..
[13] A. D. Martin, W. J. Stirling, R. S. Thorne and G. Watt, Eur. Phys. J. C**63**, 189-285 (2009).
[14] D. de Florian, R. Sassot and M. Stratmann, Phys. Rev. D**75**, 114010 (2007).
[15] K. J. Eskola, H. Paukkunen and C. .A. Salgado, JHEP **0904**, 065 (2009).
[16] D. de Florian and R. Sassot, Phys. Rev. D**69**, 074028 (2004).
[17] M. B. Johnson, B. Z. Kopeliovich and A. V. Tarasov, Phys. Rev. C**63**, 035203 (2001).
[18] K. Golec-Biernat and M. Wüsthoff, Phys. Rev. D**59**, 014017 (1998).
[19] A. H. Rezaeian, at al., Phys. Rev. D**87**, 034002 (2013).
[20] D. Antreasyan, et al., Phys. Rev. D**19**, 764 (1979); P.B. Straub, et al., Phys. Rev. Lett. **68**, 452 (1992).

Challenges of direct photon production at forward rapidities and large p_T

Michal Krelina, Jan Cepila

Czech Technical University in Prague, FNSPE, Brehova 7, 11519 Prague, Czech Republic

E-mail: `michal.krelina@fjfi.cvut.cz`

Jan Nemchik

Czech Technical University in Prague, FNSPE, Brehova 7, 11519 Prague, Czech Republic
Institute of Experimental Physics SAS, Watsonova 47, 04001 Kosice, Slovakia

Abstract. Direct photons produced in interactions with nuclear targets represent a cleaner probe for investigation of nuclear effects than hadrons, since photons have no final state interaction and no energy loss or absorption is expected in the produced hot medium. Therefore, besides the Cronin enhancement at medium-high transverse momenta p_T and isospin effects at larger p_T, one should not expect any nuclear effects. However, this fact is in contrast to the PHENIX data providing an evidence for a significant large-p_T suppression at mid rapidities in central $d + Au$ and $Au + Au$ collisions that cannot be induced by coherent phenomena (gluon shadowing, Color Glass Condensate). We demonstrate that such an unexpected results is subject to deficit of energy induced universally by multiple initial state interactions (ISI) towards the kinematic limits (large Feynman x_F and/or large $x_T = 2p_T/\sqrt{s}$). For this reason, in order to enhance the effects of coherence, one should be cautious going to forward rapidities and higher energies. In the LHC kinematic region ISI corrections are irrelevant at mid rapidities but cause rather strong suppression at forward rapidities and large p_T. Numerical calculations of invariant p_T spectra and the nuclear modification factor were performed within two different models, the color dipole formalism and the model based on k_T-factorization, which are successfully confronted with available data from the RHIC and LHC collider experiments. Finally, we perform also predictions for a strong onset of ISI corrections at forward rapidities and corresponding expected suppression can be verified by the future measurements at LHC.

1. Introduction

Direct photons provide an unique tool to study nuclear effects in proton-nucleus and heavy-ion collisions and represent a cleaner probe than hadron production since they have no final state interactions, either energy loss or absorption in the produced hot medium. For this reason, no convolution with the jet fragmentation function is required and no nuclear effects are expected besides the Cronin enhancement and small isotopic corrections. Thus, direct photons can serve as an additional tool to discriminate between overall nuclear effects and the effects coming from final state interactions typical for strongly interacting particles in heavy-ion collisions. Manifestations of nuclear effects are usually studied through the nucleus-to-nucleon ratio, the so called nuclear modification factor, $R_A(p_T) = \sigma_{pA\to\gamma+X}(p_T)/A\,\sigma_{pp\to\gamma+X}(p_T)$ for pA collisions and $R_{AB}(p_T) = \sigma_{AB\to\gamma+X}(p_T)/AB\,\sigma_{pp\to\gamma+X}(p_T)$ for minimum bias (MB) AB collisions.

At medium-high transverse momenta p_T one should take into account the Cronin effect, enhancement of particle production in pA collisions, $R_A(p_T) > 1$. This effect was studied within the color dipole formalism in [1], where the predicted shape and magnitude of the Cronin enhancement were confirmed later by the PHENIX data [2] at RHIC and recently by the ALICE measurements [3] at LHC. However, other models presented in the review [4] were not able to describe successfully the last ALICE data [3].

Since the Cronin enhancement can not be measured precisely by experiments at RHIC and LHC due to difficult identification of direct photons at small and medium-high p_T, in this paper we focused on study of possible nuclear effects in the large-p_T region. In contrast with a naive expectation about an absence of nuclear effects at large p_T the PHENIX data [2] on π^0 production in central dAu collisions provide a clear evidence for a significant suppression at midrapidity, $y = 0$. Such an observation is confirmed also by the PHENIX data on direct photon production in central $AuAu$ collisions [5]. Besides small isotopic corrections, observed attenuation can not be interpreted by the coherence effects (gluon shadowing, color glass condensate) due to large values of Bjorken x.

Alternative interpretation is based on multiple interactions of the projectile hadron and its debris during propagation through the nucleus. The corresponding energy loss is proportional to the hadron energy and the related effects do not disappear at very high energies as was stressed in [6]. In each Fock component the hadron momentum is shared between its constituents: the more constituents are involved, the smaller is the mean energy per parton. This leads to the softer fractional energy distribution of a leading parton, and the projectile parton distribution falls at large $x \to 1$ steeper on a nuclear target than on a proton.

Such softening of the projectile parton fractional energy distribution can be viewed as an effective energy loss of the leading parton due to initial state multiple interactions (ISI). Enhancement of the weight factors for higher Fock states in the projectile hadron with a large number of constituents leads to reduction of the mean fractional energy of the leading parton compared to lower Fock states which dominate the hard reaction on a proton target. Such a reduction is apparently independent of the initial hadron energy and can be treated as an effective loss of energy proportional to the initial hadron energy. A detailed description and interpretation of the corresponding additional suppression was presented also in Refs. [7, 8, 9].

The effect of initial state energy loss (ISI effect) is not effective at high energies and midrapidities. However, it may essentially suppress the cross section approaching the kinematic bound, either in $x_L = 2p_L/\sqrt{s} \to 1$ or $x_T = 2p_T/\sqrt{s} \to 1$ defined at given c.m. energy $\sqrt{s}$. Correspondingly, the proper variable which controls this effect is $\xi = \sqrt{x_L^2 + x_T^2}$.

The magnitude of suppression was evaluated in Ref. [6, 10]. It was found within the Glauber approximation that each interaction in the nucleus leads to a suppression factor $S(\xi) \approx 1 - \xi$. Summing up over the multiple initial state interactions in a pA collision with impact parameter b one arrives at a nuclear ISI-modified parton distribution function (PDF) $F_{a/p}(x, Q^2) \Rightarrow F_{a/p}^{(A)}(x, Q^2, b)$, where

$$f_{a/p}(x, Q^2) \Rightarrow f_{a/p}^{(A)}(x, Q^2, b) = C_v f_{a/p}(x, Q^2) \frac{e^{-\xi\,\sigma_{eff} T_A(b)} - e^{-\sigma_{eff} T_A(b)}}{(1-\xi)\left(1 - e^{-\sigma_{eff} T_A(b)}\right)}. \tag{1}$$

Here $\sigma_{eff} = 20\,\mathrm{mb}$ [6] is the effective hadronic cross section controlling the multiple interactions. The normalization factor C_v in Eq. (1) is fixed by the Gottfried sum rule, $T_A(\vec{b})$ is the nuclear thickness function at given impact parameter b normalized to the mass number A. It was found that such an additional nuclear suppression due to the ISI effects represents an energy independent feature common for all known reactions, experimentally studied so far, with any leading particle (hadrons, Drell-Yan dileptons, charmonium, etc.).

Using PDFs modified by the ISI energy loss, Eq. (1), one can predict much stronger onset of nuclear suppression in a good agreement with available data from the BRAHMS and STAR [11] experiments at forward rapidities (large x_L) in dA collisions [6, 10]. An alternative interpretation [12] is based on the coherence effects, which should disappear at lower energies because $x \propto 1/\sqrt{s}$ increases. However, according to Eq. (1) the suppression caused by the ISI energy loss scales in Feynman $x_F = x_L$ and should exist at any energy. Thus, by reducing the collision energy one should provide a sensitive test for the models. Expectation of no suppression following from CGC at forward rapidities and small energies is in contradiction with data from the NA49 experiments [13] at SPS obtained at much smaller energy than BRAHMS. This observation confirms an onset of suppression at forward rapidities with entirely interpretation based on the ISI energy loss.

The ISI energy loss also affects the p_T dependence of the nuclear suppression in heavy ion collisions. These effects are calculated similarly to $p(d)A$ collisions using the modified PDFs, Eq. (1), for nucleons in both colliding nuclei.

In order to test theoretical uncertainties, in this paper we calculate p_T-spectra and nuclear suppression of direct photons produced on nuclear targets at RHIC and LHC energy using two different models. Corresponding results obtained within the model based on k_T-factorisation [14] will be compared with the color dipole approach [15].

2. Model based on k_T-factorisation

Here the process of direct photon production to the leading order can be treated as a collision of two hadrons where a quark from one hadron annihilates with an antiquark from the other hadron into a real photon. In vacuum (e.g. in pp collisions), in calculations of the invariant cross section of direct photon production we employ the model proposed in [16]:

$$E\frac{d^3\sigma^{pp\to\gamma X}}{d^3p} = K\sum_{abd}\int d^2k_{Ta}d^2k_{Tb}\frac{dx_a}{x_{Ra}}\frac{dx_b}{x_{Rb}}g_p(k_{Ta},Q^2)\,g_p(k_{Tb},Q^2) \times F_{a/p}(x_a,Q^2)\,F_{b/p}(x_b,Q^2)\,\frac{\hat{s}}{\pi}\,\frac{d\hat{\sigma}^{ab\to\gamma d}}{d\hat{t}}\,\delta(\hat{s}+\hat{t}+\hat{u}), \quad (2)$$

which corresponds to the collinear factorization expression modified by an intrinsic transverse momentum dependence. In Eq. (2) $K \approx 1.0 - 1.5$ is the normalization factor depending on the c.m. energy, $F_{i/p}(x_i, Q^2) = x_i\, f_{i/p}(x_i, Q^2)$ with PDF $f_{i/p}(x_i, Q^2)$, $d\hat{\sigma}/d\hat{t}$ is the cross section of hard parton scattering, x_a, x_b are fractions of longitudinal momenta of the incoming hadrons. The radial variable is defined as $x_{Ri}^2 = x_i^2 + 4k_{Ti}^2/s$, $\hat{s}, \hat{t}, \hat{u}$ are the parton Mandesltam variables and $\vec{k}_{T_i}$ is transverse momentum of parton.

The distribution of the initial parton transverse momentum is described by the Gaussian form [16],

$$g_p(k_T, Q^2) = \frac{1}{\pi\langle k_T^2\rangle_N(Q^2)}e^{-k_T^2/\langle k_T^2\rangle_N(Q^2)} \quad (3)$$

with the scale dependent parametrization of the mean intrinsic transverse momentum from [16], $\langle k_T^2\rangle_N(Q^2) = \langle k_T^2\rangle_0 + 0.2\,\alpha_S(Q^2)\,Q^2$, where $\langle k_T^2\rangle_0 = 0.2$ GeV^2 and 2.0 GeV^2 for quarks and gluons, respectively.

For the hard parton scattering cross section we use regularization masses $\mu_q = 0.2$ GeV and $\mu_G = 0.8$ GeV for quark and gluon propagators, respectively. In all calculations we take the scale $Q^2 = p_T^2$. For PDFs we used MSTW2008 [17] parametrization.

The differential cross section for direct photon production in $p + A$ and $A + A$ collisions then can be treated as

$$E\frac{d^3\sigma^{pA\to\gamma X}}{d^3p} = \int d^2b\,T_A(\vec{b})E\frac{d^3\tilde{\sigma}^{pp\to\gamma X}}{d^3p} \quad (4)$$

and

$$E\frac{d^3\sigma^{AB\to\gamma X}}{d^3p} = \int d^2b\, d^2s\, T_A(\vec{s})T_B(\vec{b}-\vec{s})E\frac{d^3\tilde{\sigma}^{pp\to\gamma X}}{d^3p}, \tag{5}$$

respectively.

In Eqs. (4) and (5) the *pp*-invariant cross section has the same form as is given by Eq.(2) except for a modification of PDFs to nuclear ones (nPDF) $F_{i/A}(b, x_i, Q^2) = R_i^A(x, Q^2)\left(\frac{Z}{A}x_i f_{i/p}(x, Q^2) + \left(1 - \frac{Z}{A}\right) x_i f_{i/n}(x, Q^2)\right)$, where $R_i^A(x, Q^2)$ is the nuclear modification factor from EPS09 [18]. Invariant cross section $E\, d^3\tilde{\sigma}^{pp\to\gamma X}/d^3p$ in Eqs. (4) and (5) contains also a nuclear modified distribution of the initial parton transverse momentum as reads,

$$g_A(k_T, Q^2, b) = \frac{1}{\pi\langle k_T^2\rangle_A(Q^2, b)} e^{-k_T^2/\langle k_T^2\rangle_A(Q^2,b)}\,, \tag{6}$$

where impact parameter dependent variance $\langle k_T^2\rangle_A(Q^2, b) = \langle k_T^2\rangle_N(Q^2) + \Delta k_T^2(b)$ is larger than in *pp* collisions due to the nuclear k_T-broadening $\Delta k_T^2(x, b) = 2\, C(x)\, T_A(b)$ evaluated within the color dipole formalism [19]. The factor $C(x)$ is related to the dipole cross section $\sigma_{\bar{q}q}$, which describes the interaction of the $\bar{q}q$ pair with a nucleon, as $C(x) = \left.\frac{d\sigma^N_{\bar{q}q}(x,r)}{dr^2}\right|_{r=0}$. Note that for gluons the nuclear broadening is larger due to the Casimir factor 9/4. For the dipole cross section we adopt the GBW parametrization from [20].

3. Color Dipole formalism

The color dipole formalism is treated in the target rest frame, where the process of direct photon production can be viewed as a radiation of a real photon by a projectile quark [15]. Assuming only the lowest $|q\gamma\rangle$ Fock component, the p_T distribution of the photon bremsstrahlung in quark-nucleon interaction can be expressed as a convolution of the dipole cross section $\sigma^N_{q\bar{q}}(\alpha\rho, x)$ and the light-cone (LC) wave functions of the projectile $q + \gamma$ fluctuation $\Psi_{\gamma q}(\alpha, \vec{\rho})$ [15]:

$$\frac{d\sigma(qN \to \gamma X)}{d\ln\alpha d^2p_T} = \frac{1}{(2\pi)^2}\int\sum_{in,f} d^2\rho_1\, d^2\rho_2\, e^{i\vec{p}_T\cdot(\vec{\rho}_1-\vec{\rho}_2)}\, \Psi^*_{\gamma q}(\alpha, \vec{\rho}_1)\, \Psi_{\gamma q}(\alpha, \vec{\rho}_2)\, \Sigma(\alpha, \rho_1, \rho_2, x_2)\,, \tag{7}$$

where $\Sigma(\alpha, \rho_1, \rho_2, x) = \left\{\sigma^N_{\bar{q}q}(\alpha\rho_1, x) + \sigma^N_{\bar{q}q}(\alpha\rho_2, x) - \sigma^N_{\bar{q}q}(\alpha(\vec{\rho}_1 - \vec{\rho}_2, x))\right\}/2$.

The differential hadronic cross section for direct photon production in *pp* collisions can be expressed as a convolution of the differential cross section, Eq. (7) with corresponding PDFs

$$\frac{d^3\sigma^{pp\to\gamma X}}{dx_1 d^2p_T} = \frac{1}{x_1 + x_2}\int\frac{d\alpha}{\alpha}\sum_q e_q^2\left(\tfrac{x_1}{\alpha}\, f_{q/p}\left(\tfrac{x_1}{\alpha}, Q^2\right) + \tfrac{x_1}{\alpha}\, f_{\bar{q}/p}\left(\tfrac{x_1}{\alpha}, Q^2\right)\right)\frac{d\sigma^{qp\to\gamma p}}{d\ln\alpha d^2p_T}, \tag{8}$$

where e_q is a quark charge, $\alpha = p^+_\gamma/p^+_q$ is a fraction of quark LC momenta taken by the photon and Bjorken variables x_1 and x_2 are connected with the Feynman variable as $x_F = x_1 - x_2$ with $x_1 = p^+_\gamma/p^+_p$ in the target rest frame. In all calculation we use the scale $Q^2 = p_T^2$, for PDFs we take the GRV98 parametrization from [21] and for the color dipole cross section we adopt GBW parametrization [20].

Mechanism of direct photon production in *pA* and *AA* collisions is controlled by the mean coherence length, $l_c = \left\langle\frac{2E_q\alpha(\alpha-1)}{\alpha^2 m_q^2 + p_T^2}\right\rangle_\alpha$, where $E_q = x_q s/2m_N$ and $m_q = 0.2$ GeV are the energy and mass of projectile quark, respectively. The variable $x_q = x_1/\alpha$ denotes a fraction of the proton momentum carried by the quark. The onset of nuclear shadowing requires a sufficiently long coherence length (LCL), $l_c \gtrsim R_A$, where R_A is the nuclear radius. This LCL limit can be safely used for the RHIC and LHC kinematic regions especially at forward rapidities and leads to a simple incorporation of shadowing effects via eikonalization of $\sigma^N_{\bar{q}q}(\rho, x)$ [22], i.e. performing the following substitutions in Eq. (7):

$$\sigma^N_{\bar{q}q}(\alpha\rho, x) \Rightarrow \sigma^A_{\bar{q}q}(\alpha\rho, x) = 2\int d^2s\, \sigma^A_{\bar{q}q}(\vec{s}, \alpha\rho, x) \tag{9}$$

for proton-nucleus interations and

$$\sigma^N_{\bar{q}q}(\alpha\rho, x) \Rightarrow \sigma^{AB}_{\bar{q}q}(\alpha\rho, x) = \int d^2b\, d^2s \left[\sigma^B_{\bar{q}q}(\vec{s}, \alpha\rho, x)T_B(\vec{b}-\vec{s}) + \sigma^A_{\bar{q}q}(\vec{b}-\vec{s}, \alpha\rho, x)T_B(\vec{s})\right] \tag{10}$$

for heavy-ion collisions where

$$\sigma^A_{\bar{q}q}(\vec{s}, \alpha\rho, x) = 1 - \left(1 - \tfrac{1}{2A}\sigma^N_{\bar{q}q}(\alpha\rho, x)T_A(\vec{s})\right)^A. \tag{11}$$

In the LCL limit, besides the lowest $|q\gamma\rangle$ Fock state one should include also higher Fock components containing gluons. They cause an additional suppression, known as the gluon shadowing (GS). Gluon shadowing is incorporated via attenuation factor R_G [23] as the modification of the nuclear thickness function $T_A(\vec{s}) \Rightarrow T_A(\vec{s})R_G(x_2, Q^2, A, \vec{s})$ in Eq. (9) for $p+A$ interaction and $T_A(\vec{s}) \Rightarrow T_A(\vec{s})R_G(x_2, Q^2, A, \vec{s})$ and $T_B(\vec{b}-\vec{s}) \Rightarrow T_B(\vec{b}-\vec{s})R_G(x_1, Q^2, A, \vec{b}-\vec{s})$ in Eq. (10) for heavy-ion collisions.

4. Results

Figs. 1 and 2 show a comparison of both models with PHENIX [24] and CMS [25] data on direct photon production in pp collisions at midrapidity and c.m. energy $\sqrt{s} = 200$ GeV and $\sqrt{s} = 2760$ GeV, respectively For both energies the model based on k_T-factorisation (blue solid lines) and calculations within the color dipole formalism (red solid lines) agree with data reasonably. However, the former describes the data better in the low-p_T region especially at smaller energies due to an absence in this kinematic region of the precise parametrization of the dipole cross section [20] used in calculations. More precise recent parametrization (see [26], for example) improve an agreement with data at small p_T.

Fig. 3 shows a confrontation of the PHENIX data [5] on direct photon production in $AuAu$ collisions with both models. Experimental values were measured at $\sqrt{s} = 200$ GeV and at midrapidity for several centralities $0-10\,\%$, $40-50\,\%$ and minimum-bias (MB). Blue and red lines represent calculations within the model based on k_T-factorisation and the color dipole formalism, respectively. The solid and dashed lines represent calculations with and without ISI effect. As was mentioned above, at small and medium-high p_T the different shape and magnitude of the Cronin enhancement predicted within both models is caused predominantly by an absence of the precise parametrization of the dipole cross section [20] used in calculations. We expect that more precise recent parametrization [26] of the dipole cross section used in the color dipole formalism leads to a better agreement with the model based on k_T factorization in the small p_T region. Similarly as was demonstrated above, both models agree well with data in the large-p_T region. Moreover, the data on $R_{AuAu}(p_T)$ at centrality $0-10\,\%$ indicate a significant suppression at large $p_T \gtrsim 17$ GeV that can not be interpreted by coherence effects. Calculations within both models including ISI corrections clearly demonstrate the observed large-p_T attenuation.

Fig. 4 shows predictions of both models for $R_{AuAu}(p_T)$ at forward rapidity $y = 3$ and for the same centralities that are indicated in Fig 3. Here we predict a strong suppression for all centralities due to ISI effects.

In Fig. 5 we compare predictions of both models with available data from CMS experiment [25] on direct photon production in $PbPb$ collisions at c.m. energy $\sqrt{s} = 2760$ GeV for three

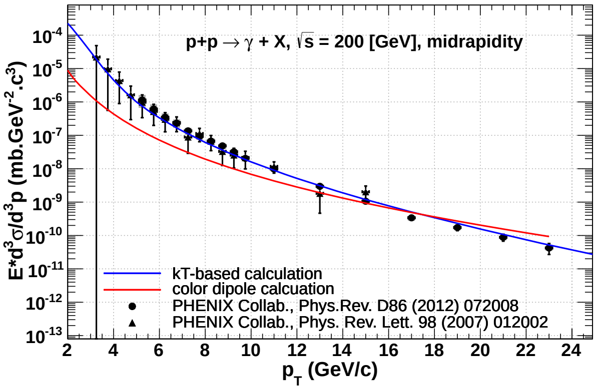

Figure 1. Invariant cross section for direct photon production in pp collisions. The data from the PHENIX experiment [24] are compared with the model based on k_T factorization (blue line) and with calculations based on color dipole formalism (red line).

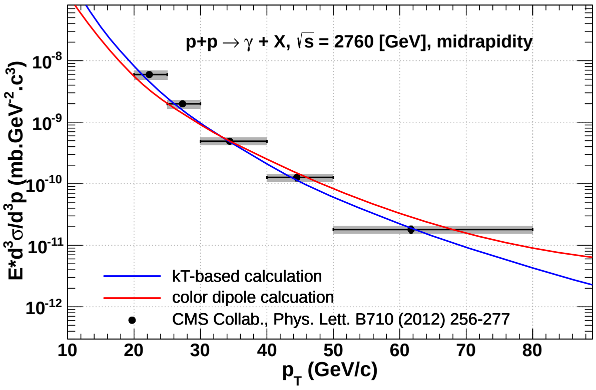

Figure 2. The same as Fig. 1 but with data from CMS experiment [25].

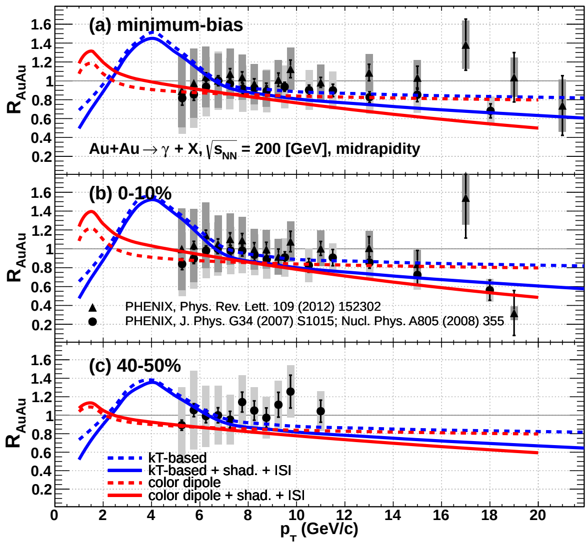

Figure 3. Comparison of the PHENIX data on R_{AuAu} [5] at midrapidity and for several centralities with the model based on k_T factorization (blue line) and with calculations based on the color dipole formalism (red lines). The solid and dashed lines represent calculations with and without ISI effects.

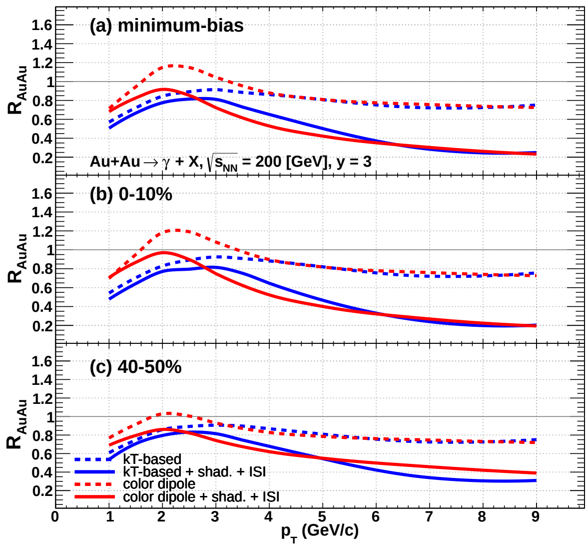

Figure 4. The same as Fig. 3 but at rapidity $y = 3$.

different intervals of centralities. The predictions of both models are qualitatively very close in good accordance with data. They also demonstrate a very weak onset of ISI corrections at large p_T.

Fig. 6 shows predictions from both models for R_{PbPb} at forward rapidity $y = 4$ for the same centrality intervals as are depicted in Fig. 5. We predict a strong suppressions for all centralities due to ISI effects.

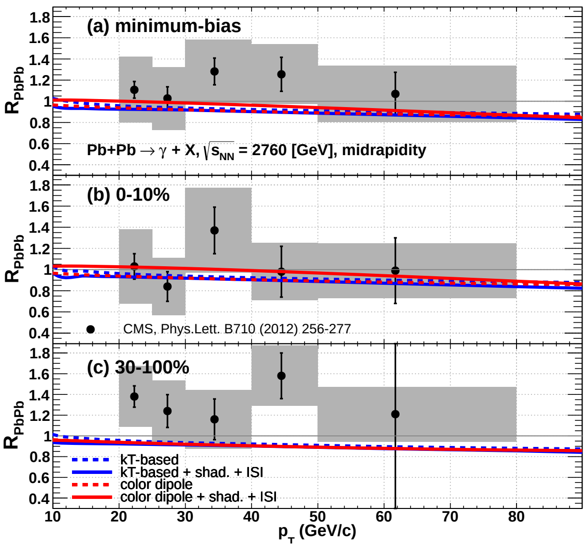

Figure 5. The same as Fig. 3 but with CMS data [25].

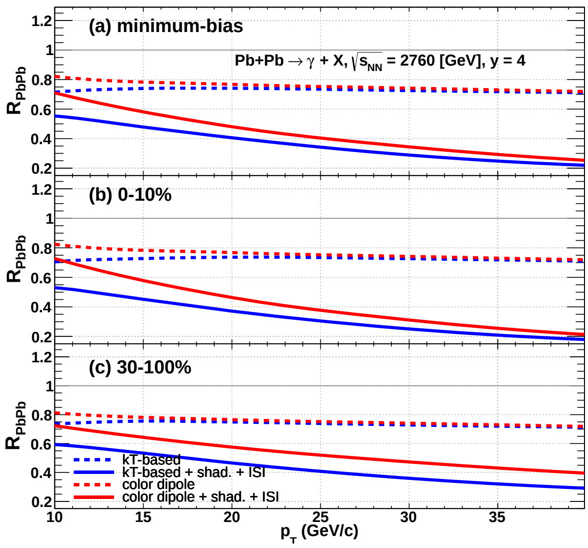

Figure 6. The same as Fig. 4 but at rapidity $y = 4$ and at c.m. energy $\sqrt{s} = 2760$ GeV.

Predictions for $R_{dAu}(p_T)$ from both models are compared in Fig. 7 with PHENIX data [27] on direct photon production in dAu collisions at midrapidity and at $\sqrt{s} = 200$ GeV. Here we predict a sizeable effect of ISI corrections that can be verified in the future by data obtained at very large $p_T \gtrsim 15 - 20$ GeV. The same Fig. 7 also clearly manifests a strong rise of ISI effects with rapidity at fixed p_T values as was discussed in Sect. 1.

Similarly as was mentioned above and presented in Fig. 3 one can see a quantitative difference between both models in predictions of the shape and magnitude of the Cronin enhancement at different rapidities.

Fig. 8 contains predictions for direct photons produced at LHC c.m. energy $\sqrt{s} = 5020$ GeV in pPb collisions at different rapidities $y = 0, 2$ and 4. Here we predict a significant large-p_T suppression due to ISI effects only at rapidities $y \gtrsim 2$. The expected rise of nuclear attenuation with rapidity can be verified in the future by experiments at LHC.

5. Conclusions

We study production of direct photons in pp, $p(d)A$ and AA collisions at RHIC and LHC energies using two different models: the model based on k_T factorization and the model based on the color dipole formalism. The main motivation for a such investigation was to test the theoretical uncertainties in predictions of corresponding variables that can be verified by available data.

Both models describe reasonable well the data on direct photon production in pp collisions. The model based on k_T-factorisation shows a better agreement with data in the low-p_T region. This fact is a consequence of an absence of the more precise determination of the dipole cross section in this kinematic region as that used in calculations within the color dipole formalism.

Investigating direct photon production on nuclear targets, at small and medium-high values of p_T we found a significant difference between predictions of the shape and magnitude of the Cronin enhancement from both models. However, we expect a better agreement between the both models using more precise recent parameterizations of the dipole cross section as is presented in [26], for example. In the large-p_T region we found a good agreement of both models with available data on nuclear modification factors R_A and R_{AA} at RHIC and LHC.

Besides the Cronin enhancement, isospin corrections and coherence effects we investigated also additional suppression due to initial state effective energy loss (ISI effects). We

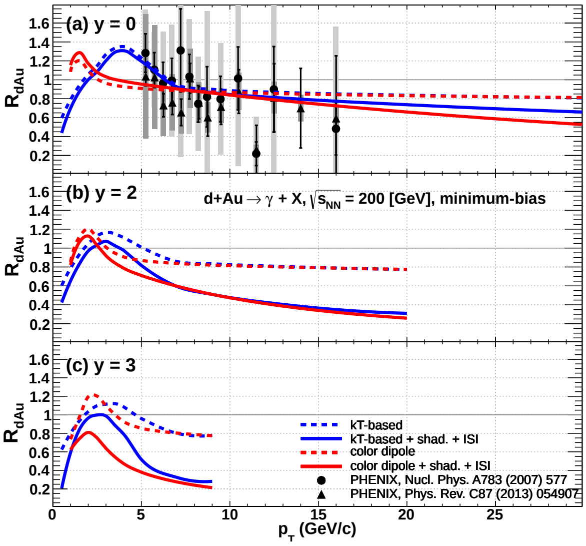

Figure 7. Predictions from both models at different rapidities $y = 0, 2$ and 3 vs. PHENIX data [27] on $R_{dAu}(p_T)$ at midrapidity and at $\sqrt{s} = 200$ GeV

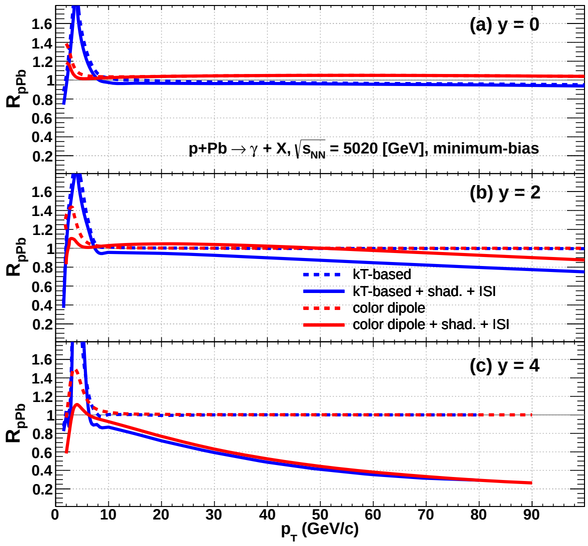

Figure 8. Predictions for R_{pPb} from both models at $\sqrt{s} = 5020$ GeV and at different rapidities $y = 0, 2$ and 4.

demonstrated that ISI effects cause a strong suppression at forward rapidities and large p_T leading so to breakdown of the QCD factorisation. In the RHIC kinematic region no coherence effects are possible at large p_T. However, the PHENIX data on direct photon production in $AuAu$ interactions clearly indicate a significant large-p_T suppression that can be explained entirely by ISI effects. The ISI effects are practically irrelevant at LHC but we predict a strong nuclear suppression at forward rapidities that can be verified by the future measurements at RHIC and LHC.

Acknowledgements

This work has been supported in part by the grant 13-20841S of the Czech Science Foundation (GAČR), by the Grant MŠMT LG13031, by the Slovak Research and Development Agency APVV-0050-11 and by the Slovak Funding Agency, Grant 2/0020/14 by the European social fund within the framework of realizing the project "Support of inter-sectoral mobility and quality enhancement of research teams at Czech Technical University in Prague", CZ.1.07/2.3.00/30.0034.

References

[1] B. Z. Kopeliovich, et al., Phys. Rev. Lett. **88**, 232303 (2002).
[2] S. S. Adler, et al. (PHENIX Collab.), Phys. Rev. Lett. **98**, 172302 (2007); Phys. Rev. Lett. **109**, 152302 (2012).
[3] B. Abelev, et al. (ALICE Collab.), Phys. Rev. Lett. **110**, 082302 (2013).
[4] J. Albacete, N. Armesto, et al., Int. J. Mod. Phys. E**22**, 1330007 (2013).
[5] S. Afanasiev et al. (PHENIX Collab.), Phys. Rev. Lett. **109**, 152302 (2012); T. Sakaguchi Nucl. Phys. A **805**, 355 (2008).
[6] B Z. Kopeliovich et al., Phys. Rev. C**72**, 054606 (2005); B. Z. Kopeliovich and J. Nemchik, J. Phys. G**38**, 043101 (2011).
[7] J. Nemchik, et al., Phys. Rev. C**78**, 025213 (2008); Nucl. Phys. A**830**, 611c (2009).
[8] B. Z. Kopeliovich and J. Nemchik, Phys. Rev. C**86**, 054904 (2012).
[9] B. Z. Kopeliovich, J. Nemchik, I. K. Potashnikova and I. Schmidt, Int. J. Mod. Phys. E **23**, 1430006 (2014).

[10] B. Z. Kopeliovich and J. Nemchik, J. Phys. G **38**, 043101 (2011).
[11] I. Arsene, et al. (BRAHMS Collab.), Phys. Rev. Lett. **93**, 242303 (2004); J. Adams, et al. (STAR Collab.), Phys. Rev. Lett. **97**, 152302 (2006).
[12] D. Kharzeev, Y.V. Kovchegov and K. Tuchin, Phys. Lett. B **599**, 23 (2004).
[13] B. Boimska [NA49 Collaboration], Ph.D. Dissertation **CERN-THESIS-2004-035**
[14] R. P. Feynman, R. D. Field and G. C. Fox, Phys. Rev. D**18**, 3320 (1978).
[15] B. Z. Kopeliovich, A. V. Tarasov and A. Schafer, Phys. Rev. C**59**, 1609 (1999).
[16] X. N. Wang, Phys. Rev. C**61**, 064910 (2000).
[17] A. D. Martin, W. J. Stirling, R. S. Thorne and G. Watt, Eur. Phys. J. C**63**, 189-285 (2009).
[18] K. J. Eskola, H. Paukkunen and C. .A. Salgado, JHEP **0904**, 065 (2009).
[19] M. B. Johnson, B. Z. Kopeliovich and A. V. Tarasov, Phys. Rev. C**63**, 035203 (2001).
[20] K. Golec-Biernat and M. Wüsthoff, Phys. Rev. D**59**, 014017 (1998).
[21] M. Gluck, E. Reya and A. Vogt, Eur. Phys. J. C**5**, 461 (1998).
[22] B. Z. Kopeliovich, L. I. Lapidus and A. B. Zamolodchikov, JETP Lett. **33**, 595 (1981).
[23] B. Z. Kopeliovich, J. Nemchik, A. Schafer and A. V. Tarasov Phys. Rev. C **65**, 035201 (2002).
[24] A. Adare, et al. (PHENIX Collab.), Phys. Rev. D **86**, 072008 (2012); S. S. Adler et al. (PHENIX Collab.), Phys. Rev. Lett **98**, 012002 (2007).
[25] S. Chatrchyan, et al. (CMS Collab.), Phys. Lett. B **710**, 256-277 (2012).
[26] A. H. Rezaeian, at al., Phys. Rev. D**87**, 034002 (2013).
[27] D. Peressounko (PHENIX Collab.), Nucl. Phys. A **783**, 577-582 (2007); A. Adare, et al. (PHENIX Collab.), Phys. Rev. C **87**, 054907 (2013).

Production of photons and hadrons on nuclear targets

Michal Krelina[1] and Jan Nemchik[1,2]

[1] michal.krelina@fjfi.cvut.cz, Czech Technical University in Prague, FNSPE, Brehova 7, 11519 Prague, Czech Republic
[2] nemcik@saske.sk, Institute of Experimental Physics SAS, Watsonova 47, 04001 Kosice, Slovakia

Abstract. We investigate nuclear effects in production of large-p_T hadrons and direct photons in pA and AA collisions corresponding to energies at RHIC and LHC. Calculations of nuclear invariant cross sections include additionally the nuclear broadening and the nuclear modification of parton distribution functions. We demonstrate that at large p_T and forward rapidities the complementary effect of initial state interactions (ISI) causes a significant nuclear suppression. Numerical results for nuclear modification factors R_A and R_{AA} are compared with available data at RHIC and LHC. We perform also predictions at forward rapidities which are expected to be measured by the future experiments.

1 Introduction

Recent experimental measurements of hadron and direct photon production [1–3] allow to investigate nuclear effects at medium and large transverse momenta p_T. This should help us to understand properties of a dense medium created in heavy ion collisions (HICs). Manifestations of nuclear effects are usually studied through the nucleus-to-nucleon ratio, the so called nuclear modification factor, $R_A(p_T) = \sigma_{pA\to h(\gamma)+X}(p_T)/A\,\sigma_{pp\to h(\gamma)+X}(p_T)$ for pA collisions and $R_{AB}(p_T) = \sigma_{AB\to h(\gamma)+X}(p_T)/AB\,\sigma_{pp\to h(\gamma)+X}(p_T)$ for minimum bias (MB) AB collisions.

In this paper we focused on suppression at large p_T, $R_A(p_T) < 1$ ($R_{AA} < 1$) indicated at midrapidity, $y = 0$, by the PHENIX data [1] on π^0 production in central dAu collisions and on direct photon production in central $AuAu$ collisions [2]. Such a suppression can not be interpreted by the onset of coherence effects (gluon shadowing, color glass condensate) due to large values of Bjorken x. The same mechanism of nuclear attenuation should be arisen especially at forward rapidities where we expect much stronger onset of nuclear suppression as is demonstrated by the BRAHMS and STAR data [3]. Here the target Bjorken x is $\exp(y)$-times smaller than at $y = 0$ allowing so a manifestation of coherence effects. However, assuming their dominance at RHIC forward rapidities then the same effects causing a strong suppression should be expected also at LHC at $y = 0$, what is in contradiction with ALICE data [4].

We interpret alternatively the main source of this suppression as multiple initial state interactions (ISI) of the projectile hadron and its debris during propagation through the nucleus. This leads to a dissipation of energy resulting in a suppressed production rate of particles as was stressed in [5, 6]. The corresponding suppression factor reads [5],

$$S(\xi) \approx 1 - \xi, \tag{1}$$

where $\xi = \sqrt{x_F^2 + x_T^2}$, and $x_F = 2p_L/\sqrt{s}$; $x_T = 2p_T/\sqrt{s}$. This factor leads to a suppression at large-p_T ($x_T \to 1$) and also at forward rapidities ($x_F \to 1$).

2 Results

Calculations of pp, pA and AA cross sections were performed employing the parton model, which corresponds to collinear factorization expression modified by intrinsic transverse momentum dependence [7].

In the RHIC energy range at $y = 0$ besides Cronin enhancement at medium-high p_T and small isotopic corrections at large p_T one should not expect any nuclear effects since no coherence effects are possible. However, the PHENIX data [1, 2] indicate large-p_T suppression, which is more evident for hadron and direct photon production in central dAu and $AuAu$ collisions, respectively, as is demonstrated in Fig. 1 (lower box) and in Fig. 2 (middle box). Such a suppression is caused by ISI effects, Eq. (1), and is depicted by the solid lines, while the dotted lines without ISI effects overestimate the PHENIX data at large p_T.

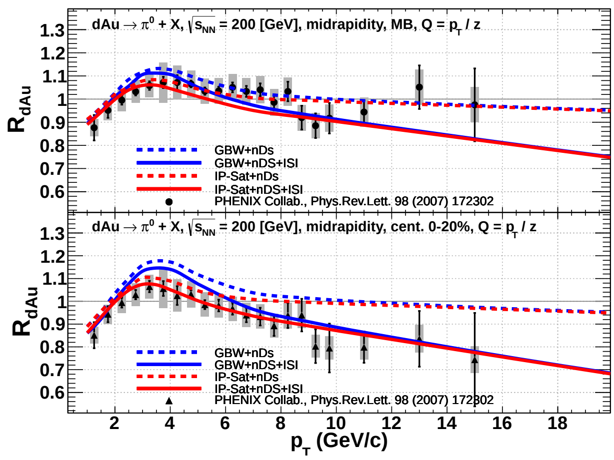

Figure 1. Nuclear modification factor $R_{dAu}(p_T)$ for π^0 production at $\sqrt{s} = 200$ GeV for MB - upper box and for the centrality interval $0 - 20\,\%$ - lower box.

In the LHC energy range at $y = 0$, we do not expect any ISI effects, Eq. (1), and the ALICE data [4] on hadron production in pPb collisions allow so to test only model predictions for the Cronin enhancement at medium-high p_T. The corresponding comparison demonstrates a good agreement as is shown in Fig. 3 by the solid and dotted lines manifesting so a weak ef-

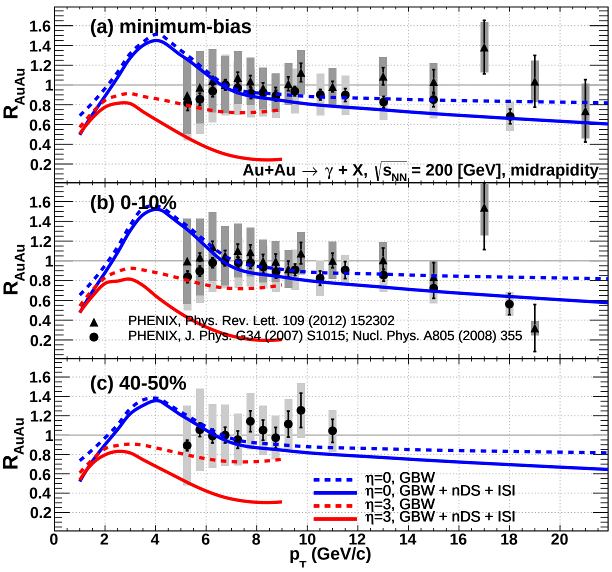

Figure 2. Nuclear modification factor $R_{AuAu}(p_T)$ for direct photon production at $\sqrt{s} = 200$ GeV for different centrality intervals at $y = 0$ and $y = 3$.

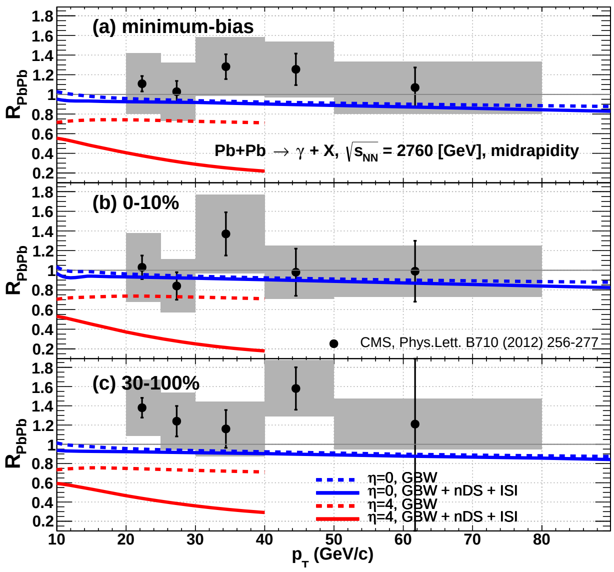

Figure 4. Nuclear modification factor $R_{PbPb}(p_T)$ for direct photon production at $\sqrt{s} = 2760$ GeV for different centrality intervals at $y = 0$ and $y = 4$.

fect of nuclear shadowing. However, ISI effects causing a significant large-p_T suppression can be arisen at forward rapidities as is depicted in Fig. 3 by the dashed and dot-dashed lines calculated at $y = 2$ and $y = 4$.

Direct photons produced in a hard reaction are not accompanied with any final state interaction, either energy loss or absorption and represent so a cleaner probe for a dense medium created in HICs. The CMS data [8] on direct photon production in $PbPb$ collisions at $y = 0$ presented in Fig. 4 show only a manifestation of isotopic corrections at large-p_T due to a weak onset of ISI effects. Similarly as for hadron production, ISI effects cause a significant large-p_T suppression at forward rapidities as is shown in Fig. 4 by the solid lines calculated at $y = 4$.

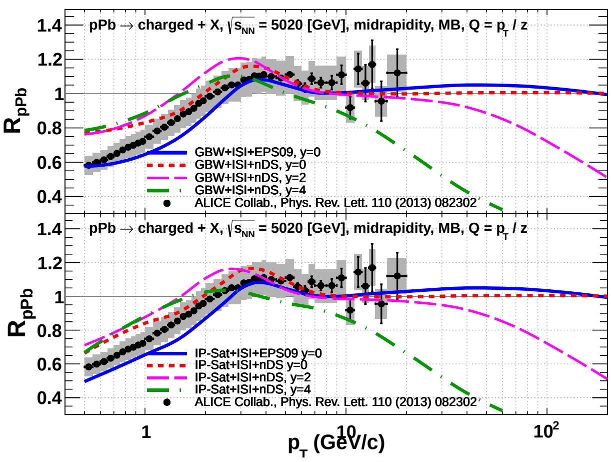

Figure 3. Nuclear modification factor $R_{pPb}(p_T)$ for charge hadron production at $\sqrt{s} = 5020$ GeV and at several rapidities, $y = 0, 2$ and 4.

3 Conclusions

Employing the parton model, corresponding to collinear factorization expression modified by intrinsic transverse momentum dependence, we predict large-p_T suppression of hadrons and direct photons produced on nuclear targets. The main source for suppression comes from ISI effects, which are dominant at large x_F and/or x_T. ISI effects at LHC are irrelevant at $y = 0$ but we predict a strong suppression at forward rapidities that can be verified by the future measurements.

Acknowledgements

This work has been supported in part by the grant 13-20841S of the Czech Science Foundation (GAČR), by the Grant MŠMT LG13031, by the Slovak Research and Development Agency APVV-0050-11 and by the Slovak Funding Agency, Grant 2/0020/14.

References

[1] S.S. Adler, et al. [PHENIX Collab.], Phys. Rev. Lett. **98**, 172302 (2007); Phys. Rev. Lett. **109**, 152302 (2012).

[2] S. Afanasiev et al. [PHENIX Collab.], Phys. Rev. Lett. **109**, 152302 (2012); T. Sakaguchi Nucl. Phys. A **805**, 355 (2008).

[3] I. Arsene, et al. [BRAHMS Collab.], Phys. Rev. Lett. **93**, 242303 (2004); J. Adams, et al. [STAR Collab.], Phys. Rev. Lett. **97**, 152302 (2006).

[4] B. Abelev et al. [ALICE Collab.], Phys. Rev. Lett. **110**, 082302 (2013).

[5] B.Z. Kopeliovich et al., Nucl. Phys. B **146**, 171 (2005).

[6] B.Z. Kopeliovich et al., Phys. Rev. C**72**, 054606 (2005); B.Z. Kopeliovich and J. Nemchik, J. Phys. G **38**, 043101 (2011).

[7] M. Krelina and J. Nemchik, Nucl. Phys. B (Proc. Suppl.)**245**, 239 (2013).

[8] S. Chatrchyan et al. [CMS Collab.], Phys. Lett. B **710**, 256 (2012).

EPJ Web of Conferences will be set by the publisher
DOI: will be set by the publisher

Systematic study of real photon and Drell-Yan pair production in p+A (d+A) interactions

M. Krelina[1,a], E. Basso[2,3], V. P. Goncalves[3,4], J. Nemchik[1,5], and R. Pasechnik[3]

[1] FNSPE, Czech Technical University in Prague, Brehova 7, 115 19 Prague, Czech Republic
[2] Instituto de Fısica, Universidade Federal do Rio de Janeiro, Caixa Postal 68528, Rio de Janeiro, RJ 21941-972, Brazil
[3] Department of Astronomy and Theoretical Physics, Lund University, SE-223 62 Lund, Sweden
[4] High and Medium Energy Group, Instituto de Fisica e Matematica, Universidade Federal de Pelotas, Pelotas, RS, 96010-900, Brazil
[5] Institute of Experimental Physics SAS, Watsonova 47, 04001 Kosice, Slovakia

Abstract. We study nuclear effects in production of Drell-Yan pairs and direct photons in proton-nucleus collisions. For the first time, these effects are studied within the color dipole approach using the Green function formalism which naturally incorporates the color transparency and quantum coherence effects. The corresponding numerical results for the nuclear modification factor are compared with available data. Besides, we present a variety of predictions for the nuclear suppression as a function of transverse momentum p_T, Feynman variable x_F and invariant mass M of the lepton pair which can be verified by experiments at RHIC and LHC. We found that the nuclear suppression is caused predominantly by effects of quantum coherence (shadowing corrections) and by the effective energy loss induced by multiple initial state interactions. Whereas the former dominate at small Bjorken x_2 in the target, the latter turns out to be significant at large x_1 in the projectile beam and is universal at different energies and transverse momenta.

1 Introduction

The color dipole approach [1] represents a phenomenological framework that effectively takes into account the higher-order and nonlinear QCD effects. There are many studies in the literature demonstrating a reliable agreement of predictions with experimental data, especially at high energies and/or small Bjorken variable x_2 in proton-proton (pp) collisions and DIS (see e.g. Refs. [2–4] and references therein).

The color dipole approach which is formulated in the target rest frame provides a consistent way of studying the nuclear effects, especially the nuclear shadowing, in both proton-nucleus (pA) and nucleus-nucleus (AA) collisions. The dynamics of pA or AA collisions is controlled by the coherence length l_c. When the coherence length is sufficiently large or small, one talks about the long coherence length (LCL) or short coherence length (SCL) approximations, respectively. In the intermediate kinematics when both approximations fail, one should employ the Green function technique which

[a] e-mail: michal.krelina@fjfi.cvut.cz

accounts for the exact coherence length l_c and naturally incorporates the color transparency and quantum coherence effects. Such a kinematic region corresponds e.g. to kinematics at RHIC fixed target experiments or planned experiments such as AFTER@LHC.

In this paper, we present numerical results on the quark-nucleus cross section within the Green function formalism for the Drell-Yan (DY) lepton pair production and production of direct photons. Besides, we include also the gluon shadowing (GS) that dominates at small Bjorken x_2 and the effective energy loss induced by multiple initial state interactions.

2 Coherence length

The rest frame of the nucleus is very convenient for study of coherence effects. The dynamics of Drell-Yan (DY) process is regulated by the coherence length l_c, which controls the interference between amplitudes of the hard reaction occurring on different nucleons and is given by

$$l_c = \frac{1}{x_2 m_N} \frac{(M^2 + p_T^2)(1-\alpha)}{\alpha(1-\alpha)M^2 + \alpha^2 m_f^2 + p_T^2}\,, \tag{1}$$

where α is the fraction of the light-cone momentum of the projectile quark carried out by the photon, and $m_q = 0.2$ GeV is an effective quark mass. Figs. 1 and 2 show the energy dependence of the mean coherence length for $x_F = 0$ and $x_F = 0.6$ corresponding to small x_2 fractions, explicitly separating the regimes with the long coherence length (LCL), $l_c > R_A$, and short coherence length (SCL), $l_c \lesssim 1 \div 2$ fm. For the transition region between both limits we used the Green function formalism as the general case with no restrictions on l_c.

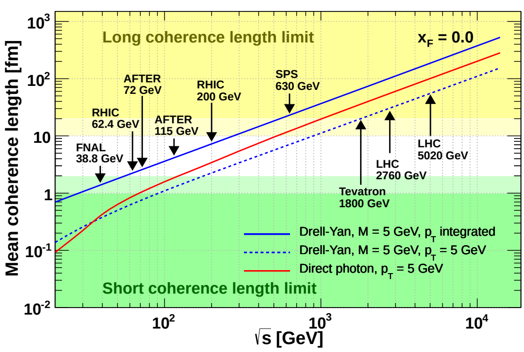

Figure 1. The mean coherence length for Drell-Yan and direct photons production for $x_F = 0$.

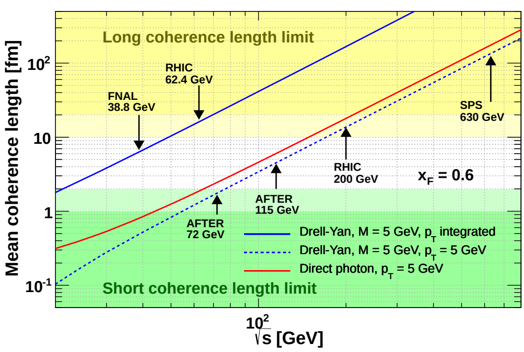

Figure 2. The mean coherence length for Drell-Yan and direct photons production for $x_F = 0.6$.

3 Color dipole approach

The DY process in the target rest frame can be treated as a radiation of a heavy photon or Z^0 boson by a projectile quark. The transverse momentum p_T distribution of photon bremsstrahlung in quark-nucleon interactions reads [5]

$$\frac{d^3\sigma^{(qN\to\gamma^* X)}}{d\ln\alpha d^2 p_T} = \frac{1}{(2\pi)^2}\int d^2\rho_1 d^2\rho_2 e^{i\vec{p}_T\cdot(\vec{\rho}_1-\vec{\rho}_2)}\Psi^*_{\gamma^* q}(\alpha,\vec{\rho}_2)\Psi_{\gamma^* q}(\alpha,\vec{\rho}_1)\Sigma(\alpha,\vec{\rho}_1,\vec{\rho}_2)\,, \tag{2}$$

where

$$\Sigma(\alpha,\vec{\rho}_1,\vec{\rho}_2) = \frac{1}{2}\left(\sigma^N_{q\bar{q}}(\alpha\vec{\rho}_1) + \sigma^N_{q\bar{q}}(\alpha\vec{\rho}_2) - \sigma^N_{q\bar{q}}(\alpha(\vec{\rho}_1 - \vec{\rho}_2))\right) \tag{3}$$

and the light-cone (LC) wave functions of the projectile $q \to q + \gamma$ fluctuation $\Psi_{T,L}(\alpha,\vec{\rho})$ can be found in Ref. [5]. For the dipole cross section $\sigma^N_{q\bar{q}}(\alpha\vec{\rho})$ we used GBW [6], KST [7] and GBWnew [8] parameterisations. The hadron cross section is given by a convolution of the qN cross section with the corresponding parton distribution functions (PDFs) f_q and $\bar{f}_q$ as follows

$$\frac{d^4\sigma^{(pp\to l^+l^-X)}}{d^2p_T dx_F dM^2} = \frac{\alpha_{\rm EM}}{3\pi^2}\frac{x_1}{x_1+x_2}\int_{x_1}^1 \frac{d\alpha}{\alpha^2}\sum_q Z_q\left(q_f(x_1/\alpha,Q^2) + \bar{q}_f(x_1/\alpha,Q^2)\right)\frac{d^3\sigma^{(qN\to\gamma^* X)}}{d\ln\alpha d^2p_T} \tag{4}$$

where Z_q is the fractional quark charge, the (anti)quark PDFs f_q and $\bar{f}_q$ are used with the leading order (LO) parameterisation from Ref. [9] at the scale $Q^2 = p_T^2 + (1-x_1)M^2$. After integration over the transverse momentum $\vec{p}_T$ we get for hadronic cross section

$$\frac{d^2\sigma^{(pp\to l^+l^-X)}}{dx_F dM^2} = \frac{\alpha_{\rm EM}}{3\pi^2}\frac{x_1}{x_1+x_2}\int_{x_1}^1 \frac{d\alpha}{\alpha^2}\sum_q Z_q\left(q_f(x_1/\alpha,Q^2) + \bar{q}_f(x_1/\alpha,Q^2)\right)\frac{d\sigma^{(qN\to\gamma^* X)}}{d\ln\alpha} \tag{5}$$

and for quark-nucleon cross section

$$\frac{d\sigma^{(qN\to\gamma^* X)}}{d\ln\alpha} = \int d^2\rho\,|\Psi_{\gamma^* q}(\alpha,\vec{\rho})|^2\sigma^N_{q\bar{q}}(\alpha\vec{\rho})\,. \tag{6}$$

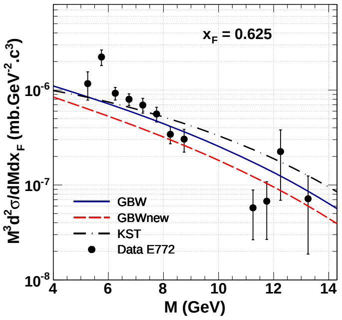

Figure 3. Differential dilepton cross sections in pp collisions vs E772 [13].

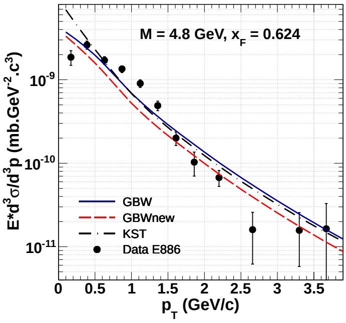

Figure 4. Differential dilepton cross sections in pp collisions vs E886 [14].

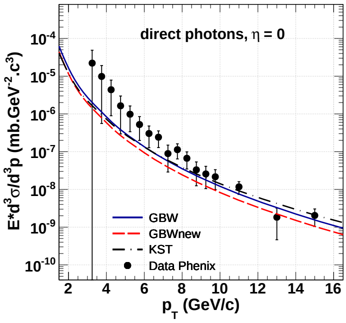

Figure 5. Differential direct photon cross sections in pp collisions vs PHENIX [15].

In Figs. 3, 4 and 5 we compare our predictions for various dipole cross section parameterisations with available DY data from E772 and E886 experiments and for direct photons from the PHENIX experiment where the dipole model predictions agree with the data reasonably well.

4 Transition to nuclear target

Within the Green function formalism the quark-nucleus cross section for DY pair production on nuclear targets reads [5]

$$\begin{aligned}\frac{d\sigma^{(qA\to\gamma^* X)}}{d\ln\alpha} &= A\frac{d\sigma^{(qN\to\gamma^* X)}}{d\ln\alpha} - \frac{1}{2}Re\int_{-\infty}^{\infty}dz_1\int_{-\infty}^{z_1}dz_2\int d^2b d^2\rho_1 d^2\rho_2 \\ &\times \Psi^*_{\gamma^* q}(\alpha,\vec{\rho}_2)\rho_A(b,z_2)\sigma^N_{q\bar{q}}(\alpha\vec{\rho}_2)G(\vec{\rho}_2,z_2|\vec{\rho}_1,z_1)\rho_A(b,z_1)\sigma^N_{q\bar{q}}(\alpha\vec{\rho}_1)\Psi_{\gamma^* q}(\alpha,\vec{\rho}_1)\,, \quad (7)\end{aligned}$$

where the Green function $G(\vec{\rho}_2,z_2|\vec{\rho}_1,z_1)$ describes the propagation of $|\gamma^* q\rangle$ Fock state between longitudinal positions z_1 and z_2 through the nucleus with initial and final separations $\vec{\rho}_1$ and $\vec{\rho}_2$, respectively. The Green function above satisfies the two-dimensional time-dependent Schroedinger equation (z_2 plays the role of time)

$$\left[i\frac{\partial}{\partial z_2} + \frac{\Delta_T(\vec{\rho}_2) - \eta^2}{2E_q\alpha(1-\alpha)} - V(z_2,\vec{\rho}_2,\alpha)\right]G(\vec{\rho}_2,z_2|\vec{\rho}_1,z_1) = 0 \quad (8)$$

with the boundary condition $G(\vec{\rho}_2,z_2|\vec{\rho}_1,z_1)|_{z_1=z_2} = \delta^2(\vec{\rho}_2-\vec{\rho}_1)$. The imaginary part of the potential $V(z_2,\vec{\rho}_2,\alpha)$ describes an absorption of the dipole in a nuclear medium and reads

$$V(z_2,\vec{\rho},\alpha) = -\frac{i}{2}\rho_A(b,z_2)\sigma^N_{q\bar{q}}(\alpha\vec{\rho})\,. \quad (9)$$

For the p_T-dependent DY production cross section we solved the Schroedinger equation analytically which is possible for quadratic $\sigma^N_{q\bar{q}}(\rho) = C\rho^2$ and the uniform nuclear density. For p_T-integrated DY production cross section we solved the Schroedinger equation numerically using an algorithm proposed in Ref. [10].

In the LCL limit the Green function formalism naturally leads to a simple modification of the dipole cross section:

$$\sigma^N_{q\bar{q}}(\vec{\rho},x) \to \sigma^A_{q\bar{q}}(\vec{\rho},x) = 2\int d^2b\left(1 - e^{-\frac{1}{2}\sigma^N_{q\bar{q}}(\vec{\rho},x)T_A(b)}\right)\,. \quad (10)$$

Besides the lowest $|qG^*\rangle$ Fock state one should include also the higher Fock components containing gluons $|\gamma^* qG\rangle$, $|\gamma^* q2G\rangle$ etc. They cause an additional suppression known as the gluon shadowing (GS). The corresponding suppression factor R_G [11] calculated as a correction to the total $\gamma^* A$ cross section for the longitudinal photon, $R_G(x,Q^2,b) \approx 1 - \frac{\Delta\sigma_L^{(\gamma^* A)}}{\sigma_{tot}^{(\gamma^* A)}}$, was included in calculations replacing $\sigma^N_{q\bar{q}}(\vec{\rho},x) \to \sigma^N_{q\bar{q}}(\vec{\rho},x)R_G(x,Q^2,b)$.

The initial state energy loss (due to ISI effects) is expected to suppress the nuclear cross section significantly towards the kinematical limits, $x_L = \frac{2p_L}{\sqrt{s}} \to 1$ and $x_T = \frac{2p_T}{\sqrt{s}} \to 1$. Correspondingly, the proper variable which controls this effect is $\xi = \sqrt{x_L^2 + x_T^2}$. The magnitude of suppression was evaluated in Ref. [12]. It was found within the Glauber approximation that each interaction in the nucleus leads to a suppression factor $S(\xi) \approx 1 - \xi$. Summing up over the multiple initial state interactions in a pA collision at impact parameter b, one arrives at the nuclear ISI-modified quark PDF

$$q_f(x,Q^2) \Rightarrow q_f^A(x,Q^2,b) = C_v q_f(x,Q^2)\frac{e^{-\xi\sigma_{eff}T_A(b)} - e^{-\sigma_{eff}T_A(b)}}{(1-\xi)(1-e^{-\sigma_{eff}T_A(b)})}\,. \quad (11)$$

Here, $\sigma_{eff} = 20$ mb is the effective hadronic cross section controlling the multiple interactions. The normalisation factor C_v is fixed by the Gottfried sum rule (for more details, see Ref. [12]), $T_A(b)$

is the nuclear thickness function at given impact parameter b normalized to the mass number A. It was found that such an additional nuclear suppression due to the ISI effects represents an energy independent feature common for all known reactions, experimentally studied so far, with any leading particle (hadrons, Drell-Yan dileptons, charmonium etc).

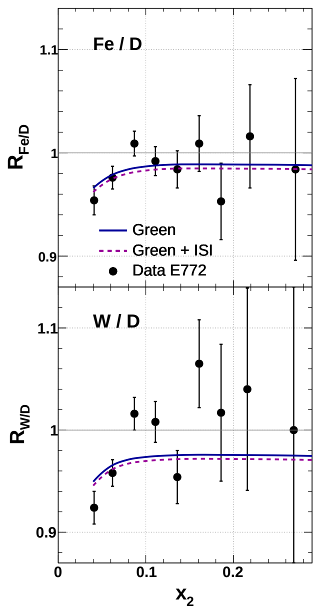

Figure 6. Comparison of the dipole model predictions for $R_{A/B}(x_2)$ with the E772 data at $\sqrt{s}$ = 38.8 GeV [13].

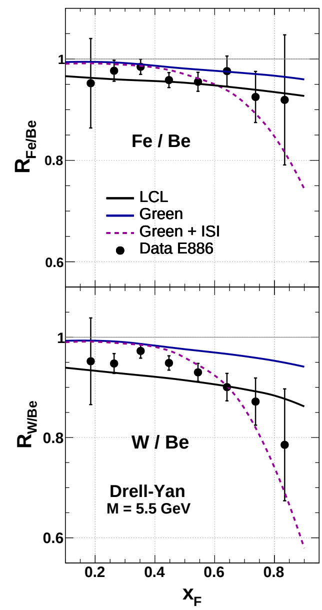

Figure 7. Comparison of the dipole model predictions for $R_{A/B}(x_F)$ with the E886 data at $\sqrt{s}$ = 38.8 GeV [14].

In Figs. 6 and 7 we compare our predictions for ratios $R_{A/B}(x_2)$ and $R_{A/B}(x_F)$ with the E772 and E886 data where the GS is not expected. We obtain a reasonable agreement with the E886 data including the ISI effects. In Fig. 8 we present our predictions for the nuclear suppression of DY pairs production at the future AFTER@LHC experiment demonstrating separate contributions from the GS and ISI effects. Fig. 9 shows the difference between calculations using the Green function formalism and the LCL limit in the RHIC kinematics region for production of direct photons and DY pairs at midrapidity. The RHIC data [15] indicate a strong large-p_T suppression that can be explained only by the ISI effects.

5 Conclusions

For the first time, we use the Green function formalism based on the color dipole approach for description of DY pair and direct photon production on nuclear targets in the kinematic regions where the SCL and LCL limits should not be used. We demonstrate that the GS and ISI energy loss causes a significant nuclear suppression. While the GS dominates at large energies and p_T, the ISI effects are important at large p_T and/or x_F. Our predictions are in a good agreement with FNAL E772 and E886 data as well as with the data from the PHENIX Collaboration. Finally, we predict a strong suppression due to the ISI effects that can be verified by the AFTER@LHC experiment in the future.

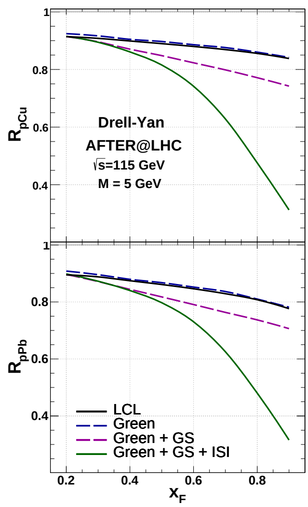

Figure 8. Predictions for the nuclear suppression R_{pA} in the DY process for the AFTER@LHC experiment.

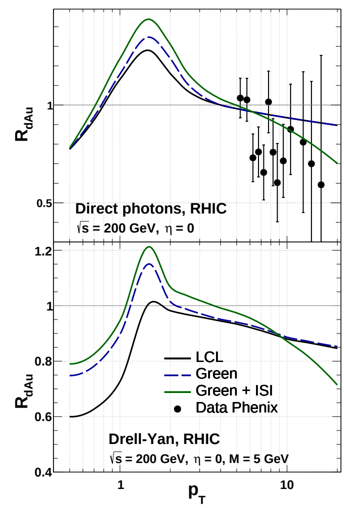

Figure 9. Comparison of R_{pA} with the data from RHIC [15] for direct photons and for the DY process with M = 5 GeV.

6 Acknowledgements

E. B. is supported by CAPES and CNPq (Brazil), contract numbers 2362/13-9 and 150674/2015-5. V. P. G. has been supported by CNPq, CAPES and FAPERGS, Brazil. R. P. is supported by the Swedish Research Council, contract number 621-2013-428. J. N. is partially supported by the grant 13-20841S of the Czech Science Foundation (GAČR), by the Grant MSMT LG13031, by the Slovak Research and Development Agency APVV-0050-11 and by the Slovak Funding Agency, Grant 2/0020/14.

References

[1] N. N. Nikolaev and B. G. Zakharov, Z. Phys. C**64**, 631 (1994).
[2] E. Basso, V. P. Goncalves, J. Nemchik, R. Pasechnik, M. Sumbera, arXiv:1510.00650 [hep-ph].
[3] B. Z. Kopeliovich, E. Levin, A. H. Rezaeian and I. Schmidt, Phys. Lett. B**675**, 190-195 (2009).
[4] B. Z. Kopeliovich, A. H. Rezaeian, H. J. Pirner and I. Schmidt, Phys. Lett. B**653**, 210-215 (2007).
[5] B. Z. Kopeliovich, A. V. Tarasov and A. Schafer, Phys. Rev. C**59**, 1609-1619 (1999).
[6] K. Golec-Biernat and M. Wüsthoff, Phys. Rev. D**59**, 014017 (1998).
[7] B. Z. Kopeliovich, A. Schafer and A. V.Tarasov, Phys. Rev. D**62**, 054022 (2000).
[8] H. Kowalski, L. Motyka and G. Watt, Phys. Rev. D**74**, 074016 (2006).
[9] A. D. Martin, W. J. Stirling, R. S. Thorne, G. Watt, Eur. Phys. J. C**63**, 189 (2009).
[10] J. Nemchik, Phys. Rev. C**68**, 035206 (2003).
[11] B. Z. Kopeliovich, J. Nemchik and A. Schafer, Phys. Rev. C**65**, 035201 (2002).
[12] B. Z. Kopeliovich *et al.*, Int. J. Mod. Phys. E**23**, 1430006 (2014).
[13] D. M. Alde *et al.* [E772 Collaboration], Phys. Rev. Lett. **64**, 2479 (1990).
[14] M. A. Vasiliev *et al.* [E886 Collaboration], Phys. Rev. Lett. **83**, 2304 (1999).
[15] S. S. Adler *et al.* [PHENIX Collaboration], Phys. Rev. Lett. **98**, 012002 (2007).

EPJ Web of Conferences will be set by the publisher
DOI: will be set by the publisher

Nuclear effects in Drell-Yan production at the LHC

M. Krelina[1,a], E. Basso[2,3], V. P. Goncalves[3,4], J. Nemchik[1,5], and R. Pasechnik[3]

[1] *FNSPE, Czech Technical University in Prague, Brehova 7, 115 19 Prague , Czech Republic*
[2] *Instituto de Fısica, Universidade Federal do Rio de Janeiro, Caixa Postal 68528, Rio de Janeiro, RJ 21941-972, Brazil*
[3] *Department of Astronomy and Theoretical Physics, Lund University, SE-223 62 Lund, Sweden*
[4] *High and Medium Energy Group, Instituto de Fisica e Matematica, Universidade Federal de Pelotas, Pelotas, RS, 96010-900, Brazil*
[5] *Institute of Experimental Physics SAS, Watsonova 47, 04001 Kosice, Slovakia*

Abstract. Using the color dipole formalism we study production of Drell-Yan (DY) pairs in proton-nucleus interactions in the kinematic region corresponding to LHC experiments. Lepton pairs produced in a hard scattering are not accompanied with any final state interactions leading to either energy loss or absorption. Consequently, dileptons may serve as more efficient and cleaner probes for the onset of nuclear effects than inclusive hadron production. We perform a systematic analysis of these effects in production of Drell-Yan pairs in *pPb* interaction at the LHC. We present predictions for the nuclear suppression as a function of the dilepton transverse momentum, rapidity and invariant mass which can be verified by the LHC measurements. We found that a strong nuclear suppression can be interpreted as an effective energy loss proportional to the initial energy universally induced by multiple initial state interactions. In addition, we study a contribution of coherent effects associated with the gluon shadowing affecting the observables predominantly at small and medium-high transverse momenta.

1 Introduction

The Drell-Yan (DY) process provides an important test of the Standard Model as well as a comprehensive tool for studies of strong interaction dynamics in an extended kinematical range of energies and rapidities. In this paper, we focus on dilepton pairs coming from decay of virtual γ^*/Z^0 as a probe of nuclear effects in proton-lead (pPb) collisions at LHC. In this case, the DY process represents a cleaner probe than typical hadron production since the dilepton pairs have no final state interactions leading to either energy loss or absorption in the hot medium. For the same reason, no convolution with the jet fragmentation function is required and no nuclear effects are expected besides the saturation effects.

First, we give a short introduction into the color dipole picture as a framework in which the DY looks like a radiation of γ^*/Z^0 boson by a quark. We also compare calculations with the existing DY data in proton-proton (pp) collisions at LHC. A more detailed recent study of DY observables for pp collisions by some of the authors can be found in Ref. [1]. Then, we demonstrate that the coherence

[a] e-mail: michal.krelina@fjfi.cvut.cz

length l_c is large enough, and the long coherence length (LCL) limit can be safely used in calculations of the DY cross section in pPb collisions.

Besides the quark shadowing which is naturally incorporated in the LCL formula, we take into account for following two important effects. The first one is the gluon shadowing which plays a greater role at LHC energies at very small fractions x and can be estimated as a correction associated with the higher Fock states $|\gamma^* qG\rangle$, $|\gamma^* q2G\rangle$, etc. The second effect is the so-called effective energy loss due to the initial state interactions (ISI). The latter describes a suppression of the cross section at large dilepton p_T which was indicated at midrapidity, $y = 0$, by the PHENIX data [2] on π^0 production in central dAu collisions and on direct photon production in central $AuAu$ collisions [3]. The same mechanism of nuclear attenuation is important, especially at forward rapidities where we expect a much stronger onset of nuclear suppression as was demonstrated by the BRAHMS and STAR data [4].

Finally, we present new results on dilepton-pion azimuthal correlation in proton-lead collisions, where the characteristic double peak structure particularly sensitive to the saturation scale is predicted.

2 Color dipole picture

The color dipole formalism is treated in the target rest frame where the process of DY pair production can be viewed as a radiation of gauge bosons $G^* = \gamma^*, Z^0$ by a projectile quark [1, 5]. Assuming only the lowest $|qG^*\rangle$ Fock component the quark–nucleon differential cross section reads [1, 5, 6]

$$\frac{d\sigma^f_{T,L}(qN \to qG^* X)}{d\ln\alpha d^2 p_T} = \frac{1}{(2\pi)^2}\int d^2\rho_1 d^2\rho_2 e^{i\vec{p}_T\cdot(\vec{\rho}_1-\vec{\rho}_2)}\Psi^{V-A}_{T,L}(\alpha,\vec{\rho}_1)\Psi^{V-A,*}_{T,L}(\alpha,\vec{\rho}_2)\Sigma(\alpha,\vec{\rho}_1,\vec{\rho}_2), \quad (1)$$

where

$$\Sigma(\alpha,\vec{\rho}_1,\vec{\rho}_2) = \frac{1}{2}\left(\sigma^N_{q\bar{q}}(\alpha\vec{\rho}_1) + \sigma^N_{q\bar{q}}(\alpha\vec{\rho}_2) - \sigma^N_{q\bar{q}}(\alpha(\vec{\rho}_1 - \vec{\rho}_2))\right) \quad (2)$$

and $\vec{p}_T$ is the transverse momentum of the outgoing gauge boson, and α is a fraction of the quark LC momentum taken by the gauge boson G^*. The vector and axial-vector wave functions are decorrelated in the simplest case of an unpolarized incoming quark [5]. In this work, we take into account the presence of both interfering $G^* = \gamma^*$ and Z^0 contributions. The corresponding wave functions $\Psi^{V-A}_{T,L}(\alpha,\vec{\rho})$ can be found in Ref. [5]. The cross section for inclusive production of a virtual gauge boson in pp collisions is found as follows [1]

$$\frac{d\sigma_{L,T}(pp \to G^* X)}{d^2 p_T d\eta dM^2} = J(\eta, p_T)\frac{x_1}{x_1 + x_2}\sum_f \int_{x_1}^1 \frac{d\alpha}{\alpha^2}\left(q_f(x_q,\mu^2) + \bar{q}_f(x_q,\mu^2)\right)\frac{d\sigma^f_{T,L}(qN \to qG^* X)}{d\ln\alpha d^2 p_T} \quad (3)$$

where $J(\eta, p_T) = \frac{2}{\sqrt{s}}\sqrt{M^2 + p_T^2}\cosh\eta$ is the Jacobian of the transformation between the Feynman $x_F = x_1 - x_2$ and the pseudorapidity η variables, with Bjorken fractions x_1 and x_2. Then, $q_f, \bar{q}_f$ denote quark and antiquark PDFs, respectively, for which the CTEQ parameterisations [7] will be used, with the hard scale $\mu^2 = p_T^2 + (1 - x_1)M^2$, where M is a dilepton mass. In practical calculations we use several parametrisations for dipole cross sections such as GBW [8], BGBK [9] and IP-Sat [10] models.

In Figs. 1 and 2 we compare our predictions for the dilepton invariant mass distributions with recent ATLAS data in the high invariant mass range and with recent CMS data covering the Z^0 boson resonance region taking into account its interference with the γ^* contribution. We can conclude that the parametrisation of the dipole cross section including the DGLAP evolution via the gluon PDF (BGBK and IP-Sat) describe the DY data better than naive GBW model as expected.

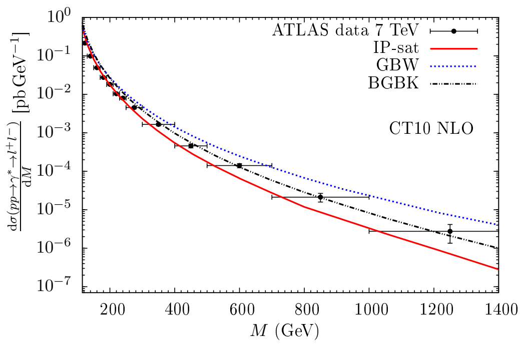

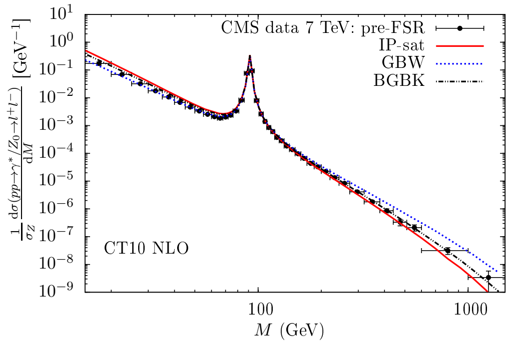

Figure 1. Predictions for the DY dilepton invariant mass distributions in pp vs. data from ATLAS [11].

Figure 2. Predictions for DY dilepton mass distributions in pp vs. data from CMS [12].

3 Proton-nucleus interactions

The dynamics of DY production on nuclear targets is controlled by the mean coherence length

$$l_c = \frac{1}{x_2 m_N} \frac{(M^2 + p_T^2)(1-\alpha)}{\alpha(1-\alpha)M^2 + \alpha^2 m_f^2 + p_T^2}, \tag{4}$$

where M is the dilepton invariant mass, m_f is the mass of a projectile quark (we take same values as in Ref. [1]) and α is the fraction of the light-cone momentum of the projectile quark carried out by the gauge boson. The condition for the onset of shadowing is that the coherence length exceeds the nuclear radius R_A, $l_c \gtrsim R_A$. In the LHC kinematic region the long coherence length (LCL) limit can be safely used in practical calculations as is demonstrated in Fig. 3. In particular, this enables us to incorporate the shadowing effects via eikonalization of $\sigma_{q\bar{q}}^N(\vec{\rho}, \alpha)$ [13]

$$\sigma_{q\bar{q}}^N(\vec{\rho}, x) \to \sigma_{q\bar{q}}^A(\vec{\rho}, x) = 2 \int d^2b \left(1 - e^{-\frac{1}{2}\sigma_{q\bar{q}}^N(\vec{\rho},x)T_A(b)}\right) \tag{5}$$

where $T_A(b)$ is the nuclear thickness function at given impact parameter b normalized to the mass number A.

In the LCL limit, besides the lowest $|qG^*\rangle$ Fock state one should include also the higher Fock components containing gluons, e.g. $|\gamma^* qG\rangle$, $|\gamma^* q2G\rangle$, etc. They cause an additional suppression known as the gluon shadowing (GS). The corresponding suppression factor R_G [15] computed as a correction to the total $\gamma^* A$ cross section for the longitudinal photon reads $R_G(x, Q^2, b) \approx 1 - \frac{\Delta\sigma_L^{(\gamma^* A)}}{\sigma_{tot}^{(\gamma^* A)}}$, was included in calculations replacing $\sigma_{q\bar{q}}^N(\vec{\rho}, x) \to \sigma_{q\bar{q}}^N(\vec{\rho}, x) R_G(x, Q^2, b)$.

3.1 Effective energy loss

The initial-state energy loss (due to ISI effects) is expected to suppress noticeably the nuclear cross section when reaching the kinematical limits, $x_L = \frac{2p_L}{\sqrt{s}} \to 1$ and $x_T = \frac{2p_T}{\sqrt{s}} \to 1$. Correspondingly, a proper variable which controls this effect is $\xi = \sqrt{x_L^2 + x_T^2}$. The magnitude of suppression was evaluated in Ref. [16]. It was found within the Glauber approximation that each interaction in the nucleus

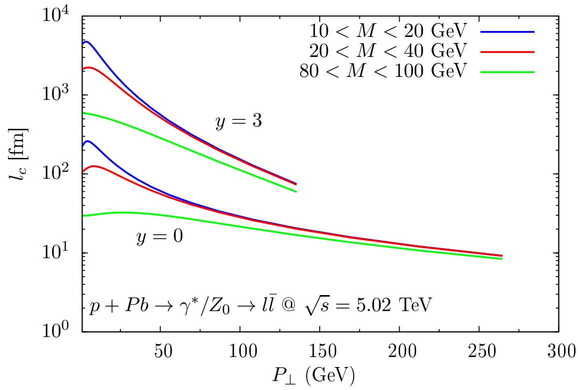

Figure 3. The mean coherence length for dilepton rapidities $y = 0, 3$ for different dilepton invariant mass intervals.

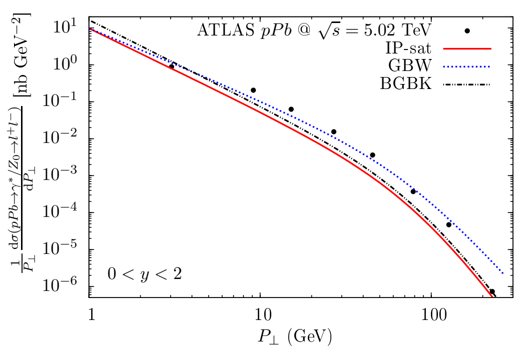

Figure 4. The dilepton p_T distribution in pPb collisions vs. ATLAS data [14].

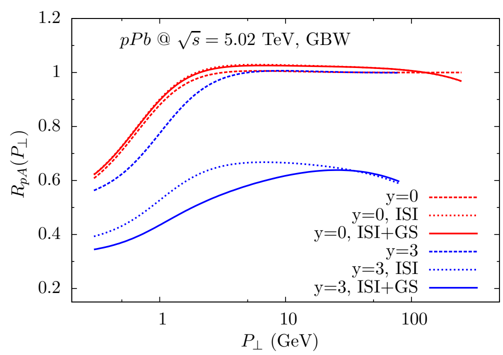

Figure 5. Predictions for the nuclear modification factor R_{pPb}.

leads to a suppression factor $S(\xi) \approx 1 - \xi$. Summing up over the multiple initial state interactions in a pA collision at impact parameter b, one arrives at a nuclear ISI-modified PDF

$$q_f(x, Q^2) \Rightarrow q_f^A(x, Q^2, b) = C_v q_f(x, Q^2) \frac{e^{-\xi\sigma_{eff}T_A(b)} - e^{-\sigma_{eff}T_A(b)}}{(1-\xi)(1 - e^{-\sigma_{eff}T_A(b)})}. \tag{6}$$

Here, $\sigma_{eff} = 20$ mb is the effective hadronic cross section controlling the multiple interactions. The normalisation factor C_v is fixed by the Gottfried sum rule (for more details, see Ref. [16]). It was found that such an additional nuclear suppression emerging due to the ISI effects represents an energy independent feature common for all known reactions experimentally studied so far, with any leading particle (hadrons, Drell-Yan dileptons, charmonium, etc).

Fig. 4 demonstrates a good agreement of our calculations for DY production in pPb collisions with the data from ATLAS experiment [14]. Fig. 5 shows predictions for the nuclear modification factor R_{pPb} as a function of p_T for production of DY pairs at distinct rapidities $y = 0, 3$ and dilepton invariant masses in the interval $66 < M < 122$ GeV typical for the ATLAS measurements. The GS and ISI effects are irrelevant at $y = 0$. However, we expect a strong nuclear suppression in the forward region $y = 3$ and large p_T's caused by the ISI effects. Here, the GS effects give a small contribution to the nuclear suppression at $p_T < 15 \div 20$ GeV.

4 Drell-Yan–Hadron correlations

The correlation function $C(\Delta\phi)$ depends on the azimuthal angle difference $\Delta\phi$ between the trigger and associate particles. The azimuthal correlations are investigated through a coincidence probability defined in terms of a trigger particle which could be either the gauge boson (dilepton) or the hadron. If we assume the former as a trigger particle then the correlation function is written as [1]

$$C(\Delta\phi) = \frac{2\pi \int_{p_T^{G^*}, p_T^h > p_T^{cut}} dp_T^{G^*} p_T^{G^*} dp_T^h p_T^h \frac{d\sigma(pp\to hG^*X)}{d^2p_T^h d\eta^h d^2p_T^{G^*} d\eta^{G^*} d^2b}}{\int_{p_T^{G^*} > p_T^{cut}} dp_T^{G^*} p_T^{G^*} \frac{d\sigma(pp\to G^*X)}{d^2p_T^{G^*} d\eta^{G^*} d^2b}} \tag{7}$$

where $\Delta\phi$ is the angle between the gauge boson and the hadron. The differential cross sections for G^* and G^*h production in momentum representation can be found in Ref. [1]. Fig. 6 demonstrates that a double peak structure emerges around $\Delta\phi = \pi$ in pp collisions considering that the photon and the pion are produced at forward rapidities, close to the limit of the phase space. Taking into account the nuclear dependence of the saturation scale in the GBW model in the LCL limit we calculated the correlation functions for proton-lead collisions as is shown in Fig. 7, where we expect again the characteristic double peak structure at forward rapidity $y = 4$. These results are in agreement with Ref. [17].

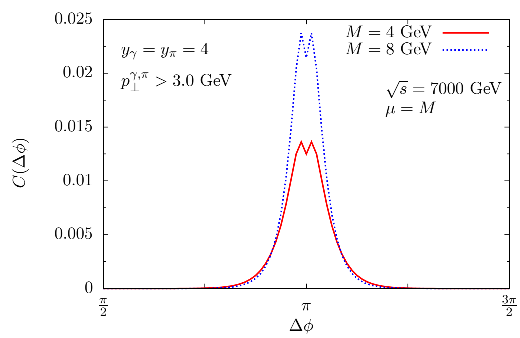

Figure 6. The correlation function for the DY–pion production in pp collisions.

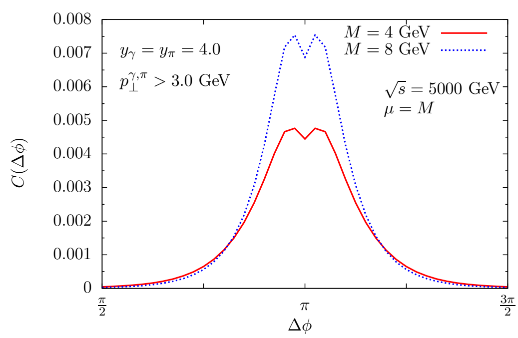

Figure 7. The correlation function for the DY–pion production in pPb collisions.

5 Conclusions

Within the color dipole picture we analyzed the DY pair production process accouning for virtual γ^* and Z^0 contributions. In the case of pp collisions, we found a good agreement of the differential cross section as a function of the dilepton invariant mass M with the ATLAS and CMS data. We demonstrate that for production of DY pairs on nuclear targets, the LCL limit can be safely employed in the LHC kinematic region. Our calculations of differential cross section for DY production in pPb collisions were compared to the ATLAS data and a good agreement has been found. We showed that the main source of a strong nuclear suppression, especially at forward rapidities expected at the LHC, comes mainly from the ISI corrections. A small onset of the GS is visible only at large $y = 3$ for $p_T < 15 \div 20$ GeV. Investigating the anglular correlation function corresponding to associated dilepton and pion production we found a characteristic double peak structure around $\Delta\phi = \pi$ not only for *pp* but also for *pPb* collisions.

6 Acknowledgements

E. B. is supported by CAPES and CNPq (Brazil), contract numbers 2362/13-9 and 150674/2015-5. V. P. G. has been supported by CNPq, CAPES and FAPERGS, Brazil. R. P. is supported by the Swedish Research Council, contract number 621-2013-428. J. N. is partially supported by the grant 13-20841S of the Czech Science Foundation (GAČR), by the Grant MSMT LG13031, by the Slovak Research and Development Agency APVV-0050-11 and by the Slovak Funding Agency, Grant 2/0020/14.

References

[1] E. Basso, V. P. Goncalves, J. Nemchik, R. Pasechnik, M. Sumbera, arXiv:1510.00650 [hep-ph].
[2] S. S. Adler *et al.* [PHENIX Collab.], Phys. Rev. Lett. **98**, 172302 (2007);
Phys. Rev. Lett. **109**, 152302 (2012).
[3] S. Afanasiev *et al.* [PHENIX Collab.], Phys. Rev. Lett. **109**, 152302 (2012);
T. Sakaguchi, Nucl. Phys. A**805**, 355 (2008).
[4] I. Arsene *et al.* [BRAHMS Collab.], Phys. Rev. Lett. **93**, 242303 (2004);
J. Adams *et al.* [STAR Collab.], Phys. Rev. Lett. **97**, 152302 (2006).
[5] R. Pasechnik, B. Z. Kopeliovich, I. Potashnikova, Phys. Rev. D**86**, 114039 (2012).
[6] B. Z. Kopeliovich, A. V. Tarasov, A. Schafer, Phys. Rev. C**59**, 1609-1619 (1999).
[7] H. Lai, M. Guzzi, J. Huston, Z. Li, P. M. Nadolsky, J. Pumplin, C. P. Yuan, Phys. Rev. D**82**, 074024 (2010).
[8] K. Golec-Biernat, M. Wüsthoff, Phys. Rev. D**59**, 014017 (1998).
[9] J. Bartels, K. Golec-Biernat, H. Kowalski, Phys. Rev. D**66**, 014001 (2002).
[10] H. Kowalski, L. Motyka, G. Watt, Phys. Rev. D**74**, 074016 (2006).
[11] G. Aad *et al.* [ATLAS Collab.], Phys. Lett. B**725**, 223 (2013).
[12] V. Khachatryan *et al.* [CMS Collab.], Eur. Phys. J. **75**, 147 (2015).
[13] B. Z. Kopeliovich, L. I. Lapidus, A. B. Zamolodchikov, JETP Lett. **33**, 595-597 (1981).
[14] G. Aad *et al.* [ATLAS Collab.], Phys. Rev. C**92**, 044915 (2015).
[15] B. Z. Kopeliovich, J. Nemchik, A. Schafer, Phys. Rev. C**65**, 035201 (2002).
[16] B. Z. Kopeliovich, J. Nemchik, I. K. Potashnikova, I. Schmidt, Int. J. Mod. Phys. E**23**, 1430006 (2014).
[17] A. Stasto, B. W. Xiao and F. Yuan, Phys. Lett. B**716**, 430 (2012).

LU TP 16-03
March 2016

Nuclear effects in Drell-Yan pair production in high-energy pA collisions

Eduardo Basso,[1,*] Victor P. Goncalves,[2,3,†] Michal Krelina,[4,‡] Jan Nemchik,[4,5,§] and Roman Pasechnik[2,¶]

[1] *Instituto de Física, Universidade Federal do Rio de Janeiro, Caixa Postal 68528, Rio de Janeiro, RJ 21941-972, Brazil*
[2] *Department of Astronomy and Theoretical Physics, Lund University, SE-223 62 Lund, Sweden*
[3] *High and Medium Energy Group, Instituto de Física e Matemática, Universidade Federal de Pelotas, Pelotas, RS, 96010-900, Brazil*
[4] *Czech Technical University in Prague, FNSPE, Břehová 7, 11519 Prague, Czech Republic*
[5] *Institute of Experimental Physics SAS, Watsonova 47, 04001 Košice, Slovakia*

The Drell-Yan (DY) process of dilepton pair production off nuclei is not affected by final state interactions, energy loss or absorption. A detailed phenomenological study of this process is thus convenient for investigation of the onset of initial-state effects in proton-nucleus (pA) collisions. In this paper, we present a comprehensive analysis of the DY process in pA interactions at RHIC and LHC energies in the color dipole framework. We analyse several effects affecting the nuclear suppression, $R_{pA} < 1$, of dilepton pairs, such as the saturation effects, restrictions imposed by energy conservation (the initial-state effective energy loss) and the gluon shadowing, as a function of the rapidity, invariant mass of dileptons and their transverse momenta p_T. In this analysis, we take into account besides the γ^* also the Z^0 contribution to the production cross section, thus extending the predictions to large dilepton invariant masses. Besides the nuclear attenuation of produced dileptons at large energies and forward rapidities emerging due to the onset of shadowing effects, we predict a strong suppression at large p_T, dilepton invariant masses and Feynman x_F caused by the Initial State Interaction effects in kinematic regions where no shadowing is expected. The manifestations of nuclear effects are investigated also in terms of the correlation function in azimuthal angle between the dilepton pair and a forward pion $\Delta\phi$ for different energies, dilepton rapidites and invariant dilepton masses. We predict that the characteristic double-peak structure of the correlation function around $\Delta\phi \simeq \pi$ arises for very forward pions and large-mass dilepton pairs.

I. INTRODUCTION

During the last two decades, a series of theoretical and experimental studies of particle production in heavy ion collisions (HICs) at Relativistic Heavy Ion Collider (RHIC) and Large Hadrons Collider (LHC) energies has been performed. These results provided us with various sources of information on properties of the hot and dense matter (Quark Gluon Plasma) formed in these collisions. Although several issues still remain open, those are mainly related to a description of nuclear effects related to the initial-state formation before it interacts with a nuclear target, as well as to the parton propagation in a nuclear medium. In this context, the phenomenological studies of hard processes in proton-nucleus (pA) collisions can provide us with an additional quantitative information about various nuclear effects expected also in HICs. This can help us to disentangle between the medium effects of different types and constrain their relative magnitudes and contributions [1].

A key feature of the Drell-Yan (DY) process is the absence of final state interactions and fragmentation associated with an energy loss or absorption phenomena. For this reason, the DY process can be considered as a very clean probe for the Initial State Interaction (ISI) effects [2]. In practice, this process can be used as a convenient tool in studies of the Quantum Chromodynamics (QCD) at high energies, in particular, the saturation effects expected to

*Electronic address: eduardo.basso@thep.lu.se
†Electronic address: victor.goncalves@thep.lu.se
‡Electronic address: michal.krelina@fjfi.cvut.cz
§Electronic address: nemcik@saske.sk
¶Electronic address: roman.pasechnik@thep.lu.se

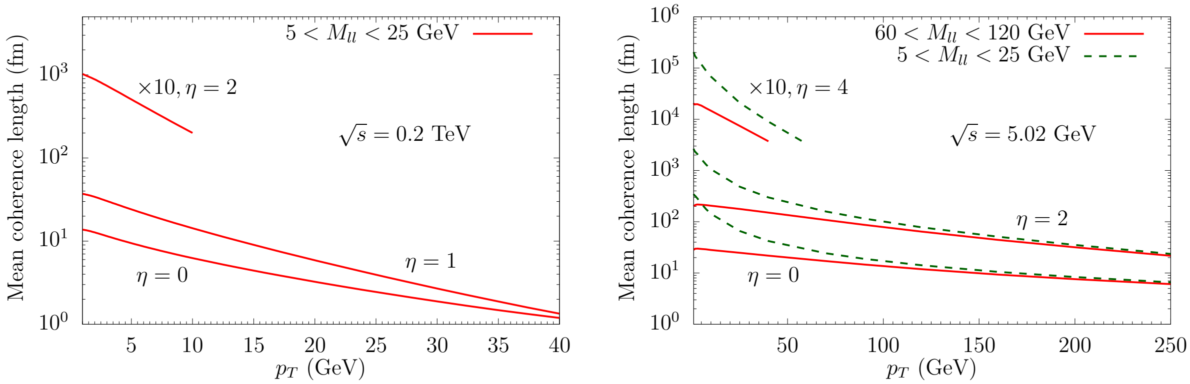

FIG. 1: (Color online) The mean coherence length l_c of the DY reaction in pA collisions at RHIC and LHC energies for different dilepton rapidities and invariant mass ranges.

determine the initial conditions in hadronic collisions as well as the initial-state energy loss due to the projectile quark propagation in the nuclear medium before it experiences a hard scattering.

In the present paper, we study the DY process on nuclear targets at high energies using the color dipole approach [3–12], which is known to give as precise prediction for the DY cross section as the Next-to-Leading-Order (NLO) collinear factorization framework and allows to include naturally the coherence effects in nuclear collisions. Moreover, the color dipole formalism provides a straightforward generalisation of the DY process description from the proton-proton to proton-nucleus collisions and is thus suitable for studies of nuclear effects directly accessing the impact parameter dependence of nuclear shadowing and nuclear broadening – the critical information which is not available in the parton model.

In contrast to the conventional parton model where the dilepton production process is typically viewed as the parton annihilation in the center of mass (c.m.) frame, in the color dipole approach operating in the target rest frame the same process looks as a bremsstrahlung of a γ^*/Z^0 boson off a projectile quark. In pA collisions assuming the high energy limit, the projectile quark probes a dense gluonic field in the target and the nuclear shadowing leads to a nuclear modification of the transverse momentum distribution of the DY production cross section. The onset of shadowing effects is controlled by the coherence length, which can be interpreted as the mean lifetime of γ^*/Z^0-quark fluctuations, and is given by

$$l_c = \frac{1}{x_2 m_N} \frac{(M_{l\bar{l}}^2 + p_T^2)(1-\alpha)}{\alpha(1-\alpha)M_{l\bar{l}}^2 + \alpha^2 m_f^2 + p_T^2} \,, \tag{1}$$

where $M_{l\bar{l}}$ is the dilepton invariant mass and p_T its transverse momentum. Moreover, α is the fraction of the light-cone momentum of the projectile quark carried out by the gauge boson. As demonstrated in Fig. 1, in the RHIC and LHC kinematic regions, the coherence length exceeds the nuclear radius R_A, $l_c \gtrsim R_A$, which implies that the long coherence length (LCL) limit can be safely used in practical calculations of the DY cross section in pA collisions.

Besides the quark shadowing effects naturally accounted for in the dipole picture, one should also take into account the nuclear effects due to multiple rescattering of initial-state projectile partons (ISI effects) in a medium before a hard scattering. The latter are important close to the kinematic limits, e.g. at large Feynman $x_F \to 1$ and $x_T = 2p_T/\sqrt{s} \to 1$ ($\sqrt{s}$ is the collision energy in c.m. frame), due to restrictions imposed by energy conservation. In the present paper, we take into account also non-linear QCD effects, which are amplified in nuclear collisions and related to multiple scatterings of the higher Fock states containing gluons in the dipole-target interactions. They generate the gluon shadowing effects effective at small Bjorken x in the target and large rapidity values.

In our study, all the basic ingredients for the DY nuclear production cross section (such as the dipole cross section parameterisations and Parton Distribution Functions (PDFs)) have been determined from other processes. Consequently, our predictions are parameter-free and should be considered as an important test for the onset of distinct nuclear effects. Note that the nuclear DY process mediated by a virtual photon has been already studied within the color dipole framework by several authors (see e.g. Refs. [7–9]). However, the results of this paper represent a further step updating and improving the previous analyses in the literature providing new predictions for the transverse momentum, dilepton invariant mass and rapidity distributions of the nuclear DY production cross section at RHIC and LHC energies as well as in comparison to the most recent data. Besides, the effects of quantum coherence at large energies including the gluon shadowing as a leading-twist shadowing correction as well as an additional contribution of the Z^0 boson and γ^*/Z^0 interference are incorporated. Moreover, the impact of the effective initial state energy loss effects on the DY nuclear production cross section is studied for the first time. We also investigate nuclear effects providing a detailed analysis of the azimuthal correlation between the produced DY pair and a forward pion taking into account the Z^0 boson contribution in addition to virtual photon, generalising thus the results presented in Ref. [13].

This paper is organized as follows. In the Section II, we present a brief overview of gauge boson production in the color dipole framework. Moreover, we discuss in detail the saturation effects, gluon shadowing and initial-state energy loss effects included in the analysis. Section III is devoted to predictions for the dilepton invariant mass, rapidity and transverse momentum distributions of the DY nuclear production cross sections in comparison with the available data. The onset of various nuclear effects is estimated in the LCL limit and the predictions for the nucleus-to-nucleon ratio, $R_{pA} = \sigma_{pA}/A\sigma_{pp}$[1], of the DY production cross sections are presented. The latter can be verified in the future by experiments at RHIC an LHC. Furthermore, the azimuthal correlation function between the produced dilepton and a pion is evaluated for pA collisions at RHIC and LHC for different dilepton invariant masses including the high-mass region. Finally, in Section IV we summarise our main conclusions.

II. DRELL-YAN PROCESS IN HADRON-NUCLEUS COLLISIONS

A. DY nuclear cross section

The color dipole formalism is treated in the target rest frame where the process of DY pair production can be viewed as a radiation of gauge bosons $G^* = \gamma^*/Z^0$ by a projectile quark (see e.g. Ref. [10, 12]). Assuming only the lowest $|qG^*\rangle$ Fock component, the cross section for the inclusive gauge boson production with invariant mass $M_{l\bar{l}}$ and transverse momentum p_T can be expressed in terms of the projectile quark (antiquark) densities q_f ($\bar{q}_f$) at momentum fraction x_q and the quark-nucleus cross section as follows (see e.g. Refs. [7, 12]),

$$\frac{d\sigma(pA \to G^* X)}{\mathrm{d}^2 p_T \, d\eta} = J(\eta, p_T) \, \frac{x_1}{x_1 + x_2} \sum_f \sum_{\lambda_G = L,T} \int_{x_1}^{1} \frac{d\alpha}{\alpha^2} \left[q_f(x_q, \mu_F^2) + \bar{q}_f(x_q, \mu_F^2) \right] \frac{d\sigma^f_{\lambda_G}(qA \to qG^* X)}{d(\ln\alpha) \, d^2 p_T} \,, \tag{2}$$

where

$$J(\eta, p_T) \equiv \frac{dx_F}{d\eta} = \frac{2}{\sqrt{s}} \sqrt{M_{l\bar{l}}^2 + p_T^2} \, \cosh(\eta) \tag{3}$$

is the Jacobian of transformation between the Feynman variable $x_F = x_1 - x_2$ and pseudorapidity η of the virtual gauge boson G^*, $x_q = x_1/\alpha$, where α is the fraction of the light-cone momentum of the projectile quark carried out by the gauge boson, and $\mu_F^2 = p_T^2 + (1 - x_1) M_{l\bar{l}}^2$ is the factorization scale in quark PDFs. As in Ref. [12] we take $\mu_F \simeq M_{l\bar{l}}$, for simplicity.

The transverse momentum distribution in Eq. (2) of the gauge boson G^* bremsstrahlung in quark-nucleus interactions can be obtained by a generalization of the well-known formulas for the photon bremsstrahlung from Refs. [5, 7, 8]. Then the corresponding differential cross section for a given incoming quark of flavour f reads,

$$\begin{aligned} \frac{d\sigma^f_{T,L}(qA \to qG^* X)}{d(\ln\alpha) \, d^2 p_T} &= \frac{1}{(2\pi)^2} \sum_{\text{quark pol.}} \int d^2\rho_1 \, d^2\rho_2 \, \exp\!\left[i \, \mathbf{p}_T \cdot (\boldsymbol{\rho}_1 - \boldsymbol{\rho}_2) \right] \Psi^{\mathcal{V}-\mathcal{A}}_{T,L}(\alpha, \boldsymbol{\rho}_1, m_f) \, \Psi^{\mathcal{V}-\mathcal{A},*}_{T,L}(\alpha, \boldsymbol{\rho}_2, m_f) \\ &\times \; \frac{1}{2} \left[\sigma^A_{q\bar{q}}(\alpha\boldsymbol{\rho}_1, x_2) + \sigma^A_{q\bar{q}}(\alpha\boldsymbol{\rho}_2, x_2) - \sigma^A_{q\bar{q}}(\alpha|\boldsymbol{\rho}_1 - \boldsymbol{\rho}_2|, x_2) \right] , \end{aligned} \tag{4}$$

where $x_2 = x_1 - x_F$ and $\boldsymbol{\rho}_{1,2}$ are the quark-G^* transverse separations in the total radiation amplitude and its conjugated counterpart, respectively. Assuming that the projectile quark is unpolarized, the vector $\Psi^{\mathcal{V}}$ and axial-vector $\Psi^{\mathcal{A}}$ wave functions in Eq. (4) are not correlated such that

$$\begin{aligned} &\sum_{\text{quark pol.}} \Psi^{\mathcal{V}-\mathcal{A}}_{T,L}(\alpha, \boldsymbol{\rho}_1, m_f) \, \Psi^{\mathcal{V}-\mathcal{A},*}_{T,L}(\alpha, \boldsymbol{\rho}_2, m_f) = \\ &= \Psi^{\mathcal{V}}_{T,L}(\alpha, \boldsymbol{\rho}_1, m_f) \, \Psi^{\mathcal{V},*}_{T,L}(\alpha, \boldsymbol{\rho}_2, m_f) + \Psi^{\mathcal{A}}_{T,L}(\alpha, \boldsymbol{\rho}_1, m_f) \, \Psi^{\mathcal{A},*}_{T,L}(\alpha, \boldsymbol{\rho}_2, m_f) \,, \end{aligned} \tag{5}$$

---

[1] Here A represents the atomic mass number of the nuclear target

where the averaging over the initial and summation over final quark helicities is performed and the quark flavour dependence comes only via the projectile quark mass m_f. The corresponding wave functions $\Psi^{\mathcal{V}-\mathcal{A}}_{T,L}(\alpha,\boldsymbol{\rho})$ can be found in Ref. [10].

Our goal is to evaluate the DY production cross section in pA collisions at high energies and a large mass number A of the nuclear target. This regime is characterised by a limitation on the maximum phase-space parton density that can be reached in the hadron wave function (parton saturation) [14]. The transition between the linear and non-linear regimes of QCD dynamics is typically specified by a characteristic energy-dependent scale called the saturation scale Q_s^2, where the variable s denotes c.m. energy squared of the collision. Such saturation effects are expected to be amplified in nuclear collisions since the nuclear saturation scale $Q^2_{s,A}$ is expected to be enlarged with respect to the nucleon one $Q^2_{s,p}$ by rougthly a factor of $A^{1/3}$.

In general, the dipole-nucleus cross section $\sigma^A_{q\bar{q}}(\rho,x)$ can be written in terms of the forward dipole-nucleus scattering amplitude $\mathcal{N}^A(\rho,x,\boldsymbol{b})$ as follows,

$$\sigma^A_{q\bar{q}}(\boldsymbol{\rho},x) = 2\int d^2\boldsymbol{b}\,\mathcal{N}^A(\boldsymbol{\rho},x,\boldsymbol{b})\,. \tag{6}$$

At high energies, the evolution of $\mathcal{N}^A(x,\boldsymbol{r},\boldsymbol{b})$ in rapidity $Y=\ln(1/x)$ is given, for example, within the Color Glass Condensate (CGC) formalism [15], in terms of an infinite hierarchy of equations known as so called Balitsky-JIMWLK equations [15, 16], which reduces in the mean field approximation to the Balitsky-Kovchegov (BK) equation [16, 17]. In recent years, several groups have studied the solution of the BK equation taking into account the running coupling corrections to the evolution kernel. However, these analyses have assumed the translational invariance approximation, which implies that $\mathcal{N}^A(\rho,x,\boldsymbol{b}) = \mathcal{N}^A(\rho,x)\,S(\boldsymbol{b})$ and $\sigma^A_{q\bar{q}}(\boldsymbol{\rho},x,\boldsymbol{b}) = \sigma_0\,\mathcal{N}(\rho,x)$, where $\mathcal{N}(\rho,x)$ is a partial dipole amplitude on a nucleon, and σ_0 is the normalization of the dipole cross section fitted to the data. Basically, they disregard the impact parameter dependence. Unfortunately, the impact-parameter dependent numerical solutions of the BK equation are very difficult to obtain [18]. Moreover, the choice of the impact-parameter profile of the dipole amplitude entails intrinsically nonperturbative physics, which is beyond the QCD weak coupling approach of the BK equation. In what follows, we explore an alternative path and employ the available phenomenological models, which explicitly incorporate an expected b-dependence of the scattering amplitude.

B. Models for the dipole cross section

As in our previous studies [19–24], we work in the LCL limit and employ the model initially proposed in Ref. [25] which includes the impact parameter dependence in the dipole-nucleus amplitude and describes the experimental data on the nuclear structure function (for more details, see Ref. [19, 26]). In particular, this model enables us to incorporate the shadowing effects via a simple eikonalization of the standard dipole-nucleon cross section $\sigma_{q\bar{q}}(\boldsymbol{\rho},x)$ such that the forward dipole-nucleus amplitude in Eq. (6) is given by

$$\mathcal{N}^A(\boldsymbol{\rho},x,\boldsymbol{b}) = 1-\exp\left(-\frac{1}{2}\,T_A(\boldsymbol{b})\,\sigma_{q\bar{q}}(\boldsymbol{\rho},x)\right)\,, \tag{7}$$

where $T_A(\boldsymbol{b})$ is the nuclear profile (thickness) function, which is normalized to the mass number A and reads

$$T_A(\boldsymbol{b}) = \int_{-\infty}^{\infty}\rho_A(\boldsymbol{b},z)dz\,. \tag{8}$$

Here $\rho_A(\boldsymbol{b},z)$ represents the nuclear density function defined at the impact parameter $\boldsymbol{b}$ and the longitudinal coordinate z. In our calculations we used realistic parametrizations of $\rho_A(\boldsymbol{b},z)$ from Ref. [27]. The eikonal formula (7) based upon the Glauber-Gribov formalism [28] resums the multiple elastic rescattering diagrams of the $q\bar{q}$ dipole in a nucleus in the high-energy limit. The eikonalisation procedure is justified in the LCL regime where the transverse separation ρ of partons in the multiparton Fock state of the photon is frozen during propagation through the nuclear matter and becomes an eigenvalue of the scattering matrix.

For the numerical analysis of the nuclear DY observables, we need to specify a reliable parametrisation for the dipole-proton cross section. In recent years, several groups have constructed a number of viable phenomenological models based on saturation physics and fits to the HERA and RHIC data (see e.g. Refs. [29–41]).

As in our previous study of the DY process in pp collisions [12], in order to estimate theoretical uncertainty in our analysis, in what follows, we consider several phenomenological models for the dipole cross section $\sigma_{q\bar{q}}$ which take into account the DGLAP evolution as well as the saturation effects.

The first one is the model proposed in Ref. [38], where the dipole cross section is given by

$$\sigma_{q\bar{q}}(\boldsymbol{\rho}, x) = \sigma_0 \left[1 - \exp\left(-\frac{\pi^2}{\sigma_0 N_c} \rho^2 \alpha_s(\mu^2) xg(x, \mu^2)\right)\right] , \tag{9}$$

where $N_c = 3$ is the number of colors, $\alpha_s(\mu^2)$ is the strong coupling constant at μ scale, which is related to the dipole size ρ as $\mu^2 = C/\rho^2 + \mu_0^2$ with C, μ_0 and σ_0 parameters fitted to the HERA data. Moreover, in this model the gluon density evolves according to DGLAP equation [42] accounting for gluon splittings only,

$$\frac{\partial xg(x, \mu^2)}{\partial \ln \mu^2} = \frac{\alpha_s(\mu^2)}{2\pi} \int_x^1 dz\, P_{gg}(z) \frac{x}{z} g\left(\frac{x}{z}, \mu^2\right) , \tag{10}$$

where the gluon density at initial scale μ_0^2 is parametrized as [38]

$$xg(x, \mu_0^2) = A_g x^{-\lambda_g} (1 - x)^{5.6} . \tag{11}$$

The set of best fit values of the model parameters reads: $A_g = 1.2$, $\lambda_g = 0.28$, $\mu_0^2 = 0.52$ GeV^2, $C = 0.26$ and $\sigma_0 = 23$ mb. In what follows we denote by BGBK the predictions for the DY observables obtained using Eq. (9) as an input in calculations of the dipole-nucleus scattering amplitude.

The model proposed in Ref. [38] was generalised in Ref. [35] in order to take into account the impact parameter dependence of the dipole-proton cross section and to describe the exclusive observables at HERA. In this model, the corresponding dipole-proton cross section is given by

$$\sigma_{q\bar{q}}(\boldsymbol{\rho}, x) = 2 \int d^2 b_p \left[1 - \exp\left(-\frac{\pi^2}{2N_c} \rho^2 \alpha_s(\mu^2) xg(x, \mu^2) T_G(\mathbf{b}_p)\right)\right] \tag{12}$$

with the DGLAP evolution of the gluon distribution given by Eq. (10). The Gaussian impact parameter dependence is given by $T_G(\mathbf{b_p}) = (1/2\pi B_G) \exp(-b_p^2/2B_G)$, where B_G is a free parameter extracted from the t-dependence of the exclusive electron-proton (ep) data. The parameters of this model were updated in Ref. [40] by fitting to the recent high precision HERA data [43] providing the following values: $A_g = 2.373$, $\lambda_g = 0.052$, $\mu_0^2 = 1.428$ GeV^2, $B_G = 4.0$ GeV^2 and $C = 4.0$. Hereafter, we will denote as IP-SAT the resulting predictions obtained using Eq. (12) as an input in calculations of $\mathcal{N}^A$, Eq. (7).

For comparison with the previous results existing in the literature, we also consider the Golec-Biernat-Wusthoff (GBW) model [29] based upon a simplified saturated form

$$\sigma_{q\bar{q}}(\boldsymbol{\rho}, x) = \sigma_0 \left(1 - e^{-\frac{\rho^2 Q_s^2(x)}{4}}\right) \tag{13}$$

with the saturation scale

$$Q_s^2(x) = Q_0^2 \left(\frac{x_0}{x}\right)^\lambda , \tag{14}$$

where the model parameters $Q_0^2 = 1$ GeV^2, $x_0 = 4.01 \times 10^{-5}$, $\lambda = 0.277$ and $\sigma_0 = 29$ mb were obtained from the fit to the DIS data accounting for a contribution of the charm quark.

Finally, we also consider the running coupling solution of the BK equation for the partial dipole amplitude obtained in the Ref. [44] using the GBW model as an initial condition such that $\sigma^p_{q\bar{q}}(\boldsymbol{\rho}, x) = \sigma_0 \mathcal{N}^p(\boldsymbol{\rho}, x)$ where the normalisation σ_0 is fitted to the HERA data.

C. Gluon shadowing corrections

In the LHC energy range the eikonal formula for the LCL regime, Eq. (7), is not exact. Besides the lowest $|qG^*\rangle$ Fock state, where $G^* = \gamma^*/Z^0$, one should include also the higher Fock components containing gluons, e.g. $|qG^*g\rangle$, $|qG^*gg\rangle$, etc. They cause an additional suppression known as the gluon shadowing (GS). Such high LHC energies allow so to activate the coherence effects also for these gluon fluctuations, which are heavier and consequently have a shorter coherence length than lowest Fock component $|qG^*\rangle$. The corresponding suppression factor R_G, as the ratio of the gluon densities in nuclei and nucleon, was derived in Ref. [45] using the Green function technique through the calculation of the inelastic correction $\Delta\sigma_{tot}(q\bar{q}g)$ to the total cross section $\sigma_{tot}^{\gamma^* A}$, related to the creation of a $|q\bar{q}\,g\rangle$ intermediate Fock state

$$R_G(x, Q^2, \boldsymbol{b}) \equiv \frac{xg_A(x, Q^2, \boldsymbol{b})}{A \cdot xg_p(x, Q^2)} \approx 1 - \frac{\Delta\sigma_{tot}(q\bar{q}g)}{\sigma_{tot}^{\gamma^* A}} \,. \tag{15}$$

GS corrections are included in calculations replacing $\sigma_{q\bar{q}}^N(\boldsymbol{\rho}, x) \to \sigma_{q\bar{q}}^N(\boldsymbol{\rho}, x)\, R_G(x, Q^2, \boldsymbol{b})$. They lead to additional nuclear suppression in production of DY pairs at small Bjorken $x = x_2$ in the target. In Fig. 2 (left panel) we present our results for the x dependence of the ratio $R_G(x, Q^2, \boldsymbol{b})$ for different vales of the impact parameter b. As expected, the magnitude of the shadowing corrections decreases at large values of b. In the right panel we present our predictions for the b-integrated nuclear ratio $R_G(x, Q^2)$ for different values of the hard scale Q^2. This figure shows a not very strong onset of GS, which was confirmed by the NLO global analyses of DIS data [46]. A weak Q^2 dependence of GS demonstrates that GS is a leading twist effect, with $R_G(x, Q^2)$ approaching unity only very slowly (logarithmically) as $Q^2 \to \infty$.

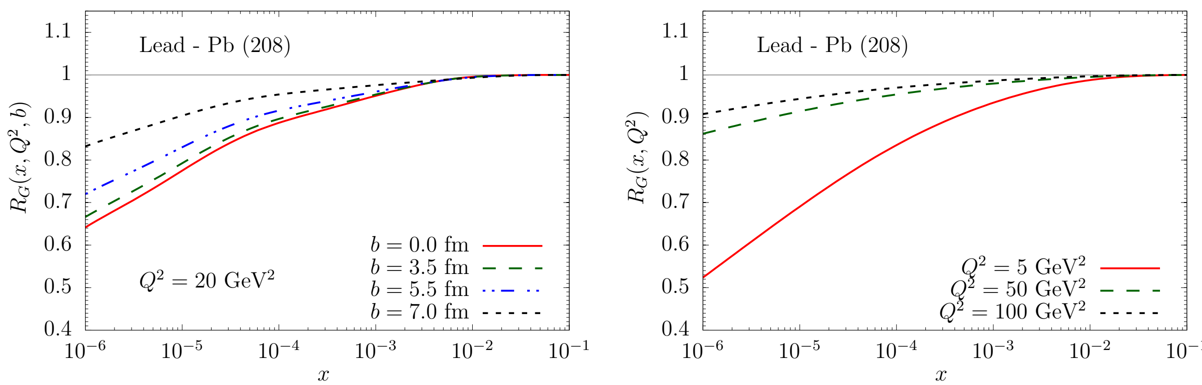

FIG. 2: (Color online) Left panel: The x-dependence of the ratio $R_G(x, Q^2, \boldsymbol{b})$ for different values of the impact parameter. Right panel: The x-dependence of the b–integrated ratio $R_G(x, Q^2)$ for distinct values of the hard scale Q^2.

D. Effective energy loss

The effective initial-state energy loss (ISI effects) is expected to suppress noticeably the nuclear cross section when reaching the kinematical limits,

$$x_L = \frac{2p_L}{\sqrt{s}} \to 1\,, \qquad x_T = \frac{2p_T}{\sqrt{s}} \to 1\,.$$

Correspondingly, a proper variable which controls this effect is $\xi = \sqrt{x_L^2 + x_T^2}$. The magnitude of suppression was evaluated in Ref. [47]. It was found within the Glauber approximation that each interaction in the nucleus leads to a suppression factor $S(\xi) \approx 1 - \xi$. Summing up over the multiple initial state interactions in a pA collision at impact parameter b, one arrives at a nuclear ISI-modified PDF

$$q_f(x, Q^2) \Rightarrow q_f^A(x, Q^2, b) = C_v\, q_f(x, Q^2)\, \frac{e^{-\xi\sigma_{\rm eff} T_A(b)} - e^{-\sigma_{\rm eff} T_A(b)}}{(1-\xi)(1 - e^{-\sigma_{\rm eff} T_A(b)})} \,. \tag{16}$$

Here, $\sigma_{\rm eff} = 20$ mb is the effective hadronic cross section controlling the multiple interactions. The normalisation factor C_v is fixed by the Gottfried sum rule (for more details, see Ref. [47]). It was found that such an additional nuclear suppression emerging due to the ISI effects represents an energy independent feature common for all known reactions experimentally studied so far, with any leading particle (hadrons, Drell-Yan dileptons, charmonium, etc). In particular, such a suppression was indicated at midrapidity, $y = 0$, and at large p_T by the PHENIX data [48] on π^0 production in central dAu collisions and on direct photon production in central $AuAu$ collisions [49], where no shadowing is expected since the corresponding Bjorken $x = x_2$ in the target is large. Besides large p_T-values, the same mechanism of nuclear attenuation is effective also at forward rapidities (large Feynman x_F), where we expect a much stronger onset of nuclear suppression as was demonstrated by the BRAHMS and STAR data [50]. In our case, we predict that the ISI effects induce a significant suppression of the DY nuclear cross section at large dilepton p_T, dilepton invariant mass and at forward rapidities as one can see in the next Section.

III. RESULTS

In what follows, we present our predictions for the DY pair production cross section in the process $pA \to \gamma^*/Z^0 \to l\bar{l}$ obtained within the color dipole formalism and taking into account the medium effects discussed in the previous Section. Following Ref. [29], we use the quark mass values to be $m_u = m_d = m_s = 0.14$ GeV, $m_c = 1.4$ GeV and $m_b = 4.5$ GeV. Moreover, we take the factorisation scale μ_F defined above to be equal to the dilepton invariant mass, $M_{l\bar{l}}$, and employ the CT10 NLO parametrisation for the projectile quark PDFs [51] (both sea and valence quarks are included). As was demonstrated in Refs. [12, 52], there is a little sensitivity of DY predictions on PDF parameterisation in pp collisions at high energies so we do not vary the projectile quark PDFs.

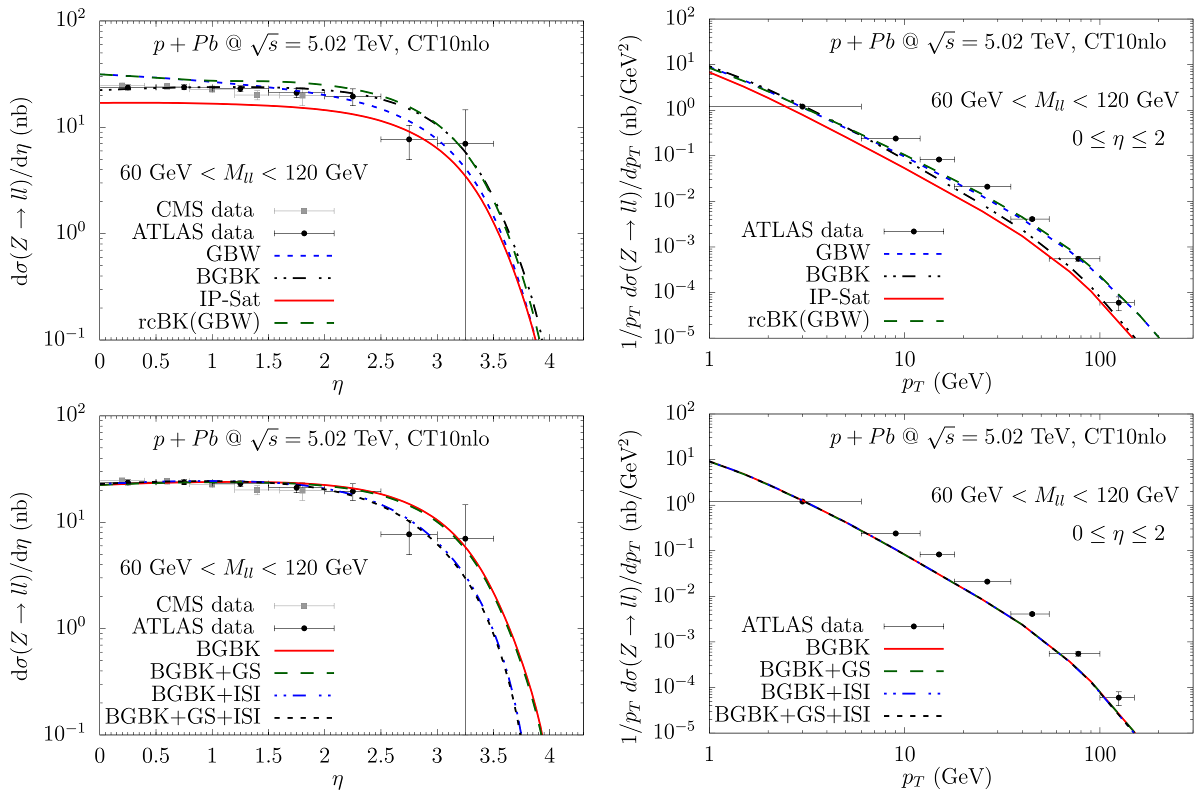

FIG. 3: (Color online) The dipole model predictions for the DY nuclear cross sections at large dilepton invariant masses compared to the recent experimental data from ATLAS and CMS experiments [53, 54] at c.m. collision energy $\sqrt{s} = 5.02$ TeV. The predictions obtained for several parameterisations of the dipole cross section described in the text are shown in the top panels while the effects of the gluon shadowing and the initial-state energy loss are demonstrated in the bottom panels.

In Fig. 3 we compare our predictions for the DY nuclear cross section with available LHC data [53, 54] for large invariant dilepton masses, $60 < M_{l\bar{l}} < 120$ GeV, taking into account the saturation effects. In the top panels, we test the predictions of various models for the dipole cross section comparing them with the experimental data for the rapidity and transverse momentum distributions of the DY production cross sections in pA collisions. As was already verified in Ref. [12] for DY production in pp collisions, the dipole approach works fairly well in description of the current experimental data at high energies. In particular, the BGBK model provides a consistent prediction describing the data on the rapidity distribution quite well in the full kinematical range. In the bottom panels of Fig. 3, we took the BGBK model and considered the impact of gluon shadowing corrections as well as the initial-state effective energy loss (ISI effects), Eq. (16). In the range of large dilepton invariant masses concerned, the gluon shadowing corrections are rather small since the corresponding Bjorken $x = x_2$ in the target becomes large. On the other hand, the ISI effects significantly modify the behaviour of the rapidity distribution at large $\eta > 2$. Unfortunately, the current data are not able at this moment to verify the predicted strong onset of ISI effects due to large error bars. In the case of the transverse momentum distribution for large invariant masses and $0 \le \eta \le 2$, the impact of both the gluon shadowing and the ISI effects is negligible.

In order to quantify the impact of the nuclear effects, in what follows, we estimate the invariant mass, rapidity and transverse momentum dependence of the nucleus-to-nucleon ratio of the DY production cross sections (nuclear

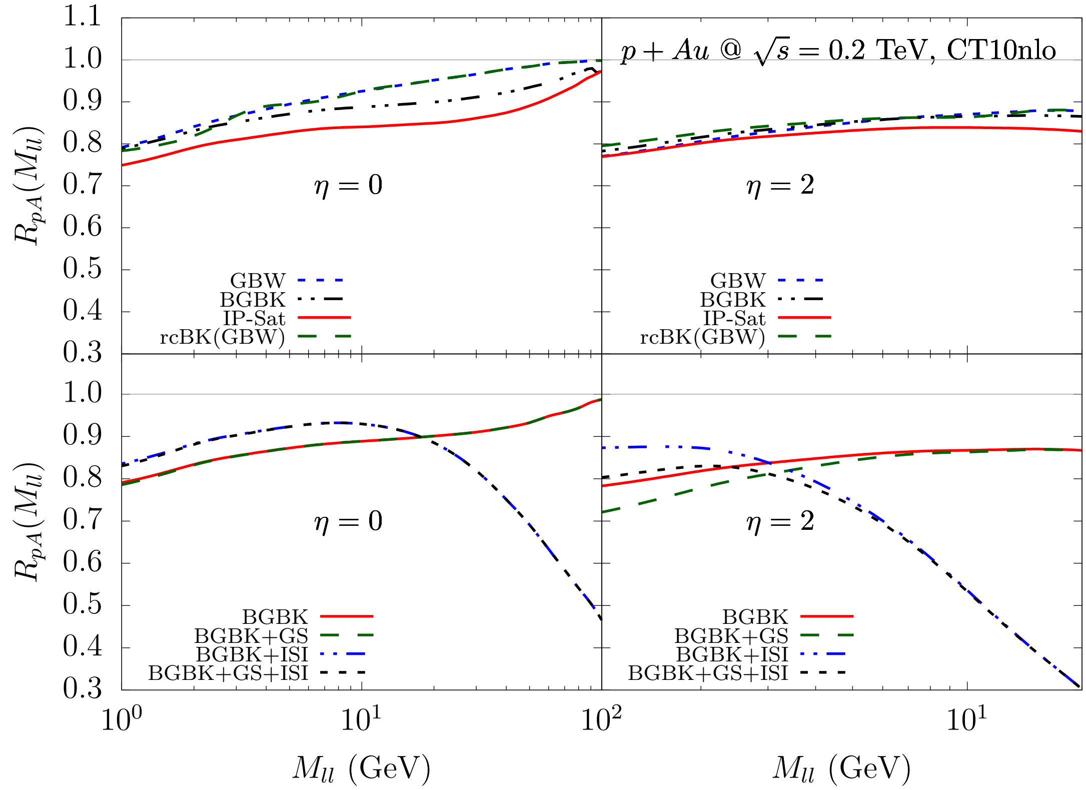

FIG. 4: (Color online) The dilepton invariant mass dependence of the nucleus-to-nucleon ratio, $R_{pA} = \sigma_{pA}^{DY}/(A \cdot \sigma_{pp}^{DY})$, of the DY production cross sections for c.m. energy $\sqrt{s} = 0.2$ TeV corresponding to RHIC experiments.

modification factor), $R_{pA} = \sigma_{pA}^{DY}/(A \cdot \sigma_{pp}^{DY})$, considering the DY process at RHIC ($\sqrt{s} = 0.2$ TeV) and LHC ($\sqrt{s} = 5.02$ TeV) energies. The color dipole predictions for the DY production cross section in *pp* collisions have been discussed in detail in Ref. [12]. For consistency, the numerator and denominator of the nuclear modification factor are evaluated within the same model for the dipole cross section as an input.

In Fig. 4 we present our predictions for the dilepton invariant mass dependence of the ratio $R_{pA}(M_{l\bar{l}})$ at RHIC considering both central and forward rapidities. In the top panels, we show that the dipole model predictions are almost insensitive to the parameterisations used to treat the dipole-proton interactions. The magnitude of the saturation effects decreases at large dilepton invariant masses and increases at forward rapidities. Such a behaviour is expected, since at smaller $M_{l\bar{l}}$ and at larger η one probes smaller values of the Bjorken-x_2 variable in the target. In the bottom panels of Fig. 4, we present the predictions taking into account also the GS corrections and ISI effects. As was mentioned above we predict a weak onset of GS corrections at central rapidities whereas GS leads to a significant suppression in the forward region. Besides, as expected, the impact of GS effects decreases with $M_{l\bar{l}}$ due to rise of the Bjorken x_2-values. In contrast to that, the ISI effects become effective causing a strong nuclear suppression at large $M_{l\bar{l}}$ and/or η. This behaviour is also well understood since large dilepton invariant masses and/or rapidities correspond to large Feynman x_F leading to a stronger onset of ISI effects as follows from Eq. (16). A similar behaviour has been predicted for the LHC energy range as is shown in Fig. 5 where the impact of saturation and GS effects is even more pronounced.

In Fig. 6 we present our predictions for rapidity dependence of the nucleus-to-nucleon ratio, $R_{pA}(\eta)$, of the DY production cross sections at RHIC and LHC energies considering two ranges, ($5 < M_{l\bar{l}} < 25$ GeV) and ($60 < M_{l\bar{l}} < 120$ GeV), of dilepton invariant mass. We would like to emphasize that the onset of saturation effects reduces $R_{pA}(\eta)$ at large rapidities and have a larger impact in the small invariant mass range. For large invariant masses, we predict a reduction of $\approx 10\%$ in the R_{pPb} ratio at LHC energy. At RHIC energy we predict a weak onset of GS effects even at large $\eta > 3$. In contrast to RHIC energy range, at the LHC the GS effects lead to a significant additional suppression, modifying thus the ratio R_{pPb} especially at small dilepton invariant masses and large rapidity values. On the other hand, the onset of the ISI effects is rather strong for both RHIC and LHC kinematic regions, and becomes even stronger at forward rapidities for both invariant mass ranges. This makes the phenomenological studies of the

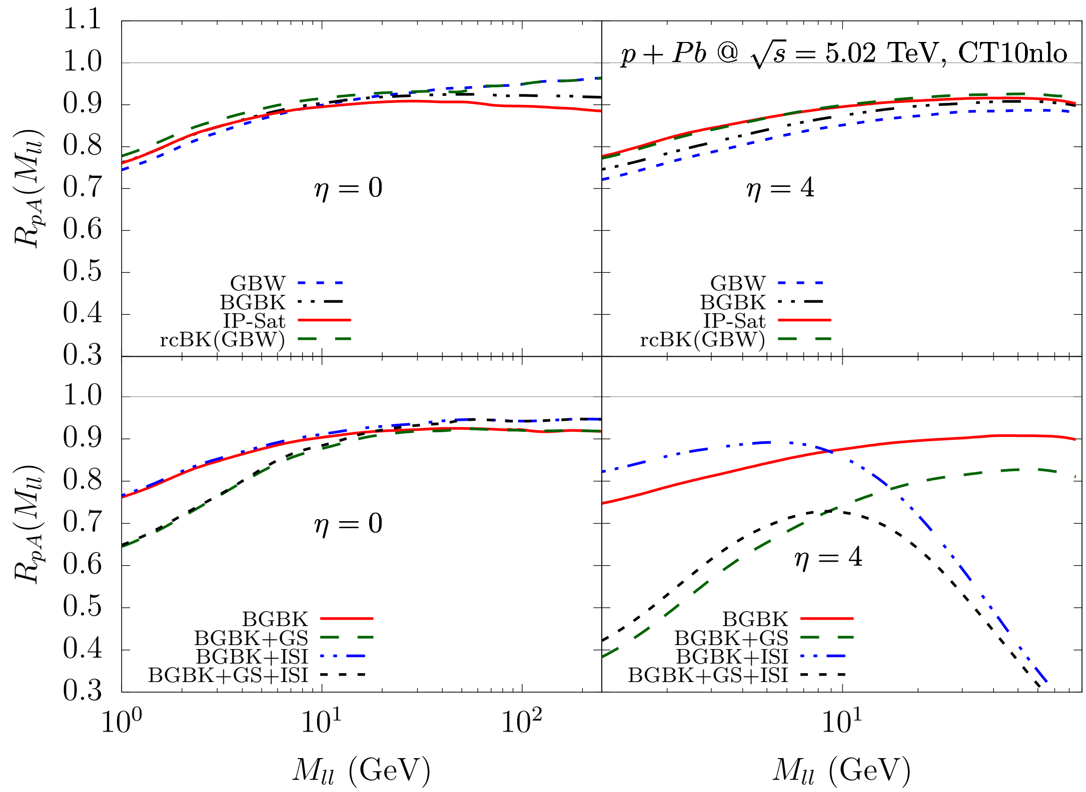

FIG. 5: (Color online) The dilepton invariant mass dependence of the nucleus-to-nucleon ratio, $R_{pA} = \sigma_{pA}^{DY}/(A \cdot \sigma_{pp}^{DY})$, of the DY production cross sections for c.m. enegy $\sqrt{s} = 5.02$ TeV corresponding to LHC experiments.

rapidity dependence of R_{pA} ideal for constraining such effects.

Fig. 7 shows our predictions for the transverse momentum dependence of the nuclear modification factor, $R_{pA}(p_T)$, for the invariant mass range $5 < M_{l\bar{l}} < 25$ GeV at RHIC c.m. energy $\sqrt{s} = 0.2$ TeV and two distinct pseudorapidity values $\eta = 0$ and $\eta = 1$. At large transverse momenta, the role of the saturation effects is negligibly small and can be important only at small $p_T \leq 2$ GeV. Similarly, the GS effects are almost irrelevant at RHIC energies. However, Fig. 7 clearly demonstrates a strong onset of ISI effects causing a significant suppression at large p_T, where no coherence effects are expected. In accordance with Eq. (16) and in comparison with $\eta = 0$, we predict stronger ISI effects at forward rapidities as is depicted in Fig. 7 for $\eta = 1$. Due to a significant elimination of coherence effects the study of the DY process at large p_T in pA collisions at RHIC is a very convenient tool for investigation of net ISI effects. On the other hand, at LHC energies (see Fig. 8) the manifestation of the saturation and GS effects rises at forward rapidities and becomes noticeable for $p_T \leq 10$ GeV. As was already mentioned for RHIC energies, the ISI effects cause a significant attenuation at large transverse momenta and forward rapidities, although no substantial suppression is expected in the DY process due to absence of the final state interaction, energy loss or absorption. For these reasons a study of the ratio $R_{pA}(p_T)$ also at the LHC especially at large p_T and at small invariant mass range is very effective to constrain the ISI effects.

In order to reduce the contribution of coherence effects (gluon shadowing, CGC) in the LHC kinematic region one should go to the range of large dilepton invariant masses as is shown in Fig. 9. Here we present our predictions for the ratio $R_{pPb}(p_T)$ at the LHC c.m. collision energy $\sqrt{s} = 5.02$ TeV for the range $60 < M_{l\bar{l}} < 120$ GeV and several values of $\eta = 0, 2, 4$. According to expectations we have found that the saturation and GS effects turn out to be important only at small p_T and large η. Such an elimination of coherence effects taking into account larger dilepton invariant masses causes simultaneously a stronger onset of ISI effects as one can seen in Fig. 9 in comparison with Fig. 8. For this reason, investigation of net ISI effects at large $M_{l\bar{l}}$ does not require such high p_T- and rapidity values, what allows to obtain the experimental data of higher statistics and consequently with smaller error bars. Fig. 9 demonstrates again a large nuclear suppression in the forward region ($\eta = 4$) over an extended range of the dilepton transverse momenta. Consequently, such an analysis of the DY nuclear cross section at forward rapidities by e.g. the LHCb Collaboration can be very useful to probe the ISI effects experimentally.

Finally, let us discuss the azimuthal correlation between the DY pair and a forward pion produced in pA collisions

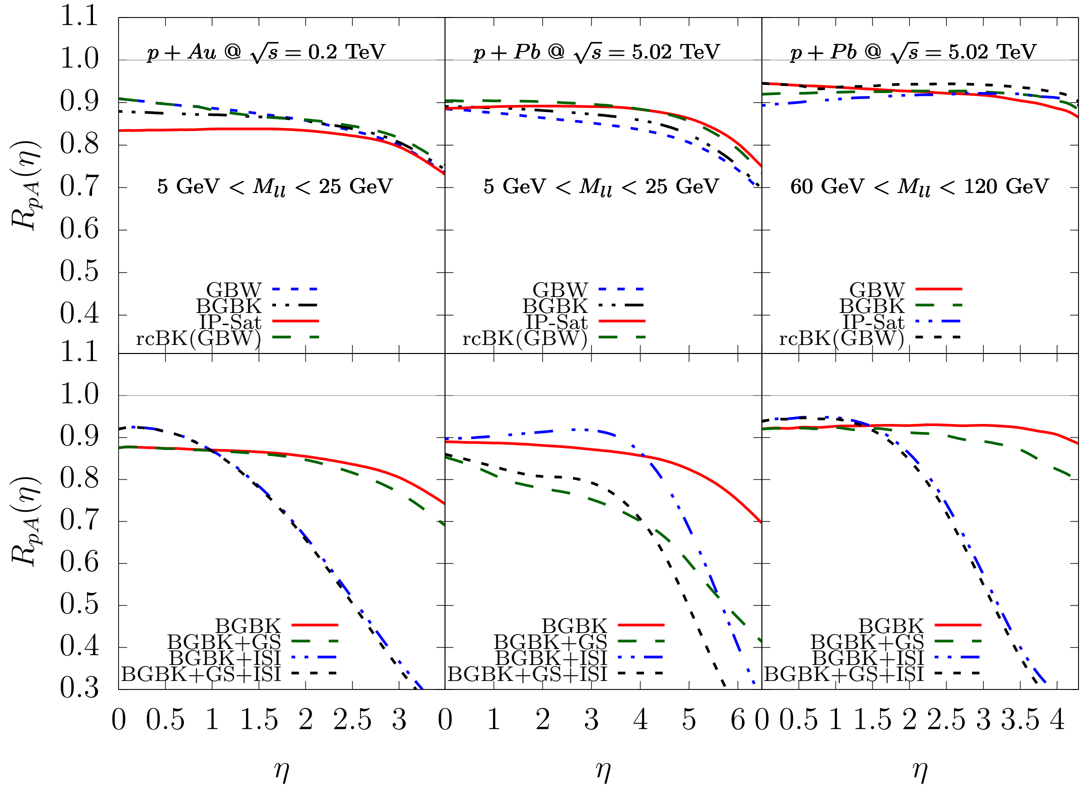

FIG. 6: (Color online) The pseudorapidity dependence of the nucleus-to-nucleon ratio, $R_{pA}(\eta)$, of the DY production cross sections at RHIC and LHC energies for two ranges ($5 < M_{l\bar{l}} < 25$ GeV) and ($60 < M_{l\bar{l}} < 120$ GeV) of dilepton invariant mass.

taking into account the Z^0 boson contribution in addition to the virtual photon as well as the saturation effects. As was discussed earlier in Refs. [12, 13, 55], the dilepton-hadron correlations can serve as an efficient probe of the initial state effects. Considering the $G^* = \gamma^*/Z_0$ boson as a trigger particle, the corresponding correlation function can be written as

$$C(\Delta\phi) = \frac{2\pi \int_{p_T, p_T^h > p_T^{\rm cut}} dp_T p_T \, dp_T^h p_T^h \, \frac{d\sigma(pA \to hG^* X)}{dY dy_h d^2p_T d^2p_T^h}}{\int_{p_T > p_T^{\rm cut}} dp_T p_T \, \frac{d\sigma(pA \to G^* X)}{dY d^2 p_T}} \,, \tag{17}$$

where $p_T^{\rm cut}$ is the experimental low cut-off on transverse momenta of the resolved G^* (or dilepton) and a hadron h, $\Delta\phi$ is the angle between them. The differential cross sections entering the numerator and denominator of $C(\Delta\phi)$ have been derived for pp collisions in Ref. [12] taking into account both the γ^* and Z^0 boson contributions and can now be directly generalised for pA collisions by accounting the nuclear dependence of the saturation scale. We refer to Ref. [12] for details of the differential cross sections. As in Ref. [13], in what follows we study the correlation function $C(\Delta\phi)$ taking the unintegrated gluon distribution (UGDF) in the following form

$$F(x_g, k_T^g) = \frac{1}{\pi Q_{s,A}^2(x_g)} \, e^{-{k_T^g}^2/Q_{s,A}^2(x_g)} \,, \tag{18}$$

where x_g and k_T^g are the momentum fraction and transverse momentum of the target gluon, ${Q_{s,A}}^2(x) = A^{1/3} c(b) \, Q_{s,p}^2(x)$ is the saturation scale and $Q_{s,p}^2(x)$ is given by Eq. (14). In numerical analysis, the CT10 NLO parametrization [51] for the parton distributions and the Kniehl-Kramer-Potter (KKP) fragmentation function $D_{h/f}(z_h, \mu_F^2)$ of a quark to a neutral pion [56] have been used. Moreover, we assume that the minimal transverse momentum ($p_T^{\rm cut}$) of the gauge boson G^* and the pion $h = \pi$ in Eq. (17) are the same and equal to 1.5 and 3.0 GeV for RHIC and LHC energies, respectively. As in our previous study [12], we assume that the factorisation scale is given by the dilepton invariant mass, i.e. $\mu_F = M_{l\bar{l}}$.

Considering our results for pp collisions [12], we have that the increasing of the saturation scale at large rapidities implies a larger value for the transverse momentum carried by the low-x gluons in the target which generates the

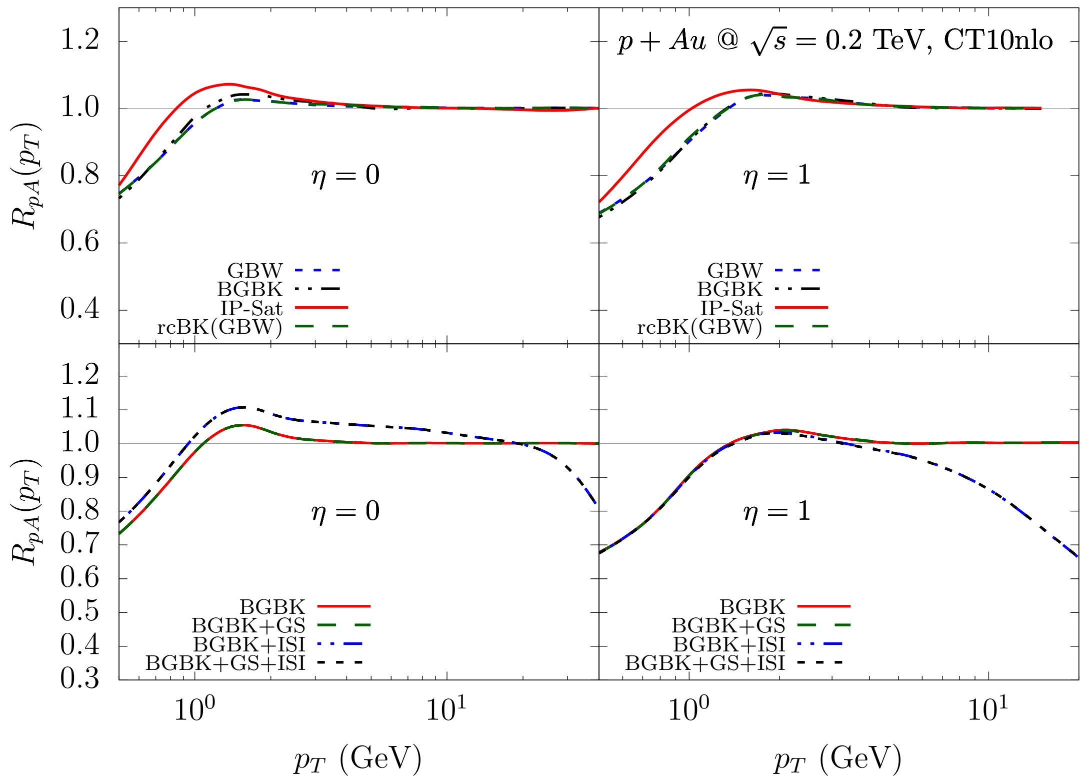

FIG. 7: (Color online) The transverse momentum dependence of the nucleus-to-nucleon ratio of the DY production cross sections, $R_{pA}(p_T)$, for the dilepton invariant mass range $5 < M_{l\bar{l}} < 25$ GeV at $\sqrt{s} = 0.2$ TeV and $\eta = 0, 1$.

decorrelation between the back-to-back jets. In the case of pA collisions, the magnitude of the saturation scale is amplified by the factor $A^{\frac{1}{3}}$. Consequently, we should also expect the presence a double-peak structure of $C(\Delta\phi)$ in the away side dilepton-pion angular correlation in pA collisions. This expectation is verified in our predictions presented in Fig. 10, where we show our predictions for the correlation function $C(\Delta\phi)$ of the associated DY pair and pion in pA collisions at LHC energies and different values of the atomic mass number. We have that larger values of A implies the smearing of the the back-to-back scattering pattern and suppress the away-side peak in the $\Delta\phi$ distribution. Our predictions for the RHIC and LHC kinematical regions are presented in Fig. 11, which agree with the results for small invariant masses presented in Refs. [12, 13]. In variance with our results for pp collisions [12], we also predict a double-peak structure for large invariant masses. This new result is directly associated with the larger value of the saturation scale present in pA collisions and to the fact that the typical momentum transverse of the produced particles is smaller in pA collisions at $\sqrt{s} = 5.02$ TeV than for pp collisions at $\sqrt{s} = 14$ TeV. As a consequence, the effect of the transverse momentum of the exchanged gluon is larger, implying the imbalance of the back-to-back jets also for large invariant masses in pA collisions, generating thus the double-peak structure observed in Fig. 11.

IV. SUMMARY

In this paper, we carried out an extensive phenomenological analysis of the inclusive DY $\gamma^*/Z^0 \to l\bar{l}$ process in pA collisions within the color dipole approach. At large dilepton invariant masses the Z^0 contribution becomes relevant. The corresponding predictions for the dilepton invariant mass and transverse momentum differential distributions have been compared with available data at the LHC and a reasonable agreement was found. The invariant mass, rapidity and transverse momentum dependencies of the nucleus-to-nucleon ratio of production cross sections, $R_{pA} = \sigma_{pA}^{DY}/(A \cdot \sigma_{pp}^{DY})$, were estimated taking into account such nuclear effects as the saturation, gluon shadowing GS and initial state energy loss effects (ISI effects).

In comparison with other processes with inclusive particle production, the DY reaction is very effective tool for study of nuclear effects since no final state interaction is expected, either the energy loss or absorption. For this reason the DY process represents a cleaner probe for the medium created not only in pA interactions but also in

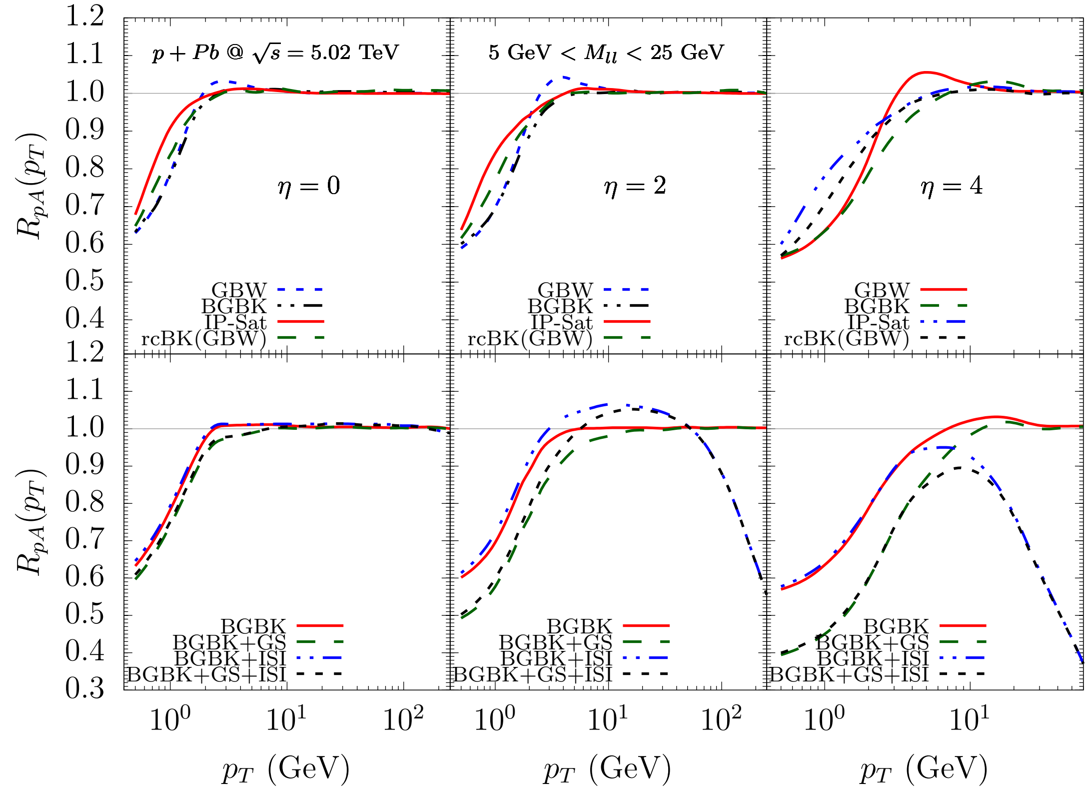

FIG. 8: (Color online) The transverse momentum dependence of the nucleus-to-nucleon ratio of the DY production cross sections, $R_{pA}(p_T)$, for the dilepton invariant mass range $5 < M_{l\bar{l}} < 25$ GeV at $\sqrt{s} = 5.02$ TeV and $\eta = 0, 2, 4$.

heavy ion collisions. Our results demonstrate that the analysis of the DY process off nuclei in different kinematic regions allows us to investigate the magnitude of particular nuclear effects. We found that both GS and ISI effects cause a significant suppression in DY production. Whereas GS effects dominate at small Bjorken-x in the target the ISI effects (in accordance with Eq. (16)) become effective at large transverse momenta p_T and invariant masses $M_{l\bar{l}}$ of dilepton pairs as well as at large Feynman x_F (forward rapidities). Consequently, at forward rapidities in some kinematic regions at the LHC one can investigate only a mixing of both effects even at large p_T- values. However, in contrast to other inclusive processes, the advantage of the DY reaction arises in elimination of the GS-ISI mixing by elimination of coherence effects going to larger values of the dilepton invariant mass. Then an investigation of nuclear suppression at large p_T represents a clear manifestation of net ISI effects even at forward rapidities as is demonstrated in Fig. 9. Such a study of nuclear suppression at large dilepton invariant masses, transverse momenta and rapidities especially at the LHC energy favours the DY process as an effective tool for investigation of net ISI effects.

Besides, we have analysed the correlation function $C(\Delta\phi)$ in azimuthal angle $\Delta\phi$ between the produced dilepton and a forward pion, which results by a fragmentation from a projectile quark radiating the virtual gauge boson. The corresponding observable has been studied at various energies in pA collisions in both the low and high dilepton invariant mass ranges as well as at different rapidities of final states. We found a characteristic double-peak structure of the correlation function around $\Delta\phi \simeq \pi$ at various dilepton mass values and for a very forward pion. The considering observable is more exclusive than the ordinary DY process. Such a measurement at different energies at RHIC and LHC is therefore capable of setting further even stronger constraints on saturation physics.

Acknowledgements

E.B. is supported by CAPES and CNPq (Brazil), contract numbers 2362/13-9 and 150674/2015-5. V.P.G. has been supported by CNPq, CAPES and FAPERGS, Brazil. R.P. is supported by the Swedish Research Council, contract number 621-2013-428. J.N. and M.K. are partially supported by the grant 13-02841S of the Czech Science Foundation (GAČR) and by the Grant MŠMT LG15001. J.N. is supported by the Slovak Research and Development Agency

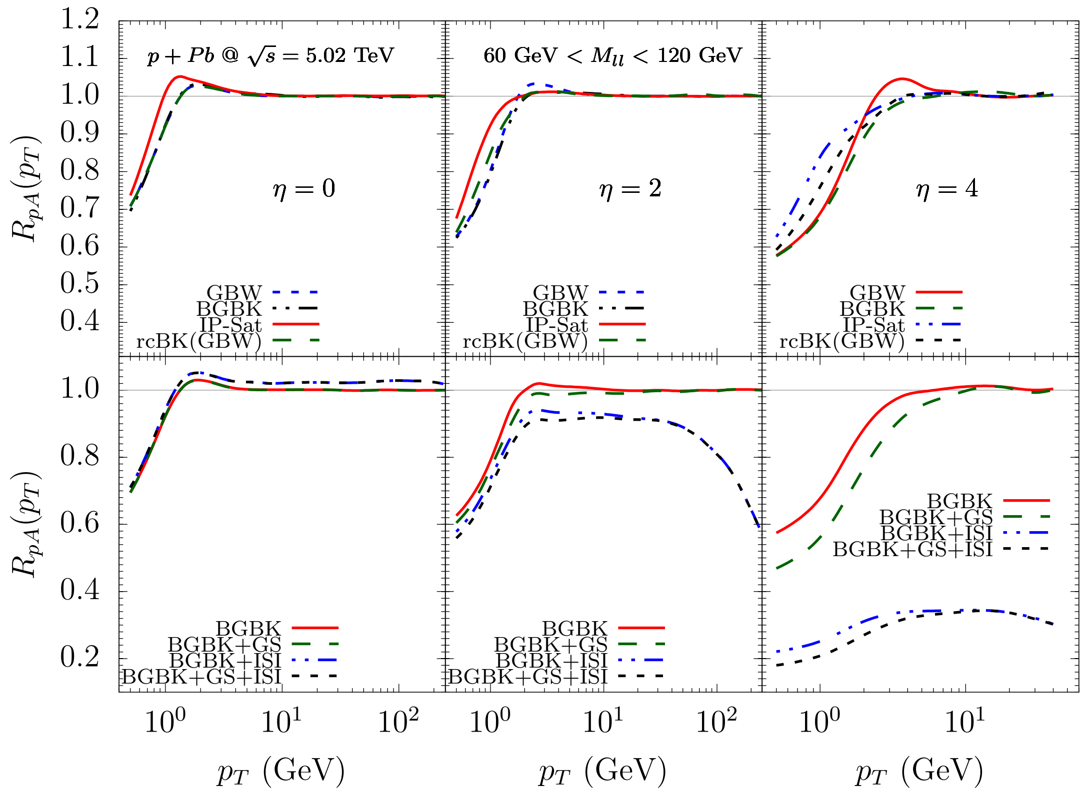

FIG. 9: (Color online) The transverse momentum dependence of the nucleus-to-nucleon ratio of the DY production cross sections, $R_{pA}(p_T)$, for the dilepton invariant mass range $60 < M_{l\bar{l}} < 120$ GeV at $\sqrt{s} = 5.02$ TeV and $\eta = 0, 2, 4$.

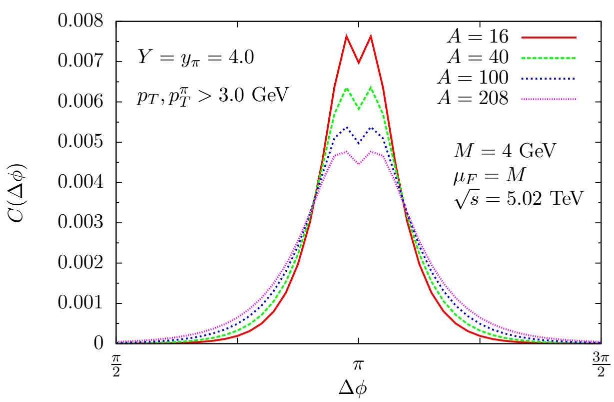

FIG. 10: (Color online) The correlation function $C(\Delta\phi)$ for the associated DY pair and pion production in pA collisions at the LHC ($\sqrt{s} = 5.02$ TeV) for different mass numbers A.

APVV-0050-11 and by the Slovak Funding Agency, Grant 2/0020/14.

[1] C.A. Salgado *et al.*, J. Phys. G**39**, 015010 (2012).
[2] J.C. Peng and J.W. Qiu, Prog. Part. Nucl. Phys. **76**, 43 (2014).
[3] B.Z. Kopeliovich, in *Proceedings of the international workshop XXIII on Gross Properties of Nuclei and Nuclear Excitations, Hirschegg, Austria, 1995*, edited by H. Feldmeyer and W. Nörenberg (Gesellschaft Schwerionenforschung, Darmstadt, 1995),

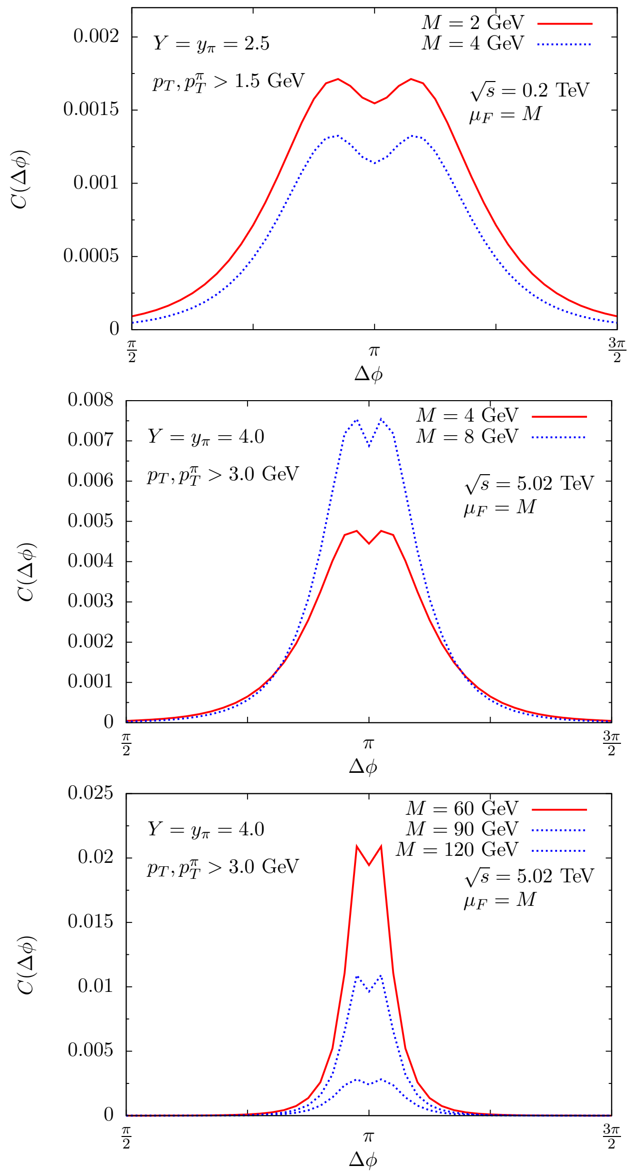

FIG. 11: (Color online) The correlation function $C(\Delta\phi)$ for the associated DY pair and pion production in pA collisions at RHIC ($\sqrt{s} = 0.2$ TeV) and LHC ($\sqrt{s} = 5.02$ TeV) energies and different values of the dilepton invariant mass.

p. 385.

[4] S.J. Brodsky, A. Hebecker and E. Quack, Phys. Rev. D**55**, 2584 (1997).

[5] B.Z. Kopeliovich, A. Schafer, and A.V. Tarasov, Phys. Rev. C**59**, 1609 (1999).

[6] B.Z. Kopeliovich, J. Raufeisen, and A.V. Tarasov, Phys. Lett. B**503**, 91 (2001).

[7] B.Z. Kopeliovich, J. Raufeisen, A.V. Tarasov and M.B. Johnson, Phys. Rev. C**67**, 014903 (2003).

[8] J. Raufeisen, J.C. Peng and G.C. Nayak, Phys. Rev. D**66**, 034024 (2002);
M.B. Johnson, B.Z. Kopeliovich, M.J. Leitch, P.L. McGaughey, J.M. Moss, I.K. Potashnikova and I. Schmidt, Phys. Rev. C**75**, 035206 (2007);
M.B. Johnson, B.Z. Kopeliovich and I. Schmidt, Phys. Rev. C**75**, 064905 (2007).

[9] M.A. Betemps, M.B.G. Ducati and M.V.T. Machado, Phys. Rev. D**66**, 014018 (2002);
M.A. Betemps, M.B.G. Ducati, M.V.T. Machado and J. Raufeisen, Phys. Rev. D**67**, 114008 (2003);
M.A. Betemps and M.B.G. Ducati, Phys. Rev. D**70**, 116005 (2004); Phys. Lett. B**636**, 46 (2006);
M.A. Betemps, M.B.G. Ducati and E.G. de Oliveira, Phys. Rev. D**74**, 094010 (2006);
M.B.G. Ducati and E.G. de Oliveira, Phys. Rev. D**81**, 054015 (2010);
M.B.G. Ducati, M.T. Griep and M.V.T. Machado, Phys. Rev. D**89**, 034022 (2014).

[10] R.S. Pasechnik, B.Z. Kopeliovich, and I.K. Potashnikova, Phys. Rev. D**86**, 114039 (2012).
[11] E.A.F. Basso, V.P. Goncalves and M. Rangel, Phys. Rev. D**90**, 094025 (2014).
[12] E. Basso, V.P. Goncalves, J. Nemchik, R. Pasechnik and M. Sumbera, Phys. Rev. D**93**, 034023 (2016).
[13] A. Stasto, B-W Xiao and D. Zaslavsky, Phys. Rev. D**86**, 014009 (2012).
[14] F. Gelis, E. Iancu, J. Jalilian-Marian and R. Venugopalan, Ann. Rev. Nucl. Part. Sci. **60**, 463 (2010);
E. Iancu and R. Venugopalan, arXiv:hep-ph/0303204;
H. Weigert, Prog. Part. Nucl. Phys. **55**, 461 (2005);
J. Jalilian-Marian and Y.V. Kovchegov, Prog. Part. Nucl. Phys. **56**, 104 (2006);
J.L. Albacete and C. Marquet, Prog. Part. Nucl. Phys. **76**, 1 (2014).
[15] J. Jalilian-Marian, A. Kovner, L. McLerran and H. Weigert, Phys. Rev. D**55**, 5414 (1997);
J. Jalilian-Marian, A. Kovner and H. Weigert, Phys. Rev. D**59**, 014014 (1999), *ibid.* **59**, 014015 (1999), *ibid.* **59** 034007 (1999);
A. Kovner, J. Guilherme Milhano and H. Weigert, Phys. Rev. D**62**, 114005 (2000);
H. Weigert, Nucl. Phys. A**703**, 823 (2002);
E. Iancu, A. Leonidov and L. McLerran, Nucl. Phys. A**692**, 583 (2001);
E. Ferreiro, E. Iancu, A. Leonidov and L. McLerran, Nucl. Phys. A**701**, 489 (2002).
[16] I.I. Balitsky, Phys. Rev. Lett. **81**, 2024 (1998); Phys. Lett. B**518**, 235 (2001);
I.I. Balitsky and A.V. Belitsky, Nucl. Phys. B**629**, 290 (2002).
[17] Y.V. Kovchegov, Phys. Rev. D**60**, 034008 (1999); Phys. Rev. D**61**, 074018 (2000).
[18] K.J. Golec-Biernat and A.M. Stasto, Nucl. Phys. B**668**, 345 (2003);
J. Berger and A. Stasto, Phys. Rev. D**83**, 034015 (2011); Phys. Rev. D**84**, 094022 (2011).
[19] E.R. Cazaroto, F. Carvalho, V.P. Goncalves and F.S. Navarra, Phys. Lett. B**671**, 233 (2009).
[20] V.P. Goncalves, M.S. Kugeratski, M.V.T. Machado and F.S. Navarra, Phys. Rev. C**80**, 025202 (2009).
[21] E.R. Cazaroto, F. Carvalho, V.P. Goncalves, M.S. Kugeratski and F.S. Navarra, Phys. Lett. B**696**, 473 (2011).
[22] F. Carvalho, V.P. Goncalves, F.S. Navarra and E.G. de Oliveira, Phys. Rev. C**87**, 065205 (2013).
[23] V.P. Goncalves and D.S. Pires, Phys. Rev. C**91**, 055207 (2015).
[24] V.P. Goncalves, F.S. Navarra and D. Spiering, arXiv:1510.01512 [hep-ph].
[25] B.Z. Kopeliovich, L.I. Lapidus, A.B. Zamolodchikov, JETP Lett. **33**, 595-597 (1981).
[26] N. Armesto, Eur. Phys. J. C**26**, 35 (2002).
[27] H.De Vries, C.W.De Jager and C.De Vries, Atomic Data and Nucl. Data Tables **36**, 469 (1987).
[28] V.N. Gribov, Sov. Phys. JETP **30**, 709 (1970) [Zh. Eksp. Teor. Fiz. **57**, 1306 (1969)].
[29] K.J. Golec-Biernat, M. Wusthoff, Phys. Rev. D**59**, 014017 (1998).
[30] E. Iancu, K. Itakura, S. Munier, Phys. Lett. B**590**, 199 (2004).
[31] D. Kharzeev, Y.V. Kovchegov and K. Tuchin, Phys. Lett. B**599**, 23 (2004).
[32] A. Dumitru, A. Hayashigaki and J. Jalilian-Marian, Nucl. Phys. A**765**, 464 (2006).
[33] V.P. Goncalves, M.S. Kugeratski, M.V.T. Machado and F.S. Navarra, Phys. Lett. B**643**, 273 (2006).
[34] D. Boer, A. Utermann, E. Wessels, Phys. Rev. D**77**, 054014 (2008).
[35] H. Kowalski, L. Motyka and G. Watt, Phys. Rev. D**74**, 074016 (2006);
G. Watt and H. Kowalski, Phys. Rev. D**78**, 014016 (2008).
[36] J.T. de Santana Amaral, M.B. Gay Ducati, M.A. Betemps, and G. Soyez, Phys. Rev. D**76**, 094018 (2007);
E.A.F. Basso, M.B.G. Ducati and E.G. de Oliveira, Phys. Rev. D**87**, 074023 (2013).
[37] G.Soyez, Phys. Lett. B**655**, 32 (2007).
[38] J. Bartels, K. Golec-Biernat, and H. Kowalski, Phys. Rev. D**66**, 014001 (2002).
[39] H. Kowalski and D. Teaney, Phys. Rev. D**68**, 114005 (2003).
[40] A.H. Rezaeian, M. Siddikov, M. Van de Klundert and R. Venugopalan, Phys. Rev. D**87**, 034002 (2013).
[41] A. Rezaeian and I. Schmidt, Phys. Rev. D**88**, 074016 (2013).
[42] V.N. Gribov and L.N. Lipatov, Sov. J. Nucl. Phys. **15**, 438 (1972);
G. Altarelli and G. Parisi, Nucl. Phys. B**126**, 298 (1977);
Yu.L. Dokshitzer, Sov. Phys. JETP **46**, 641 (1977).
[43] F.D. Aaron *et al.* [H1 and ZEUS Collaborations], JHEP **1001**, 109 (2010);
H. Abramowicz *et al.* [H1 and ZEUS Collaborations], Eur. Phys. J. C**73** 2311 (2013).
[44] J.L. Albacete, N. Armesto, J.G. Milhano and C.A. Salgado, Phys. Rev. D**80**, 034031 (2009).
[45] B.Z. Kopeliovich, A. Schaefer, and A.V. Tarasov, Phys. Rev. **D62**, 054022 (2000);
B.Z. Kopeliovich, J. Nemchik, A. Schaefer, Phys. Rev. C**65**, 035201 (2002);
B.Z. Kopeliovich, J. Nemchik, I.K. Potashnikova, I. Schmidt, J. Phys. G**35**, 115010 (2008).
[46] D. de Florian and R. Sassot, Phys. Rev. D**69**, 074028 (2004);
M. Hirai, S. Kumano and T.H. Nagai, Phys. Rev. C**70**, 044905 (2004).
[47] B.Z. Kopeliovich, J. Nemchik, I.K. Potashnikova, M.B. Johnson, I. Schmidt, Phys. Rev. C**72**, 054066 (2005);
B.Z. Kopeliovich, J. Nemchik, I.K. Potashnikova, I. Schmidt, Int. J. Mod. Phys. E**23**, 1430006 (2014).
[48] S.S. Adler *et al.* [PHENIX Collab.], Phys. Rev. Lett. **98**, 172302 (2007);
Phys. Rev. Lett. **109**, 152302 (2012).
[49] S. Afanasiev *et al.* [PHENIX Collab.], Phys. Rev. Lett. **109**, 152302 (2012);
T. Sakaguchi, Nucl. Phys. A**805**, 355 (2008).
[50] I. Arsene *et al.* [BRAHMS Collab.], Phys. Rev. Lett. **93**, 242303 (2004);

J. Adams *et al.* [STAR Collab.], Phys. Rev. Lett. **97**, 152302 (2006).
[51] H.L. Lai, M. Guzzi, J. Huston, Z. Li, P.M. Nadolsky, J. Pumplin and C.P. Yuan, Phys. Rev. D**82**, 074024 (2010).
[52] E. Basso, C. Bourrely, R. Pasechnik and J. Soffer, arXiv:1509.07988 [hep-ph].
[53] V. Khachatryan *et al.* [CMS Collaboration], arXiv:1512.06461 [hep-ex].
[54] G. Aad *et al.* [ATLAS Collaboration], Phys. Rev. C**92**, 044915 (2015).
[55] J. Jalilian-Marian and A.H. Rezaeian, Phys. Rev. D**86**, 034016 (2012);
A.H. Rezaeian, Phys. Rev. D**86**, 094016 (2012).
[56] B.A. Kniehl, G. Kramer and B. Potter, Nucl. Phys. B**582**, 514 (2000).